Physico-chemical characterisation of water soluble non-starch polysaccharides.

Wang, Qi

KING'S College LONDON
Founded 1829

Physico-chemical characterization of water soluble non-starch polysaccharides

Qi Wang BSc MSc

October 1997

A thesis submitted to the University of London
for the degree of Doctor of Philosophy

King's College London
University of London

ALL MISSING PAGES ARE BLANK

IN

ORIGINAL

Abstract

This thesis is concerned with the development of physico-chemical techniques to characterise the properties of water soluble non-starch polysaccharides (s-NSP). The first part of this project was to characterise the structure and solution properties of s-NSP extracted from a plant, *Detarium senegalense* Gmelin. The extracted s-NSP was analysed by GLC and found to be similar in structure to tamarind xyloglucan. This was confirmed by comparing the oligosaccharides released on enzymatic digestion with those obtained from tamarind xyloglucan. Histochemical examination of detarium seed showed the presence of xyloglucan in highly thickened cell walls. The intrinsic viscosity of detarium gum was found to be high, indicating that the sample was of high molecular weight. The semi-dilute solution characteristics investigated by steady and dynamic shear rheometry, suggest that detarium gum is a well behaved linear polymer entanglement system. Static light scattering was also successfully applied to examine the molecular weight and architecture of the detarium xyloglucan macromolecules.

The physiological behaviour of s-NSP when consumed is critically dependent on their physico-chemical properties, including the rate and degree of hydration. In the second part of the project a method for determining the hydration rate of a powdered form of s-NSP was developed. A logarithmic model for describing the hydration kinetics of guar gum was also established. This model was used to investigate the effects of polymer concentration (C), molecular weight (M), and particle size on the hydration rate of guar gum. The results showed that there was a significant inverse relationship between hydration rate and M and mean particle size, respectively. The hydration rate increased with increasing C at a low concentration range, but decreased when C>1.2% (w/w).

The pH in the lumen of the gastrointestinal tract of human is acidic, usually between 2.0 and 1.5 after a meal. The stability of guar gum in acidic conditions was investigated at temperatures 25, 37 and 50°C. The results indicated that there was unlikely to be significant acidic degradation of guar gum in the human gastrointestinal tract. The pH condition was also found to influence the hydration rate of guar gum. In general, the hydration rate was lower in an acid environment than it was in neutral conditions.

Acknowledgements

I am particularly grateful to my supervisors Dr. Peter Ellis and Professor Simon Ross-Murphy of King's College London for their excellent guidance and full support during the performance of this programme. Their dedication and constant encouragement have ensured that I could get this far.

I would like to thank Prof. J.S.G. Reid and Dr. M. Edwards of the University of Stirling for their expert supervision of the chemical structure analysis of detarium gum. I also wish to thank Prof. W. Burchard for his expert assistance with the light scattering work described in this thesis. My thanks are extended to Dr H. Englyst for the analysis of the starch content of detarium flour.

I gratefully acknowledge a number of people at King's College: Dr. U. Onyechi for providing the detarium samples. Mr. V. Dawes and Dr. X. Zeng of Pharmacy Department for their assistance and helpful advice on particle size analysis and Dr. A. Cullen in the EM Unit for his assistance with preparing the SEM photomicrographs. I would like to thank all the members of the Biopolymers Group at King's for their help and friendship which have made my time in UK so enjoyable. I am particularly grateful to Pip, Atsumi, Gaynor, Diane and Yilong for their assistance and invaluable comments.

I gratefully acknowledge the financial support from Meyhall Chemical AG (Rhône-Poulenc Group), Switzerland and the ORS award from the Committee of Vice-chancellors and Principals of UK Universities. I particularly wish to thank Mrs. C. Guittard (Rhône-Poulenc Group) for her constant interest and support, Dr. W.C. Wielinga and Dr. J. Runyon (Meyhall Chemical AG) for preparing some of the guar samples and helpful discussions.

Finally, I would like to thank Xijin, Wu and all my family and friends who have supported me during the last four years. I am especially indebted to my mother-in-law Mrs. Z. Xiang for her encouragement and selfless support.

Table of Contents

Abbreviations and Symbols

Abbreviations

AACC	American Association of Cereal Chemists
DF	dietary fibre
DM	diabetes mellitus
DMSO	dimethyl sulfoxide
EM	electron microscopy
EMC	equilibrium moisture content
FAO	Food and Agriculture Organisation
Gal	galactose (syl)
GI	gastrointestinal
GLC	gas-liquid chromatography
Glc	glucose (syl)
HPAEC	high-performance anion-exchange chromatography
LBG	locust bean gum
NSP	non-starch polysaccharides
ORS	overseas research studentships
RFSII	Rheometrics Fluids Spectrometer II
r.p.m.	revolutions per minute
S.D.	standard deviation
S.E.	standard error
SEM	scanning electron microscope
s-NSP	water-soluble non-starch polysaccharides
TLC	thin-layer chromatography
WHO	World Health Organisation
w/v	weight/volume
w/w	weight/weight
XG	xyloglucan
Xyl	xylose (syl)

Symbols

A_{sp}	specific surface area of particles
A_2, A_3, ...	the second, third, ... virial coefficients
α	exponent in Mark-Houwink equation; time scale parameter in Weibull function; anomeric configuration of sugars
α_{sv}	surface-volume shape coefficient
β	shape factor in Weibull function; anomeric configuration of sugars
C, c	polymer concentration
c_s	solubility of the sample, i.e. the maximum concentration of solution under a given condition
c_t	polymer concentration at time t
D	diffusion coefficient
df	degrees of freedom
D_m, d_m	surface volume mean diameter of particles
$\bar{DP}_n$, $\bar{DP}_w$	the number-average, weight-average degree of polymerisation
δ	phase difference between strain and stress wave
Δ	change in (difference)
ΔG	change of Gibbs free energy
ΔH	enthalpy change
ΔS	entropy change
f	functionality of polymer molecules
F_g	gel-solid front during hydration of polymer
F_s	solid-polymer front during hydration of polymer
φ	integration constant
G	dissolution rate per unit area (V/S dc/dt)
G', G"	shear storage, shear loss modulus
G*	complex shear modulus
G(t)	time dependant shear modulus
γ	interfacial tension; shear strain
$\dot{\gamma}$	shear rate
h	thickness of the film layer formed around a particle during hydration

η	shear viscosity
$[\eta]$	intrinsic viscosity
η_r	relative viscosity
η_{red}	reduced viscosity
η_{sp}	specific viscosity
η_0	zero-shear viscosity
η^*	complex dynamic viscosity
η_∞	limiting viscosity at infinite shear rate; 'ultimate viscosity' of a solution
I	intensity of the light
J(t)	time dependent shear compliance
k, K	general constant
K	optical contrast constant; Kelvin (temperature unit)
λ	wavelength
m	maximum hydration rate; meter
M_v, M_w, M_n	viscosity, weight and number average molecular weight, respectively
n_0	solvent refractive index
ν	hydration index, i.e. the maximum hydration rate divided by the time needed to reach this hydration rate
P(q), P(u)	particle scattering factor
π	osmotic pressure
q	the magnitude of the scattering vector
θ	scattering angle
R	gas constant
R_g	the z-average radius of gyration
$<R^2>_0$	the mean square end-to-end distance
R_θ	Rayleigh ratio
r^2	correlation coefficient
S	surface area of particles; radius of gyration
s	velocity of dissolution
s^2	variance (= sum of squares/degrees of freedom)
T	temperature in K
t	time

$t_{0.8}$	hydration index, i.e. the time needed for a dispersion to reach 80% of the ultimate viscosity during hydration process
τ	relaxation time
V	volume of solution or dispersion
W, w	sample weight
Ω	location factor in Weibull function
ω	oscillatory frequency
ψ_d	shape factor for transforming the results between two methods of particle sizing

Chapter 1

Introduction

1.1 Background

1.1.1 Physico-chemical and functional properties of NSP

Polysaccharides are linear or branched carbohydrate polymers which form a major constituent of food consumed by humans. Among the polysaccharides, starch occupies a unique position because of its wide usage as a major food carbohydrate source. The remainder are collectively known as non-starch polysaccharides (NSP), which are the main subject studied in this thesis. The molecular structures of NSP are complicated and diverse as will be described in Chapter 2. This leads to various physical properties and functionality of NSP with wide applications in a range of industries. These polymers may alter the properties of aqueous solutions (dispersion) by increasing viscosity, forming gels (or weak gels) and affecting surface properties of foams. The functionality of these polymers is largely dependent on their physico-chemical properties. Therefore, the investigation of the physical and chemical characteristics of these polymers is fundamental to the prediction of their functionality in practical applications.

However, most polysaccharides have been used for a long time without there being concerned with the underlying chemistry and physics of polysaccharide systems. In particular, most of these substances had received relatively little attention from physical chemists until the 1960s (Tanford, 1961). During the last few decades, one of the advances in polysaccharide research has been to relate the molecular constitution of polysaccharides to their physical properties and hence functionality, which was inspired originally by the work of D.A. Rees and co-workers in the 1960s and 1970s (Rees, 1977). Since then, there has been a significant growth in interest in this area. The

success in employing a range of modern techniques, such as light scattering and rheology techniques, for characterising the physico-chemical properties of these polymers has stimulated studies in this area. Consequently, a number of important theories and models have been proposed to describe the polysaccharides and other biopolymers both on the molecular and macromolecular levels. These theories have enabled us to have a deeper understanding of the mechanisms underlying the functional effects of these polymers.

1.1.2 Biological and nutritional role of NSP

NSP represent a large group of biopolymers which can be obtained in nature from plants, micro-organisms and animals. In nature they have a wide range of functions. Some of them form the principal bulk carbohydrate reserve in plant seeds and are mobilised after germination, such as guar gum and tamarind gum. Some others contribute to the integrity and mechanical strength of plant tissues, examples here being cellulose and pectin.

From a nutritional standpoint, NSP contribute to the major components of dietary fibre (DF). The role of DF in human nutrition and health has become increasingly appreciated since the late 1960s. In recent years, the nutritional and therapeutic benefits of NSP, notably in the treatment of metabolic disorders, such as diabetes mellitus and hyperlipidemia, have been more widely appreciated (Ellis, 1994). It has been known that NSP mainly from plant food sources have marked effects on the physical properties of digesta at all sites of the gastrointestinal (GI) tract (Edwards, 1995). The consumption of NSP, in the form of plant cell walls or purified extracts, can strongly influence GI functions, including the rate and extent of nutrient absorption in the small intestine and bacterial fermentation in the large intestine. Therefore, the study of the mechanism underlying the physiological effects of NSP has been one of the hottest topics in the nutritional research areas during the past few decades. Although numerous research reports have been published, the mechanisms by which different NSP influenced physiological processes have not yet been elucidated (Edwards, 1995).

Dietary fibre consisting of mainly water-insoluble NSP has been added to food for promoting health for more than 30 years. However, for a long time, the inclusion of water-soluble NSP (s-NSP) in foods has rarely been used for changing their nutritional qualities, but only to assist processing, or changing structural and textural properties. But in recent years, s-NSP have been incorporated into a variety of food products with the aim of changing their nutritional properties. These NSP-supplemented foods developed for nutritional and health purposes are often termed 'functional foods'.

1.1.3 Hydration property in relation to the physiological effects of s-NSP

It has been known that many s-NSP can significantly modulate carbohydrate and lipid metabolism in experimental animals and man (Jenkins, *et al.* 1976; Gee, *et al.* 1983; Ellis, *et al.*, 1991). The mechanisms by which these types of dietary fibre elicit their physiological effects are still not completely understood. Nevertheless, it has been widely accepted that the physiological action of soluble NSP largely depends on the capacity of these polymers to hydrate and increase the viscosity of digesta in the upper gastrointestinal tract (Jenkins, *et al.,* 1978; Edwards, 1995; Ellis, *et al.,* 1995). From this point of view, the rheological behaviour of s-NSP in solution is likely to be used as an indicator of their potential biological function.

The critical importance of the rate and degree of hydration of s-NSP in determining the biological activity of these polymers has been demonstrated by a number of research groups (O'Connor, *et al.,* 1981; Heppell and Rainbird, 1985; Ellis and Morris, 1991). Those s-NSP with high molecular weight cannot confer their full viscosity until they are properly hydrated. The disappointing performance of some commercial guar granules in lowering post-prandial levels of blood glucose and insulin may simply due to their inability to dissolve during their transit time along the upper GI tract (Ellis and Morris, 1991).

Like many other substances, the hydration properties of s-NSP are inevitably affected by a range of physico-chemical properties and the environmental conditions where they hydrate. Study of the effects of these factors on the hydration properties is obviously fundamental to understanding the physiological mechanisms and clinical role of these polymers. The development of a rheological method for studying the hydration kinetics of s-NSP is not only useful for evaluating some of the nutritional properties of these materials, but is also important in investigating their functional properties in general (i.e. viscosity enhancing). Such a technique may also have value in studying the relationship between the rheological properties of digesta in the small intestine and the digestion and absorption kinetics of starch and other nutrients.

Guar gum has been selected as an example of s-NSP for the hydration kinetic study in this project. This is because guar gum is not only one of most well-characterised s-NSP, but it is also mostly commonly used as a model soluble dietary fibre in clinical nutrition. Moreover, it is commercially available in a range of average molecular weights. There is a practical need to investigate the hydration behaviour of different grades of guar gum in order to study their physiological effects.

1.2 Aims

This thesis is concerned with the development of physico-chemical techniques to characterise the structure and properties of non-starch polysaccharides, in particular those related to nutritional aspects. The project was divided into two phases involving studies of two different polysaccharides. The first phase involved characterising the structure and macromolecular solution properties of purified s-NSP from a traditional Nigerian plant: *Detarium senegalense* Gmelin. The aims of this work was: (1) to determine the molecular structure of detarium polysaccharides by the use of total acid hydrolysis and enzymatic hydrolysis methods; (2) to examine molecular weight and architecture of detarium polysaccharides using rheological and laser scattering techniques and (3) to investigate the macromolecular solution properties by steady and dynamic shear rheometry.

The second part of this project was concerned with developing a rheological method for studying the hydration kinetics of a s-NSP, namely, guar gum. A range of commercial food grade guar gum flours were selected for this study. The aims of this study was: (1) to develop an hydration technique for measuring the hydration rate; (2) to seek an appropriate empirical model for describing the hydration process of guar gum powders. Attempts were made to develop a simple empirical model by mathematical curve fitting approaches, and (3) to study a number of physico-chemical variables that are likely to influence the hydration behaviour of guar gum powders using the same hydration technique and model. These factors include polymer concentration, molecular weight, particle size and pH levels.

1.3 Outline of thesis

This thesis is divided into ten chapters. After a brief introductory chapter there follows a review of the general literature (Chapter 2). The review starts with the general description of polysaccharides, focusing on their basic molecular structures and physical and functional properties. Some individual polysaccharides that are commonly used in research and industry are described. The rheological and light scattering techniques have been two important methods for studying the physico-chemical properties of polysaccharides in this thesis. The basic theory and a number of important studies on rheology and light scattering of polysaccharide systems are also reviewed in this chapter. In subsequent sections of Chapter 2, there is a review of the physiological aspects of NSP, when they are used as a major ingredient of the diet. The recent development in the area of physiological effects of NSP (mainly s-NSP) and the underlying mechanisms are summarised in reasonable detail. This has led to recognising the important role of the hydration behaviour of s-NSP in determining their physiological functions. Therefore, a number of important research studies carried out on the hydration kinetics of polymers were subsequently reviewed. The experimental techniques that were used throughout this research project are described in Chapter 3. Other techniques used are given in the appropriate chapters. Chapters 4 and 5 describe the characterisation of a new polysaccharide sample from detarium gum, using a wide range of physico-chemical

techniques. Chapter 4 includes the results of the isolation of the polymers and the determination of the molecular structure of these polymer extracts. The molecular weight and macromolecular solution properties of these polysaccharides are then investigated in Chapter 5 using rheological and static light scattering techniques.

The second phase of the work is described in Chapters 6-9, and discuss the results of experiments designed to study hydration kinetics of guar gum. Chapter 6 involves developing a rheological method for the measurement of hydration rate of polysaccharide powders. It also includes the establishment of an empirical mathematical model for describing the hydration rate of these guar gum flours. A number of other hydration models previously developed are also discussed in this chapter. In Chapter 7, the effects of polymer concentration and molecular weight on the hydration rate of guar gum flours were investigated using the hydration technique and the mathematical model developed in Chapter 6. The hydration behaviour of a range of commercial food grades of guar gum flour of different average molecular weights was examined. The effects of particle size of guar gum on hydration rate was comprehensively studied and discussed in Chapter 8. The polynomial regression method was applied to describe the hydration rate and a useful hydration index was defined for the comparison of hydration rate of different samples. In Chapter 9, the stability of guar gum polysaccharides under acidic conditions was investigated using dilute solutions at temperature 25, 37 and 50°C. The effects of pH on the hydration rate of guar gum under acidic conditions were also investigated using the hydration model developed in Chapter 6.

In the final chapter of the thesis (Chapter 10), there is a summary of the main conclusions drawn from this project and a discussion of the possible future experiments that need to be carried out.

1.4 Publications and presentations relevant to thesis

Wang, Q., Ellis, P.R., Ross-Murphy S.B. and Burchard, W. (1997). Solution characteristics of the xyloglucan extracted from *Detarium senegalense* Gmelin. *Carbohydrate Polymers* **31**, (In press).

Ross-Murphy S.B., Wang, Q. and Ellis, P.R. (1997). Structure and mechanical properties of polysaccharides. *Macromolecular Symposia* (In press).

Wang, Q., Ellis, P.R. and Ross-Murphy S.B. (1997). Development of a rheological method for studying the hydration kinetics of water-soluble non-starch polysaccharides. *16th International Congress of Nutrition (Conference Abstract).*

Wang, Q., Ellis, P.R., Ross-Murphy S.B. and Reid, J.S.G. (1996). A new polysaccharide from a traditional Nigerian plant food: *Detarium senegalense* Gmelin. *Carbohydrate Research* **284**, 229-239.

Ellis, P.R., Rayment, P. and Wang, Q. (1996). A physico-chemical perspective of plant polysaccharides in relation to glucose absorption, insulin secretion and the entero-insular axis. *Proceeding of the Nutrition Society* **55**, 881-898.

Wang, Q., Ellis, P.R. and Ross-Murphy S.B. (1995). Solution properties of polysaccharide extracted from a traditional Nigerian plant food: *Detarium senegalense* Gmelin. *Cereal Food World* **40** (9), P645.

Wang, Q., Ellis, P.R., Ross-Murphy, S.B. and Reid, J.S.G. (1995). A new polysaccharide from a traditional Nigerian plant food: *Detarium senegalense* Gmelin. The *Royal Society of Chemistry Spring Meeting of the Carbohydrate Group.* University of Leeds.

Chapter 2

Literature review

2.1 Polysaccharides

2.1.1 General structures and physical properties

Polysaccharides are high-molecular-weight carbohydrates which can be viewed as condensation polymers in which monosaccharides have been joined by *O*-glycosidic linkages with elimination of water. The term polysaccharide is limited generally to those polymers containing ten or more monosaccharide residues. The carbohydrates comprising 2-10 monosaccharide units are called oligosaccharides. Most polysaccharides as found in nature contain a hundred to several thousand monosaccharide units.

Polysaccharides show considerable diversity in structure and are often named according to the constituent sugars and their glycosidic linkages. In such a classification, polysaccharides hydrolysing to only one monosaccharide type are termed homoglycans, while polysaccharides hydrolysing to two or more monosaccharide types are termed heteroglycans. The same type of monosaccharide units can be linked in various ways to give polysaccharide of different macromolecular structures and physical properties. Conversely, different monosaccharides linked in the same way often give polysaccharides with closely similar properties. For example, Fig. 2.1 illustrates some of the inter-residue linkage patterns and their resulting secondary structures. Each type of bonding pattern gives rise to a characteristic ordered structure with associated characteristic physical properties. In Fig. 2.1a the residues are linked together through equatorial bonds diagonally opposite each other across the sugar ring, so that the bonds to and from each residue are almost parallel. This linkage pattern gives a flat, ribbon-like

secondary structure and the polymer chains tend to packed tightly together into ordered assemblies such as cellulose microfibrils. When the bonds to and from each residue are not parallel as shown in Fig. 2.1b, a systematic twist in chain direction is introduced. This type of linkage often gives a helical ordered structure which is usually stabilised by packing together co-axially. One of the examples of this type of structure is amylose which is composed of (1→4)-α-D-glucopyranose repeating units. In Fig. 2.1c, although the bonds to and from each residue are still parallel and opposite to each other, they are in the axial position rather than equatorial one. This again results in an ordered ribbon-like, but highly buckled structure, so that the chains usually pack together giving cavities which can accommodate site-bound counterions when the chains are charged.

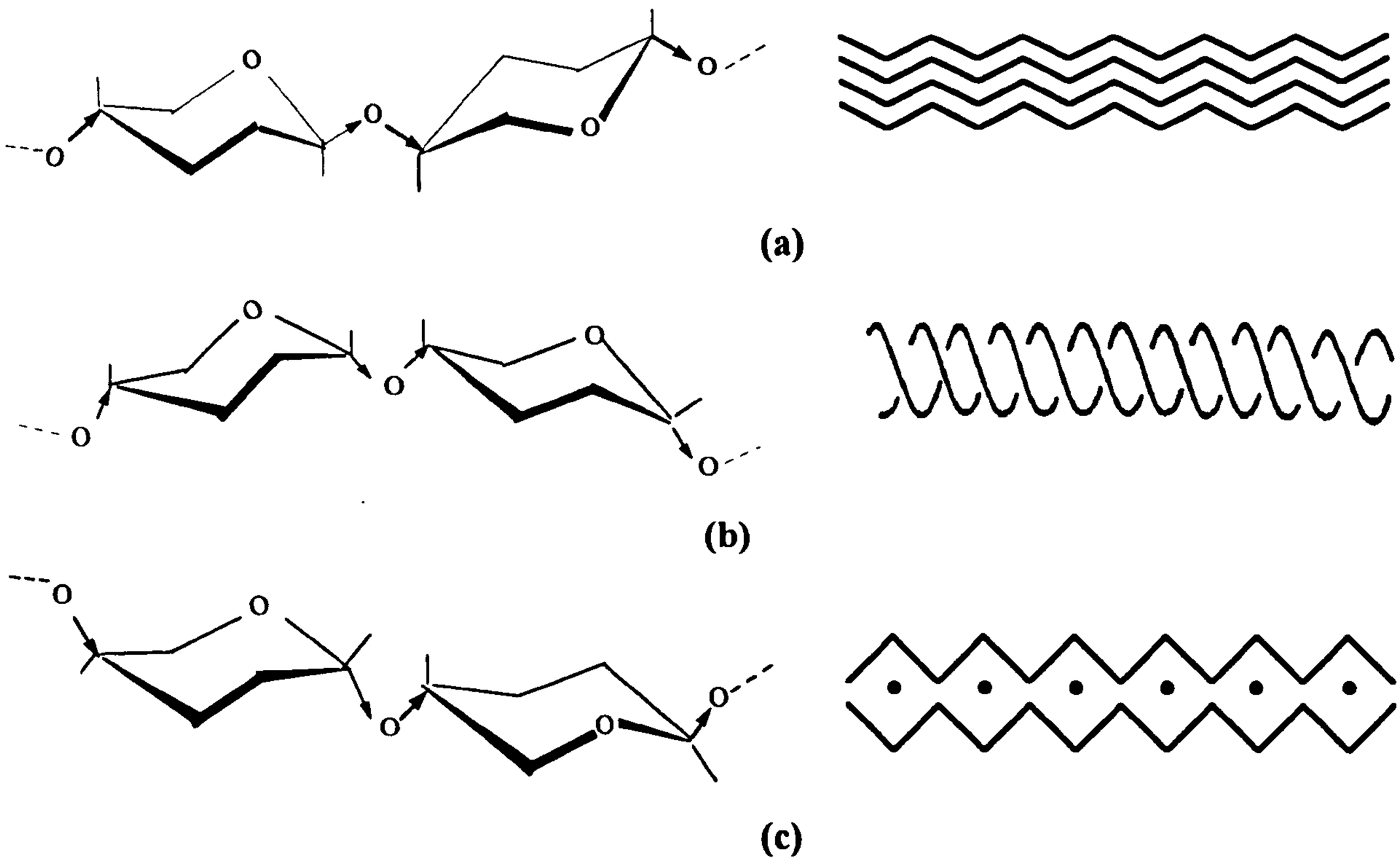

Fig. 2.1 Inter-residue linkage patterns of polysaccharide chains and their resulting secondary structures. (a) flat ribbons, (b) hollow helices, and (c) buckled ribbons. Bolded arrows denote the linkage bonds to and from each residue are parallel (a and c) or not parallel (b) (Morris, 1990b).

In contrast to the highly ordered structures of polysaccharides which are often mechanically strong and almost totally insoluble in water as, for example, in the case for

cellulose, the disordered chains of polysaccharides can exist in solution as fluctuating coils, giving entanglement networks above the critical concentration C* (Fig. 2.2a). The rheological properties of this entanglement system will be discussed further in the next section. In between the above two extreme cases, polysaccharides can also contain both ordered and disordered regions within the same polymer chains. In this case, a three dimensional, cross-linked gel system may be formed under certain conditions by the co-existence of the disordered soluble regions (solubilizing sequences) and ordered insoluble regions (junction zones) as shown in Fig. 2.2b.

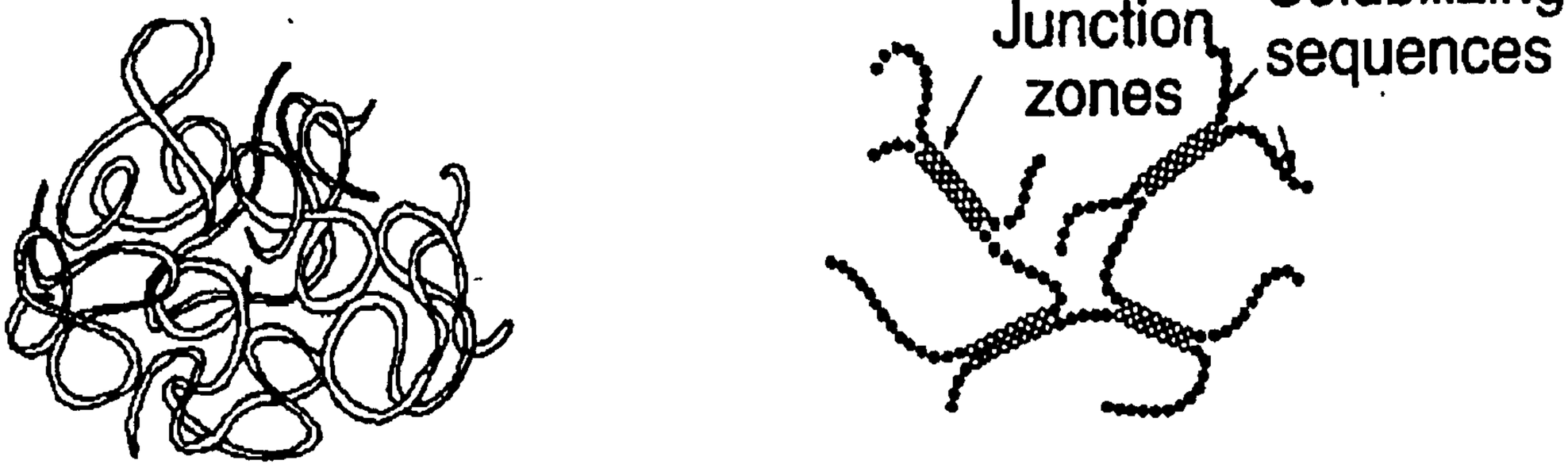

(a) **(b)**

Fig. 2.2 Schematic representation of the polysaccharide system in solutions giving (a) entangled disordered coils and (b) gel systems (Morris, 1990b).

The relationship between the chemical structure of polysaccharide and its physical properties has begun to receive notably attention since the past few decades. The diversity in structure of polysaccharides causes a wide variety of physical and functional properties. The usefulness of these functional properties has resulted in an enormous application of polysaccharides in industry. For example, the water-soluble polysaccharides have been widely used in industry because of their capacity to modify the properties of aqueous phases, that is their capacity to thicken, emulsify, stabilise, encapsulate, or to form gels and films etc. Only recently, the nutritional significance of the polysaccharides other than starch in our diet has become apparent and this aspect will be discussed in more detail later in this chapter. The following sections we will

briefly review the most commonly used polysaccharides in research and industry, particularly in food and pharmaceutical industries, according to the sources of the polysaccharides, namely, plant, marine and microbial polysaccharides.

2.1.2 Plant polysaccharides

2.1.2.1 α-glucans (Starch)

Starch is a major reserve polysaccharide of plants and probably the second most abundant carbohydrate in nature next to cellulose. Therefore, the structures, properties and utilisation of this polysaccharide have been the subject of many investigations since the beginning of modern chemistry and biochemistry. Starch usually appears in the form of granules within the protoplasm of many plant cells. It is a mixture of two structurally different polysaccharides: the linear type molecules are defined as amylose, and the remainder, the largely branched molecules, as amylopectin. Both amylose and amylopectin are composed of D-glucopyranose units as shown in Fig. 2.3. In amylose, more than 300 units at least are uniformly linked by (1→4)-α-glucosidic bonds, which tend to induce a spiralling of the molecule in a helix-like fashion. In amylopectin, the majority of the units are also connected (1→4) with α links, but there are (1→6)-α-glucosidic bonds at the branch points.

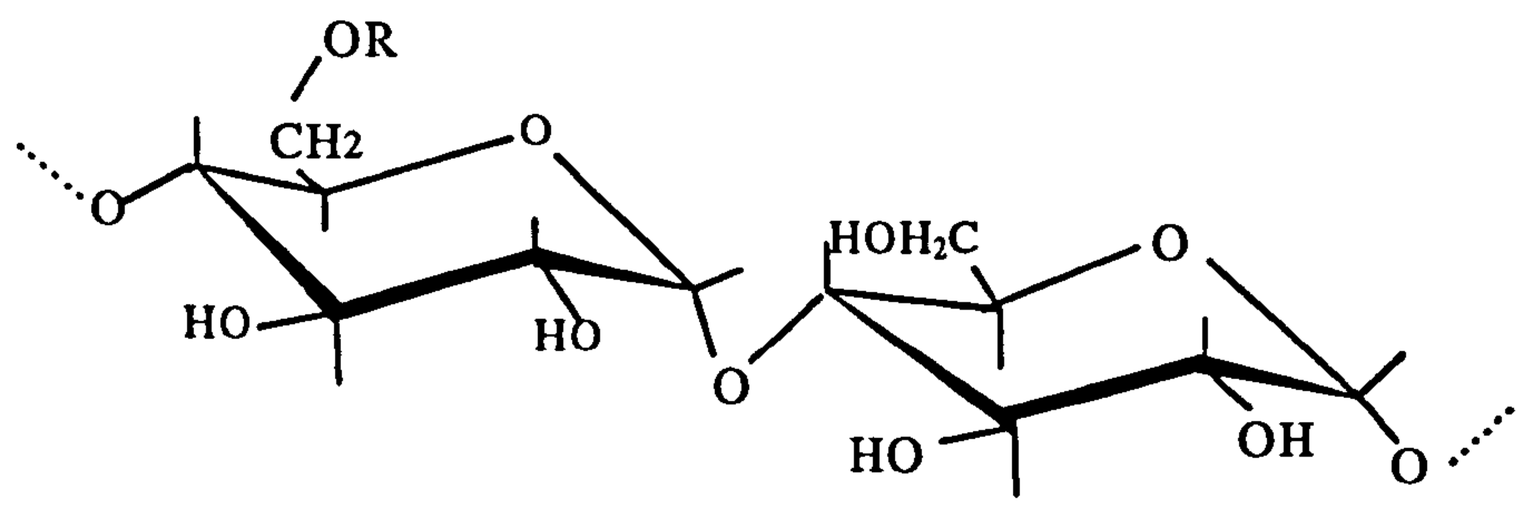

Fig. 2.3 Representative of the chemical structure of starch, where R = H in amylose and R = (1→6)-α-D-glucopyranose in amylopectin.

The majority of starches of different sources have nearly identical ratios of amylose to amylopectin. The most prevalent composition found in corn, wheat, potato starches, etc., is 20 - 28% amylose and 72 - 80% amylopectin (Whistler and Corbett, 1957). The relative amounts of amylose and amylopectin are significant in relationship to the application of a starch. The manifold functions of starch and its derivatives, such as their ethers, esters and depolymerized starch, enable these materials to be used in a wide range of food and many other industries. It can yield viscous dispersions, solutions, or gels depending on concentration and temperature conditions. Therefore, it can work as a thickener, a gelling agent, an absorber of water, a source of energy in fermentation and a bulking agent. The physico-chemical and functional properties of starch have been reviewed comprehensively by Eliasson and Gudmundsson (1996).

Although starch is readily digested in the human small intestine and thereby utilised as a source of carbohydrate, not all the starch in food is necessarily available to human digestion. For example, the starches in raw potatoes and unripe bananas are in a crystalline form that is highly resistant to intestinal hydrolysis. The so-called "resistant starch" which is usually formed when starchy material is heated in the absence of abundant water, cannot be digested by endogenous digestive enzymes of human. These fractions of starch can therefore be classified as an insoluble fibre component.

2.1.2.2 β-Glucans

2.1.2.2.1 Cellulose

Cellulose, the most abundant organic chemical on earth, is an essential component of most plant cell walls. It is a high molecular weight linear polymer consisting of (1→4)-β-D-glucopyranose with at least 3000 units (Fig. 2.4). The solid state conformations of cellulose are extended flat-ribbon arrangement maintained by intramolecular hydrogen bonding. The essentially linear structure of cellulose molecules results in a compact and tightly-bonded aggregate by the intermolecular association and hydrogen bonding of parallel molecules. Therefore, cellulose is virtually insoluble in aqueous solutions and resistant to all but the most vigorous chemical treatments. For instance, it can be made

soluble in 72% (w/w) sulphuric acid because sulphonation takes place at the C6 hydroxyl group, thereby breaking the hydrogen bonds and intermolecular association.

Cellulose and its modified forms, such as hydroxyethyl- and hydroxypropylmethyl-cellulose, carboxymethylcellulose and methylcellulose, are used in a large number of industrial applications. These modified celluloses have many different functional properties compared to native cellulose. Many of them are soluble in water or alcohol-water mixtures giving viscous dispersions. They are used in cosmetics and health care products because of good compatibility with surfactants and salts. Other applications of these polymers include membrane manufacturing (Uragami and Shinomiya, 1992), textile aids, adhesives, coatings, detergents, and building materials (Lapasin and Pricl, 1995).

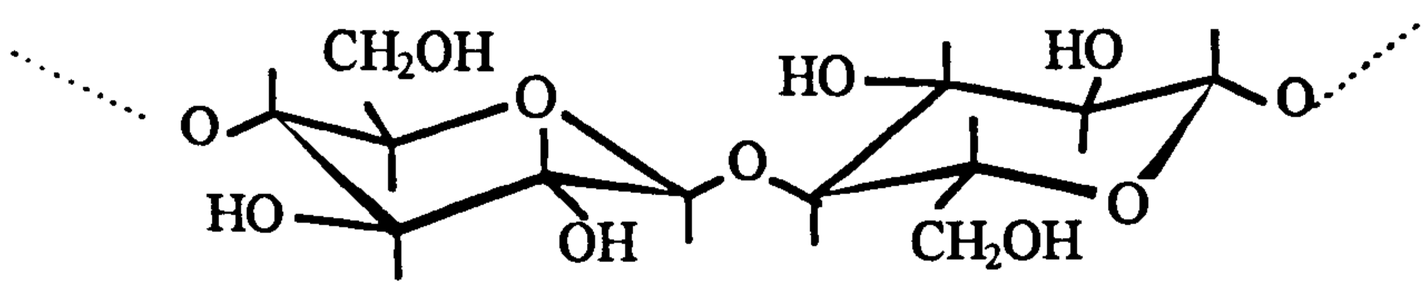

Fig. 2.4 Chemical structure of cellulose.

2.1.2.2.2 Oat gum

Oat gum isolated from starchy endosperm cell wall of oats (*Avena Sativa* L.) is mostly β-glucan consisting mainly of β-(1→4)-linked, 3-O-β-cellobiosyl- and 3-O-β-cellotriosyl-D-glucopyranose as shown in Fig. 2.5 (Wood, *et al.*, 1978). The aqueous solution of oat gum is highly viscous and it is a typical non-gelling polysaccharides. Wood *et al.* (1978) found that oat gum extracted from dehulled oats with alkaline solution has a greater viscosity than most commercial products of oat gum and barley gum. Barley gum is also rich in β-glucan but consisted mainly of cellotriosyl and cellotetraosyl units joined together by single (1→3)-β-linkages (Bathgate, *et al.*, 1974). Oat gum has received much attention recently because of its cholesterol-lowering effects and other beneficial effects to human health (Wood, *et al.*, 1992; Braaten, *et al.*, 1993).

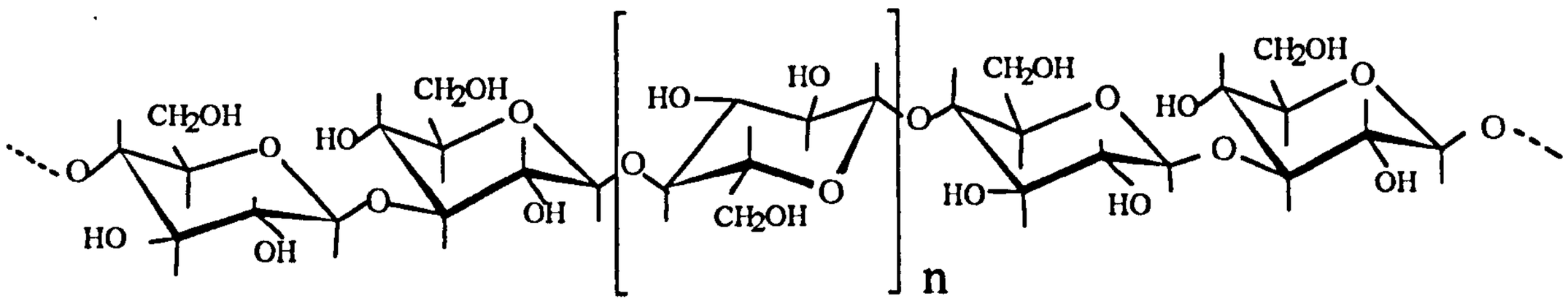

Fig. 2.5 Repeating units of oat β-glucan, n = 1 or 2.

2.1.2.3 Substituted β-mannans

This is a group of cell wall storage polysaccharides which are all based on a linear (1→4)-β-D-mannopyranan backbone. They may be subdivided into two major groups: glucomannans in which some of the D-mannopyranose residues in the backbone are replaced by D-glucopyranose, and galactomannans in which the backbone carries (1→6)-α-D-galactopyrannosyl substituents.

2.1.2.3.1 Galactomannans

Galactomannans are one of the best characterised of all the storage carbohydrates which reflects their industrial importance. Structurally, seed galactomannans consist of a (1→4)-β-D-mannopyranose backbone with heavy substitution of single (1→6)-α-D-galactopyranosyl side chains (Fig. 2.6). The ratio of galactose to mannose varies with origins. The two mostly commonly used galactomannans are guar and locust bean gum.

Guar gum

Guar gum is produced from the seed endosperm of the leguminous plant *Cyamopsis tetragonoloba* (L.), a native plant of India. The native guar gum is of high molecular weight (Barth and Smith, *et al.*, 1981; Herald, 1986; Reid, *et al.*, 1987) and the molecular weight of extracted polymer has been estimated to range from $0.5x10^6$ to $1.1x10^7$. The ratio of galactose to mannose is typically 1:2. Guar gum products with a wide range of average molecular weight are also commercially available.

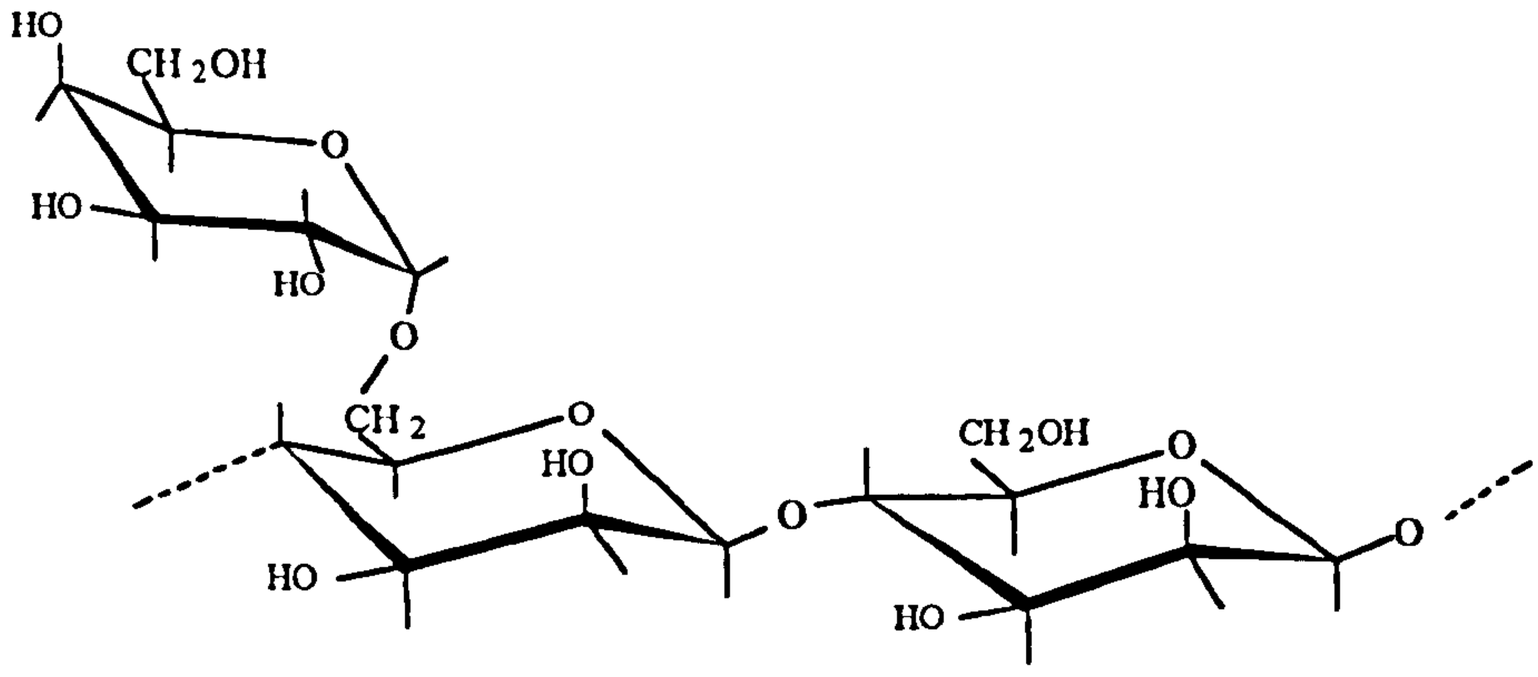

Fig. 2.6 Chemical structure of a typical galactomannan.

Guar gum hydrates in both cold and hot water to give high viscosity solutions. The hydration rate and final viscosity depend on factors such as particle size, pH, and temperature etc. Guar gum solutions are reported to be stable over the approximate pH range 4.0 - 10.5, and highest hydration rate is reported to be at pH 8.0 (Sandford and Baird, 1983). Hydration rates are reduced in the presence of dissolved salts and other water-binding agents such as sucrose.

Guar gum is compatible with most other hydrocolloids. Like other non-ionic polymers, guar gum and its derivatives also exhibit viscosity synergism in solution when combined with anionic surfactants and especially anionic polymers. For example, there is a useful synergistic increase in viscosity given by blends of guar gum with xanthan gum and κ-carrageenan. Viscosity of these mixtures can be many times greater than that of either component alone.

The high thickening efficiency and good compatibility combined with wide availability have resulted in guar gum being the most extensively used gum in food and pharmaceutical industries. Apart from this, guar gum and its derived polymers are leading processing aids in mining and mineral industry for the recovery and separation of some metals from ores. Its derivatives, such as, hydroxypropyl- and carboxymethyl-hydroxypropyl-guar gum, cross-linked with Al^{3+} and Ti^{4+}, have been commonly used in the oil recovery operations. Furthermore, an aqueous solution of guar gum is generally

the oil recovery operations. Furthermore, an aqueous solution of guar gum is generally recognised to be a model entanglement network system (Robinson, *et al.*, 1982; Richardson and Ross-Murphy, 1987a) in polymer studies.

Locust bean gum

Locust bean gum (LBG) is another type of galactomannan obtained from the ground endosperm of *Ceretonia siliqua* (L.), a leguminous tree grown in the Mediterranean countries. The ratio of galactose to mannose of LBG is about 1:4~5. This lower degree of branching is believed to account for the differences in properties between LBG and guar gum. One estimation of the average molecular weight of LBG is $3x10^5$ (Gaisford, *et al.*, 1986).

Locust bean gum is only slightly soluble in cold water and must be heated to 80°C and re-cooled to obtain the maximum viscosity of a highly-viscous pseudoplastic solution. However, cold-water-soluble LBG can be prepared, for example, by heating LBG in the presence of small amounts of guar gum or simple sugars, which prevent reassociation of LBG's crystalline D-galactosyl-free regions on cooling. Locust bean gum has a more pronounced synergistic interaction with other polysaccharides compared to guar gum. For example, neither xanthan gum nor locust bean gum will form significant gels by their own. However, mixtures of these two gums at a total concentration of above 0.5% can form thermally reversible gels with unique textural properties.

2.1.2.3.2 Glucomannan

Konjac mannan is a typical glucomannan type polysaccharide which is isolated from the tubers of *Amorphophallus konjac*. Native konjac mannan is a partially acetylated linear polysaccharide containing mainly (1→4)-β-D-mannopyranose and (1→4)-β-D-gluco-pyranose in a molar ratio of approximately 1.6:1 (Kato, *et al.*, 1970; Maeda, *et al.*, 1980). A small amount of (1→3) branching has also been reported (Maeda, *et al.*, 1980). Enzymatic hydrolysis analysis (Kato, *et al.*, 1970; Shimahara, *et al.*, 1975) suggests that this polysaccharide does not contain a regular repeating sequence or substantial lengths of either mannan or glucan blocks. The molecular weight of konjac

mannan samples have been estimated to range from $4.7x10^5$ to $6.8x10^5$ (Nishinari and Williams, 1992; Kohyama, *et al.,* 1993).

Konjac mannan has been used as an ingredient in food recipes in China, Japan, Pakistan and India for centuries. It is water soluble and produces highly viscous, pseudoplastic solutions. A characteristic property of konjac mannan is its strong ability for gel formation in alkaline media, although it does not form gels at neutral pH. Konjac mannan was reported to have a more pronounced synergistic interaction with κ-carrageenan and xanthan gum than galactomannans (Dea and Morrison, 1975; Dalbe, 1991; Williams, *et al.,* 1991) to produce strong and elastic gels.

2.1.2.4 Xyloglucans

A large number of species of plant seeds have been reported to contain xyloglucans as reserve materials other than starch. These xyloglucans are stored in the cell wall of endosperm or storage cotyledons and are known as cell wall storage polysaccharides. Xyloglucans are often termed 'amyloids' because of the characteristic blue stain that is produced with iodine/potassium iodide solution (Kooiman, 1960).

One of the well-characterised xyloglucans comes from tamarind seed gum, which is obtained from the seeds of the *Tamarindus indica*, an evergreen tree of south-east Asia. The major polysaccharide in tamarind seed gum is a galactoxyloglucan composed of a cellulosic type backbone (i.e. (1→4)-β-D-glucan) with side chains of α-D-xylopyranose (1→6)- and β-D-galactopyranosyl-(1→2)-α-D-xylopyranose-(1→6)- linked to the main chain (as shown in Fig. 2.7). The ratio of galactose:xylose:glucose may vary slightly depending on the origin of the seed but is generally close to 3:2:1 (Meier and Reid, 1982; Glicksman, 1986). A small proportion of arabinose residues has been reported in acid hydrolysates of preparations of tamarind seed polysaccharide. It has been suggested that this is due to a minor polysaccharide containing branched (1→5)-α-L-arabinofuranan and unbranched (1→4)-β-D-galactopyranan (Gidley, *et al.*, 1991).

Tamarind xyloglucan is soluble in water. Recent studies have shown that tamarind seed xyloglucan exhibits a strong tendency to aggregate in aqueous solution (Gidley, *et al.*, 1991; Lang and Burchard, 1993). This was described as bundle-shaped lateral aggregation of single polymer strands. This behaviour results in a marked increase in polymer stiffness which in turn means that the solution of the tamarind gum is highly viscous.

A crude preparation of tamarind powder is used in textile sizing and weaving, and as an adhesive or binding agent in other industries (Gerard, 1980). The isolated polysaccharides are used as thickening, stabilising and gelling agent in foods, particularly in Japan where they are permitted food additives.

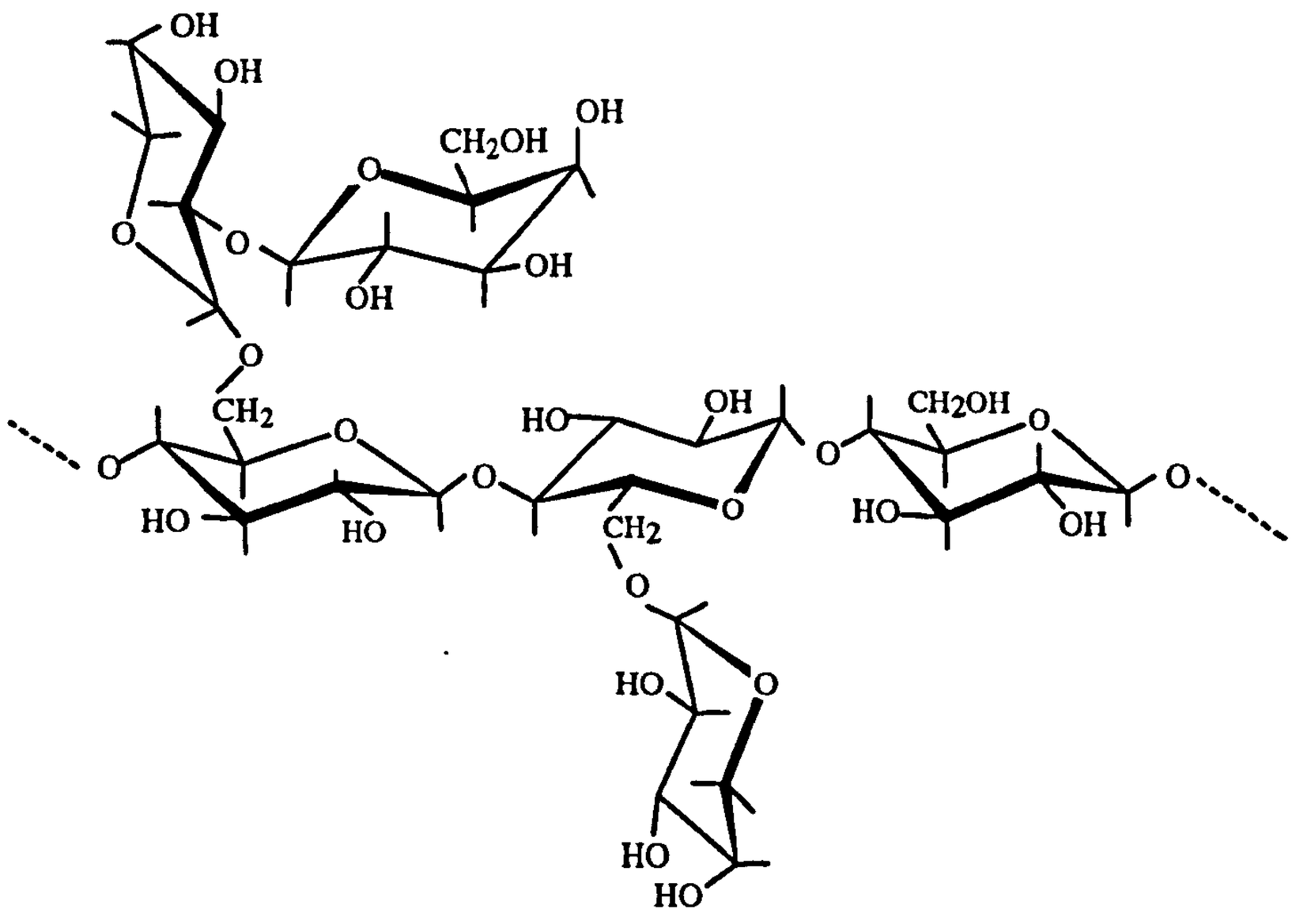

Fig. 2.7 Representative structure of a xyloglucan (such as tamarind gum).

2.1.3 Marine polysaccharides

2.1.3.1 Carrageenans

Carrageenan is a general name for a family of sulphated linear polysaccharides which are extracted as matrix components of the red seaweed, *Rhodophyceae*. Among all the

various types of carrageenans, three are most commercially important, namely, τ-, κ- and λ- carrageenans. Their representative structures are shown in Fig. 2.8. The τ- and κ-carrageenan polymers consists of alternating (1→3)-β-D-galactopyranose-4-sulphate and (1→4)-3,6-anhydro-α-D-galactose-2-sulphate (τ-carageenan) or (1→4)-3,6-anhydro-α-D-galactose (κ-carageenan) monomers. λ-carrageenan is mainly composed of (1→3)-β-D-galactose-2-sulphate and (1→4)-α-D-galactose-2,6-disulphate and contains few anhydride residues.

The most prominent feature of the carrageenans is their diversity in chemical structure and physical properties. Non-gelling and gelling samples may be obtained depending on the algal source and the method of preparation. Among the different types of carrageenans, κ- and τ-carrageenans are highly valued due to their ability to form thermo-reversible gels in the presence of specific cations (Morris, *et al.*, 1980; Hermansson, *et al.*, 1991). These two materials have found applications in structuring and stabilising of aqueous phases in numerous food products, e.g. chilled, frozen and for fat replacement.

(a)

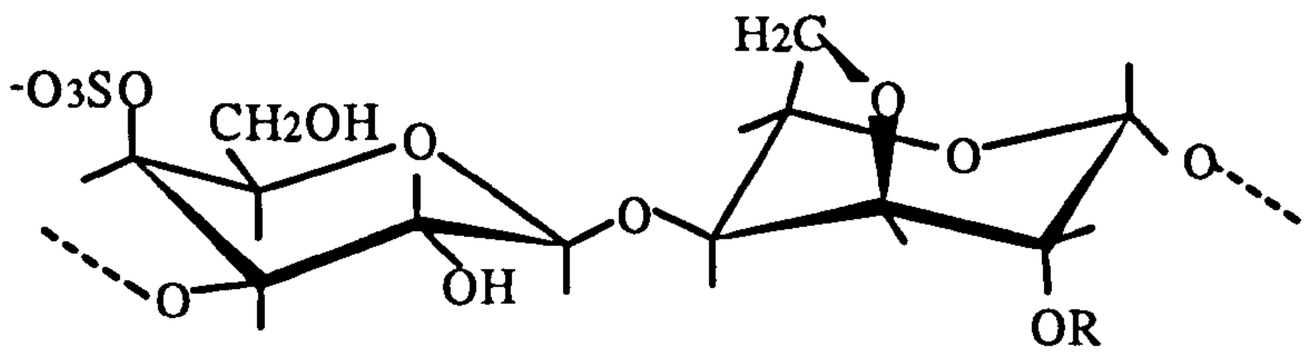

(b)

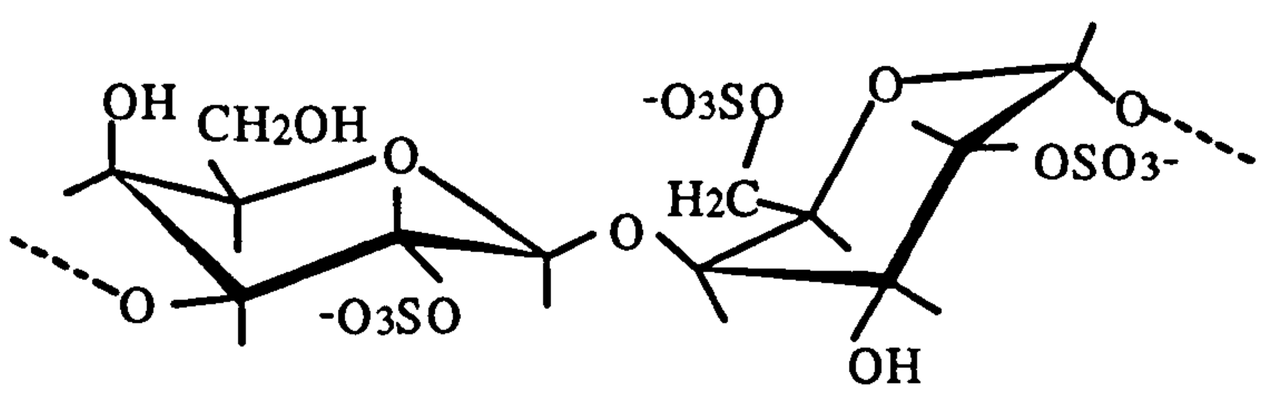

Fig. 2.8 Chemical structure of three carrageenans, where (a) R = H in κ-carrageenan and R = SO_3^- in τ-carrageenan; (b) λ-carrageenan.

2.1.3.2 Agar

Agar is the collective term for a complex mixture of polysaccharide components extracted from certain species of red seaweed. The major fraction that is of commercially importance is a neutral polysaccharide called agarose, which usually accounts for 50-90% of the total agar. Agarose is a linear polymer composed of a disaccharide repeating unit of the AB type, which is, alternating (1→3)-β-D-galactopyranose (A) and (1→4)-3,6-anhydro-α-L-galactopyranose (B) as in Fig. 2.9. Variable amounts of 6-O-methyl-D-galactopyranose (1-20%) may also be present in agarose depending on the sources.

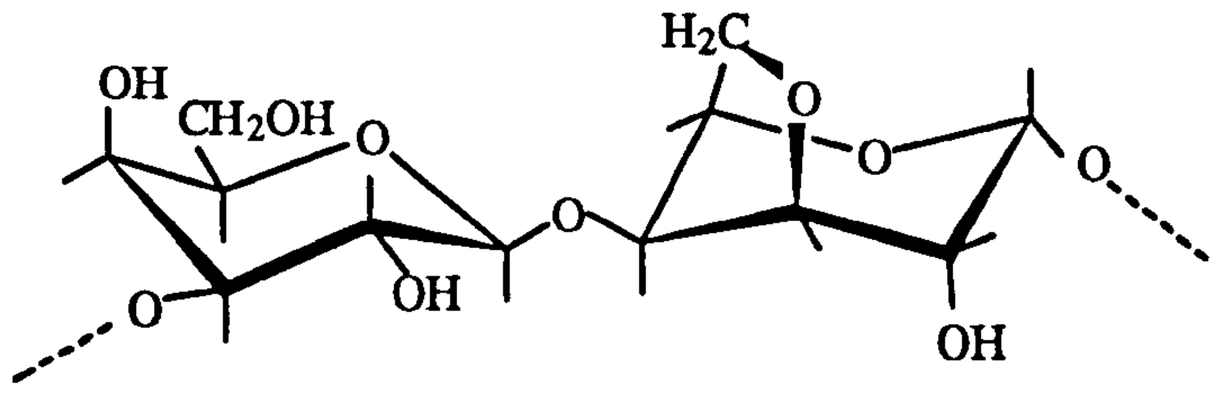

Fig. 2.9 Chemical structure of agarose.

Unlike alginate, agarose can form thermo-reversible gels without metal ions. The gelation is believed to be induced by double helix formation and subsequent association of the helices. Agar is unique among polysaccharides in that gelation occurs at low temperature (30 - 40 °C), which is also far below the gel melting point (70 - 90 °C). This property has a variety of applications in the food industry.

2.1.4 Microbial polysaccharides

2.1.4.1 Xanthan

Xanthan, the extracellular polysaccharide from *Xanthomonas campestris* pv. *campestris* is one of the major commercial biopolymers produced from bacteria. The structure of xanthan is a pentasaccharide repeat unit, which is of particular interest as it consists of trisaccharide side-chains attached to a cellulosic backbone (Fig. 2.10). At C3, alternate

glucopyranose residues in the backbone carry the side-chains composed of 6-O-Ac-(1→3)-α-D-mannopyranose, (1→2)-β-D-glucuronic acid and 4,6-O-(1'-carboxyethylidene)-(1→4)-β-D-mannopyranose. The level of substitutions by acetic and pyruvic acid on the side chain is different depending on the source.

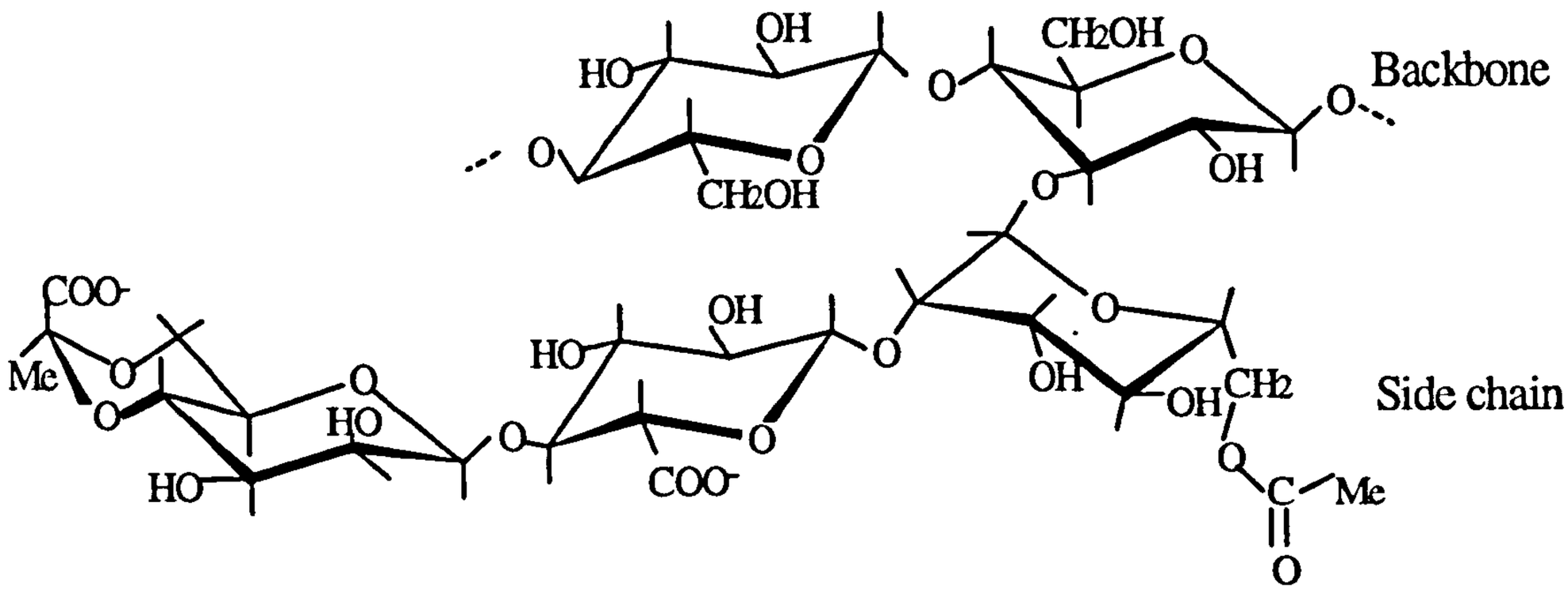

Fig. 2.10 Representative structure of xanthan.

Aqueous solutions of xanthan are highly pseudoplastic and the dispersions of the polymer have been considered to behave as weak gel-like networks of highly associated molecules (Richardson and Ross-Murphy, 1987b). It shows very good suspending properties and rapidly regains viscosity on removal of shear stress. Xanthan gum forms thermo-reversible gels when mixed with certain plant galactomannans and glucomannans (Dea and Morris, 1977).

The relatively rigid helical conformation of xanthan renders it stable over a wide range of pH, ionic strength and temperatures. It is also compatible with many salts and other food ingredients. At present, xanthan is the only bacterial polysaccharide approved and widely used by the food industry in the world.

2.1.4.2 Curdlan

Curdlan is a neutral, (1→3)-β-D-glucan (Fig. 2.11) of relatively low molecular weight, produced from bacteria *Agrobacterium* and *Rhizobium*. It is insoluble in cold water but can be dissolved in hot water. Curdlan forms a thermally reversible weak gel when

heated up to 54-80 °C. Further heating to above 80 °C increase the gel strength and produces a firm, irreversible gel. Curdlan is a permitted food additive in Japan for use in improving the texture of various foods such as bean curd and fish pastes.

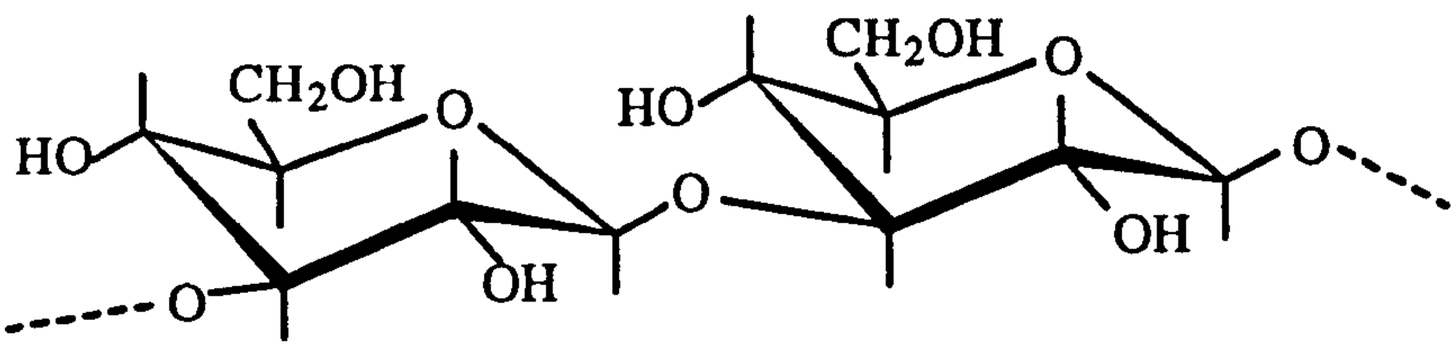

Fig. 2.11 Chemical structure of curdlan.

2.1.4.3 Gellan

Gellan gum is the trivial name given to the extracellular polysaccharide produced by a type of micro-organism called *Sphingomonas paucimibilis* (Pollock, 1993). It is a linear, anionic heteropolysaccharide consisting of tetrasaccharide repeat units, containing (1→4)- or (1→3)-β-D-glucopyranose, (1→4)-β-D-glucuronic acid and (1→4)-α-L-rhamno-pyranose in a molar ratio of 2:1:1 (Fig. 2.12). The polysaccharide is partially substituted at the (1→3)-linked D-glucose residue at C2 with L-glycerate and at C6 with acetate.

Native gellan gum forms weak, elastic thermo-reversible gels when hot gellan solutions cool in the presence of divalent cations such as Ca^{2+}. The cations associate with the carboxyl groups of the glucuronic acid residues cross-linking double helical sections together to form the junction zones of the gel. A range of gel textures can be produced through control of the degree of acylation of the polymer.

Gellan has been approved in the US and Japan for food use as a stabilizer and thickener. It is likely to become the second bacterial polysaccharide to be used widely by the food industry. It is also used as a culture medium in biotechnology because it forms a transparent gel which is resistant to heat and acid in the presence of Ca^{2+}.

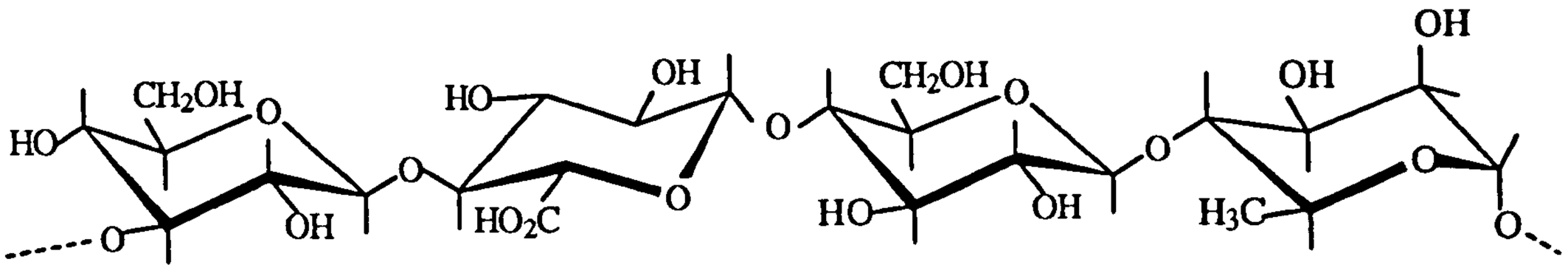

Fig. 2. 12 Basic repeat unit structure of gellan.

2.2 Rheology of water soluble polysaccharide systems

2.2.1 Background

The rheological behaviour of polysaccharides in solvents can be significantly affected by several factors. On the molecular scale, the polymer backbone and its related features, such as its length (molecular size), shape, stiffness and the presence of ionizable groups, play a major role in determining the macroscopic properties of the system including its rheology. In general, the functional properties of polysaccharides are less directly governed by their primary sequence structure rather than their second or tertiary structures. With the help of the advanced theories and techniques it has been possible to relate the experimental data to the molecular structure of the biological macromolecules including polysaccharides.

Many polysaccharides can exhibit specific rheological properties in solvent depending upon their structure, type of solvent present and sometimes the polymer concentration. They can form highly viscous solutions, gels or weak gels, and may have synergistic effects with other polymers. The current thesis deals with only neutral non-starch polysaccharides which have potential uses in clinical nutrition. Most of these polysaccharides form entanglement systems in water solutions. Therefore, in the following sections the rheology of polysaccharide entanglement systems will be discussed.

2.2.2 Intrinsic viscosity and molecular weight

Intrinsic viscosity [η] is the measure of the hydrodynamic volume that an isolated polymer molecule occupied in a given solvent. It is defined by, $[\eta]=(\eta_{sp}/c)_{c\rightarrow 0}$, in which $\eta_{sp} = \eta_r - 1$ is specific viscosity, and η_r is the relative viscosity η/η_s, which is the viscosity increase due to the contribution of the polymer over the solvent. [η] is a characteristic property of an isolated polymer molecule in a given solvent, and it depends primarily on molecular weight, chain rigidity and solvent quality. A number of models have been established to describe the relationship between intrinsic viscosity, molecular weight and molecular structural parameters. Following is a brief description of these models.

2.2.2.1 Equivalent sphere model

In this model the polymer coil and the solvent bound to it are treated as an equivalent sphere. Intrinsic viscosity, radius of gyration S, which is the distance of the elements of a molecular chain from its centre of gravity, and molecular weight M are related through the Fox-Flory equation (Flory, 1953) written as:

$$[\eta] = \phi 6^{3/2} S^3 / M \qquad (2.1)$$

where ϕ is the Flory viscosity function. For a flexible polymer $\phi=2.6\times10^{26}$ kg $^{-1}$. Since most of natural polysaccharides are polydisperse in molecular size, the z-average radius of gyration R_g and the weight average molecular weight are usually used in equation 2.1 (Ross-Murphy, 1994).

2.2.2.2 Random flight model for flexible chain molecules

In this model the polymer molecule is described by an equivalent random flight chain composed of N rods of length I. When the chain is sufficiently long the mean-square end-to-end distance $\langle R^2\rangle_0$ can be represented as:

$$<R^2>_0 = NI^2 \qquad (2.2)$$

where I is the length of the statistical Kuhn segment. For linear chains, when the end-to-end distance follows a Gaussian distribution, $<R^2>_0$ and the radius of gyration (S) are related by:

$$<R^2>_0 = 6\ <S^2>_0 \qquad (2.2.a)$$

For a given polymer only differing in average molecular weight, equation 2.2 implies that $<R^2>_0$ is proportional to the average molecular weight. If $<R'^2>_0 = N'l'^2$ represents the relationship when there is no restriction on bond rotation and all bond angles between rods are allowed, the characteristic ratio of $<R^2>_0/<R'^2>_0$ reflects the intrinsic chain flexibility of the polymer.

In practise, polysaccharides in water tend to expand due to the excluded volume effects. This is because of the fact that two segments cannot occupy the same volume and an effective small intrachain repulsive force is thus produced. Therefore, $<R^2>_0$ is no longer proportional to molecular weight and $<R^2>_0/M$ or $<S^2>_0/M$ actually increases with molecular weight.

2.2.2.3 Mark and Houwink equation

The power-law relationship between intrinsic viscosity and molecular weight was first suggested by Staudinger and corrected independently by Mark and Houwink, and Sakurada. However it is generally known as the Mark-Houwink equation and expressed as:

$$[\eta] = k\ M_v^{\alpha} \qquad (2.3)$$

where M_v is the (viscosity) average molecular weight and the parameter k is related to local flexibility of the polymer. The exponent α is related to the long distance structure

(*i.e.* the excluded volume). For most random coil linear polymers, including polysaccharides, the exponent should lie in the range 0.5 - 0.8. However, for highly branched polymers values smaller than 0.5 can be observed, whereas it increases with increasing chain stiffness up to 1.8 for rigid rods (Launay, *et al.*, 1986). Values for α = 0.723 and k = 3.8×10^{-4} dl/g have been reported for guar gum galactomannans (Robinson *et al.*, 1982).

The intrinsic viscosity is conventionally determined from the double extrapolation of Huggins and the Kramer equations :

$$\eta_{sp}/C = [\eta] + K'[\eta]^2 C + o(C^2) \qquad (2.4)$$

$$\ln(\eta_r)/C = [\eta] + (K' - 0.5)[\eta]^2 C + o(C^2) \qquad (2.5)$$

where C is the polysaccharide concentration, and K' is the Huggins coefficient. [η] was estimated as the average of the two ordinate intercepts from the two extrapolations to C=0% (Stokke, *et al.*, 1992). The notation $o(C^2)$ is used to denote second and higher order terms of such power series expansion of η_{sp}/C and $\ln(\eta_r)/C$ around C = 0%. Since the plots are essentially linear such terms are of negligible importance in this case.

2.2.3 Concentration and zero-shear viscosity

For a given polysaccharide system another parameter that is of primary important in controlling its rheological properties is the polymer concentration, more specifically, the space occupancy by the polymer molecules in a solution or dispersion. According to this polysaccharide solutions can be classified as a dilute solution, semi-dilute solution and concentrated solution.

A dilute polymer solution is one in which each flexible polymer coil and the solvent associated with it occupies a hydrodynamic impenetrable domain within the solution. The single macromolecules afford their individual contribution to the rheological properties of the system independent of the imposed shear rate. This means that under a

given flow condition, the differences in rheological behaviour can be ascribed to distinct molecular characteristics.

As the concentration of polymer increases from the dilute state, a stage is soon reached at which the coils begin to touch one another throughout the solution. This corresponding concentration is called the overlap concentration C*, i.e. the total occupancy concentration. The zero-shear viscosity η_0 of a polymer solution increases generally with increasing concentration. This relationship normally can be described by power-law type correlation:

$$\eta_{sp} = aC^b \qquad (2.6)$$

η_{sp} is zero-shear specific viscosity. However, at some concentration above C^* there is a more pronounced increases in both the zero-shear viscosity and the shear rate dependence of viscosity, reflected by two different values of the exponent b. The transition between these two regimes appears to be a continuous regime other than a sharp discontinuous as illustrated in Fig. 2.13. Therefore, another two concentrations have been defined (Ross-Murphy, 1994) (Fig. 2.13). One is the critical concentration C_{cr}, which is the concentration at which the change of slope in zero-shear viscosity is seen to occur, i.e. the breakpoint. Another is C^{**}, which is the starting point of the second slope of the high concentration regime. $C_{cr} = 4/[\eta]$ has been reported for many polysaccharides (Morris, *et al.,* 1981; Robinson, *et al.,* 1982). Conventionally, solutions with $C<C_{cr}$ are known as dilute, whereas $C>C_{cr}$ are called semi-dilute solution to distinguish them from concentrated solutions. For most of the random coil polysaccharides the exponent b lies between 1~1.5 when $C<C^*$, and 3.5~5 at $C>C^{**}$ (Ross-Murphy, 1984)

Precisely, the viscosity generated by disordered polymer coils is dependent on the degree of space-occupancy by the polymer, which is characterised by the dimensionless product of concentration and intrinsic viscosity $C[\eta]$. That is the reason for using $C[\eta]$ instead of concentration itself in Fig. 2.13. It also implies that the higher the $[\eta]$ of a polymer, the lower concentration needed to attain a given viscosity. Morris *et al.* (1981)

found that double-logarithmic plots of zero-shear specific viscosity η_{sp} *vs.* C[η] for a number of different disordered polysaccharides and different molecular weights of the same polysaccharides are virtually identical.

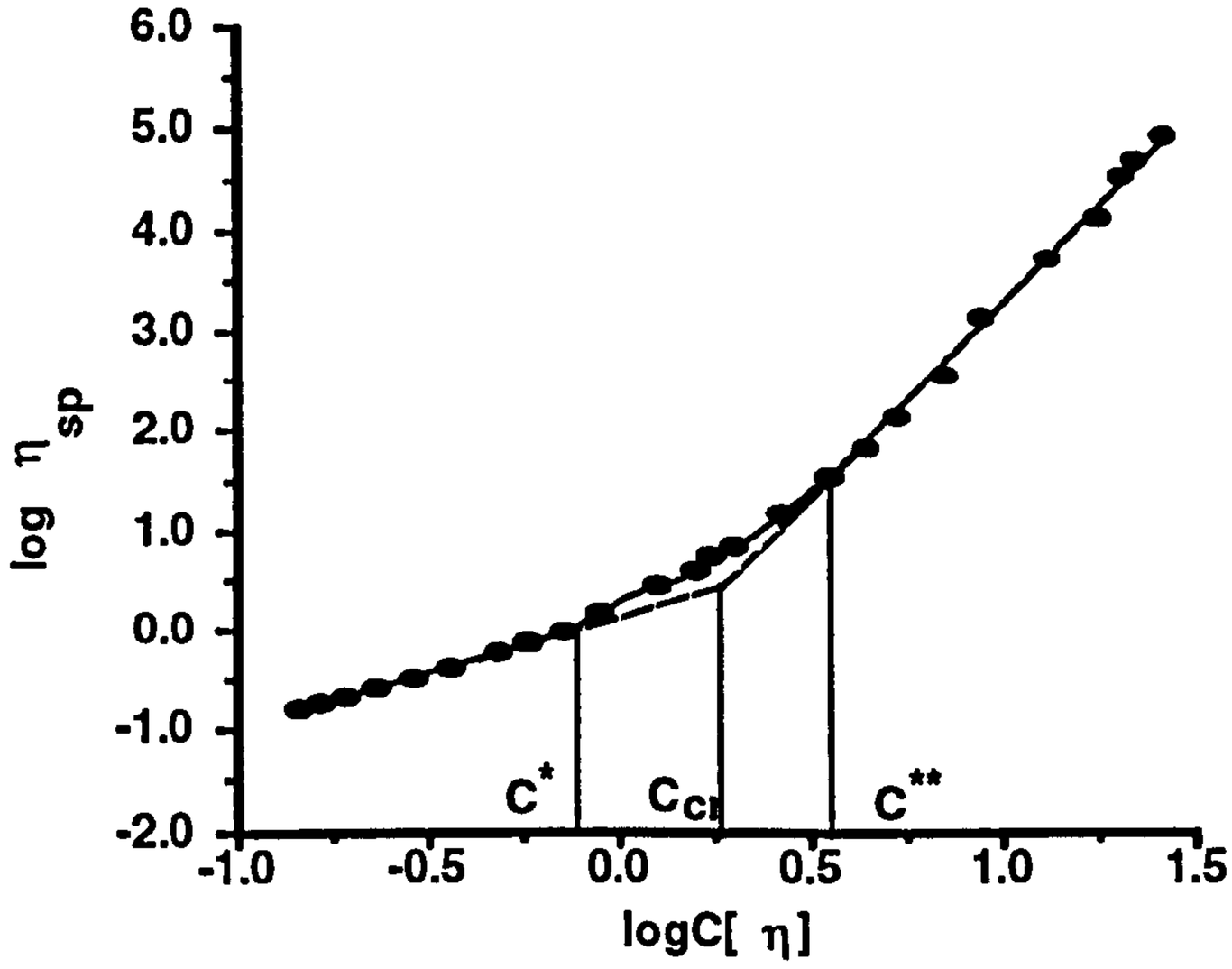

Fig. 2.13 Effect of concentration on the viscosity of polysaccharides.

2.2.4 Shear thinning properties

Many polysaccharide solutions of sufficiently high molecular weight and concentration form entangled network systems. The shear-thinning nature of this system under flow has been well recognised for many polysaccharide solutions. Doi and Edwards (1978) used a "tube" model to describe the molecular motion of concentrated polymeric systems under flow. In this model each single molecule is constrained by the surrounding macromolecules which form a tube-like region. A relaxation time is needed for the disengagement of the polymer chain from the tube by the reptation process. At low shear rates the polymer chains are free to move through the system unperturbed by their neighbouring molecules. No tube effect is present at this stage. The system has a short relaxation time resulting in no net change in the extent of entanglements and therefore no effect on the viscosity of the system. This corresponds to the Newtonian region of the viscosity-shear rate flow curves. However, as the shear rate is increased the polymer chain is forced to associate with their neighbour molecules, i.e. the polymer chain is

confined to a tube-like region. When the disengagement time of the polymer chain is shorter than the relaxation time of the "tube" shear-thinning occurs. In another words, with increasing shear rate the rate of re-entanglement of polymer chain falls behind the rate of forced disentanglement; thus, the viscosity decreases.

Many attempts have been made to describe mathematically the shear-thinning behaviour of polymeric systems (Graessley, 1967; de Gennes, 1971; Ferry, 1980; Povolo, 1992). Amongst all these models the Cross equation has been found to be the best empirical model for describing the flow behaviour of semi-dilute polysaccharide solutions (Launay, 1982; 1986). The Cross equation is written as:

$$\eta = \eta_\infty + (\eta_0 - \eta_\infty)/[1 + (\tau\dot{\gamma})^m] \qquad (2.7)$$

η_0 and η_∞ are limiting viscosity at zero and infinite high shear rate. τ is a relaxation time and m is a non-dimensional exponent. Both τ and m are adjustable parameters. Sharman *et al.* (1978) have claimed that the Cross equation with $\eta_\infty = 0$ and $m = 2/3$ can fit the flow curves of galactomannans from various botanical sources. A further simplification was suggested by Morris (1990a) in the specific case of random coil polysaccharides by supposing $\eta_\infty = 0$, $m = 0.76$, and $\tau = 1/\dot{\gamma}_{1/2}$ ($\dot{\gamma}_{1/2}$ is the shear rate required to reduce η to $\eta_0/2$). It has been found that by expressing measured viscosity η relative to η_0, and applied shear rate relative to $\dot{\gamma}_f$ (the shear rate required to reduce η to $f\eta_0$) the flow curves can be reduced to a single 'master curve' (Morris *et al.,* 1981). Therefore, the two parameters η_0 and $\dot{\gamma}_{1/2}$ characterise completely the differences in viscosity and shear-thinning for different solutions of commercial random coil polysaccharides.

2.2.5 Viscoelastic properties

Polysaccharides are said to be viscoelastic substances, which have both solid and liquid characteristics. Indeed practically, most materials are viscoelastic, depending upon the timescale of the deformation imposed. The viscoelasticity of polymer materials has been

described and analysed by two classic mechanical models, the Maxwell model and Voigt model. The detailed description of these models can be found in a number of polymer text books such as the one written by Hiemenz (1984). Both models use a spring displaying the Hookean elastic response, and a dashpot displaying the Newtonian response. The spring and dashpot are connected in a series in the Maxwell model and parallel in the Voigt model as illustrated in Fig. 2.14.

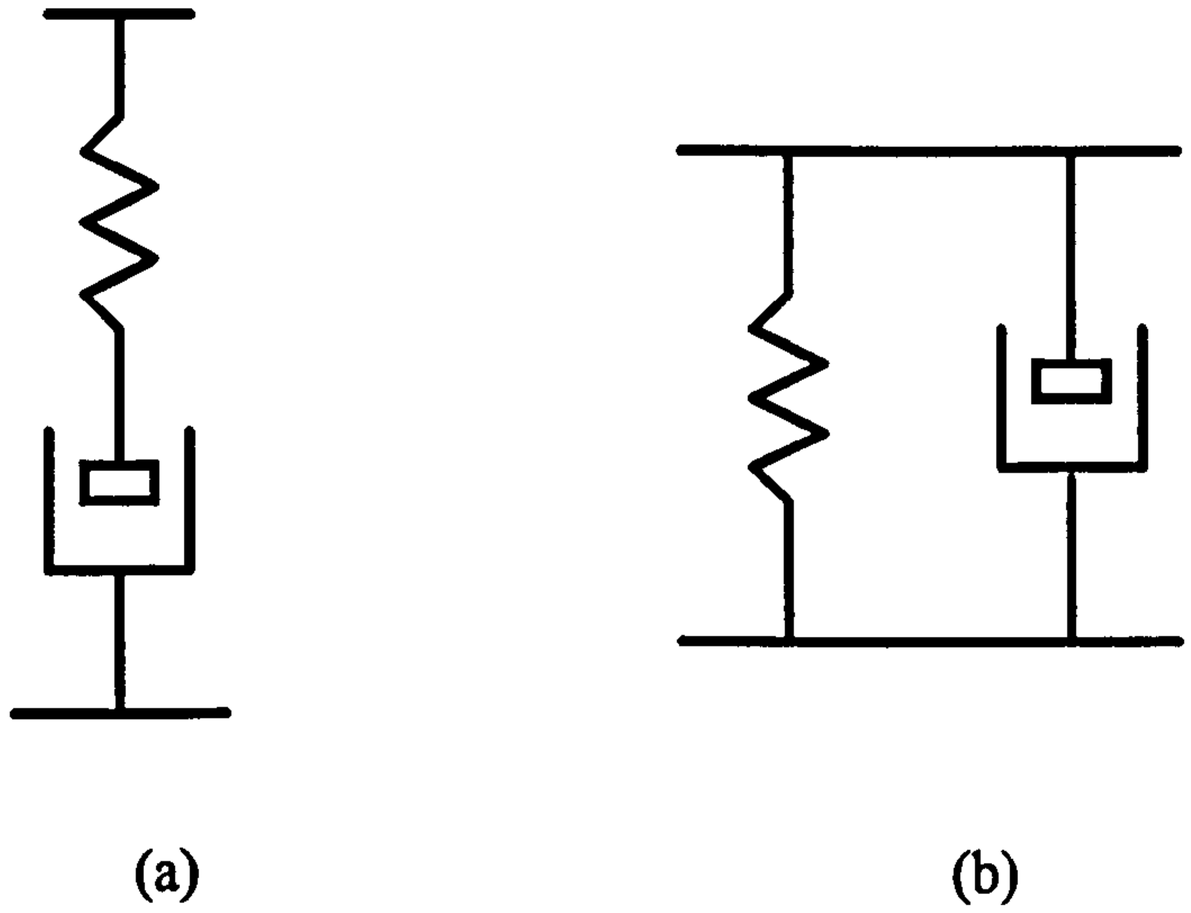

Fig. 2.14 Maxwell model consisting of a spring and dashpot in series (a) and Voigt model consisting a spring and dashpot in parallel (b).

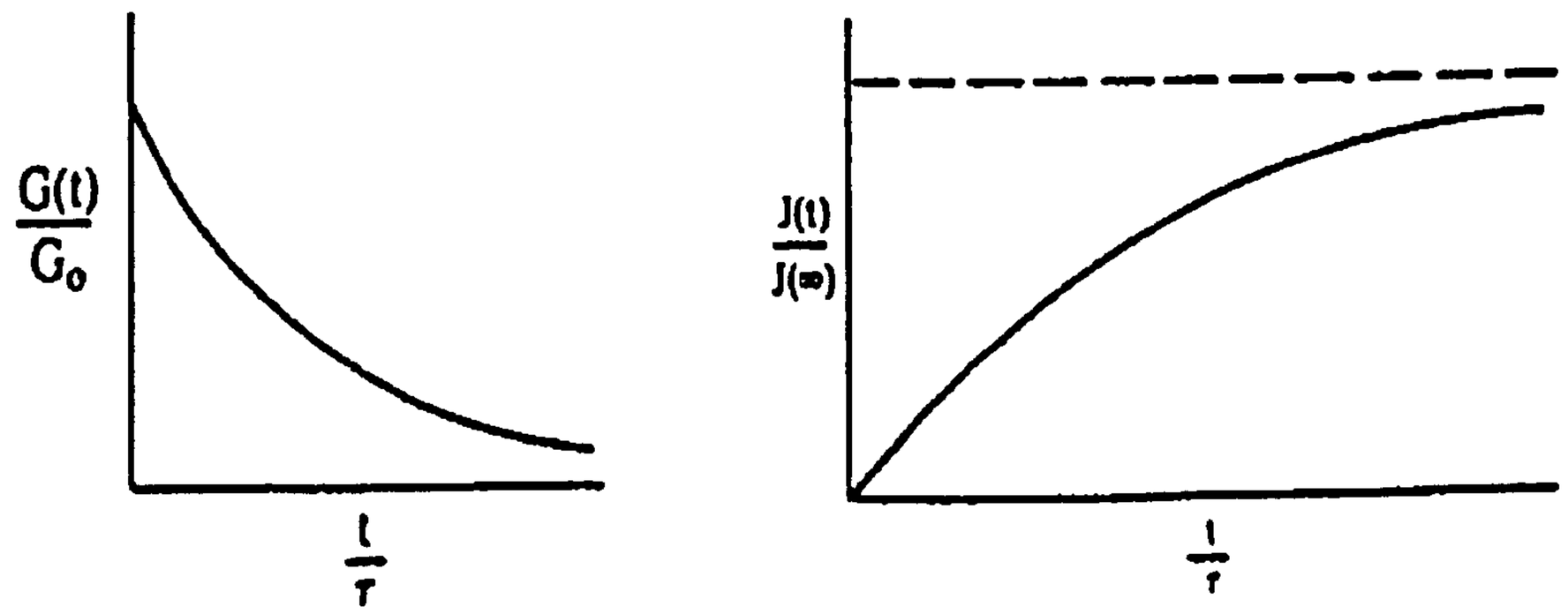

Fig. 2.15 Time-dependent shear modulus (a) (as $G(t)/G_0$) and shear compliance (b) (as $J(t)/J(\infty)$) versus time (as t/τ), where τ is experimental relaxation time, G_0 is the value of shear modulus at $t = 0$ and $J(\infty)$ is the maximum value of the shear compliance at $t \rightarrow \infty$.

The Maxwell model is interpreted by a stress relaxation test, where a constant strain is rapidly applied to a sample and the results yield a time-dependent stress relaxation modulus (Fig. 2.15a). The Voigt model describes the exact inverse case of the relaxation experiment, the creep experiment. In the creep tests, the stress is maintained at a constant value and the time dependence of the strain is measured (Fig. 2.15 b).

Another experimental approach to evaluate the viscoelasticity of a polymer material is to undertake a dynamic experiment, which involves stresses and strains varying periodically. In a dynamic oscillatory experiment the reciprocal of frequency (ω) gives the period of the oscillation and thus defines the time scale of the experiment. By varying the frequency range the maximum amount of information may be obtained from a dynamic mechanical experiment for a viscoelastic substance. More details regarding this experimental technique will be given in Chapter 3.

The use of dynamic tests gives the possibility of distinguishing the specific features of entire classes of polysaccharides by providing a criterion for a discrimination on the basis of strain and frequency dependence of the viscoelastic quantities, such as G^*, G' and G'' (The definitions of these parameters are given in Section 3.3.1.3). This is particularly true for a comparison between polysaccharide solutions, weak and strong gels. Fig. 2.16 illustrates schematically the viscoelastic parameters G', G'' and η^* as a function of frequency (Ross-Murphy, 1994). For a dilute solution of polysaccharides, $G'' > G'$ with $G'' \propto \omega$ and $G' \propto \omega^2$ (Fig. 2.16a). The dynamic viscosity is relatively independent of frequency. For a semi-dilute solution in which an entanglement network has been formed (Fig. 2.16b), the system is characterised by a crossover point of G' and G'' at a certain stage, and both G' and G'' become less frequency dependent as the frequency is increased; a 'rubbery' plateau of G' is seen at high frequency. Fig. 2.16c shows that polymer gels have a very different spectrum, G' and G'' slightly increase as frequency is increased, with $G'>G''$ at all the frequency range. The spectrum of a gel is different from that of a Hookean solid in that the moduli of the later are independent of frequency. A number of applications of using viscoelastic parameters to study polymer behaviour can be found in the monograph by Ferry (1980).

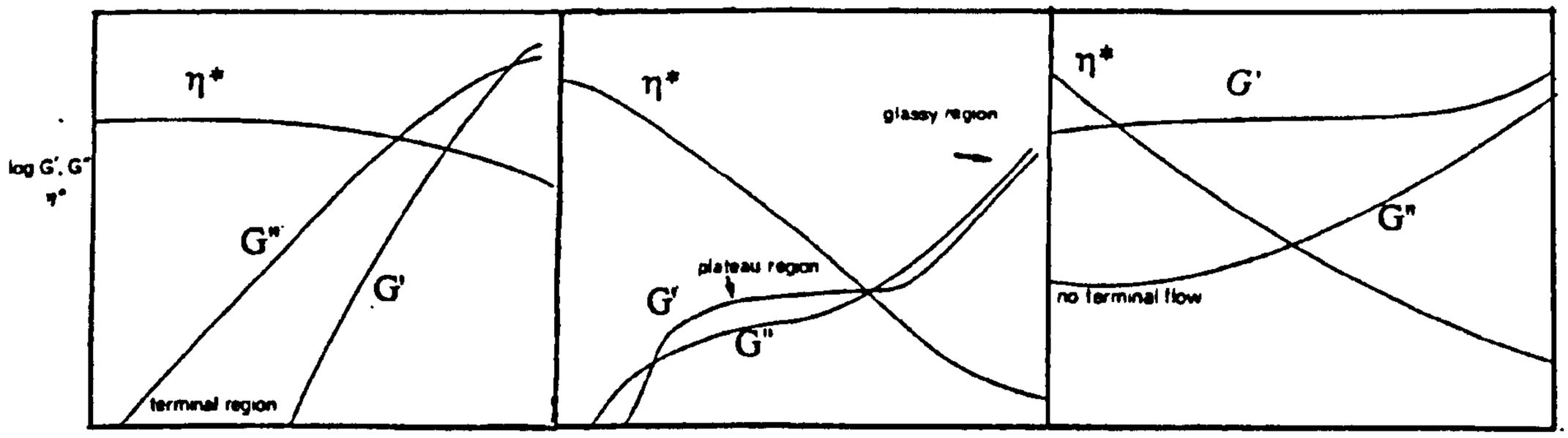

Fig. 2.16 Mechanical spectra, the storage modulus G′, the loss modulus G″ and the dynamic viscosity η^* *, plotted logarithmically against frequency* ω *for (a) a dilute solution, (b) a more entangled semi-dilute solution and (c) a gel. (From Ross-Murphy, 1994).*

2.3 Static light scattering technique

2.3.1 General concepts

While the rheological techniques allow the measurement of the macroscopic properties of a polymer, the study of scattering properties of polymers in solution provides a more direct approach to measure the molecular parameters. Using techniques such as small-angle X-ray scattering, small-angle neutron scattering and light scattering, the molecular structure can be investigated in different scales. In general, the local structure can be better examined by shorter wavelength sources. Light scattering, including static and dynamic light scattering, is an important technique for the study of polymer solutions yielding information about the molecular weight, size and shape, together with intermolecular structures. Static light scattering takes the time average of the scattered intensity hence studying the time-averaged system, while dynamic light scattering yields information of the dynamics of the system from analysis of the fluctuations in the scattered intensity as a function of time. In the present thesis, only static light scattering

technique was involved and thus is briefly described below with the references by Burchard (Burchard, 1983; 1994). We start from the definitions of the basic parameters and equations and then extend this to several examples of the use of this technique for evaluating the molecular weight and structures of polysaccharides.

2.3.1.1 Rayleigh ratio R_θ and optical contrast constant K

R_θ is also called normalised scattering intensity, which is defined as:

$$R_\theta = (I_\theta / I_0)\, r^2 \qquad (2.8)$$

where I_0 and I_θ are the intensity of the primary light and scattered light at scattering angle θ. r is the distance of the detector from the centre of the scattering volume.

The optical contrast constant K describes the contrast of the scattering intensity of the solute over that of the pure solvent. When vertically polarized incident light is used, K is given as:

$$K = (4\pi^2 / \lambda_0^4 N_A)\, n_0^2 \left(\frac{dn}{dc}\right)^2 \qquad (2.9)$$

where n_0 is the solvent refractive index, dn/dc is the refractive index increment, c is the polymer concentration in g/ml, λ_0 is the wavelength of the primary beam *in vacuo* and N_A is the Avogadro's number.

For small particles,

$$R_\theta = KcRT \left(\frac{dc}{d\pi}\right) \qquad (2.10)$$

where R is gas constant, T is temperature in K and π is the osmotic pressure. For large particles built up of monomeric units, we have:

$$R_\theta = KcRT\left(\frac{dc}{d\pi}\right) P(q, c), \qquad (2.11)$$

here the term P(q, c) is included because the interference effects resulting from interparticle distance have additional influence on the scattering intensity.

2.3.1.2 Particle scattering factor P(q)

The particle scattering factor P(q) describes the decrease of the scattering intensity as a function of scattering angle. Its value depends on the molecular architecture. Zimm (1948) derived the following relationship for large particles of fully interpenetrable chain structure:

$$Kc/R_\theta = 1/MP(q) + 2A_2 c + 3A_3 c + \ldots\ldots \qquad (2.12)$$

here, M is the molar mass of the particles. $q = 4\pi\sin(\theta/2)/\lambda$ is the magnitude of the scattering vector. $A_2, A_3, \ldots\ldots$ are virial coefficients.

2.3.1.3 The radius of gyration

At small values of q the particle scattering factor P(q) in equation 2.12 can be expanded in a Taylor series:

$$P(q) = 1 - \frac{1}{3}(R_g^2 q^2) + \ldots \qquad (2.13)$$

where $R_g^2 = \langle S^2 \rangle$ is the mean square radius of gyration, which is given by a sum over all distances of the scattering elements from the centre of mass or the sum over all intramolecular distances in a macromolecule. Often simply R_g is used in the literature instead of the more precise definition of $\langle S^2 \rangle^{1/2}$.

The radius of gyration depends on the molar mass of the particles, and in many cases can be described by a power-law behaviour such as:

$$R_g = k M^{\nu} \qquad (2.14)$$

The exponent v is a characteristic parameter for a molecular structure. Many of these exponents have been give in the literature (Burchard, 1994). For example, for linear random coil or star molecules with long arms, $v = 0.6$ in good solvents and $v = 0.5$ in ideal or θ-conditions.

2.3.2 Measurement of molecular weight and size

For solutions of macromolecules, equation 2.12 provides a direct means for measurement of molecular weight. In order to evaluate the molecular weight of large particles, we must thus extrapolate values of Kc/R_θ not only to vanishing concentration c, but also to vanishing angle θ. In practice, a plot originally suggested by Zimm allows for simultaneous graphical extrapolation of concentration and scattering angle. In the Zimm plot, Kc/R_θ is plotted against $q^2 + kc$, where k is an arbitrary constant in order to separate the angle-dependent curves from each other. Two sets of lines are drawn through the experimental points: one for constant values of scattering angle, the other at constant concentration. Both sets are extrapolated to yield lines at $\theta = 0$ and $c = 0$. The two extrapolated lines should meet at the axis. Their common intercept marks 1/M. The line at $\theta = 0$ represents the virial expansion. From its initial slope the second virial coefficient can be calculated. The line at $c = 0$ reflects the function $P^{-1}(\theta)$, and its initial slope divided by the intercept yields the radius of gyration of the particles.

For polydisperse macromolecules, the weight-average molecular weight M_w and the z-average square of the radius of gyration are measured through light scattering (Munk, 1989).

2.3.3 Structure determination

As mentioned above, in a Zimm plot from the limiting curve of the angular dependence at zero concentration, P(q) is given by $1/P(q) = M\,(Kc/R_\theta)_{\theta=0}$. A plot of this reciprocal particle scattering factor against $u^2 = q^2R_g^2$ results in curves that all have the same initial slope of 1/3. Deviations from this straight line occur only in the asymptotic region of

large u, and these deviations are characteristic of various architectures. For instance, if an upturn is observed then a globular or highly branched particle is present. If a downturn is observed then a stiff chain is probably present. However, the effect of polydispersity also has to be considered in this procedure. It has been shown that the upturn caused by branching can be balanced by the polydispersity of the chains.

The Zimm plot only gives the first hint for a qualitative check of the structure of particles in dilute solution. A more quantitative picture is obtained if structure-specific plots are employed that emphasise the asymptotic part of the particle scattering factor at large q. One of most relevant in this respect is the Kratky plot.

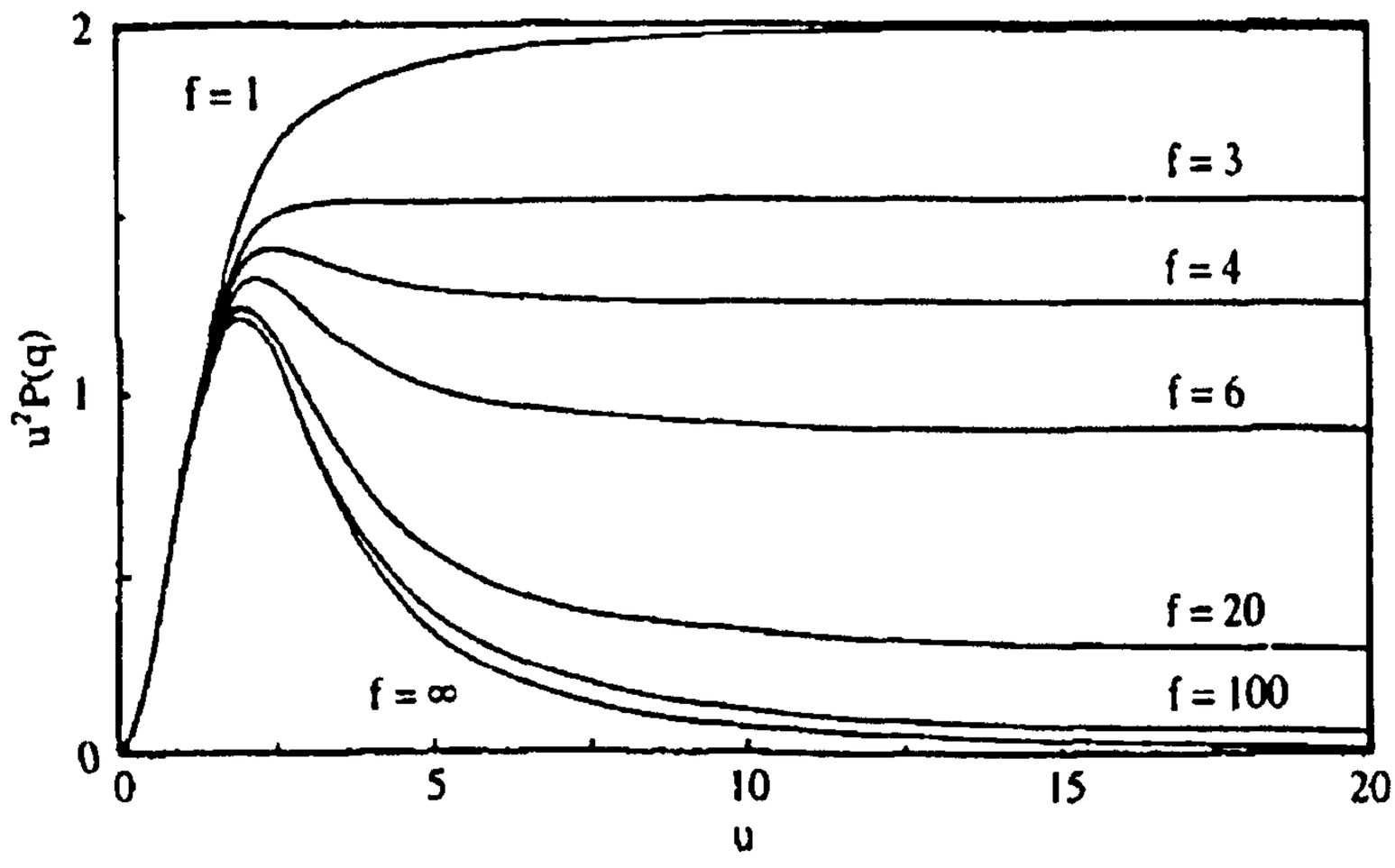

Fig. 2.17 Kratky plot for regular star-molecules. f denotes the functionality of polymer molecules (Burchard, 1994).

The Kratky plot (Burchard, 1994) has been found very useful to detect branching structures. Here $u^2P(u)$ is plotted against u, with $u = qR_g$. Linear random coiled chains exhibit an angular independent asymptote which has a value of 2 for monodisperse coils and 3 for polydisperse chains, if the distribution of the chains obey $M_w/M_n = 2$. The striking feature with branched chains is the appearance of a maximum for stars and other regular branched chains. This maximum become more and more pronounced with increasing branching density. Random f-functional polycondensates have the same

behaviour as polydisperse linear chains with $M_w/M_n = 2$. For random cross-linked chains, if the primary chains obey the most probable length distribution, behaviour identical to a polydisperse linear chain is observed. However, if the primary chains are less broad in distribution (including monodisperse chains), the characteristic maximum shows up again. Fig. 2.17 represents schematically the Kratky plot.

2.4 Dietary fibre

2.4.1 Definition of dietary fibre

The term dietary fibre was first introduced by Hipsley in 1953 to assess the epidemiological evidence linking fibre-deficient diets to the incidence of pregnancy toxaemia. Trowell in 1974 traced the history of the fibre hypothesis and definitions and gave his own definition as "the remnants of plant cells resistant to hydrolysis by the alimentary enzymes of man" (Trowell, 1972; 1974). According to this definition dietary fibre includes plant cell wall substances (cellulose, hemicelluloses, pectin, and lignin) as well as intracellular polysaccharides such as gums and mucilage. Later his definition was expanded by other investigators. Southgate (1977) suggested a chemical definition based on the fact that the sum of lignin and the non-α-glucan polysaccharides (i.e. non-starch polysaccharides) is the best index of the dietary fibre in the diet. Trowell and Spiller (1976) expanded the concept of dietary fibre to "dietary fibre complex" which also includes other substances that are undigested by human digestive enzymes. In spite of all the modifications, the early physiological definition by Trowell (1976) remains the most acceptable definition for dietary fibre.

NSP are the major constituent of dietary fibre. In current research work there is a tendency to divide dietary fibre into two categories based on the different physiological functions, namely the water-insoluble dietary fibre, such as cellulose, and water-soluble types of dietary fibre, such as guar gum. It is important to note that in broad terms these two categories of substances have widely different physiological effects. For example, insoluble fibre have more significant effects on bowel habit and faecal composition since

they are more resistant to bacterial degradation. However, many types of soluble fibre are extensively fermented in the proximal colon and have minimal effects on stool output. In contrast, guar gum as well as other viscous soluble fibre have repeatedly been demonstrated to be able to modulate the carbohydrate and lipid metabolism, whilst many types of insoluble fiber have consistently failed in this respect.

2.4.2 Main sources of dietary fibre

Dietary fibre can be supplied as either purified or partially purified polysaccharide extraction or crude heterogeneous food preparations which comprise a wide range of different polymers mainly in the form of plant cell wall materials, such as wheat bran. Isolated polysaccharides can be obtained from marine, plant and microbial fermentation. In recent years, many new and useful polysaccharides of scientific and commercial interest have been obtained from microbial fermentation. Xanthan gum obtained from *Xanthomonas campestris* is an example in this instance. However, the most widely used types of dietary fibre in physiological and nutritional purpose are still those of plant origin.

2.4.2.1 Examples of water-insoluble dietary fibre

Purified cellulose preparations as a form of insoluble dietary fibre has been extensively studied in nutrition and widely used as a source of water insoluble dietary fibre in diet. This is due to the acceptance of cellulose-type fibre as an established and recommended fibre to be used in purified diets (Penner and Liaw, 1990). For example, purified cellulose has been incorporated up to 10% by weight into the commercial calorie reduced breads in many countries.

Wheat bran, as a true food ingredient, is another most commonly used insoluble fibre source. It is a very heterogeneous material which varies in chemical composition and fractions (Robert and Verne, 1990). Commercial wheat bran contains a range of tissues, including the pericarp with attached testa, aleurone layer, and some endosperm. The

main polysaccharides in wheat bran are arabinoxylans, β-D-glucan, and small amount of cellulose and glucomannan. The structure of arabinoxylan varies depending on the source. For example, the cell wall of beeswing wheat bran comprise mainly highly branched and slightly branched acidic arabinoxylans. The arabinoxylans of the aleurone layer are neutral and much less branched than those found in the beeswing wheat bran layer. Only a small proportion of the arabinoxylans are soluble in hot water, and the rest require alkaline conditions.

2.4.2.2 Examples of water-soluble dietary fibre

Table 2.1 includes the major types of polysaccharides that are commonly used as food additives and as models for water soluble dietary fibre in experimental studies (Spiller, 1993). The main structural features of most of these polymers have been described in the previous section.

Table 2.1 Examples of polysaccharides used as water soluble dietary fibre.

Polysaccharides	Major sources	Principal types in use
Pectin	Citrus and apple cellular residues	High methoxyl Low methoxyl, amidated
Galactomannan gums	Endosperm of specific leguminous plants	Guar gum Locust bean gum
Algal polysaccharides	Cell wall of algae	Agar Alginates Carrageenans
Modified cellulose	Cellulose from delignified woody tissues	Methyl cellulose Carboxymethyl and carboxyethyl cellulose
Bacterial gums	Biosynthetically produced gums	Xanthan

Apart from the substances listed in Table 2.1, oat bran is another important food source of soluble fibre. Oat gum has received much attention recently because of its cholesterol-lowering effect (Wood, *et al.,* 1992; Braaten, *et al.,* 1993). It is produced from fractionating the ground oat groat or rolled oats. Commercial products of oat bran contain at least 5.5% (dry weight basis) of water soluble β-glucan and 16.0% (dry weight basis) of total dietary fibre. Thus, at least one third of dietary fibre in oat bran is thought to be water soluble.

2.4.3 Physiological effects of s-NSP and the underlying mechanisms

It is well established that dietary supplements of s-NSP can significantly modulate the carbohydrate and lipid metabolism. For instance, when polysaccharide gums were incorporated into foods, beneficial therapeutic effects were achieved by attenuation of postprandial plasma glucose and insulin levels in both diabetic and non-diabetic subjects (Jenkins, *et al.,* 1976; Aro, 1981). The cholesterol-lowering effect of dietary fibre also has been well documented (Kay and Truswell, 1980; Anderson and Tietyen-Clark, 1986; Reiser, 1987). The mechanisms responsible for the physiological effects of soluble fibre are still under investigation. However, a key factor in explaining the mode of action of s-NSP is their capacity to generate a high viscosity in the lumen of the gastrointestinal tract (Edwards, 1995).

One of the earliest studies to suggest the role of viscosity in relation to physiological properties of s-NSP was that carried out by Jenkins *et al.* (1978). In this study they investigated the effects of a number of types of dietary fibre on glucose tolerance including guar gum, pectin, gum tragacanth, methylcellulose, wheat bran and Cholestyramine. The most viscous fibre, guar gum was found to produce the greatest flattening of the blood glucose response curve. In addition, a hydrolysed form of guar gum, producing a much lower viscosity in aqueous solution than standard guar gum, was found to have no apparent physiological effects. Jenkins and his colleagues concluded that viscosity was the important determining factor to explain plasma glucose-lowering effect of guar gum.

Much other evidence has shown that the action of dietary fibre in improving carbohydrate and lipid metabolism is due to the delayed absorption of nutrients (Jenkins, *et al.,* 1978; Blackburn, *et al.*, 1984). This delayed absorption is ascribed to the high viscosity generated by s-NSP contained in the meals. In most cases this is thought to be a slowing of absorption rather than an inhibition or reduction in total amount absorbed (Jenkins, *et al.,* 1978). Increasing viscosity in the gut has been proposed to affect upper gastrointestinal function including the absorption of nutrients in the following number of ways.

2.4.3.1 Slowing gastric emptying

In general, viscous polysaccharides slow the emptying of liquids from the stomach, and this effect was thought to be responsible for the reduced rate of absorption of rapidly absorbed substances (Holt, *et al.,* 1979). A study by Meyer and Doty (1988) in fistulated dogs also suggested that both delayed gastric emptying as well as the changing of particle size distribution of food material leaving the stomach were important part of the overall mechanism together with slowed small bowel absorption. However, a number of other studies (Blackburn, *et al.,* 1984; Edwards, *et al.*, 1987) have suggested there is no direct relation between delayed gastric emptying time and the decrease in postprandial glucose. The argument for this is that some NSP have no significant effects on gastric emptying or even accelerate gastric emptying still reduce postprandial glycaemia (Edwards, *et al.*, 1987). Although soluble fibre such as guar gum may reduce the rate of gastric emptying under some conditions, this is unlikely to be the most predominant mechanism by which it acts (Rainbird, *et al.*, 1986; Blackburn, *et al.*, 1984).

2.4.3.2 Reducing the mixing movements of intestinal contents

Within the small intestine the interaction of enzymes and nutrients, the movement of small molecules to the mucosa and therefore absorption are all dependent on good mixing. Any factor which reduces the effectiveness of this mixing, such as increasing viscosity, should therefore slow digestion and absorption. Edwards *et al.* (1988) used a

dialysis tube and by compressing and releasing it to mimic a small intestinal segment, they found that 1% (w/v) guar gum solution abolished the increase in movement of glucose caused by an increase in the contraction rate. Similar effects have been observed by other research groups (Blackburn, *et al.,* 1984). Viscous polysaccharides have been shown to increase the viscosity of the unstirred layer and thus slow convective solute movement to the underlying intestinal villi (Johnson, *et al.*, 1981).

A number of studies also suggest that the activity of some enzymes in digesta containing viscous fibre is reduced, although *in vivo* more enzymes may be secreted by the pancreas to compensate. Isaksson *et al.* (1982) examined the effects of s-NSP, such as pectin and guar gum, on pancreatic enzyme activity under different conditions of pH, ionic strength, and time of incubation. Both high methyl esterified pectin and guar gum reduced enzyme activities, particularly lipase and increased the viscosity of the duodenal juice. A similar *in vitro* study (Schneeman and Gallaher, 1986) indicates that lipase activity in human pancreatic juice or human duodenal samples can be inhibited by pectin, guar gum and xylan. This is thought to occur because the degree of enzyme-substrate contact is inhibited, thus reducing enzyme activity.

The effect of s-NSP on enzyme activity can certainly be explained in terms of differences in the physico-chemical properties of different s-NSP. Some charged fibre such as pectin may bind enzymes, while in the case of neutral s-NSP such as guar gum, the enzymes are likely to be physically separated from the substrates because of poor mixing as a result of presence of viscous s-NSP.

2.4.3.3 Decreasing the availability of bile acids

Many types of dietary fibre may affect bile acid absorption in the small intestine through their viscosity properties, leading to decreased micelle formation and entrapment of bile acids and lipids (Selvendran, 1987). Thus, the availability of bile acid for optimal fat digestion and absorption was reduced. The effects of different fibres on faecal bile acids excretion have been reviewed in detail by Cassidy and Calvert (1993). In general, fibres that have significant hypocholesterolemic effects in humans also significant increase

faecal bile acid excretion although a few exceptions have been reported (Kritchevsky and Story, 1993).

2.4.3.4 Other proposed mechanisms

There are a number of other mechanisms which are not well defined and further work is needed to evaluate their role on the physiological effects of s-NSP. s-NSP are known to decrease serum insulin concentration and increase peripheral insulin sensitivity whilst altering other pancreatic and gastrointestinal hormone levels. Because of the important role these hormones play in cholesterol and fatty acid metabolism, it is thought that changes in hormone levels could affect lipid synthesis and metabolism. Most s-NSP are fermented in the colon to produce short-chain fatty acids, which may also have potential effects on carbohydrate metabolism. For example, acetate and propionate may stimulate insulin secretion and reduce blood glucose levels in experimental animals (Asplund, *et al.*, 1985; Brockman, 1982). Finally, Brennan, *et al.* (1996) studied the inhibitory effects of guar gum on the digestion rate of wheat bread starch by microscopy and *in vitro* digestibility methods. Their results suggested that, in addition to the viscosity effects of s-NSP in delaying glucose absorption in the small intestine, guar gum may also act at the level of the bread matrix during starch digestion. Thus, guar gum "coated" around the starch granules may function as a physical "barrier" to amylase-starch interaction and /or the release of the products of the hydrolysis from guar bread matrix into the aqueous phase of the digesta.

2.5 Hydration of s-NSP in relation to their physiological effects

2.5.1 Background

One of the first studies to investigate the rate of hydration and ultimate viscosity of

s-NSP preparations in relation to their physiological properties was carried out by O'Connor *et al.* (1981). They tested guar gums from four industrial sources including two flours, one granulate and one wax-coated granulate. Comparisons were made between the viscosity of guar gum solutions at 22°C and 37°C and pH 1.0 and 4.0 *in vitro* and the effect of 5g guar gum on postprandial glycaemia in response to an oral glucose tolerance test. Their results indicated marked difference in the rate of hydration of different grades samples of guar gum. The viscosity achieved was dependent on the extent of the hydration of the guar gum, which in turn was dependent on the physical form of the guar gum used. The two guar flours which hydrated more quickly and produced the highest final viscosity *in vitro* were equally effective *in vivo*. Although this study was not very well designed in some aspects it did highlight the importance of the nature of guar gum and its mode of administration, if optimum viscosity is to be obtained.

The critical importance of the rate and degree of hydration of s-NSP in determining the biological activity of these polymers has been further demonstrated by Heppell and Rainbird (1985) and Ellis and Morris (1991). In the latter study, they investigated six different samples of guar gum including four pharmaceutical preparations and two food grades of guar flour. Marked differences in hydration rate between the different samples were observed. Three of the four pharmaceutical preparations were lower in viscosity than the food grade guar gum flour during the first hour of hydration. Two of the preparations hydrated so slowly that even after 5 h they attained viscosity levels of only 60% of their ultimate viscosity. These two preparations have been shown to have little or no effect on glycaemic control in both pigs (Heppell and Rainbird, 1985) and humans (Baker, 1988; Holman, *et al.*, 1987). Their results provided a useful explanation for the poor clinical effects, particularly glycaemic control, of these two preparations. Thus, from the *in vitro* experiments, it was concluded that guar gum samples that had poor hydration properties in the laboratory were unlikely to hydrate sufficiently in the gastrointestinal tract to affect glucose absorption.

The process by which a solid substance dissolves in a solvent to form a solution or dispersion is called dissolution. In this thesis and many other related literature the word

"hydration" has often been used rather than dissolution for s-NSP to specify that water is the solvent used. In addition, the dissolution process normally refers to a true solution being formed rather than a suspension or dispersion as in the case of most polysaccharides. In this section we first give a brief review on the fundamental theory (models) of dissolution. Following this, we will focus on the experimental study of the hydration behaviour of high molecular weight polymers.

2.5.2 Thermodynamics of polymer solutions

For most linear and branched polymers, liquids can usually be found which will dissolve the polymer completely to form a homogeneous solution. When an amorphous polymer is mixed with a suitable solvent, it disperses in the solvent and behaves as though it too is a liquid. The ability of a polymer to be solvated is governed by the fundamental thermodynamic equation:

$$\Delta G = \Delta H - T\Delta S \qquad (2.15)$$

where, ΔG, ΔH and ΔS are the changes of Gibbs free energy, enthalpy and entropy of mixing respectively and T is the temperature of the system. A homogeneous solution is obtained when the Gibbs free energy of mixing is negative, $\Delta G < 0$. For an ideal system, ΔH is small, so the mixing will be an entropically driven process.

The solvents can be divided into three classes according to the compatibility with the polymer, i.e. good, poor and theta solvents. A good solvent is one which is highly compatible with the polymer and there is strong polymer-solvent interactions. This interaction expands the polymer coil from its unperturbed dimensions to some extent. A poor solvent is less compatible with the polymer. As a result, there are fewer polymer-solvent interactions and there is less coil expansion in a poor solvent compared to a good one. The so-called theta (θ) solvent is associated with the phase separation phenomenon. For a solvent at the theta temperature, only short range interference exists, the excluded volume effects (or long range interference) are eliminated and the polymer coil is in an unperturbed condition. Below the theta temperature the polymer segments

will attract each other and for very high molecular weight samples phase separation will occur. The second virial coefficient gives an indication of the solvent quality. In a good solvent $A_2 > 0$, whilst in the theta condition $A_2 = 0$.

2.5.3 Dissolution mechanisms

2.5.3.1 Fundamental theories

The interest in the hydration behaviour of polysaccharides is fairly new, and as far as we know, has not been extensively studied. The use of rheological methods to monitor the hydration rate has not been well established either. However, the concept of dissolution, as a fundamental phenomenon has been evident for some time. Dissolution gained a new interest in the pharmaceutical sciences in the late fifties and early sixties when the correlation between the dissolution rate of most drugs and their physiological availability was recognised (Nelson, 1957; Levy, 1961). Studies of the relationship between *in vivo* bioavailability and *in vitro* dissolution is still currently being investigated.

Dissolution can be considered as a specific type of heterogeneous reaction in which a mass transfer results as a net effect between the escape and deposition of soluble molecules at a solid surface. These reactions can be classified into three main categories (Wurster and Taylor, 1965) according to the controlling step during the process:

(a) The reaction at the interface is much faster than the transport processes. In this case the dissolution rate is controlled by the diffusion or convective transport of solute from the interfacial boundaries to the bulk of the solution.

(b) The process of liberating and depositing the solute molecules at the interfaces proceeds at a significantly slower speed than the transport process, and therefore it becomes the rate-controlling step.

(c) The rate constants of both processes are approximately equivalent, and in this case, the rate of dissolution would be a fraction of both the rate of the reaction at the interface as well as the rate of the transport process.

A number of theoretical models have been developed for interpreting the dissolution behaviour. The main three will be given below.

2.5.3.1.1 Diffusion layer model

This is the simplest model with the widest application for dissolution. It assumes that dissolution belongs to the first type of reaction where the rate is determined by the transport process. The earliest model of diffusion theory is Fick's first law of diffusion which states that at a steady state:

$$J_{ix} = - D_i \, \partial c_i/\partial x \qquad (2.16)$$

Where J_{ix} is the "diffusion current" or flux, D_i is the diffusion coefficient, c refers to concentration and $\partial c_i/\partial x$ is the spatial concentration gradient from the particle surface to the bulk of the dissolution.

However, as the concentration of the solute changes with time Fick's second law of diffusion could be derived from equation 2.16 as:

$$\partial c/\partial t = D(\partial^2 c/\partial x^2) \qquad (2.17)$$

where, t refers to time and $\partial c/\partial t$ is the dissolution rate. Based on Fick's first and second law of diffusion, Brunner and Tolloczko (1900) and Nernst (1904) proposed that a thin film, i.e. a stagnant layer h, is formed around the particle. Diffusion occurs from this layer at the boundary to the bulk of the solvent. They established a fundamental equation for dissolution when the surface area S was constant:

$$\frac{dc}{dt} = k\frac{DS}{Vh}(c_s - c_t) \qquad (2.18)$$

where c_s is the solubility of the sample, i.e. the maximum concentration of solution under a given test condition, c_t is the concentration at time t. V is the volume of the solution

and k is a constant. Equation 2.18 describes first-order dissolution kinetics; that is, if log c is plotted *vs.* time t, a straight line is obtained, the slope of which is the dissolution rate constant. In deriving this equation it was assumed that both h and S remained constant during the dissolution process.

Hixson and Crowel (1931) modified the above equation by allowing for a change in surface area with time and assumed that $S = kW^{2/3}$. They represented the model as:

$$W_0^{1/3} - W_t^{1/3} = Kt \qquad (2.19)$$

where W_0 is the initial powder weight, W_t is the powder weight at time t, K is the dissolution rate constant including the diffusion coefficient, particle density and solution viscosity. Equation 2.19 is known as Hixson and Crowell's 'Cubic Root Law' for dissolution.

2.5.3.1.2 Interfacial barrier model

In this model, the escape of solute molecules from the solid surface is considered to be a slow step. The solid-liquid interface forms the barrier to the process where the release of molecules of solute is retarded due to a high activation energy requirement. In contrast, in the diffusion layer model the transport process is much faster than the interfacial reaction. Therefore, the latter becomes the rate-limiting step of the dissolution process.

An equation that describes this model accurately has not yet been proposed. Higuchi (1967) discussed the interfacial barrier and recommended that the true surface area (not the geometric one) should be considered. The first-order dependence of dissolution rate from the factor (c_s-c_t) also was used for this model:

$$G = k (c_s - c_t) \qquad (2.20)$$

where G is the dissolution rate per unit area (i.e. $\frac{V}{S} \times \frac{dc}{dt}$) and k is the effective interfacial transport constant. The reason for an un-specified generalised constant k lies in the difficulty of expression of the true surface area involved in the process.

2.5.3.1.3 Danckwerts' model

This is also known as surface renewal theory, and was proposed by Danckwerts in 1951. In this model the assumption of the stagnant film covering the solid particles made for the previous two models is no longer valid. Instead, macroscopic packets of solvent which surrounded the solid particles are assumed to reach and attach to the solid surface area absorbing solute molecules by normal diffusion and then carrying them back to the bulk solution. The continuous arrival of fresh packets of solvent creates a continuous renewal of the surface area, which is essentially the determining factor of the rate of transport of solute molecules. The rate of transport is ultimately the rate of dissolution of solid. The basic equation for this model is:

$$G = (\gamma D)^{1/2} (c_s - c_t) \qquad (2.21)$$

where γ is the mean rate of production of fresh surface (or the interfacial tension).

Goyan, in 1965, developed a mathematical treatment of this model for a small spherical particle which can be written as:

$$\frac{dw}{dt} = (\frac{SD}{r} + \sqrt{\gamma D})(c_s - c_t) \qquad (2.22)$$

where w is the weight of the undisolved sample and r is the radius of the particle.

2.5.3.1.4 Interrelationships between above models

Although the above models try to describe dissolution according to different mechanisms the mathematical equations underlying the process reveal an interrelation

between them. The interfacial concept may be combined with the diffusion layer model by introducing the factor $(1+\frac{D}{hk})$ into equation 2.18 and representing it as:

$$G = \frac{Vdc}{Sdt} = \frac{D}{h(1+\frac{D}{hk})}(c_s - c_t) \qquad (2.23)$$

where the symbols have the same meaning as in equations 2.18 and 2.20. Nevertheless, equation 2.23 can be transformed into equations 2.18 and 2.20 in an extreme cases where one model predominates kinetically over the other. That is, if $k >> D/h$, which means the interfacial transport is much faster than the transport in the stagnant film, then, it reduces back to the basic diffusion film theory equation 2.18. However, if $k << D/h$, it reduces to the interfacial barrier equation 2.20.

In a similar manner, a factor of the form $(1+\frac{\sqrt{\gamma D}}{k})$ can be used to demonstrate the interrelation between Danckwerts' model and the interfacial barrier model through equation 2.24:

$$G = \frac{\sqrt{\gamma D}}{1+\frac{\sqrt{\gamma D}}{k}}(c_s - c_t) \qquad (2.24)$$

Again, the transformation of equation 2.24 to the basic Danckwerts' equation (i.e. equation 2.21) and the interfacial barrier model is obvious if $k >> \sqrt{\gamma D}$ or $k << \sqrt{\gamma D}$, respectively.

Above all, no matter what mechanism and model is considered, the proportionality between the dissolution rate and the term of concentration $(c_s - c_t)$ is commonly recognised. Therefore a general expression for dissolution results:

$$G = F(c_s - c_t) \qquad (2.25)$$

where F is a proportionality constant to specify the controlling step involved in the process.

2.5.3.2 Empirical kinetic models

2.5.3.2.1 First order kinetics

First order kinetics has been most popular model in describing chemical reactions and physical process including hydration. This model can be explicable in terms of the general expression for dissolution, i.e. equation 2.25:

$$\frac{dc}{dt} = k(c_s - c_t) \qquad (2.26)$$

The key and definitions are same as in previous section. Rewrite the above equation as $dc/(c_s - c_t) = kdt$ and integrate both sides giving rise to:

$$\ln (c_s - c_t) = kt + \varphi \qquad (2.27)$$

since when $t = 0$, we have $c_t = 0$, that is the starting point of the dissolution, substitute this into above equation results: $\varphi = \ln c_s$. Thus, equation 2.27 becomes:

$$\ln (1-c_t/c_s) = kt \qquad (2.28)$$

To *et al.* (1994) used this first order kinetic model to describe the growth in viscosity with time following the hydration of guar gum and xanthan gum flours:

$$\ln (1-\eta_t/\eta_\infty) = -kt \qquad (2.29)$$

where η_t is the viscosity of the dispersion at time t, η_∞ is the "ultimate" viscosity and k is the time constant relating to the rate of viscosity development.

For most polysaccharide dispersions the relationship between zero shear viscosity and the concentration of hydrated polymer is approximately $\eta_0 = C^{3.5 \cdot 4}$ (Ross-Murphy, 1994). Assuming the exponent 3.5, the following relationship can be derived from equation 2.28:

$$\ln (1-\eta_t^{1/3.5}/\eta_\infty^{1/3.5}) = -kt \qquad (2.30)$$

The hydration constant k in equations 2.29 and 2.30 can be obtained from the plots of $\ln (1- \eta_t/\eta_\infty)$ or $\ln (1-\eta_t^{1/3.5}/\eta_\infty^{1/3.5})$ *vs.* time t, respectively.

According to To and his colleagues, reasonable linearity was obtained from their experimental data ($r^2 > 0.9$) with equation 2.29. The aims of their study was to mimic the processes of preparation of solutions of polysaccharide powders on an industrial scale. Therefore, an extremely high shear condition was used, rather than the low shear used in our study which is more likely to approximate the conditions in the gastrointestinal tract.

2.5.3.2.2 Weibull distribution function

Langenbucher (1972) used a distribution function to describe the dissolution curves for some pharmaceutical tablets. The function was originally proposed by Weibull to describe the effect of the weakest link in a chain (Weibull, 1951). The chain could be anything from electric light bulb filaments to the life of a human. When applied to dissolution data, the Weibull equation expresses the accumulated fraction:

$$f(t) = 1 - \exp (-(t-\Omega)/\alpha)^{\beta} \qquad (2.31)$$

In our experiment f(t) can be conventionally considered as the fraction remaining undissolved at time t, which is expressed as $(\eta_\infty - \eta_t)/\eta_\infty = 1-\eta_t/\eta_\infty$. In this equation α is a scale parameter which defines the time scale of the process. Ω is the location parameter, represents the time lag before the actual onset of the process. β is a shape parameter characterising the shape of the process curves.

Equation 2.31 may be converted to a linear transform as following:

$$1- f(t) = \exp(-(t-\Omega)/\alpha)^{\beta}$$

$$\ln(1/(1-f(t)) = ((t-\Omega)/\alpha)^{\beta}$$

$$\ln\ln(1/(1-f(t)) = \beta\ln(t-\Omega) - \beta\ln\alpha$$

$$\ln\ln(\eta_{\infty}/\eta_{t}) = \beta\ln(t-\Omega) - \beta\ln\alpha \qquad (2.32)$$

The use of the linearization of dissolution curves by the Weibull distribution has been discussed by Langenbucher (1972).

2.5.4 Factors affecting the rate of hydration of polymers

Similar to the low molecular weight substances, the hydration rate of amorphous polymer materials is also significantly influenced by many physicochemical properties, such as the solubility, particle size and crystallinity. Other physical properties such as density, viscosity and surface property contribute to the general dissolution problems of flocculation, flotation and agglomeration, and these have been well documented in the books, for example, by Abdou (1989). In this section we will only review the effect of molecular weight, the most distinguishing characteristic of polymeric materials from low molecular weight substances, on the hydration rate of polymers.

The polystyrene-toluene system has been the most commonly used for the study of polymer dissolution. Ueberreiter (1968) investigated the influence of molecular weight (M) of polystyrene on its velocity of dissolution (s) in toluene by microscopy techniques. Over a wide range of molecular weight, s and M were found to follow the relationship described as:

$$s = kM^{a} \qquad (2.33)$$

This implies that the plot of log s *vs.* log M yields a straight line with a slope of a.

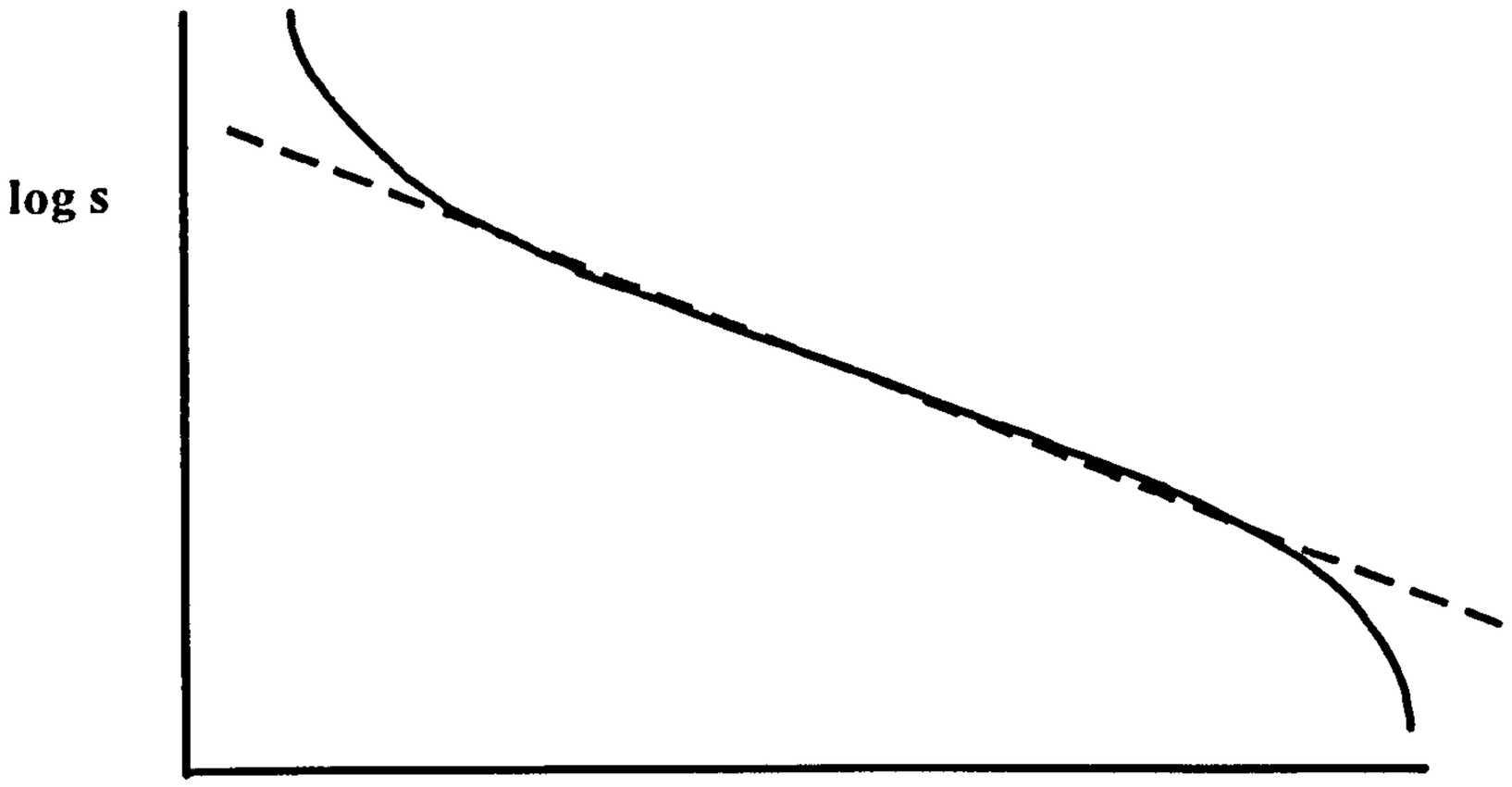

Fig. 2.18 Schematic plot showing the velocity of dissolution (s) as function of molecular weight (M) in polystyrene-toluene system (Ueberreiter, 1968).

The lower and upper limits in molecular weight, for which equation 2.33 is applicable, were found to be about 10^3 and $2x10^5$ at 25 °C, respectively. Below the lower limit the oligomers were in a rubber-like state at this temperature and possessed a much bigger velocity of dissolution, whereas above this upper limit the velocity of dissolution fell rapidly as shown in Fig. 2.18. They ascribed this to the rapidly increasing polymer chain entanglement of the very large chains which increased the thickness of the swollen surface layer.

The reptation theory has been applied to polymer dissolution processes in several studies (Brochard and de Gennes, 1983; Papanu, *et at.,* 1989; Herman and Edwards, 1990) and it has been found useful in the study of the effect of molecular weight on the hydration behaviour of polymers. In this approach, as already discussed in Section 2.2.4, a polymer chain in a entanglement network is assumed to be contained in a hypothetical tube, which is placed initially in a three dimensional network formed from the other entangled chains. A particular chain moves snake-like through the tube and escapes at

the tube end. The motion can be characterised by a reptation time, or more accurately by a relaxation time, τ, which is a measure of the time required for a chain to escape completely from its tube. The fundamental result of the reptation model is that the relaxation time (τ) is proportional to the cube of the chain length.

Brochard and de Gennes (1983) proposed a relaxation-controlled polymer dissolution kinetics model with a dissolution flux proportional to the difference between the polymer stress gradient and the solvent osmotic pressure gradient. They postulated that a gel-like swollen polymer phase will exist at small times. The dissolution of the networks from the swollen phase was predicted to be governed by the rate of stress relaxation, which was estimated to be of the order of the reptation time. Thus, from the reptation model, for a certain polymer the higher the molecular weight, the slower the hydration rate should be.

Peppas *et al.* (1994) also developed a polymer dissolution rate model by incorporating the polymer chain disentanglement mechanism into the relevant transport equations. The dependence of the gel layer thickness and the polymer dissolution rate on polymer molecular weight were derived by use of reptation theory. The effect of molecular weight on the gel layer thickness was investigated for nine monodisperse polystyrene samples, with molecular weight ranging from 28,000 to 2,830,00. Their experimental results showed that the gel layer thickness increased with increasing molecular weight. Thus, according to their model the dissolution rate decreased with increasing molecular weight. Furthermore, this effect was found more prominent in the high molecular weight region.

2.6 Degradation of polysaccharides under acidic conditions

Many polysaccharides may be rapidly and totally hydrolysed to monosaccharides by strong acidic solutions, such as 12M H_2SO_4. In more gentle acid conditions, they will

only be partially hydrolysed to produce a variable mixture of monosaccharides, oligosaccharides and polysaccharides with a broad range of degrees of polymerisation. Kinetic studies of hydrolysis of polysaccharides so far mainly involves the use of cellulose and starch. Recently, the acidic hydrolysis of carrageennans has been studied by several groups (Ekström, *et al.*, 1983; 1985; Capron, *et al.*, 1996). As far as we are aware, no kinetic studies of the acidic hydrolysis of guar galactomannan has been reported. At present, we can assume that the acid hydrolysis of guar gum galactomannan is a non-specific degradation (random scission), i.e. the glycosidic linkages are broken at random. A brief description of random scission kinetics is given as following.

Assuming that the degradation of a linear polysaccharide in solution is a random scission process, N_0 is the total number of the monosaccharide molecules in the polymer sample mixture and N_0p is the number of glycosidic bonds, then $N_0(1-p)$ is the number of unbonded positions with p is the extent of polymerisation. From the statistics of random polymerisation the number-average (denoted by subscript n) and weight-average (denoted by subscript w) degree of polymerisation ($\overline{DP}$) and molecular weight (M) are given as (Flory, 1936):

$$\overline{DP}_n = N_0/N_0\,(1 - p) = 1/(1 - p) \tag{2.34}$$

$$M_n = M_0\,\overline{DP}_n = M_0/(1 - p) \tag{2.35}$$

$$M_w = M_0\,\overline{DP}_w = M_0\,(1 + p)/(1 - p) \tag{2.36}$$

where M_0 is the contribution of each monomeric unit to the polymer molecular weight.

With random scission, the rate at which bonds are broken is proportional to the total number of the intact bonds. Thus,

$$-d(N_0p)/dt = kN_0p \tag{2.37}$$

where k is a rate constant.

The solution of equation 2.37 with the boundary condition $p = p_0$ at time $t = 0$ is that:

$$p = p_0 e^{-kt} \tag{2.38}$$

Combining equation 2.38 with equations 2.34 and 2.36 gives the average degree of polymerisation as a function of time:

$$\frac{1}{\bar{DP}_n} = 1 - p = 1 - p_0 e^{-kt} \tag{2.39}$$

$$\frac{1}{1+\bar{DP}_w} = \frac{1-p}{2} = \frac{1}{2}(1 - p_0 e^{-kt}) \tag{2.40}$$

In the initial stages of the reaction p remains close to p_0, so that e^{-kt} must be close to unity. i.e. we can set $e^{-kt} = 1 - kt$. Thus, equations 2.39 and equation 2.40 can be approximately written as:

$$\frac{1}{\bar{DP}_n} = 1 - p_0(1 - kt) = (1 - p_0) + kp_0t = \frac{1}{(\bar{DP}_n)_0} + kp_0t \tag{2.41}$$

$$\frac{1}{1+\bar{DP}_w} = \frac{1}{2}(1 - p_0(1 - kt)) = \frac{1}{2}(1 - p_0) + \frac{1}{2}kp_0t$$

$$= \frac{1}{1+(\bar{DP}_n)_0} + \frac{1}{2}kp_0t \tag{2.42}$$

Both these equations indicate that the reciprocal of number-average and weight-average degree of polymerisation are linear functions of time.

Degradation is often followed experimentally by determination of the molecular weight as a function of time, by using light scattering or viscosity (usually through measurement of intrinsic viscosity) as a measure of molecular weight. The former gives the weight-average molecular weight and the latter gives viscosity-average molecular weight M_v. The magnitude of M_v is between M_w and M_n and is usually more close to M_w. In the case of condensation polymers in which there is no change in reactivity of functional groups

with chain length, M_v/ M_w and M_v/ M_n are constants independent of molecular weight. In this case, the intrinsic viscosity [η] can also be used to measure M_w and M_n if calibration is carried out. The approximation $M_v \approx M_w$ was made without calibration in the present study since the change in molecular weight is more important here than an accurate determination of it. From equation 2.36, $\frac{1}{\bar{DP}_w} \propto \frac{1}{M_w}$, therefore there is approximately $\frac{1}{\bar{DP}_w} \propto \frac{1}{M_v}$.

Chapter 3

Experimental techniques

3.1 Introduction

A range of physical and chemical techniques for characterising polysaccharide gums have been used in the project reported in this thesis. In this chapter, only those techniques that have been used repeatedly in the project are described in detail. The other techniques used in the project are presented in specific chapters, except the light scattering technique, the principals and method of which are also described in Chapter 3.

3.2 Chemical characterisation techniques

3.2.1 Chemical analysis of polysaccharide gums

The moisture content of sample was measured after leaving the sample in an oven at 104°C for 16 hours (AACC methods 44-15A) (AACC, 1983). Crude fat (Soxhlet; light petroleum, bp 40-60°C, diethyl ether extraction) was also analysed according to AACC methods 30-26. Crude protein (N x 5.7) was estimated by the Kjeldahl method (Egan, *et al.*, 1981). Ash (total minerals) was analysed by slowly heating a 5g sample in a muffle furnace to 525°C and leaving for 12 hours at that temperature (Egan, *et al.*, 1981). The Englyst method (Englyst, *et al.*, 1992) was employed to determine the total and insoluble non-starch polysaccharides (NSP). This method will be described in detail in Section 3.2.3.

3.2.2 Extraction and purification of s-NSP

The water soluble non-starch polysaccharides (s-NSP) were extracted and purified by a modification of the method of Girhammar and Nair (1992). Detarium seed flour or guar

gum samples were boiled with 80% (v/v) ethanol for 1 hour under reflux to inactivate enzymes, denature protein and remove ethanol-soluble substances. The residue obtained by filtration was washed with 95% (v/v) ethanol and air-dried at room temperature. The dried residue was then extracted with 7 volumes of distilled water at about 40 °C followed by centrifugation at 9000 g for 10 min. The supernatant was collected, adjusted to pH 7.5 with 10% (w/w) NaOH solution, and digested for removal of protein and starch with porcine pancreatin (1% of the weight of the boiled samples), and pullulanase (0.5 Units for 10g sample) at 34 °C for 24 h with continuous stirring in the presence of 0.05% (w/v) NaN_3, which was added to inhibit microbial growth. Both enzymes were obtained from Sigma Chemical Co., St Louis, USA. The solution was then centrifuged at 9000 g for 15 min and the s-NSP in the supernatant was precipitated by the addition of absolute ethanol to give a final concentration of 80% (v/v) ethanol. The precipitate was collected by filtration (Whatman No. 541 filter paper), washed with 95% (v/v) ethanol, acetone and diethyl ether, then freeze-dried and stored at 4°C until analysis.

3.2.3 Analysis of constituent sugars of polysaccharides

The Englyst method (Englyst, *et al.*, 1992) was used to analyse the constituent monosaccharides of polysaccharide gums with small modification. In this method, total acid hydrolysis of the polysaccharide samples was employed to produce the constituent sugars, which were then converted to the alditol acetate derivatives. The derivatives were analysed by GLC (Pye Unicam Series 204) fitted with a flame ionisation detector and computing integrator, using a Supelco Sp-2330 wide-bore capillary column (Englyst, *et al.*, 1992). The uronic acid content was determined by a sulphuric acid-dimethylphenol colorimetric assay (Englyst, *et al.*, 1992). Absorption was measured at 400 and 450 nm. The reading at 400 nm was subtracted from that at 450 nm to correct for the interference from hexoses. The major procedures of this method are summarised in the following flow chart (Fig. 3.1).

In the original method, the total and insoluble NSP were determined and the soluble fraction was determined as the difference between total NSP and insoluble fraction. The

samples for the measurement of the insoluble fraction were hydrated overnight in phosphate buffer, as opposed to the 40 min suggested by Englyst *et al.* (1992), in order to allow complete hydration of the galactomannan. This method produced a significantly lower concentration of insoluble NSP than the standard technique.

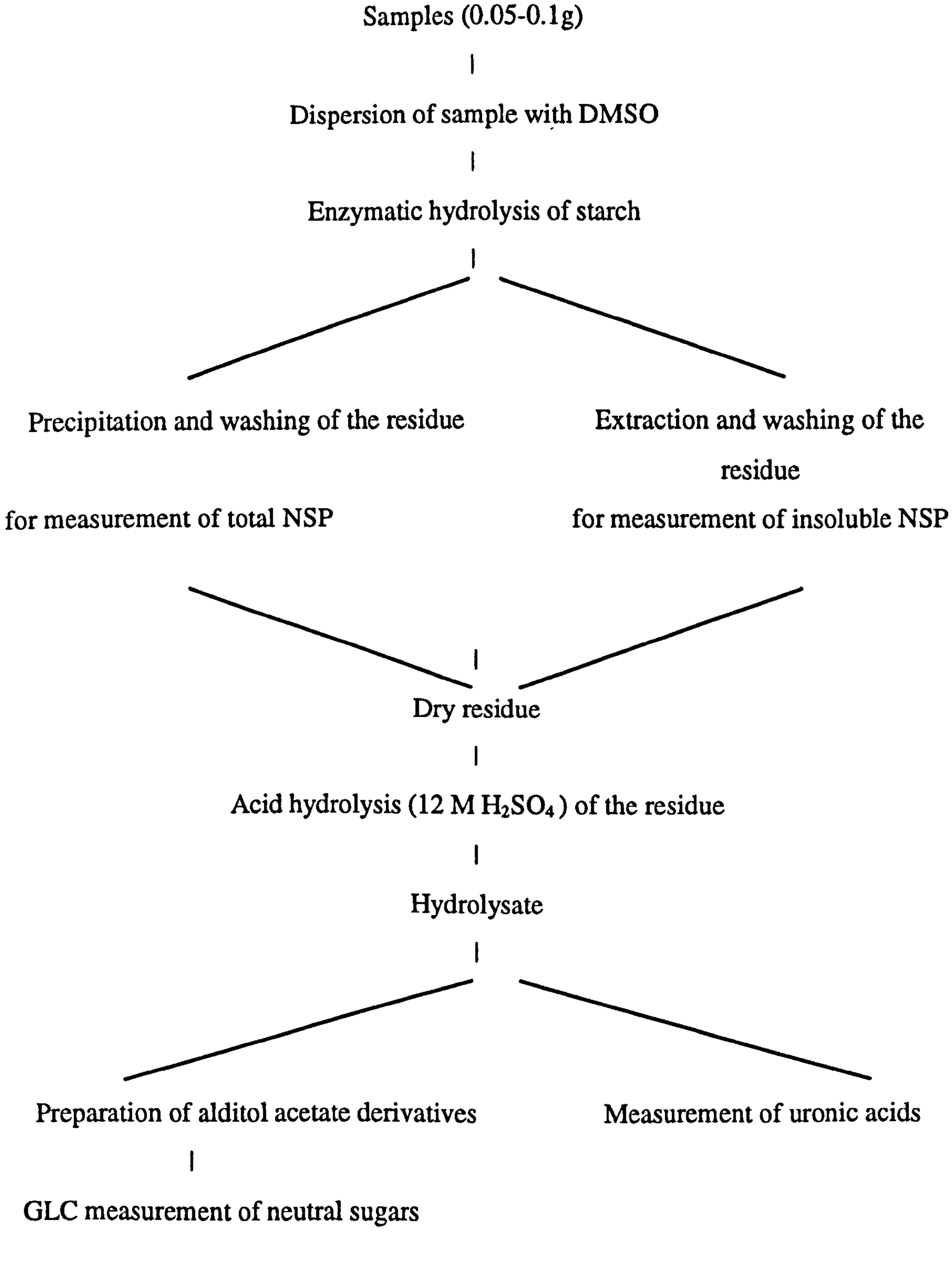

Fig. 3.1 Main procedures of Englyst method for analysis of NSP.

3.3 Physical characterization techniques

3.3.1 Rheological techniques

3.3.1.1 Intrinsic viscosity determination

The intrinsic viscosity [η] was conventionally determined from the double extrapolation of the Huggins and Kramer equations :

$$\eta_{sp}/C = [\eta] + K'[\eta]^2 C + o(C^2) \qquad (3.1)$$

$$\ln(\eta_r)/C = [\eta] + (K' - 0.5)[\eta]^2 C + o(C^2) \qquad (3.2)$$

where C is the polysaccharide concentration, and K' is the Huggins coefficient. [η] was estimated as the average of the two ordinate intercepts from the two extrapolations to C = 0%. The notation $o(C^2)$ is used to denote second and higher order terms of such power series expansion of η_{sp}/C and $\ln(\eta_r)/C$ around C = 0%. Since the plots are essentially linear such terms are of negligible importance in this case.

Unless specified, solutions for measurement of intrinsic viscosity were prepared by dispersing the known weights of samples of polysaccharide in deionized water for 1 h at 80 °C and then mixed overnight by magnetic stirring at room temperature. The solutions were filtered through a 0.45 μm syringe filter before measurements were taken. The concentrations of s-NSP used for calculating [η] were based on the polysaccharide content (measured by the Englyst method) of the purified samples rather than the dry matter content.

Viscosity measurements were performed in a dilution capillary viscometer (Cannon Ubbelohde Dilution B glass viscometer, size 50, 0.8 - 4.0 cst. Glass Artefact (Viscometers), UK) immersed in a water bath to maintain the temperature as 25 °C ± 0.1°C. Precautions were taken to ensure the viscometer was aligned vertically, and flow

times (>250 s) were measured in triplicate using a simple computer timing system; agreement between triplicates was within ± 1 s. Under the prevailing flow conditions no flow kinetic energy correction was required.

The molecular weight of guar samples were then calculated by the Mark and Houwink equation (equation 2.3), where $k = 3.8 \times 10^{-4}$ and $\alpha = 0.723$ were used (Robinson, *et al.*, 1982).

3.3.1.2 Steady shear flow measurements

A steady shear experiment is the most commonly used technique for investigating the flow properties of a liquid under "steady" shear force, which means that the axial direction of the shear deformation is constant during the measurement. As previously discussed in Chapter 2, at some concentration above C* there is a sudden change in flow properties, which is represented by a more pronounced increases in both zero-shear viscosity and the shear rate dependence (usually shear thinning for most polysaccharide in solution). In order to investigate this behaviour the steady rate sweep experiments are usually conducted on different concentrations of polymers at a concentration range as wide as possible. In each experiment the viscosity of a sample at different shear rate is measured, from which the dependence of viscosity on shear rate can be obtained over several decades using a rheometer such as the RFSII (described later in this chapter). From these measurements zero-shear viscosity can then be estimated at different concentrations.

In the first part of present project, steady shear experiments on detarium gum solutions prepared at different concentrations (0.1-3.0 %, w/w) were performed on the Rheometrics Fluids Spectrometer (RFSII, Rheometric Scientific Ltd, Epsom, UK.) with a cone and plate configuration (diameter 50 mm, cone angle 0.02 radians). From the measurements, the zero shear viscosity at different concentrations were calculated using the Cross equation (equation 2.7 in Chapter 2). Most of the steady shear measurements were carried out at shear rates of 0.05-1000 s^{-1} with a reduction in rate at the higher concentrations. All the measurements were conducted at 25°C.

The steady rate sweep test was also used to study the hydration behaviour of guar gum in the second part of this thesis (Chapters 6-9). In these cases, a time course of (zero-shear) viscosity development over some time period needs to be recorded. Because of the limitation to the measurement time for each time point, the viscosity measurements were taken only over two decades of shear rate at the lowest possible shear rate range. In this case, the Cross equation was found not to be suitable for estimating the zero-shear viscosity. Instead, the average of the first few test points at the lowest shear rate, corresponding to the Newtonian plateau, was estimated to be the zero-shear viscosity.

3.3.1.3 Dynamic measurements

As mentioned earlier, many polymer systems are actually viscoelastic materials. Although the viscoelastic properties can be evaluated by steady measurement, i.e. by the relaxation test of strain or stress, it is more convenient to adopt the dynamic measurement to study the viscoelasticity of the materials. In contrast to steady measurement, a time-dependent strain is applied to the sample in the dynamic measurements and various types of dynamic strain can be used such as sinusoidal, triangular and stepwise. In the current experiment, the oscillatory sinusoidal strain was used because of the ease of data analysis.

In the dynamic measurements the viscoelasticity of a material can be studied by comparing the applied strain wave with the resulting stress wave. If a sinusoidal strain as in Fig. 3.2 (a) is applied to an ideal Hookean material (Fig. 3.2 (b)), the resultant stress is expected to be also a sinusoidal wave with exactly the same frequency (ω) and phase angle. However, for a ideal liquid the resulting stress will be exactly 90° out of phase with the imposed strain wave (Fig. 3.2 (c)). As illustrated in Fig. 3.2 (d), for a real viscoelastic material the response stress to imposed strain is in between these two ideal cases, with a phase difference, $0°<\delta<90°$. In this case, the total resultant stress is traditionally separated to the in-phase and 90° out-phase components with respect to the strain vector (γ), which can be expressed as:

$$\tau = G'\gamma + iG''\gamma \qquad (3.3)$$

where G' is called 'shear storage modulus', which represents the elastic component of the stress, while G'' is called 'shear loss modulus' and this represents the viscous component of the stress. The complex shear modulus G* can be defined as:

$$G^* = G' + iG'' \tag{3.4}$$

Thus, we have $|G^*| = \sqrt{G'^2 + G''^2}$. The complex viscosity η^* is defined in the similar way such as:

$$|\eta^*| = \sqrt{\eta'^2 + \eta''^2} \tag{3.5}$$

and

$$|\eta^*| = \frac{|G^*|}{\omega} \tag{3.6}$$

The ratio of G' to G'' is the tangent of the phase difference (δ) between the strain wave and total stress wave. Therefore, tan δ is a measure of the viscous/elastic properties of the materials.

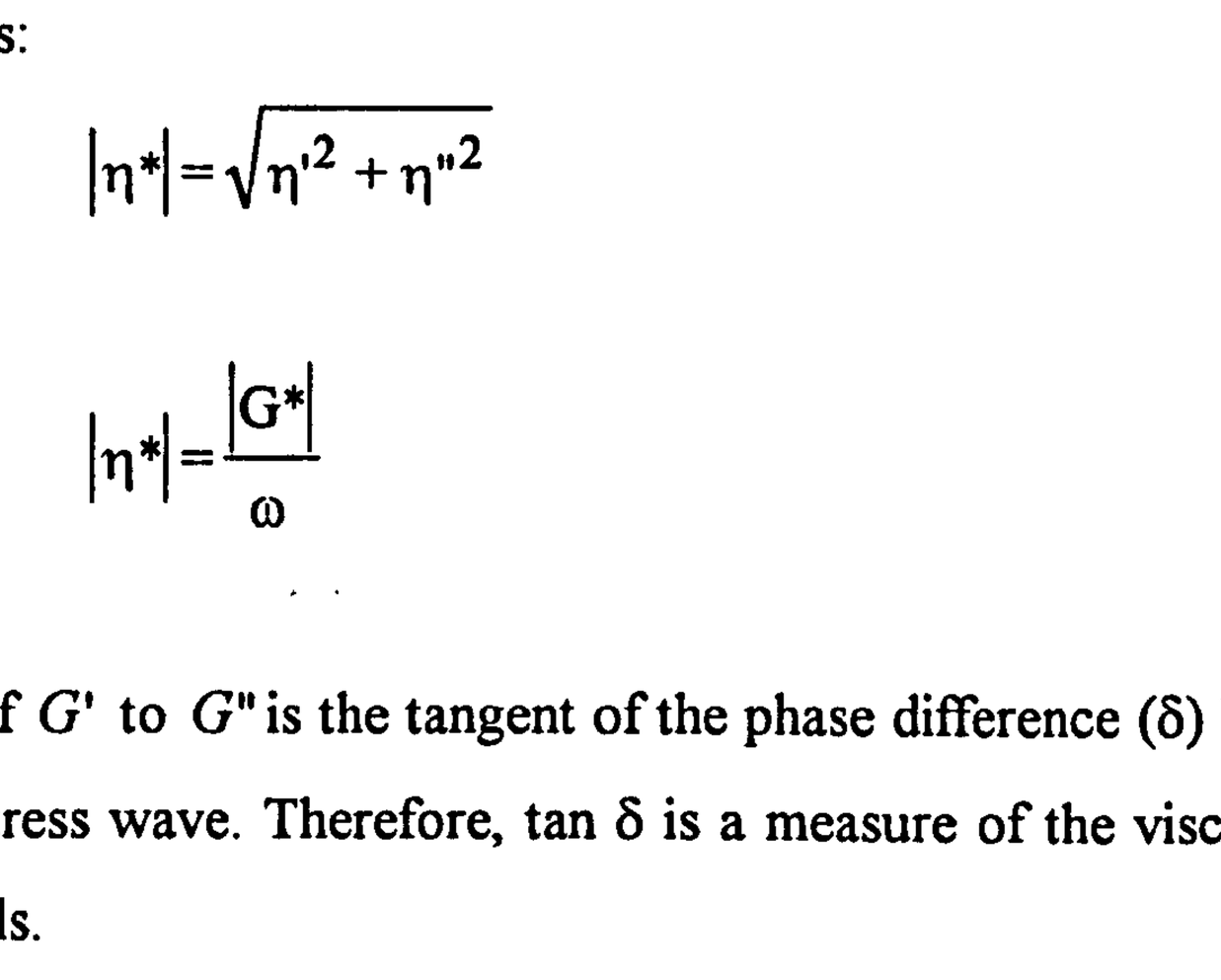

Fig. 3.2 Relationship between strain (a) and resulting stress for: (b) ideal solid, (c) ideal liquid and (d) viscoelastic material.

All the oscillatory experiments carried out on detarium solutions were performed on the RFSII using the same geometry as steady shear measurements described above. In this apparatus, a sinusoidal strain wave with frequency ω was applied to the lower plate and the response of the sample exerted on the upper plate was detected by the transducer system. The strain sweep experiments were carried out in order to determine the linear viscoelastic range of selected polysaccharide solutions. The complex shear modulus (G*) and dynamic viscosity (η*) were measured at a strain range of 0.1%-100 % in 5% increments at a frequency 1 or 10 rad. s^{-1}.

In frequency sweep measurements the strain was selected at 35%, which was within the linear viscoelastic limit established from the above experiments. The frequency of the applied strain wave was varied from 0.1-100 rad. s^{-1} with 5 points per decade. The viscoelastic parameters, namely the dynamic viscosity (η*), storage modulus (G') and loss modulus (G") were extracted.

3.3.1.4 Instruments

3.3.1.4.1 Rheometrics Fluid Spectrometer (RFS II)

Most rheological measurements in this thesis were performed on a Rheometrics Fluid Spectrometer (RFS II). This instrument is a typical strain controlled rheometer consisting of several main parts as shown in Fig. 3.3. The main unit includes a transducer, measuring system, motor and control panel. The transducer system has a dual torque range of 0.002-10 g·cm and 0.02-100 g·cm for measurement of the shear force. It has also a normal force transducer. The temperature is controlled by the water circular bath which is attached to the lower plate of the measuring system.

There are several types of measuring geometry that can be used with RFS II, including plate-plate, cone-plate, couette (cylinder) and concentric double cylinder. The first three geometries were used in the current project and are therefore briefly described here. In this instrument, the lower plate (or outer cylinder in the couette geometry) is driven by the motor to exert a certain shear strain (steady or dynamic) on the sample and the

resulting shear stress through the sample to the upper plate (inner cylinder in the couette geometry) is measured by the transducer.

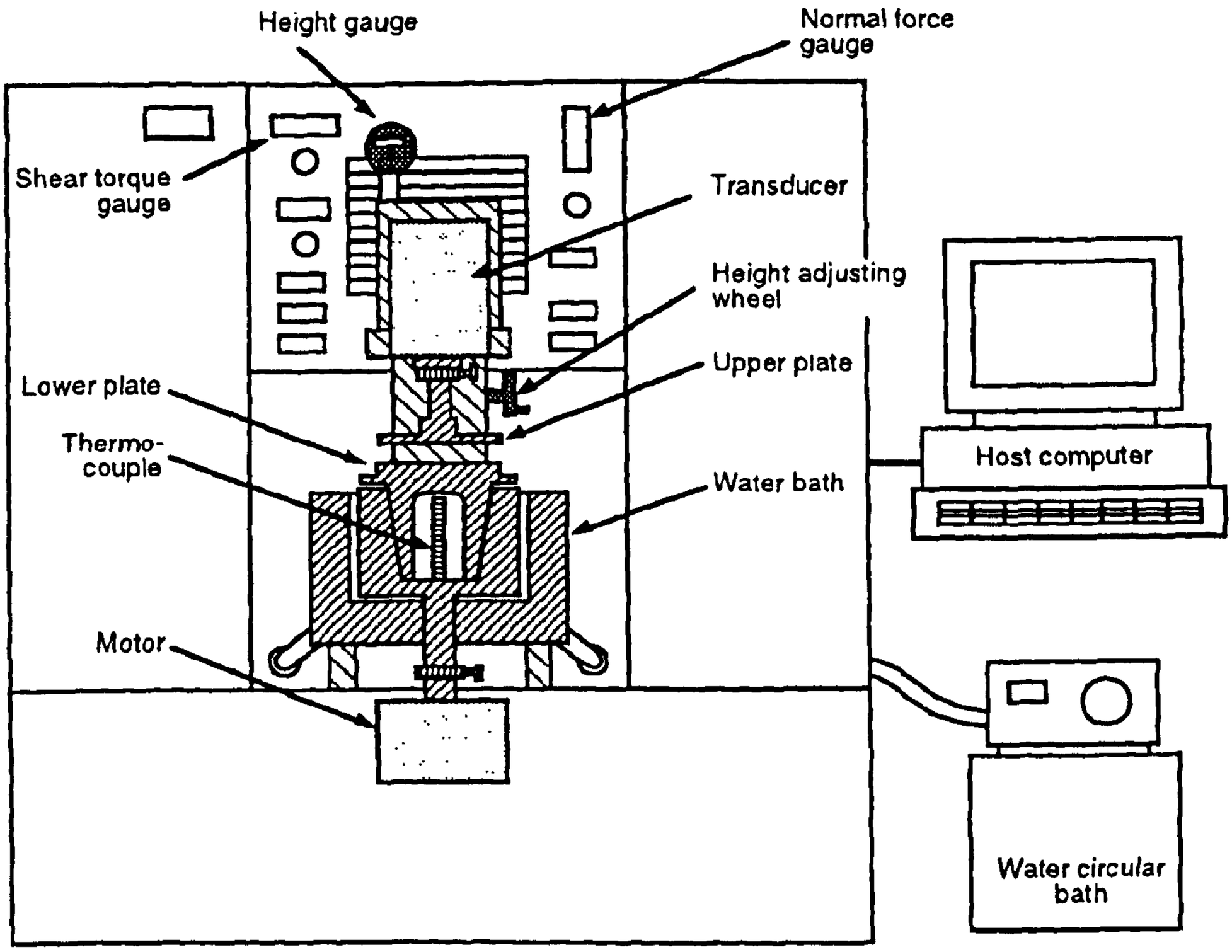

Fig. 3.3 Rheometrics Fluid Spectrometer RFSII - strain controlled rheometer.

In the cone and plate geometry (Fig. 3.4 (a)) the velocity gradient (thus, the shear rate) is designed to be constant throughout the gap. This is especially important when time-dependent behaviour is being studied since the shear history is identical for the whole sample. The major disadvantage for this system being used in particulate suspensions is that small particles may have a disproportionate effect on the behaviour near the cone apex, and the coarse particles may even become jammed between two plates.

In the parallel plate geometry (Fig. 3.4 (b)), the shear rate is not constant across the gap. Therefore, when studying the non-Newtonian materials the shear history is not identical for the whole sample. However, this geometry is found to be more suitable for studying

the particulate suspensions such as partially hydrated guar gum suspensions compared to the cone-plate system.

The concentric cylinder geometry (Fig. 3.4 (c)) consists of two cylinders with a narrow gap in between. Shear flow takes place between inner and outer cylinders. Because of the relatively large measuring surface this geometry is particularly suitable for measuring low viscosity samples when the sample amount is not limited. The main disadvantage of the geometry is again that the shear rate is not constant in the gap. One other practical difficulty of this kind of geometry is that the end effects need to be corrected when accurate absolute measurement is demanded.

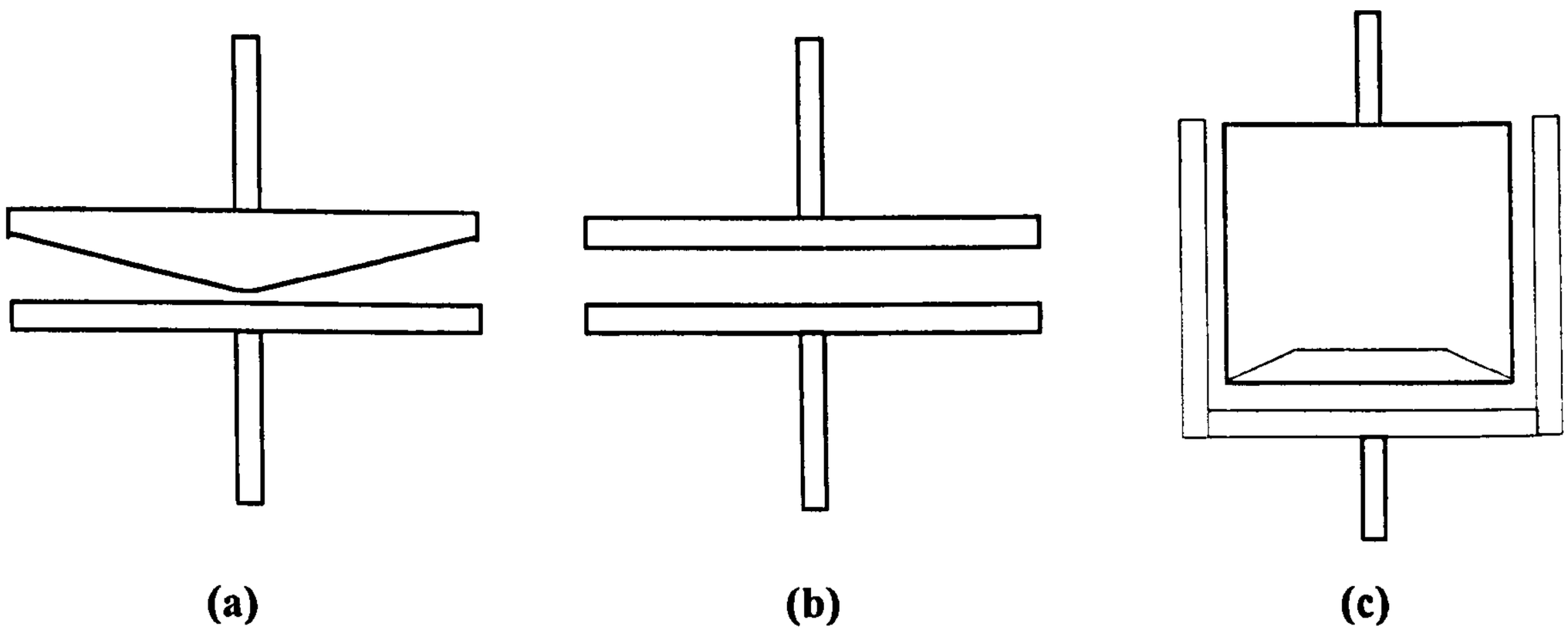

Fig. 3.4 Measuring system used with Rheometrics Fluid Spectrometer RFS II: (a) Cone-plate, (b) Plate-plate and (c) Couette geometry.

3.3.1.4.2 Brookfield viscometer (LVDV-II)

This is a much cheaper rotational viscometer which is widely used in the food and paint industries. In this viscometer a spindle is driven through a calibrated spring in the test fluid and the torque necessary to overcome the viscous resistance is measured by the spring deflection. This deflection is measured with a rotary transducer. The full scale torque of the calibrated spring for LVDV-II is 673 dyne·cm. The viscosity measurement

range is 0.003-1600 Pa.s with different spindles. Temperature control was achieved by an attached water bath.

One problem with this instrument is that it is difficult to state the exact shear rate that the sample is subjected to, because that the width of the sample in shear flow is not well defined. Therefore, the experiment results are normally presented in the form of apparent viscosity against rotational speed. In the experiments presented in this thesis a small sample adapter (chamber) was used. This makes the measuring system similar to the concentric cylinder geometry, which gives relatively accurate viscosity and shear rate determinations.

A set of spindles is provided with the Brookfield viscometer. During the measurements the viscometer can be operated at a series of rotating speeds and shear rates were then calculated using the conversion chart provided with each spindle used. With the small sample adapter the shear rate range usually covers less than two decades for each spindle.

3.3.2. Light scattering technique

Static light scattering technique was used to study the solution properties of detarium gum. The principle of this technique has been discussed in Chapter 2 in detail. Here we just discuss the experimental aspects of this technique. In this thesis the static light scattering measurements were performed with a fully computerised and electronically modified SOFICA photogoniometer (Baur Instrumentenbau, Hausen, Germany). Fig. 3.5 is a schematic diagram of this instrument.

The incident light beam from the laser (1) passes through a neutral density light filter (2) before reaching the quartz scattering vat window (3). The neutral density filter is necessary to reduce the incident light intensity so that at 90° the signal value of a toluene standard is around 4000, which ensures that the sample scattering can be covered by the full range of the analysis electronics. The sample cuvettes (4) are made of quartz and the scattering vat (5) is filled with a solvent which closely matches the refractive index of

quartz; this minimises signal flare. The resulting scattered light then passes through a series of slits and prisms (6 - 10) before reaching the photomultiplier tube (11). The photomultiplier tube is mounted on a goniometer which rotates to allow measurements to be made over an angular range.

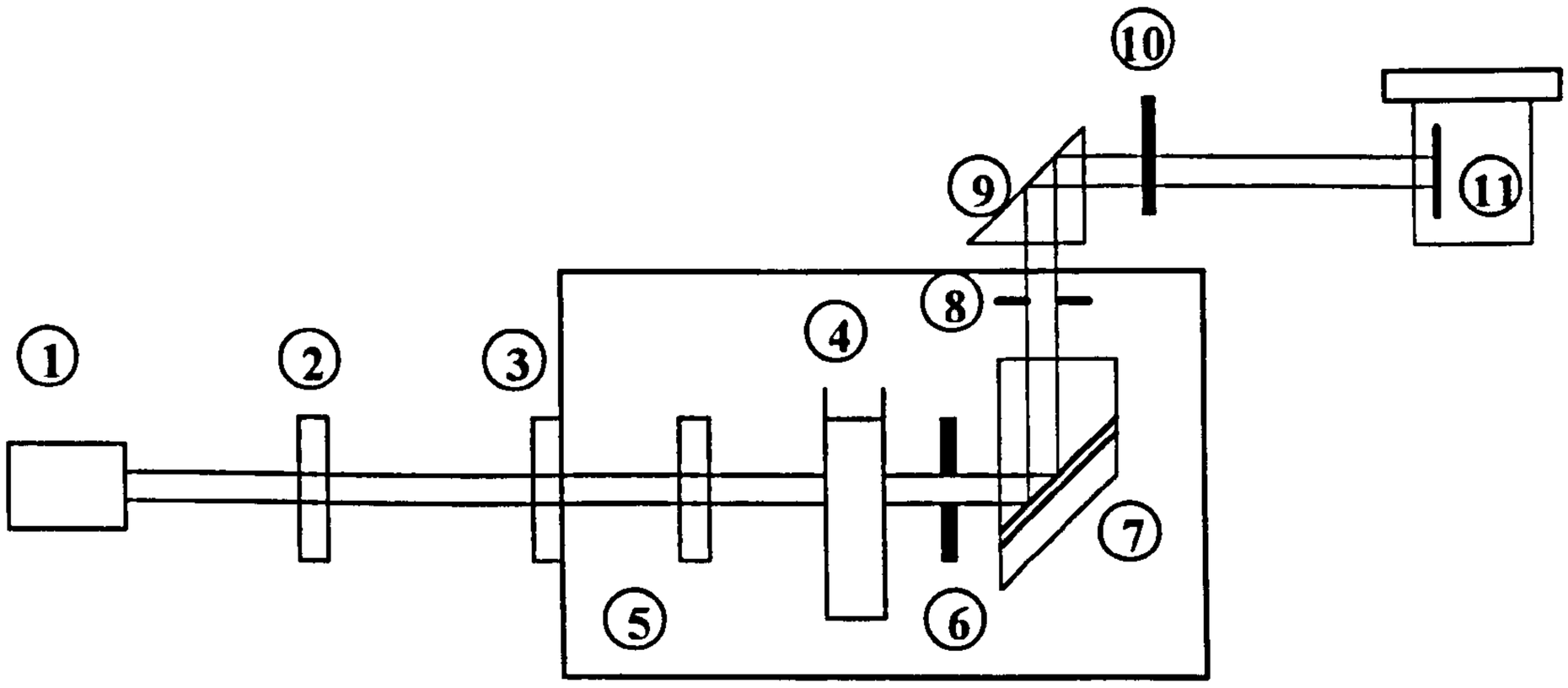

Fig. 3.5 Schematic representative of the modified Sofica light scattering apparatus. (1) Argon, blue laser, (2) density light filter, (3) vat window, (4) sample cuvette, (5) scattering vat, (6) - (10) slits or prisms and (11) photomultiplier tube.

Measurements were performed at 25°C in the angular range from 30^0 to 150^0 in steps of 5^0 (25 angles). An argon ion source (λ_0 = 488 nm) was the light source, and the scattering of toluene was used as the primary standard. The instrument automatically repeats measurements until data less than a predefined noise level (2%) are obtained. The refractive index increment, dn/dc was chosen as 0.152 ml g^{-1}, a value close to that employed for other polysaccharides at this wavelength.

Detarium solutions for light scattering were prepared by heating ca. 20 ml of solution close to C* (~ 0.1% w/w) to high temperatures (130°C to 160°C), sealed under a pressure of 15 bar N_2, for varying times. The autoclaved solution and serial dilution (1.0, 0.8, 0.6, 0.4, 0.2, 0.1) were then filtered (3 times) directly into the light scattering cuvettes (precision NMR tubes, total volume ca. 2 ml) using 0.22μm Millipore syringe filters. All solution preparation stages were carried out in a laminar air flow cabinet to minimise contamination with dust.

Following the pressure heating process, a small amount of non-dissolved material was seen. In order to see if this made up a significant fraction of the sample, 50 ml of the ca. 100 ml of solution was freeze dried after filtering, and the yield of material estimated. This was found to be ~ 95.5%, so in subsequent determinations the presence of this undissolved fraction was ignored. Subsequent filtration through 0.45μm Millipore filters was easy, as no real pressure had to be applied. This intimated that the solutions were largely aggregate free.

The light scattering measurements were performed at the Institute of Macromolecular Chemistry, Freiburg-i-Br, Germany by Professor S.B. Ross-Murphy.

3.4 Particle size analysis

The choice of methods for particle size analysis is limited by the particle size range and also the available experimental conditions. Since the sample involved in this project have a wide range of particle size, several techniques have been used for particle size analysis. They are the traditional sieving method, measurement of permeability by Fisher sub-sieve sizer, Malvern laser diffraction method and microscopy method.

3.4.1 Sieving method

The minimum number of sieves needed in order to obtain some information on the cumulative particle size distribution is usually five (Jelinek, 1970). Sieves should be selected so as to have the median average of particle size on the central sieve. The sieves used in this experiment forms the series of $d_n = \sqrt{2}\, d_{n-1}$, where d is the average aperture. The sample size required for the analysis depend upon the sieve area, particle fineness and density of the particles. Conventionally 20-60 grams of fine grained sample is used for sieves 200 mm in diameter.

The sieving process was performed on a mechanical sieve shaker [Endecott test sieve shaker, Endecotts Ltd., London SW19, UK). 30 gram of each sample was placed on the

top coarse sieve. In a sieving operation, a particle will not necessarily pass through the appropriate mesh, particularly if it will only pass through when presented in a particular orientation as with elongated particles. For all such particles to pass through, the sieving time would approach infinity. For the present study the sample was first automatically sieved for one hour. Then a soft paint brush was used to help the fine particle pass through the sieves. The sieving process was assumed finished when the rate of weight reduction for each mesh was less than 0.2 g/min. Each sample was analysed in duplicate.

3.4.2 Malvern laser diffraction particle sizer

The principle of this instrument is to analyse the diffraction from the particles selected. A low power visible laser transmitter produces a parallel, monochromatic beam of light which illuminates the particles suspended in an appropriate solvent in the sample cell. The particles must not dissolve or swell in the selected solvent and the solvent has to keep the particles well suspended. The incident light is diffracted by the particles illuminated to give a stationary diffraction pattern regardless of particle movement. As particles enter and leave the illuminated area the diffraction pattern that evolves always reflects the instantaneous size distribution in these areas. Thus, by integration over a suitable period and using a continuous flux of particles through the illuminated area, a representative bulk sample of the particles contributes to the final measured diffraction pattern.

A Fourier transform lens focuses the diffraction pattern onto a multi-element photo-electric detector which produces an analogue signal proportional to the incident light intensity. This detector is directly interfaced to a computer which reads the diffraction pattern and performs the necessary integration digitally. The result of the analysis is basically a size distribution by volume or weight, but it may be presented in a variety of ways. The cumulative volume undersize and volume frequency are tabulated together with useful derived parameters.

In our experiment guar gum samples were dispersed in butan-1-ol solvent and left in an ultrasonic bath for five minutes in order to break up any aggregates of particles. During

measurements a magnetic stirrer was used to ensure homogenised suspension of particles. No swelling or dissolution of samples was observed in this solvent when examined by light microscopy.

3.4.3 Measurement of permeability by Fisher sub-sieve sizer

This technique measures the specific surface area by the measurement of gas-flow resistance of the sample. A weighed quantity of the test sample, in a cylindrical container, is compacted to a definite volume. Then a stream of air is passed through, and the pressure drop caused by the plug of power is measured. From this, the specific surface area, A_{sp}, can be calculated from the Kozeny Carman equation (Lauer, 1966):

$$A_{sp} = 14[(p\ F\ e^3)/(v\ \eta\ L)]^{1/2}/b\ (1 - e) \qquad (3.7)$$

where: F is the cross section of sample, L is the length of sample, b is the sample density, e is porosity (the ratio of the spaces between the particles in the plug of sample to the volume it occupies), p is the pressure drop, v and η are the flow rate and viscosity of the air used respectively. Surface volume mean diameter D_m can be calculated from A_{sp} as follows:

$$D_m = 6x10^{-4}/\ b\ A_{sp} \qquad (3.8)$$

The current available Fisher sub-sieve sizer enable the operator to read the surface volume mean diameter D_m directly, from which the specific surface area can be calculated from equation 3.8.

The density of the guar gum sample was measured using Beckman Model 930 Air Comparison Pycnometer. This instrument measures the volume of powder precisely and rapidly. The measurements obtained should be repeatable to better than 0.05 cm^3. Samples were weighed to the accuracy of 0.01g.

3.5 Morphological observations

3.5.1 Light microscope

Detarium seed cotyledon were immersed in 75% (v/v) ethanol and cut into 1 mm^3 cubes. Samples were fixed in 4% (v/v) paraformaldehyde in phosphate buffered saline for 24 hours at room temperature, dehydrated by graded ethanol serial dilution (5%, 25%, 40%, 55%, 70%, 95%, 100%, v/v) and finally infiltrated and embedded in glycolmethacrylate (GMA) using a JB-4 embedding kit (Polyscience Ltd.).

Sections were cut at 7μm thickness on a Reichert-Jung 150 Autocut Microtome fitted with a glass knife. Then the sections were stained with an iodine-potassium iodide reagent (Kooiman, 1960) or with the plant lectin from *Bandeiraea simplicifolia* (BS-1; Sigma Chemical, Poole BH17 7BR, UK), which is labelled with fluorescein isothiocyanate (FITC) and is highly specific for α-D-galactose residues (Hayes, 1974). Samples were examined under light or epifluorescence using a Leitz Dialux 22 FB microscope with appropriate barrier filters (A2, excitation range 270-380 nm). Images were photographed with a Wild MP551 camera system.

For guar gum flours the samples were dispersed onto clean microscope slides using butan-1-ol as a mounter. Slides were then examined.

3.5.2 Scanning electron microscope

The scanning electron microscope (SEM) is widely used to study the surface, or near surface structure of the materials. This method employs a beam of electrons directed to the specimen. This incident electrons was dissipated resulting in various secondary emissions from the specimen. Among these emissions the secondary electrons and backscattered electrons were detected to yield the images of the specimen. Fig. 3.6 is a schematic diagram showing the main components and the mode of operation of a simple SEM.

A electron gun, usually of the tungsten filament thermionic emission type, produces electrons, and accelerates them to an energy between about 2 KeV and 40 KeV. Two or three condenser lenses then demagnify the electron beam, so that as it hits the specimen it may have a diameter of only 2-10 nm. The fine beam of electrons is scanned across the specimen by the scan coils, while a detector counts the number of low energy secondary electrons given off from each point on the surface. At the same time, the spot of a cathode ray tube (CRT) is scanned across the screen, while the brightness of the spot is modulated by the amplified current from the detector.

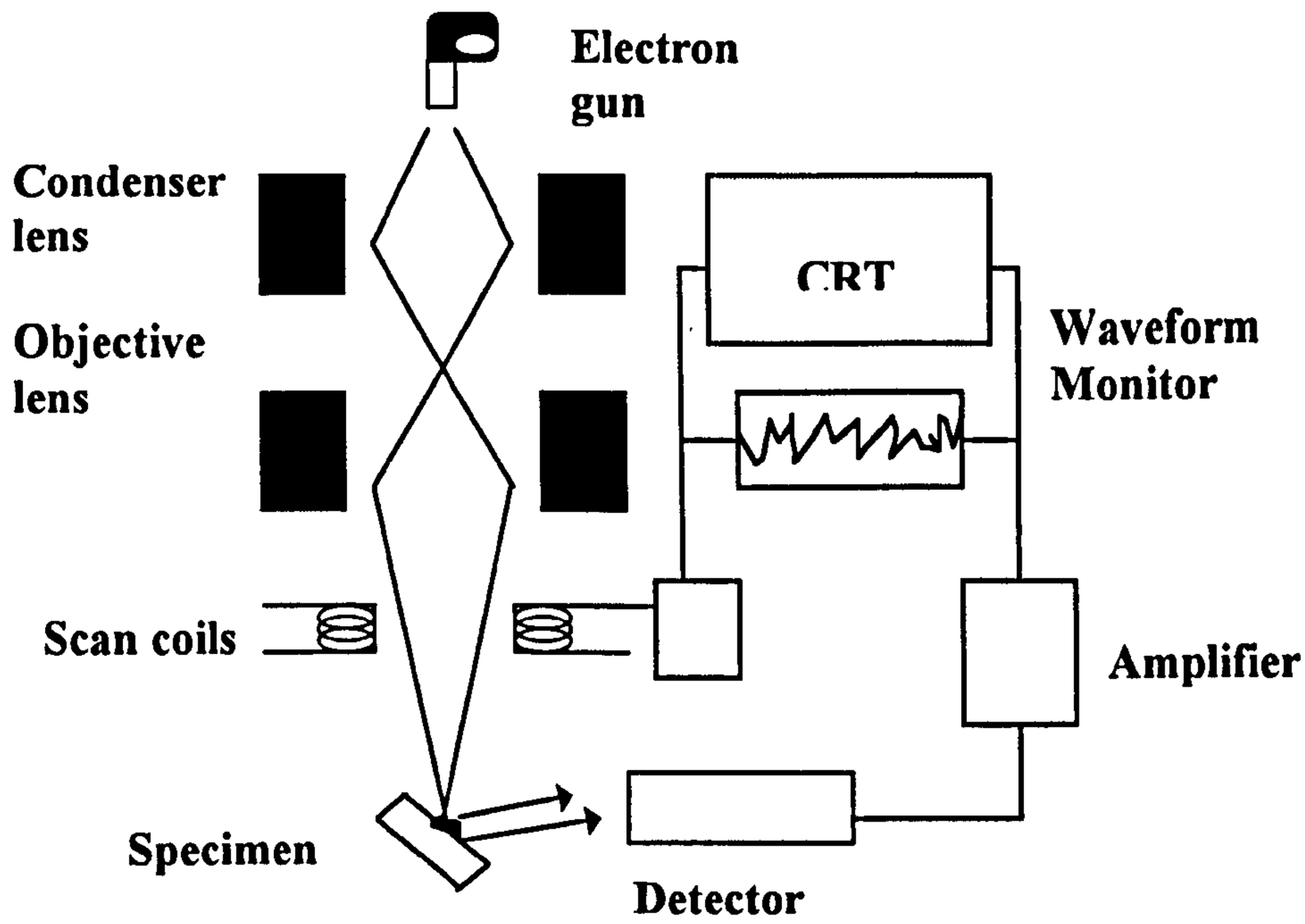

Fig. 3.6 Schematic diagram showing the main components of a SEM.

The most critical part of scanning electron microscopy is adequate preparation of the specimen. The specimen is usually mounted on a aluminium stub with an electrically conductive adhesive material. It is important for the specimen to be in close and tight contact with the stub. Materials such as biopolymers do not conduct electricity and heat very well, therefore, have to be coated with a conductive substance. In our experiment, double sided adhesive tape was used to mount the specimen to the stub. The tape was firstly firmly attached to the stub and the sample powder was scattered carefully over its

surface. The stub with the specimen then were sputter coated with a thin layer of gold (Polaron Equipment Ltd, SEM coating unit, E5100) to make the specimen conductive. The specimens were examined in a Philips SEM 501B. Photographic images were recorded on Ilford film ISO 125, 220.

3.6 Hydration method

The hydration method used in this study is a modified technique previously developed for measuring the hydration rate of pharmaceutical preparations of guar gum (Ellis and Morris, 1991). The hydration of guar gum powder was performed in a mixing box (constructed in the King's College workshop, Fig. 3.7). The mixing box was fitted inside an incubator to allow good control of experimental temperature. 500 ml sample dispersion was sealed in a screw-top glass jar (diameter 84 mm, volume 675 ml) which rotated end-over-end during the hydration process. The average rotating radius is 65 mm. The hydration process is monitored by measuring viscosity development and the zero-shear viscosity was determined as described in Section 3.3.1.2.

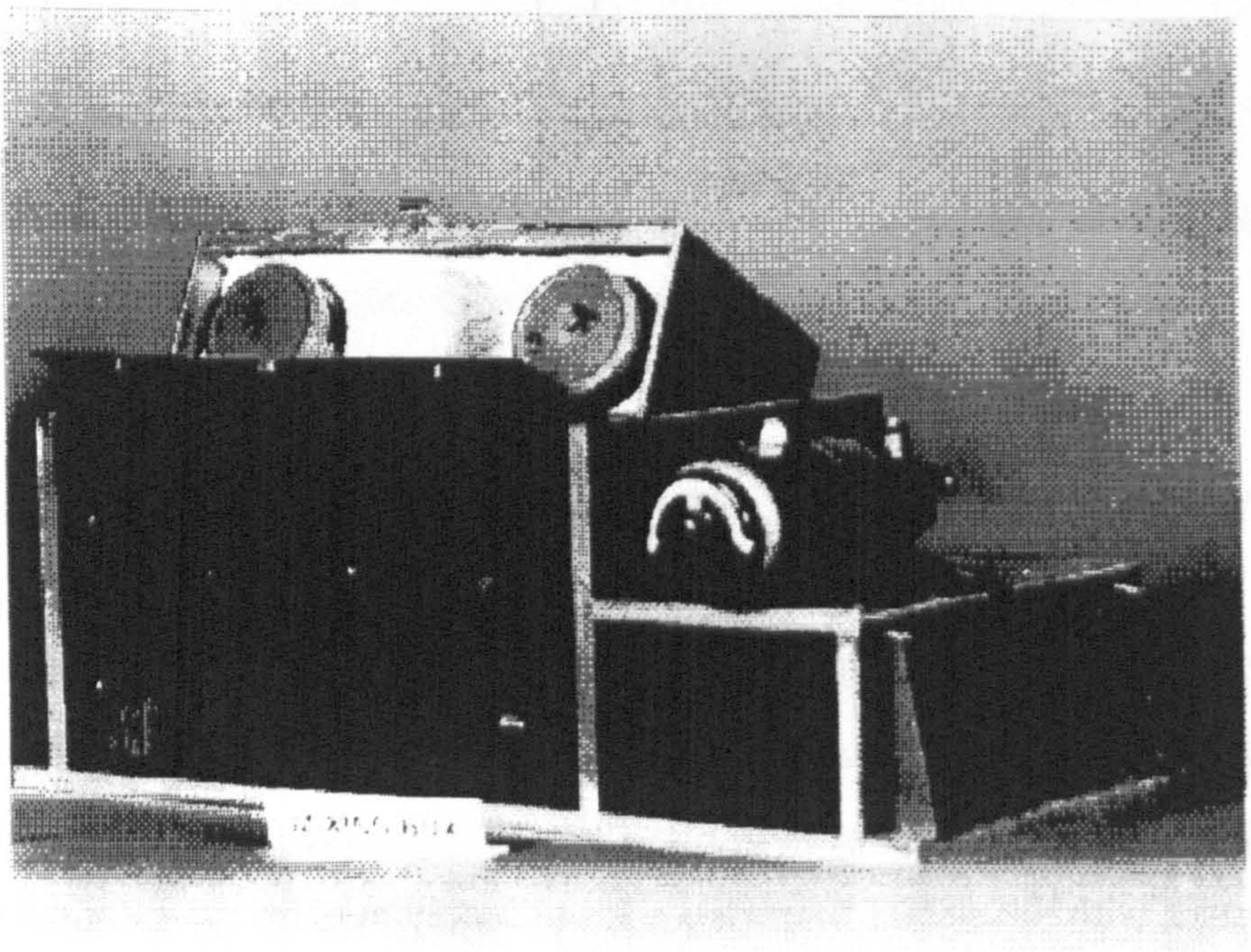

Fig. 3.7 Rotating box for hydration of samples.

The procedure involved carefully sprinkling the guar gum into a rapidly swirling vortex of distilled water in the glass jar. A magnetic stirrer was used to create the vortex in the distilled water. A ring shaped sieve (355μm in aperture, Fig. 3.8) was used to disperse samples into the water. This ensured the sample could be dispersed evenly and rapidly into the wall of the water vortex created by the magnetic stirrer. This technique also effectively reduced aggregation of particles. The time taken to add the whole of each sample to the water did not exceed 90 s. The start of hydration was taken as the moment the guar gum made contact with water. The glass jars were then immediately sealed and rotated end-over-end in the mixing box at a predetermined speed. The viscosity was measured at every 10 min in the first hour and thereafter every 30 min until 5 h. About 2 ml aliquot was taken from the batch solution at each time point. It took about 3 min for the process of viscosity measurement. An additional measurement was taken following thorough homogenising with an Ultra-turret mixer. This measurement is referred to as the "ultimate" viscosity, the point at which it was considered that the samples had been completely hydrated. This hydration method was slightly modified in the experiments described in different chapters and these modifications are specified in each chapter.

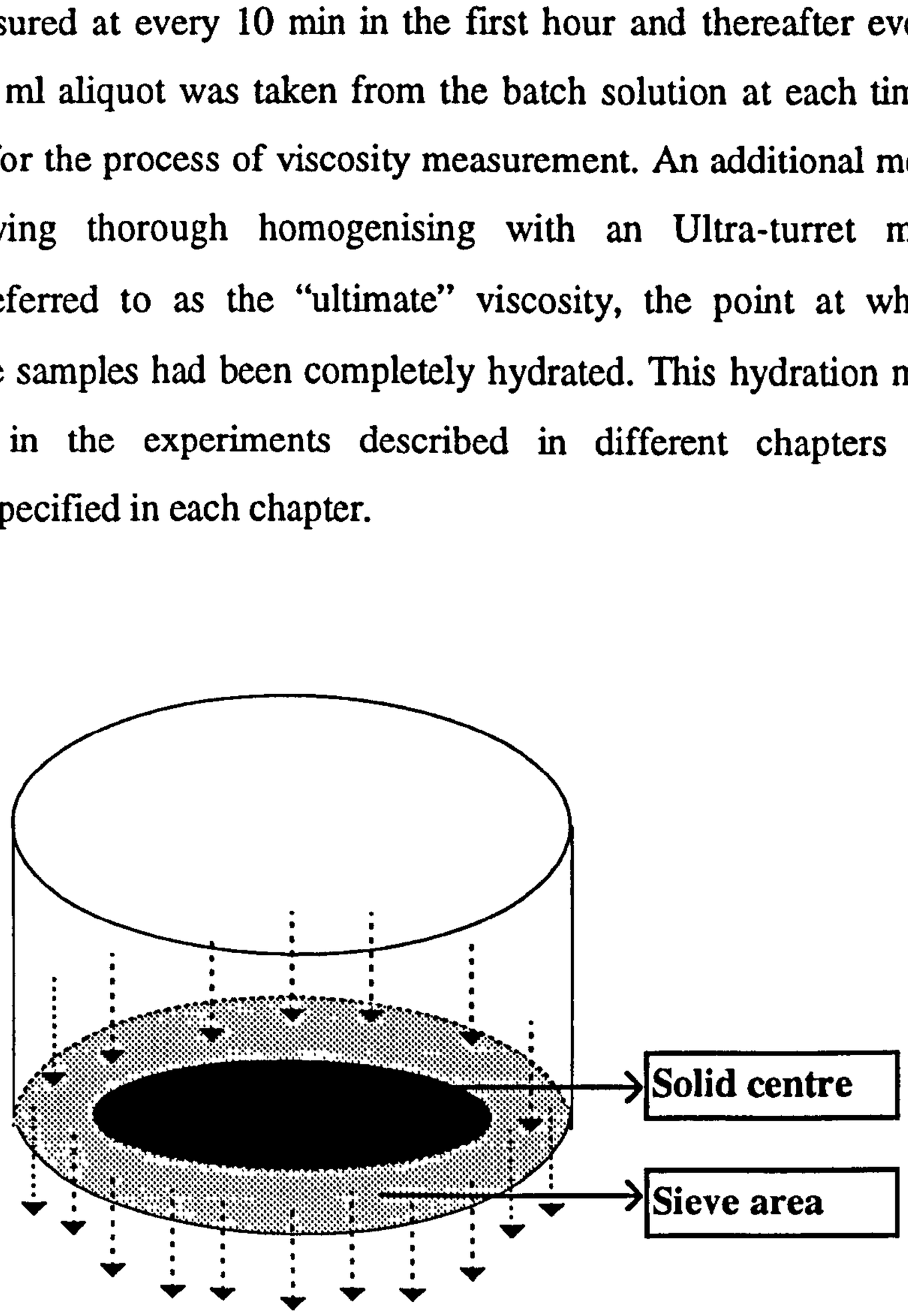

Fig. 3.8 Figure to show the ring shaped sieve for dispersion of the guar samples into the water vortex in sample jar.

Chapter 4

Isolation and chemical characterization of s-NSP from detarium seeds

4.1 Introduction

Detarium senegalense Gmelin is an under-exploited and previously largely uncharacterised leguminous crop. The seed flour of detarium is used traditionally in Nigeria as a food condiment for the thickening of soups and stews. This food material was one of a number of indigenous African plant foods, which are used in Nigeria as thickeners for foods, to be evaluated for their potential therapeutic application in treating patients with diabetes mellitus (DM) (Onyechi, 1995). The underlying hypothesis for the work on these foods is that they contain a high level water soluble non-starch polysaccharides (s-NSP), which may therefore assist in improving carbohydrate metabolism in patients with DM. It has been known since 1970's that s-NSP reduce postprandial hyperglycaemia in these patients (Jenkins, *et al.*, 1976; 1978).

In recent clinical trials, significant reductions in the post-prandial rise in blood glucose and insulin concentrations were seen in healthy (Onyechi, *et al.*, 1993) and diabetic (Onyechi, 1995) human subjects given foods supplemented with detarium seed flour. This implies that detarium has potential clinical use in the treatment of diabetes mellitus and other metabolic disorders, although the mechanism of this is still unclear.

Chemical analysis by Bell *et al.* (1993) showed that detarium seeds have a high level of s-NSP (43% by dry weight). Monosaccharide analysis of s-NSP indicated that the main polymer was similar in composition to tamarind seed (*Tamarindus indica* L.) xyloglucan (Bell, *et al.*, 1993). A preliminary study of solution properties of a purified extract of

this polymer showed that it was similar to the behaviour of solutions of a commercial grade of guar gum (Ellis, *et al.*, 1991). As has been mentioned in Chapter 2, the physiological effects of guar gum and similar hydrocolloids are strongly dependent on their capacity to generate high levels of viscosity in the upper gastrointestinal tract (Ellis *et al.*, 1995). It seems likely that the s-NSP fraction of the detarium seed is of high molecular weight polysaccharide and, at least in part, responsible for its biological activity.

Exploiting new and cheap sources of s-NSP has always been of considerable interest to a range of industries. Indeed it may be that the seeds are a potential cash crop ripe for exploitation. Thus, the purpose of this study was to further characterise the structure and solution properties of purified s-NSP extracted from the seed cotyledons of detarium, and to investigate its location within the seed using histochemical techniques. The current chapter will concentrate on the chemical characterization of detarium gum, the solution properties of which will be investigated in Chapter 5.

In the current and subsequent chapters, an unambiguous shorthand nomenclature for xyloglucan oligosaccharides is used (Fry, *et al.*, 1993). Each (1→4)-β-linked D-glucosyl residue in the backbone is given a 1-letter code according to its substituents. Thus, G = unsubstituted glucose residue; X = xylose-substituted glucose residue; L = galactosyl-xylose-substituted glucose residue; F = fucosylgalactosylxylose-substituted glucose residue. Sequences always read towards the reducing end of the molecule.

4.2. Experimental

4.2.1 Characteristics of detarium seed and preparation of seed flour

Detarium senegalense Gmelin belongs to the subdivision *Caesalpinoideae* (Balogun and Fetuga, 1986; FAO, 1988). Its tree is small to medium-size, normally 5-7 m high,

occasionally larger, and it is mainly found in West Africa, Chad and Sudan. The pods, each of which contain one seed, are usually rounded, oval or flattened and are about 4 cm in diameter. The seed samples used in the present study were purchased at a local market in Nsukka, Enugu State, Nigeria and then stored at -20°C for later use.

The detarium seed flour was prepared in the following way. The seed coats (testae), which are a deep brown purple colour, were removed after boiling in water for about 1h. The cotyledons were soaked in cold water for 1 h, washed three times and left to soak in cold water overnight. The cotyledons were then air-dried for about 24 h and ground into a fine powder (to pass through a 1 mm screen) using a coffee grinder. The powder was further dried at room temperature for 24 h and stored at -20°C.

4.2.2 General methods

A number of general experimental methods used in this chapter have been described in Chapter 3. These include:

(1) Analysis of chemical compositions of detarium seed flour and s-NSP extracts (Section 3.2.1).

(2) Extraction and purification of s-NSP from detarium seed flour (Section 3.2.2).

(3) Analysis of constituent sugars by gas-liquid chromatography (Section 3.2.3).

(4) Morphological observations of detarium seeds (Section 3.5.1).

4.2.3 Structural analysis of detarium polysaccharide

4.2.3.1 Enzymatic digestion of detarium and tamarind polysaccharides

Cellulase from *Trichoderma species* was purchased from Megazyme Pty. Ltd. (North Rocks, New South Wales, Australia). It was dialysed exhaustively against 50 mM ammonium acetate buffer at pH 5.0 (Dialysis tubing-Visking, size 1-8/32″, Medicell International Ltd, London N1, 1LX). Because the dialysis tubes selected are made of cellulose, the dialysis process has to be carried out at very low temperature (4 °C).

200 µl (12 mg/ml) of both detarium polysaccharide and xyloglucan from tamarind seed (Glyloid 3S, Dainippon Pharmaceutical Corporation, Osaka, Japan) were incubated with 80 µl cellulase (approximately 8 Units) in 200 µl ammonium acetate buffer (50 mM, pH 5.0). Aliquots of the incubation were taken at time points 0.5 h, 1 h, 2 h and 4 h. The enzyme reaction was terminated by heating the samples in a boiling water bath for 2 min. The extent of hydrolysis was monitored by thin layer chromatography (TLC) (see below for details). The hydrolyses were considered complete when there was no apparent change in the pattern of oligosaccharides produced. The oligosaccharides of the final hydrolysate were analysed quantitatively by Dionex HPAE chromatography (see below).

4.2.3.2 Thin layer chromatography

Thin-layer chromatography was carried out on aluminium foil-backed silica-gel layers with 0.2 mm in thickness (Merck DC-Alufolien, Kieselgel 60, E. Merck, Darmstadt). The developing solvent used was propan-1-ol 5 : nitromethanol 2 : distilled water 3 (by volume). The development was repeated 3 times and the plates were spray dried before the next run. The oligosaccharides were then detected by spraying lightly with a 10% (w/w) sulphuric acid solution in concentrated ethanol and the plates were heated in a dark oven at 140 °C for 5 minutes.

4.2.3.3 High-performance anion-exchange chromatography

As practical instruments for high-performance anion-exchange chromatography (HPAEC) became commercially available, HPAEC has become a powerful tool for carbohydrate research. In HPAEC, strong alkaline solutions, usually NaOH, are used as eluent. Under these conditions the hydroxyl groups of carbohydrates are transformed into oxyanions, thereby enabling carbohydrates to be chromatographed as anions (Lee, 1990).

The current HPAEC analysis of oligosaccharides from detarium and tamarind polysaccharides digest was carried out using a Dionex BioLC chromatography equipped

with CarboPac PAI anion-exchange column (250 x 4 mm Dionex, Camberley, UK), pulsed amperometric detector and microinjection system. The sample (2-10 μg) was applied to the column and the column was then eluted with a gradient of sodium acetate (50-100 mM) in sodium hydroxide (100 mM).

4.3 Results and discussion

4.3.1 Chemical compositions of detarium flour and s-NSP extract

The macronutrient composition of the detarium seed flour (Table 4.1) indicated that most of the polysaccharide material was in the form of water-soluble, non-starch polysaccharide (59.8 g/100g dry matter). A high yield of s-NSP was extracted from the original detarium seed flour (51.4 ± 1.7 g/100g dry matter) using the method described in Chapter 3.

Table 4.1 Macronutrient composition of detarium flour (g/100g dry matter).

Component	Amount	S.D.[a](±)
Protein	14.1	0.03
Fat	8.2	0.8
Starch	0.4	0[b]
s-NSP	59.8	0.9
Total NSP	62.2	1.1
Ash	2.7	0.03

[a] S.D. = standard deviation. [b] Single value only.

The s-NSP content of the extract was found to be 91.8 ± 1.7 g/100g dry matter measured by the Englyst method (see Chapter 3). The results of the compositional analysis are presented in Table 4.2 and Fig. 4.1. The main monosaccharide components of s-NSP were glucose, xylose and galactose in the ratio of ~ 2.67 (± 0.04): 1.92 (± 0.04): 1 (± 0.02), respectively. This was close to the values reported for tamarind seed

xyloglucan which was ~ (2.8-2.9): (2.1-2.25): 1, respectively (Gidley, *et al.*, 1991; Buckeridge, *et al.*, 1992).

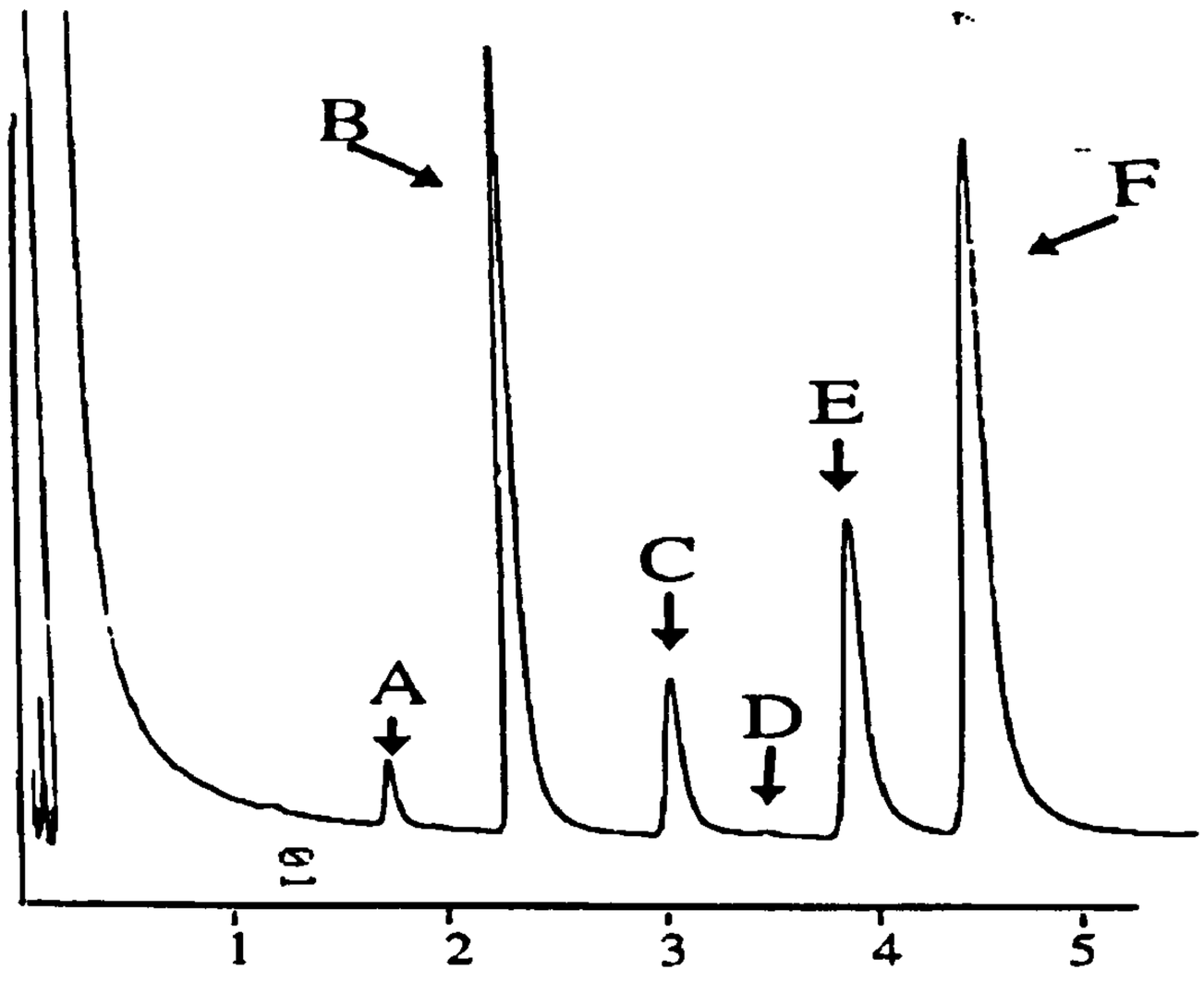

Fig. 4.1 Gas-liquid chromatogram of the alditol acetates from a hydrolysate of water-soluble non-starch polysaccharide extracted from detarium seeds, where A, arabinose, B, xylose, C, allose, D, mannose, E, galactose and F, glucose.

4.3.2 Structural analysis

To determine whether or not the s-NSP extract of detarium is a xyloglucan similar to that from tamarind seeds, samples of both polysaccharides were digested with a pure endo-(1→4)-β-D-glucanase of fungal origin. This enzyme is known to hydrolyse tamarind and other seed xyloglucans to a mixture of the four subunit oligosaccharides XXXG, XLXG, XXLG, XLLG as shown in Fig. 4.2 (York, *et al.*, 1990; Fanutti, *et al.*, 1991; Buckeridge, *et al.*, 1992).

Table 4.2 Monosaccharide composition of the water-soluble non-starch polysaccharide extract and flour from detarium seeds (g/100g dry matter).

	Polysaccharide extract		Flour	
Monosaccharides	Mean	S.D. (±)	Mean	S.D. (±)
Arabinose	1.75	0.14	2.24	0.04
Xylose	30.49	0.53	18.84	0.58
Mannose	0.72	0.14	0.55	0.04
Galactose	15.91	0.52	10.90	0.93
Glucose	42.19	1.21	26.81	1.23
Uronic acid	0.75	0.14	2.81	0.56
Total	91.81	1.71	62.15	0.63

S.D. = Standard deviation

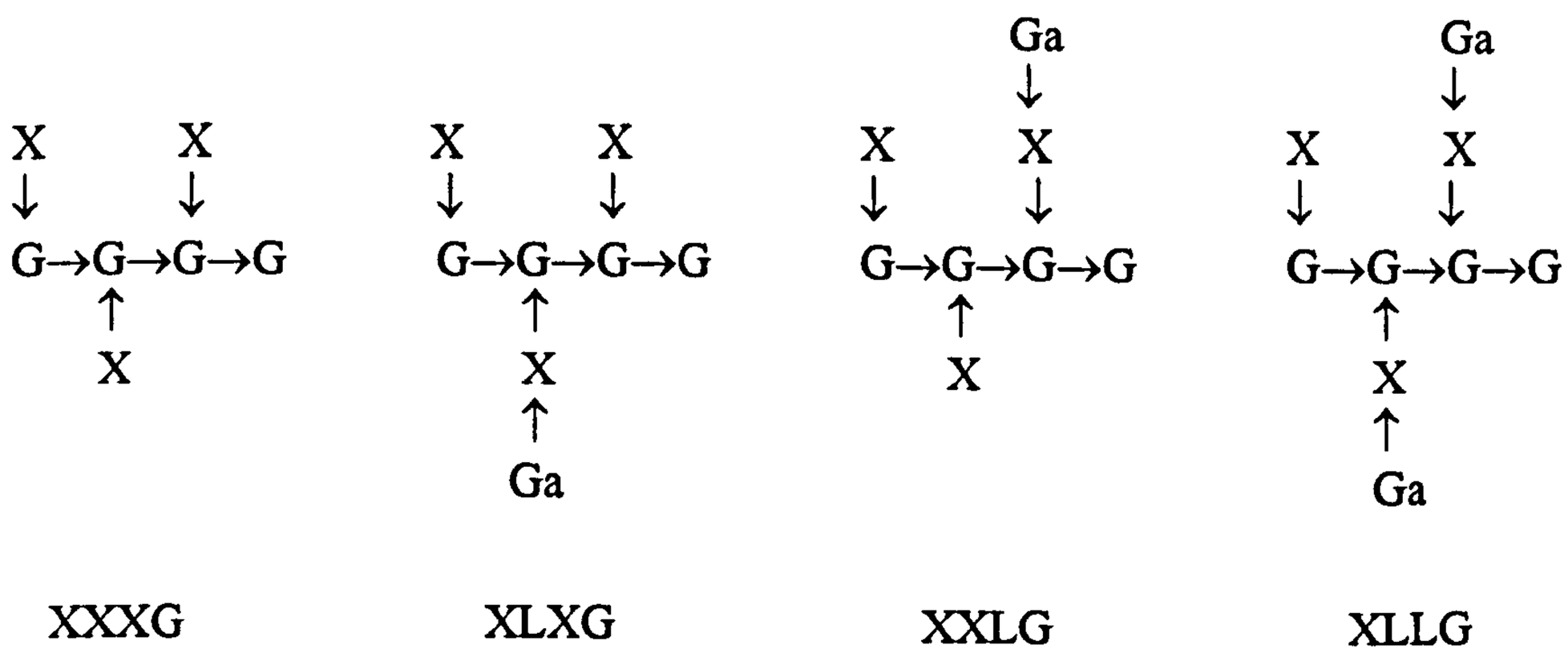

Fig. 4.2 Structure of seed xyloglucan subunit oligosaccharides, where X = xylose, G = glucose, Ga = Galactose.

TLC analysis of the progress of the hydrolysis of tamarind xyloglucan showed that a 4 h incubation was sufficient for the complete conversion of the polysaccharide to three components, previously identified as XXXG, XLXG and XXLG (unresolved) and XLLG (Fig. 4.3, lanes 5-8) (Fanutti, *et al.*, 1991). Exactly the same components were obtained from the s-NSP of detarium over the same time period, indicating that the s-

NSP was also a xyloglucan (Fig. 4.3, lanes 9-13). To confirm this, and to obtain fine-structural information, the two 4 h digests were subjected to HPAE chromatography (Fig. 4.4). As has been observed previously (York, *et al.*, 1990; Fanutti, *et al.*, 1991), the tamarind digest contained peaks corresponding to XXXG, XLXG, XXLG, XLLG in the relative proportions 1.00: 0.42: 2.07: 6.20. The detarium s-NSP contained indistinguishable peaks, but in the relative proportion 1.00: 0.30: 5.60: 6.20. These results confirm that the detarium s-NSP is a xyloglucan, consisting of a cellulosic backbone with single-unit α-D-xylopyranosyl substituents attached to carbon-6 of the glucosyl residues, and with some of the xylose residues further substituted at carbon-2 by β-D-galactopyranosyl residues.

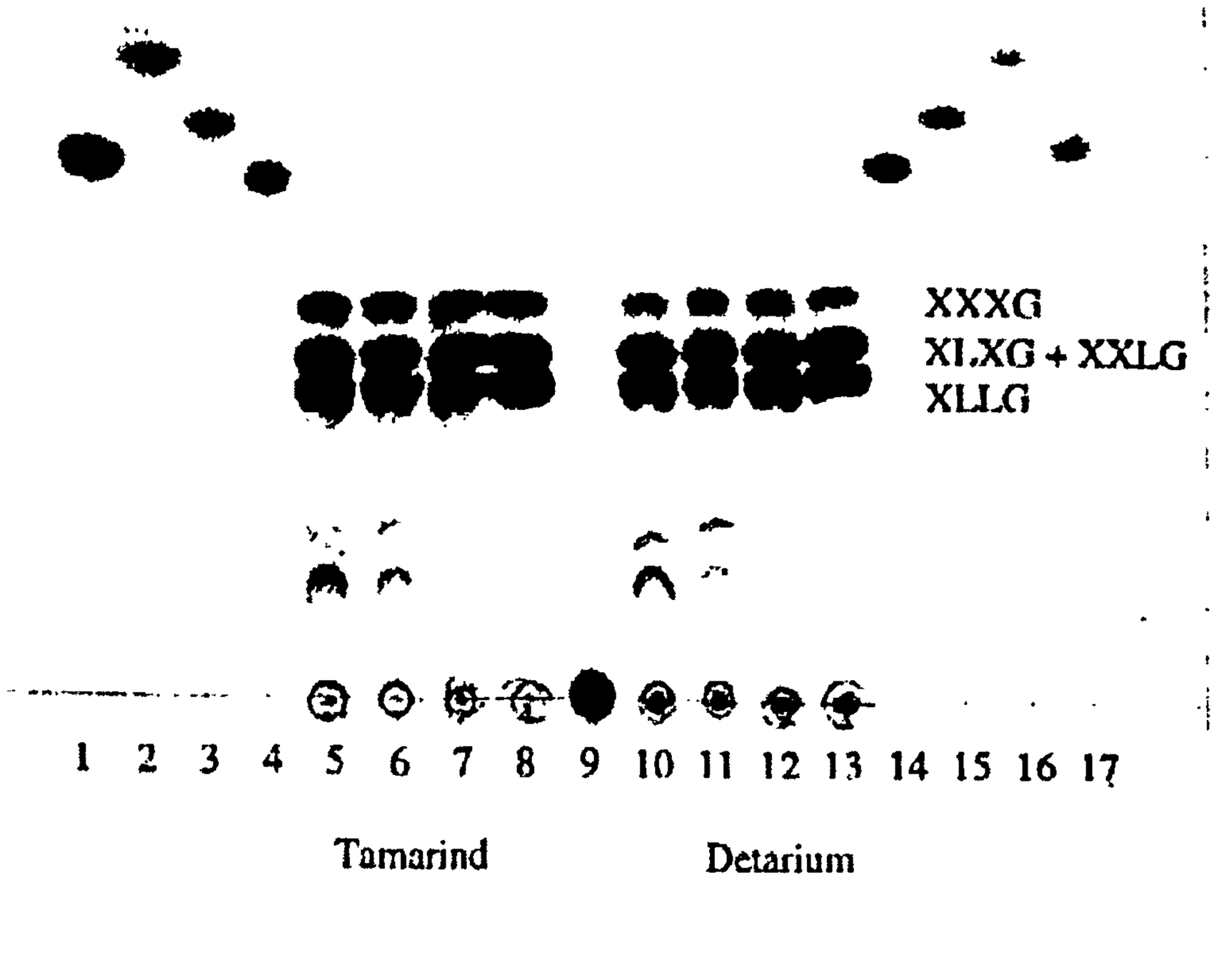

Fig. 4.3 TLC plate showing time-course of endo-(1→4)-β-glucanase hydrolysis of detarium and tamarind polysaccharides. Lanes 1, 17, galactose standard; Lanes 2, 16, xylose standard; 3, 15, glucose standard; 4, 14, cellobiose standard. Lanes 5, 6, 7, 8, digest of tamarind xyloglucan after 0.5, 1, 2, 4 h, showing conversion to XXXG, XLXG and XXLG (unresolved), XLLG. Lanes 9-13, digest of s-NSP after 0, 0.5, 1, 2, 4 h.

The quantitative information on the relative amounts of the four oligosaccharides given by Dionex HPAE analysis allowed deduction of the glc:xyl:gal ratio of the polysaccharides. They were in close agreement with the value obtained by direct hydrolysis (Table 4.3). The degree of galactose substitution of the xyloglucan core is lower in detarium than tamarind. It is interesting to note that in both polysaccharides there is a high amount of the subunit XXLG relative to XLXG. This indicates a non-random distribution of galactosyl-substituents in both polysaccharides.

Table 4.3. Results of HPAEC showing quantitatively oligosaccharides fractions converted from tamarind and detarium xyloglucan when treated with endo-(1→4)-β-glucanase.

	Oligosaccharides ratio				Deduced monosaccharides		
	XXXG	XLXG	XXLG	XLLG	Xyl	Gal	Glu
Tamarind	1.00	0.42	2.07	6.20	1.00	0.51	1.34
Detarium	1.00	0.30	5.60	6.20	1.00	0.46	1.33

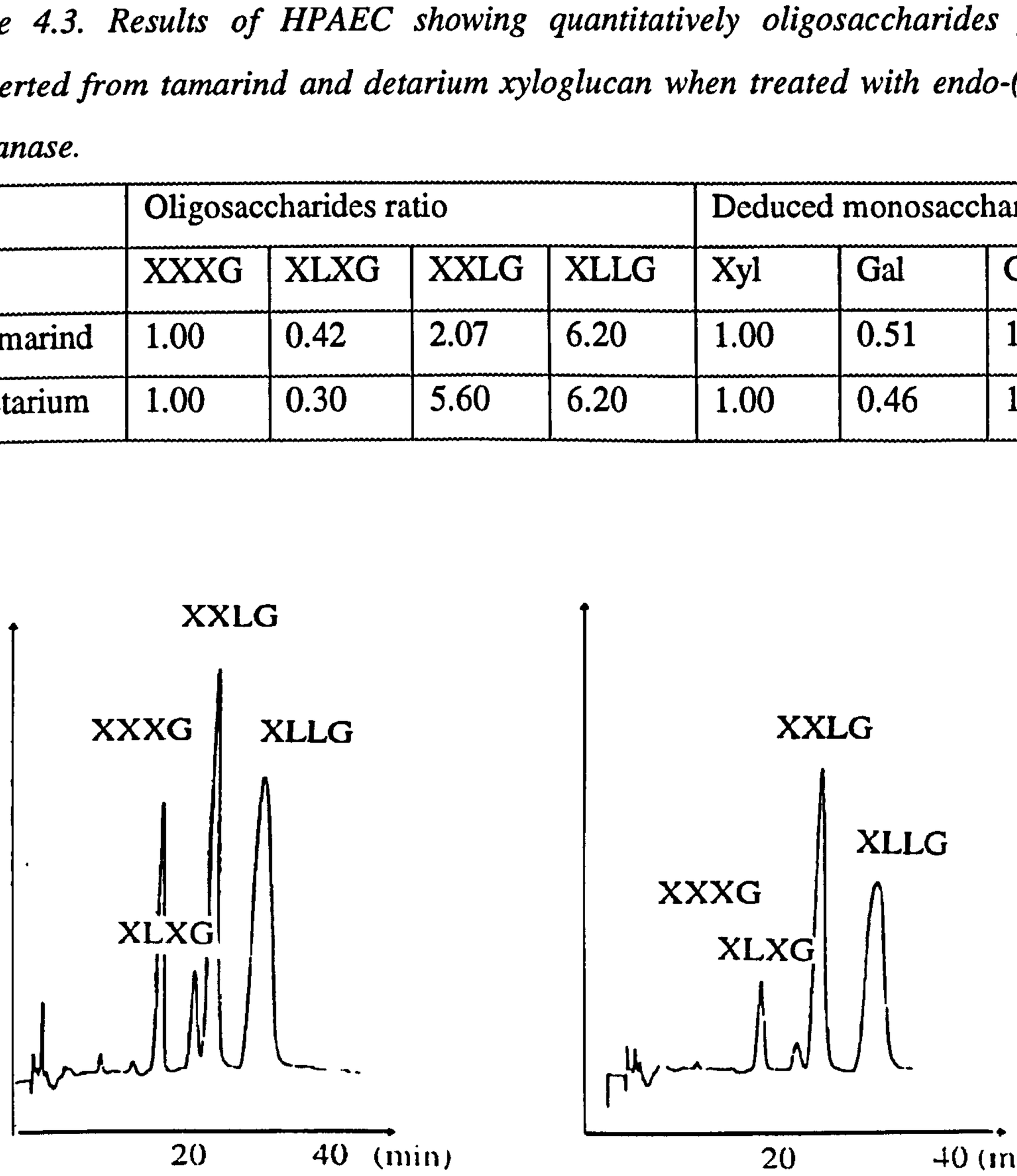

Fig. 4.4 HPAEC trace showing oligosaccharides produced from tamarind xyloglucan and detarium xyloglucan when treated with endo-(1→4)-β-glucanase.

4.3.3 Anatomical observations

Light microscopic examination of the detarium cotyledonary sections showed highly thickened cell walls, which stained bright blue with iodine reagent and were particularly prominent at the cell junctions (Fig. 4.5). This and other morphological characteristics are remarkably similar to those seen for cotyledonary material of tamarind seed (ungerminated), which like many other species of seed xyloglucan, show a blue colour (amyloid reaction) with iodine (Kooiman, 1960a, 1960b). The positive staining of the fluorescein-labelled lectin (BS-1), which is specific for α-D-galactose residues (Hayes and Goldstein, 1974), confirms the presence of xyloglucan in the thickened cell walls of detarium cotyledon. These results suggest strongly that the xyloglucan of detarium seed, which is clearly present as large deposits, functions as a cell wall storage polysaccharide like other seed xyloglucans (Reid, 1985), although germination experiments need to be carried out to confirm this.

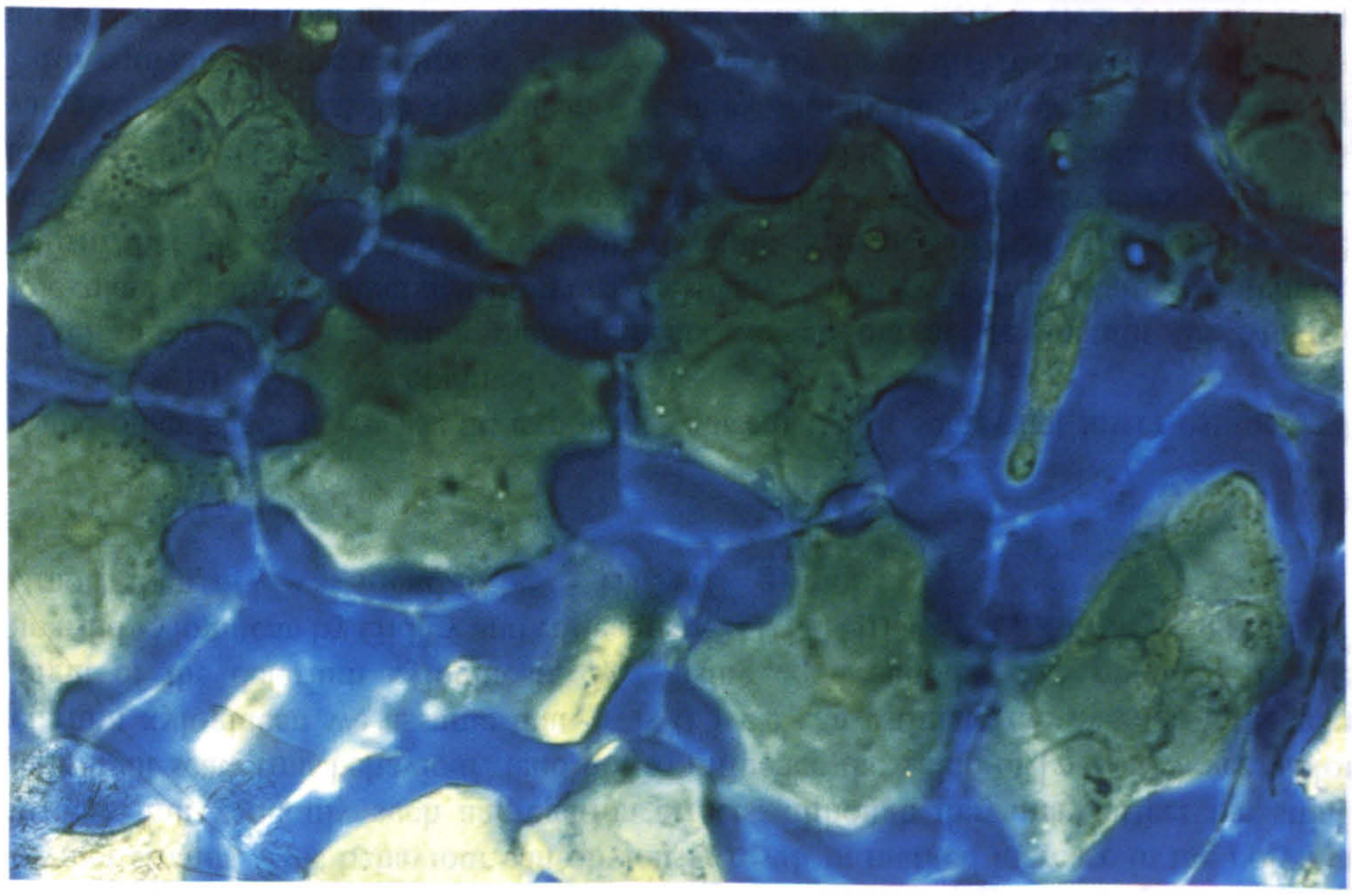

Fig. 4.5 Bright field image of storage cell wall xyloglucan in Detarium seed endosperm stained with iodine-potassium iodide. (magnification 400x).

4.4 Conclusions

Studies of a seed flour extracted from the leguminous plant *Detarium senegalense* Gmelin indicate that it is rich in s-NSP, comprising mainly glucose, xylose and galactose in the ratio ~ 2.67: 1.92: 1.00. The s-NSP component is structurally similar to tamarind seed xyloglucan, but with less galactose substitution on the detarium xyloglucan core than that found in tamarind. Histochemical examination of the detarium seed, using bright field and epifluorescence microscopy, indicated that the xyloglucan was located in highly thickened cell walls.

Chapter 5

Solution characteristics of the xyloglucan extracted from detarium seeds

5.1 Introduction

In the previous chapter it was established that detarium seeds contain a high concentration of water-soluble, non-starch polysaccharides, the main fraction of which is a xyloglucan structurally similar to that extracted from tamarind gum, although the proportion of galactose, relative to xylose and glucose, is somewhat lower than that found in tamarind gum. In the present chapter, we extend our previous characterization of detarium, by including measurements of viscosity at finite concentrations, both well above and well below C*, the coil overlap concentration, together with detailed studies of the molecular weight and chain properties obtained from intensity light scattering measurements.

Detarium xyloglucan has possible clinical use in the dietary management of diabetes mellitus and other metabolic disorders. Moreover, in common with many other polysaccharide gums, it has also potentially important commercial applications, particularly in the pharmaceutical and food industries for controlling drug release and modifying texture, respectively (Lapasin and Pricl, 1995).

Therefore, one aspect of this study was to further characterise the solution properties of purified xyloglucan, so that this can be related to therapeutic activity and other functional properties of the polymer. More generally, few detailed investigations of solution properties of xyloglucans have appeared in the literature, and the only extensive study is that on tamarind gum (Gidley, *et al.*, 1991; Lang and Burchard., 1993).

However, according to one of the co-authors of the latter paper (W. Burchard, personal communication), the light scattering measurements in these studies were complicated by time dependence and strong aggregation effects. In the present work, the pressure heating method of Vorwerg and Radosta (1993) has been employed. Recent work by these authors (Aberle, *et al.*, 1994) has shown that reliable time and aggregation independent scattering results can be obtained for starch polymers by employing this technique. The present work is the first application of this method to s-NSP.

5.2 Experimental

The detarium xyloglucan was extracted and purified using the method described in Chapter 3. Solutions for rheological measurements were prepared by dispersing the known weights of a freeze-dried sample of purified detarium gum in deionized water for 1 h at 80°C and then mixed overnight using a magnetic stirrer at room temperature. The xyloglucan content and intrinsic viscosity of the purified detarium xyloglucan were determined using the methods described in Chapter 3.

Steady shear and dynamic frequency sweep experiments on the detarium gum solutions prepared at different concentrations (0.1-3.0%, w/w) were performed on the Rheometrics Fluids Spectrometer (RFSII, Rheometric Scientific Ltd, Epsom, UK.) with a cone and plate configuration (diameter 50 mm, cone angle 0.02 radians). All the measurements were conducted at 25°C (see Chapter 3 for other details).

Static light scattering measurements were performed at 25°C with a fully computerised and electronically modified SOFICA photogoniometer. Full details of this method are given in Chapter 3.

5.3 Results

5.3.1 Intrinsic viscosity [η]

The [η] was determined with the glass capillary viscometer at polysaccharide concentrations ranging from 0.01 % to 0.1% (w/v). In this case, the viscosity relative to that of the solvent (water) lies in the range $1.2 < \eta_r < 2.0$. The experiments carried out at higher concentrations and at a range of different shear rates suggest that under these conditions (i.e. $1.2 < \eta_r < 2.0$) the solution viscosity is essentially Newtonian. The [η] of detarium gum was found to be ~8.9 ± 0.2 dl/g (Fig. 5.1), which is significantly higher than the value reported for tamarind-seed xyloglucan ([η]=6.0 ± 0.5 dl/g) (Gidley, *et al.*, 1991). Since the [η] of detarium gum is rather high, this gives a very low C* (i.e. C* = 1/[η] = 1/8.9 g/dl = 0.11% w/w), which means of course that solutions of detarium polysaccharide have significant viscosity effects even at relatively low concentrations.

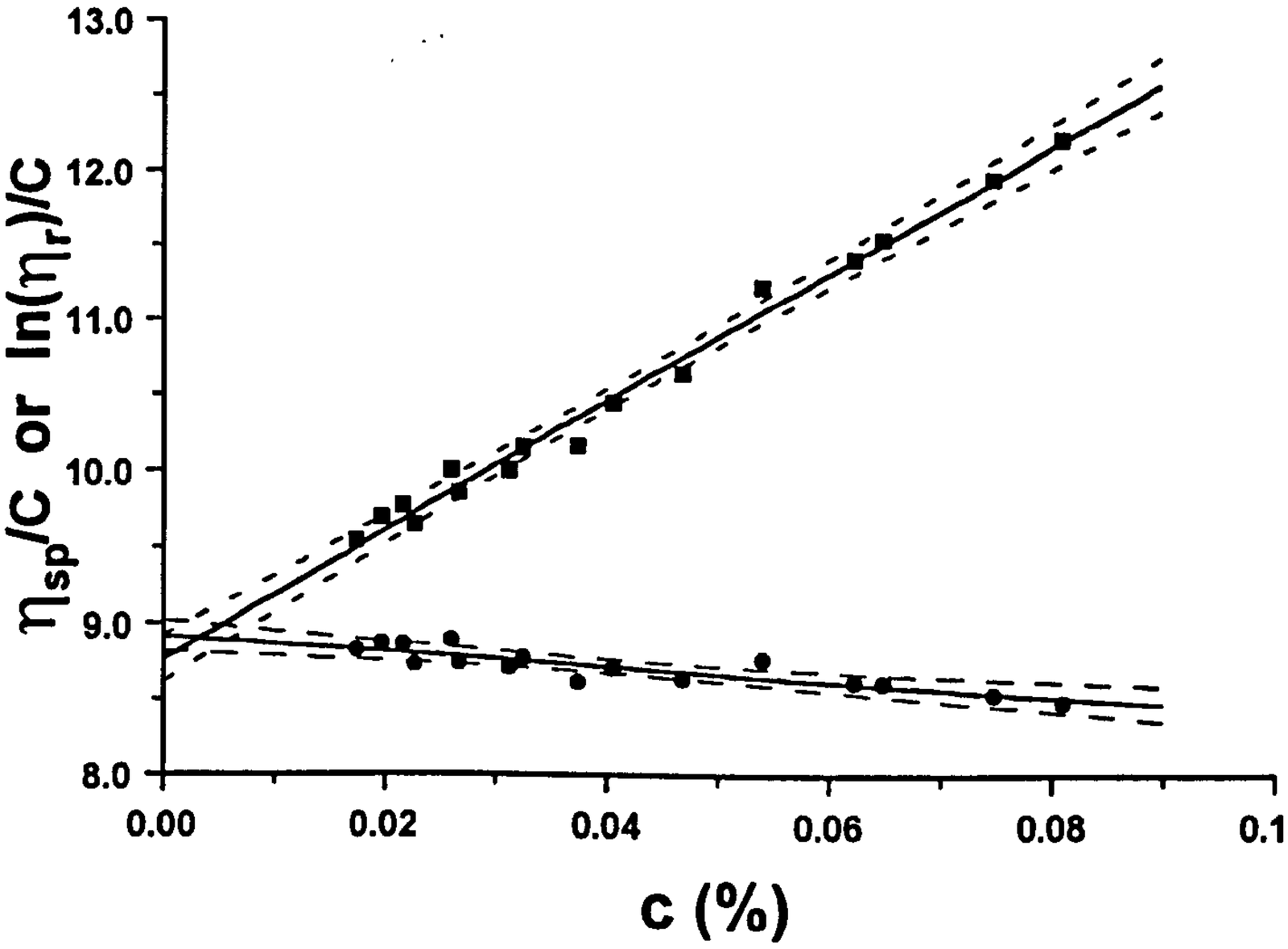

Fig. 5.1 Estimating intrinsic viscosity of detarium polysaccharide from plots η_{sp}/C vs. C (%) (■) and $ln(\eta_r)/C$ vs. C (%) (•). Dotted lines indicate 95% confidence intervals.

Since an increase in the intrinsic viscosity of any polymer reflects both the short range intramolecular interactions (chain flexibility) and its molecular weight, this difference could be due either to the fact that a decrease in galactose residues attached to the xyloglucose backbone of detarium increases chain stiffness (persistence length or chain characteristic ratio) or, more likely, that the detarium xyloglucan has a relatively higher molecular weight. Note that such an increase need not indicate that the native molecular weight is higher, but merely that it has been reduced to a lesser extent by the extraction regime employed. However, it is clear that the detarium xyloglucan is of high molecular weight.

The Mark-Houwink relationship (equation 2.3) allows an estimation of the (viscosity) average molecular weight by intrinsic viscosity measurement. For most random coil linear polymers, including polysaccharides, the exponent α should lie in the range 0.5 - 0.8 (Ross-Murphy, 1994). Recent studies show that xyloglucan exhibits a strong tendency to aggregate in aqueous solution (Gidley, *et al.*, 1991; Lang and Burchard, 1993; Lang, *et al.*, 1993,); this was described as bundle-shaped lateral aggregation of single polymer strands. This behaviour can obviously result in marked increase in the polymer stiffness, but generally such aggregation effects, although they may affect the small angle light scattering behaviour, tend not to influence the value of $[\eta]$. This is because the aggregates, although very high in molecular weight (thus in weight fraction) are usually small in number fraction. Moreover, they are usually fairly compact. Since $[\eta]$ (M_v) reflects a slightly lower M_w average ($M_n<M_v<M_w$) and effectively measures the size (radius) of the aggregate particle, it tends not to be sensitive to the aggregate fraction.

If for detarium xyloglucan we assume that α is 0.5, the average molecular weight of the detarium xyloglucan, M_D, can be estimated using equation 5.1 and the data obtained for the tamarind xyloglucan by Gidley and colleagues (Gidley, *et al.*, 1991) (i.e. $[\eta]_T = 6.0$ g/dl, $M_T = 8.8 \times 10^5$ g/mol). From this M_D was found to be ~ 1.9×10^6 g/mol.

$$M_D = ([\eta]_D \, M_T^{\alpha}/[\eta]_T)^{1/\alpha} \qquad (5.1)$$

On the other hand, if we use an exponent value of 0.8, a somewhat lower estimate of $M_D \sim 1.3x10^6$ g/mol is obtained.

5.3.2 Steady shear flow measurements

The response of semi-dilute detarium xyloglucan solutions to steady shear rate experiments was studied over a wide range of concentration (0.1-3.0 %, w/w). Fig. 5.2 shows the shear viscosity versus shear rate ($\dot{\gamma}$) in the range of 10^{-2}-10^3 s^{-1} on a double logarithmic scale. No shear rate viscosity dependence was shown in the range of $\dot{\gamma}$ used for concentrations lower than 0.3 %. However, for solutions of concentration above this level, obvious shear-thinning behaviour was seen at high shear rate range, and, as expected, this shear thinning became more pronounced as the concentration increased.

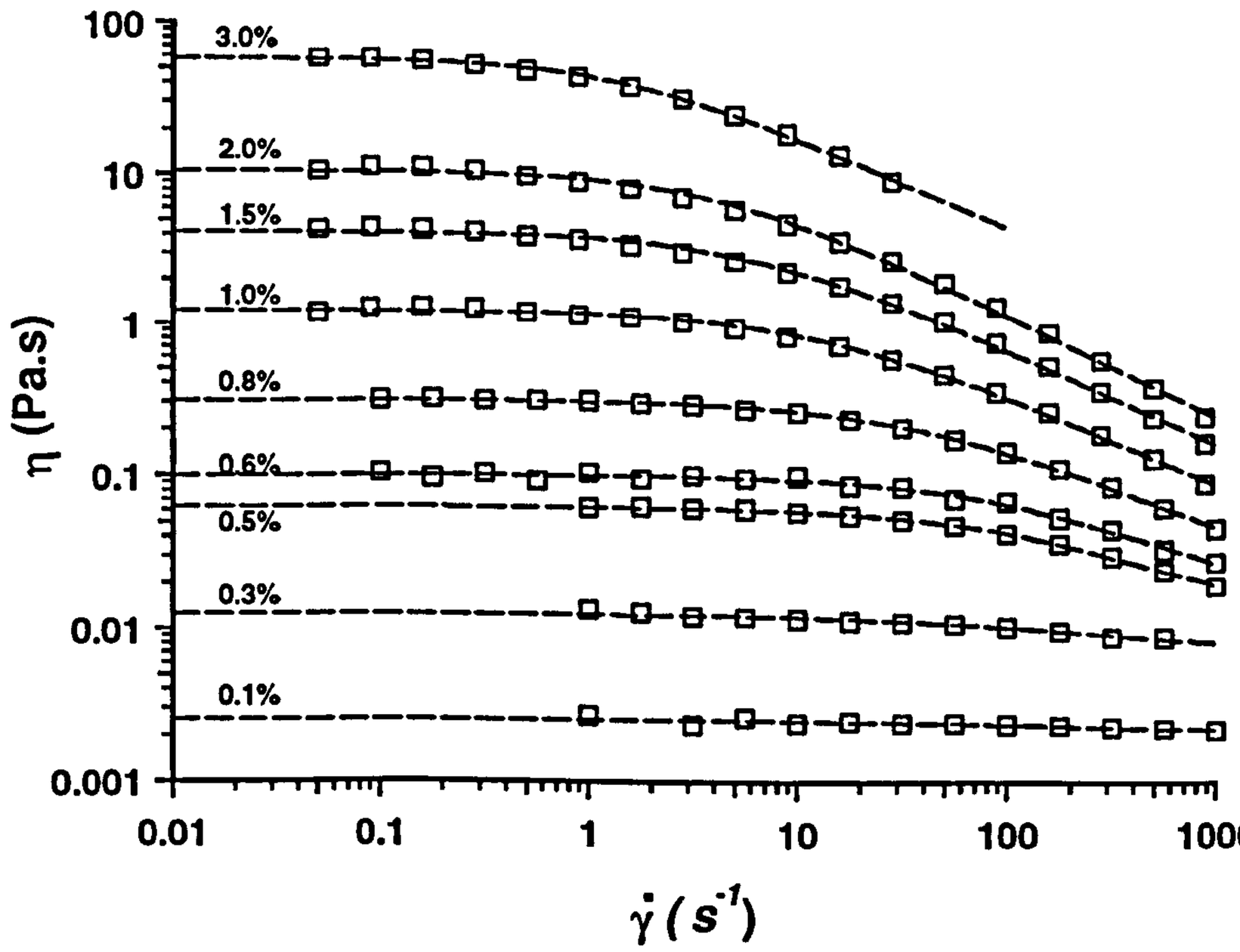

Fig. 5.2 Shear rate ($\dot{\gamma}$) dependence of viscosity (η) for different concentrations of detarium xyloglucan solutions. Dotted lines represent the least squares fitted Cross equation.

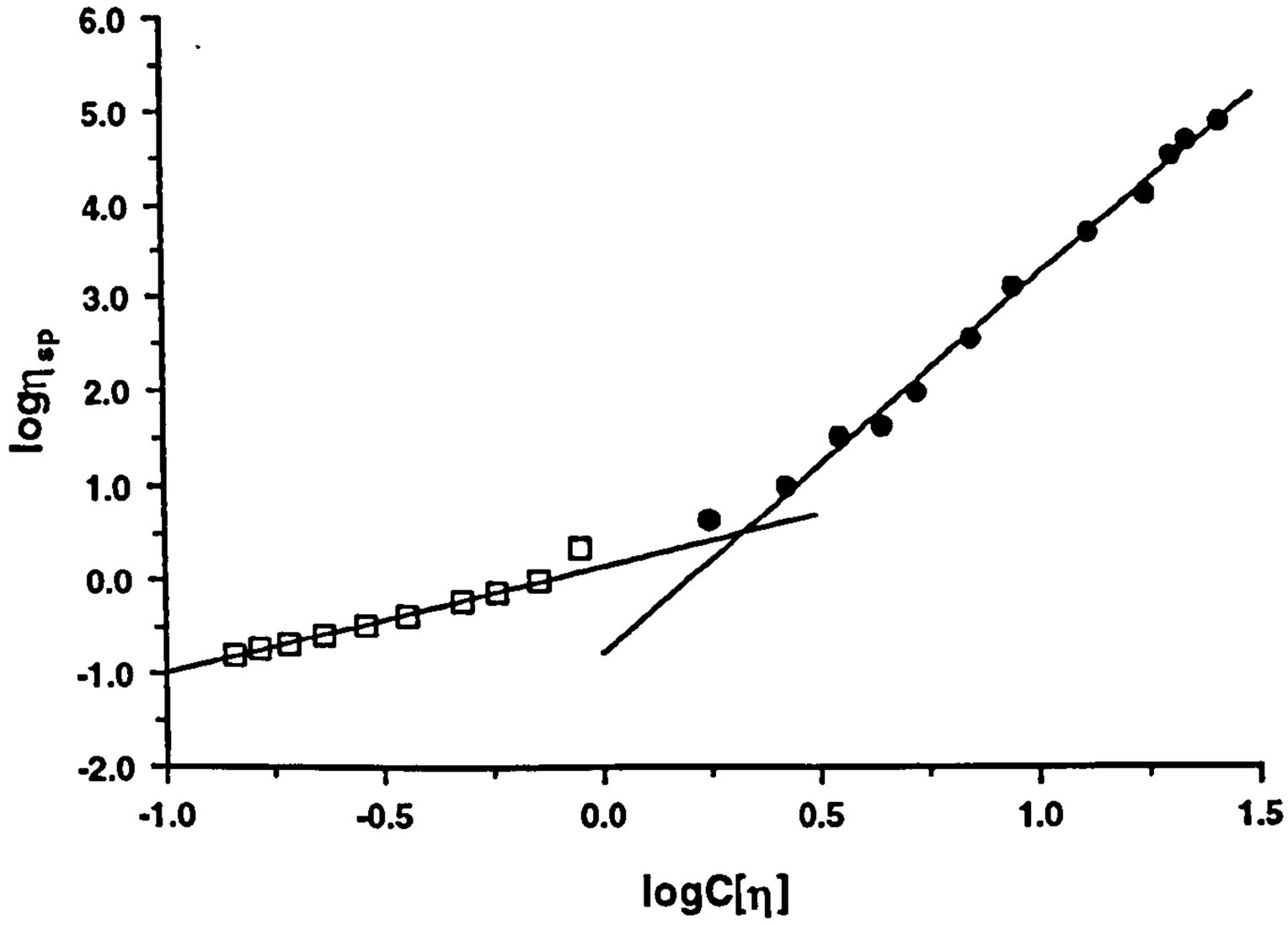

Fig. 5.3 Variation in the zero-shear specific viscosity of detarium xyloglucan solutions. Experimental points ( ) between concentrations 0.02-0.08% (w/w) were obtained by using the glass capillary viscometer. Other experimental points (•) were obtained with the RFSII.

The Cross equation (equation 2.7, Chapter 2) has been used to calculate the zero-shear viscosity η_0 of the steady shear measurements by employing a non-linear least squares fit. From these data, the concentration dependence of the zero-shear specific viscosity (η_{sp}) can be presented conveniently as a double logarithmic plot of η_{sp} against the coil overlap parameter $C[\eta] = C/C^*$ (Fig. 5.3). In Fig. 5.3, the experimental points between polymer concentrations 0.02 - 0.08% (w/w) were obtained by using the glass capillary viscometer, while the rest of the data were obtained with the RFSII. Two distinct linear regimes of slope can be identified from this plot, which is consistent with data seen for many other polysaccharide solutions. The first regime with a slope of ~1.3 corresponds to the dilute solution, and the second one with a slope of 4.0 represents semi-dilute solutions. This means that when $C < C^*$, $\eta_{sp} \propto C^{1.3}$, while at $C > \sim 2C^*$, $\eta_{sp} \propto C^{4.0}$, which is very similar to data published for guar gum (Robinson, *et al.*, 1982). The highest slope value (i.e. 4.0) is almost the same as that obtained for most linear polymers interacting by purely topological entanglements. From the intersection between the extrapolations

of the two straight lines the consequent concentration C_{cr} was calculated to be 0.21%, i.e. ~ 2C*. It is also worth mentioning that between the two linear regions there is an intermediate region in which our data shows a continuous curvature. Although some workers have apparently introduced a third linear region to describe this behaviour, this has no any real significance, particularly for polydisperse materials.

5.3.3 Dynamic measurements

As far as dynamic viscoelastic measurements are concerned, the coupling of strain γ and strain rate is critical, since only in the small-strain limit will G* and η* be independent of strain. This upper limiting strain depends strongly on the nature of the system and must be determined by careful experiments. The dependence of G* on strain γ for 1%, 2% and 3% detarium gum solutions was illustrated in Fig. 5.4. The G* are reasonably independent of strain at all three concentrations up to γ of ~ 0.35. There is no clear evidence that this limit was affected by different concentrations in the concentration range studied. Therefore, all the following frequency sweep experiments were conducted at $\gamma \sim 0.35$.

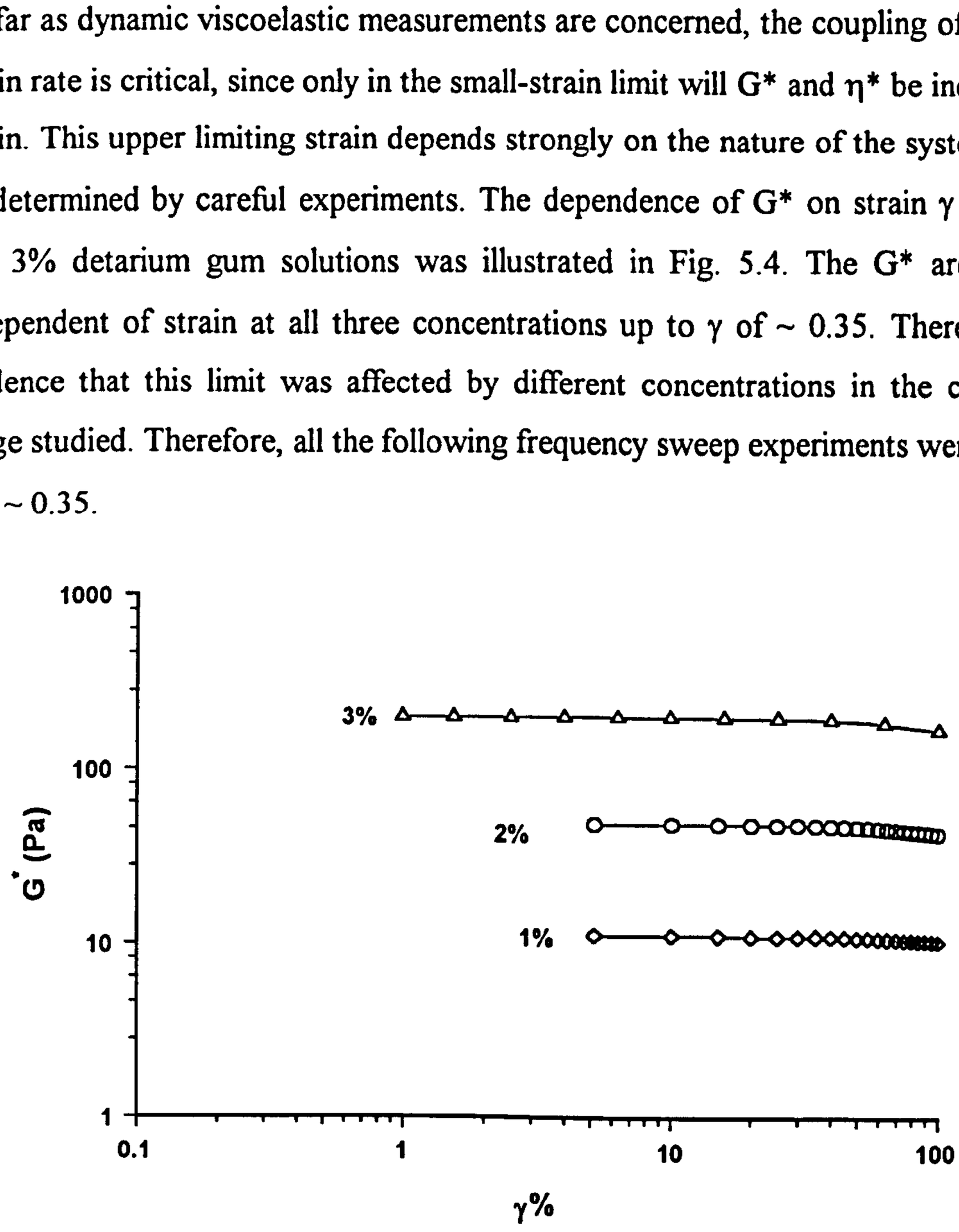

Fig. 5.4 Dependence of G on strain γ for 1, 2 and 3% (w/w) detarium xyloglucan solutions.*

The storage and loss moduli G′ and G″ for 1, 2 and 3% solutions of detarium xyloglucan are plotted against frequency ω in Fig. 5.5. G″ was always greater than G′ for all three concentrations when in the low frequency range (< ~10 rad. s^{-1}), indicating therefore, that the solutions were predominantly liquid-like. Since G′ increased faster than G″ with increasing frequencies, there was a cross-over point between G′ and G″ at 100, 35, 15 (rad. s^{-1}) for solutions of 1, 2 and 3%, respectively. This denotes a change of solution response from predominantly liquid-like to solid-like behaviour, which occurs at lower frequencies for solutions of high polymer concentration.

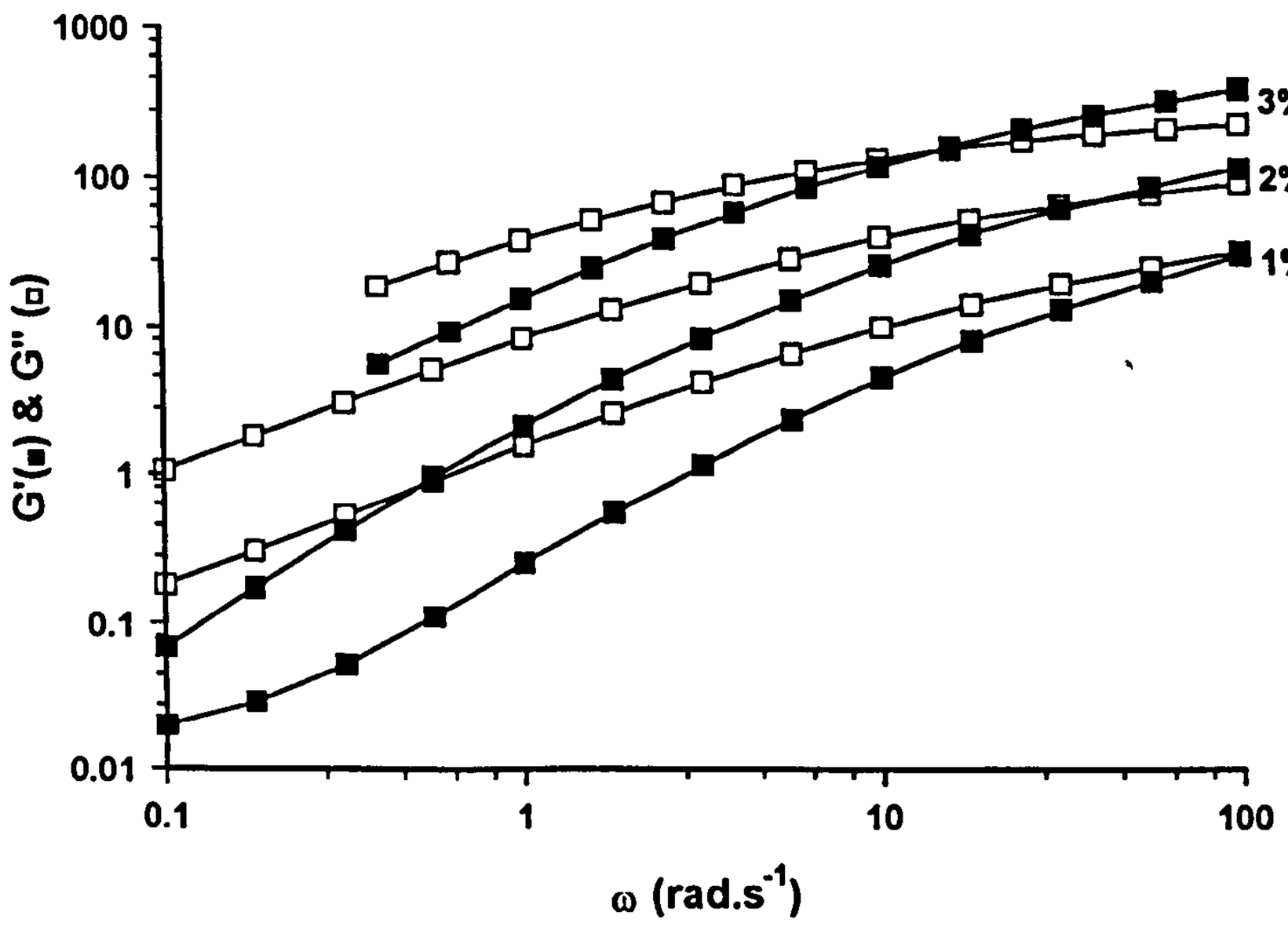

Fig. 5.5 G' and G" for different concentrations of detarium xyloglucan solutions.

The dynamic viscosity $\eta^*(\omega)$, which is defined as $(G'^2+ G''^2)^{1/2}/\omega$ (see Chapter 3), exhibits a similar profile when frequencies change as $\eta(\dot{\gamma})$ *vs.* $\dot{\gamma}$. At low frequencies a Newtonian plateau is seen while at high frequencies shear-thinning behaviour is exhibited. The η_0^* values were also calculated using the Cross equation in order to compare corresponding $\eta(\dot{\gamma})$ and $\eta^*(\omega)$ values. Good superposition of $\eta(\dot{\gamma})$ and $\eta^*($

ω) were found for solutions of concentration from 1.0-3.0 %. Within experimental error, and as always seen, within the lower shear rate ranges, the Cox-Merz rule (Ross-Murphy, 1994; Lapasin and Pricl, 1995) is obeyed perfectly as shown in Fig. 5.6.

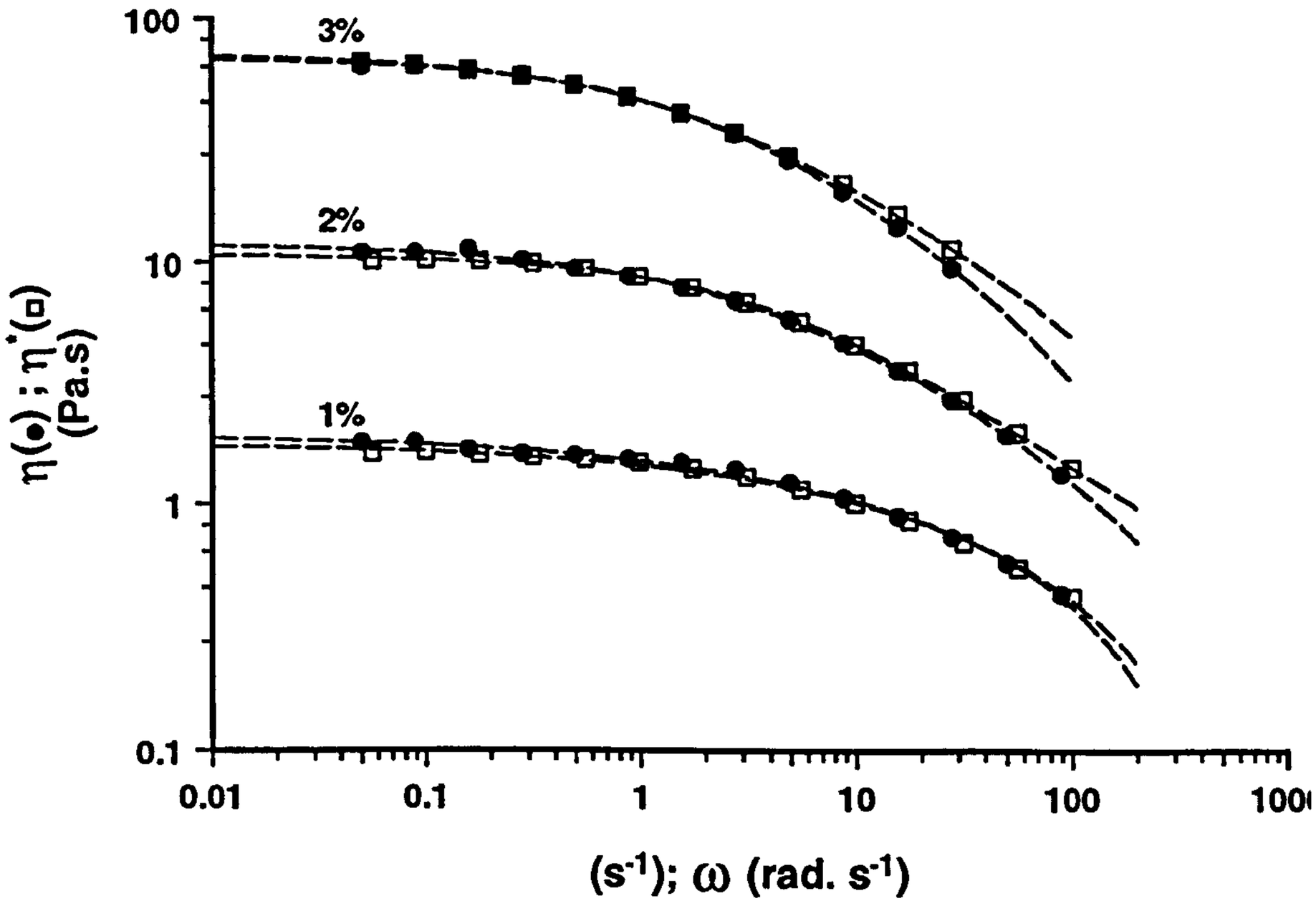

Fig. 5.6 Steady and dynamic viscosity data for 1 (i.e. C/C~9), 2 and 3.0% (w/w) detarium xyloglucan solutions.*

5.3.4 Light scattering measurements

Preliminary light scattering measurements carried out in Freiburg (Dr. H. Urakawa, Kyoto Institute of Technology, personal communication) suggested that a wide range of molecular weights could be obtained for detarium gum, some of them $>10^7$, depending on pre-measurement heating temperature (at atmospheric pressures) and solvent. This suggested that a more rigorous solubilization technique was required if reliable measurements were to be obtained using deionized water which, in turn, suggested the employment of the pressure heating cell.

In all experiments the scatter of data obtained for deionized water at scattering angles $<40^0$ was very large, a reflection of the use of water as the scattering medium, and the small cell size and scattering volume. Other measurements were very reproducible and good data could be obtained for all higher angles and $C < C^*$. Because of the obvious curvature seen in all Zimm plots, the data were replotted in the Berry form, that is plotting the square root of the abscissa (Kc/R_θ) of a conventional Zimm plot (Burchard, 1983; 1994). This curvature reflects the structure-dependent angular behaviour of the scattering data, which is analysed below.

Results from the light scattering measurements are given in Table 5.1, and a typical Berry plot is illustrated in Fig. 5.7. The weight average molecular weights, M_w, from independent zero angle and zero concentration extrapolations matched well in almost all cases, and good data were obtained for the (root of z-average mean square) radius of gyration, R_g (Table 5.1). As is usual for water-soluble neutral polysaccharides of high molecular weight, estimates for the second virial coefficient, A_2, were far less reliable, and although all values were positive, they were quite small.

Table 5.1 Summary of static light scattering results.

Sample	Treatment	M_{W1}[a] ($x10^{-6}$)	M_{W2}[a] ($x10^{-6}$)	R_g[b] (nm)	A_2[c] ($x10^4$)
XG1	130°C for 20 mins	2.75	2.75	119	1.5
XG2	Same sample after 24 hrs	Scattering essentially unchanged			
XG3	Repeat of XG1	2.58	2.53	112	0.4
XG4	130°C for 120 mins	2.75	2.75	123	3.1
XG5	160°C for 20 mins	2.72	2.72	114	1.9
Mean			2.69	117	
±SD			0.08	4.3	

[a] M_{W1} and M_{W2} correspond to the zero concentration and zero angle extrapolations of the Berry plot. XG = Xyloglucan.

[b] R_g = Z-average root mean square radius of gyration.

[c] A_2 = Second virial coefficient in units of reciprocal concentration, viz. mol ml/g

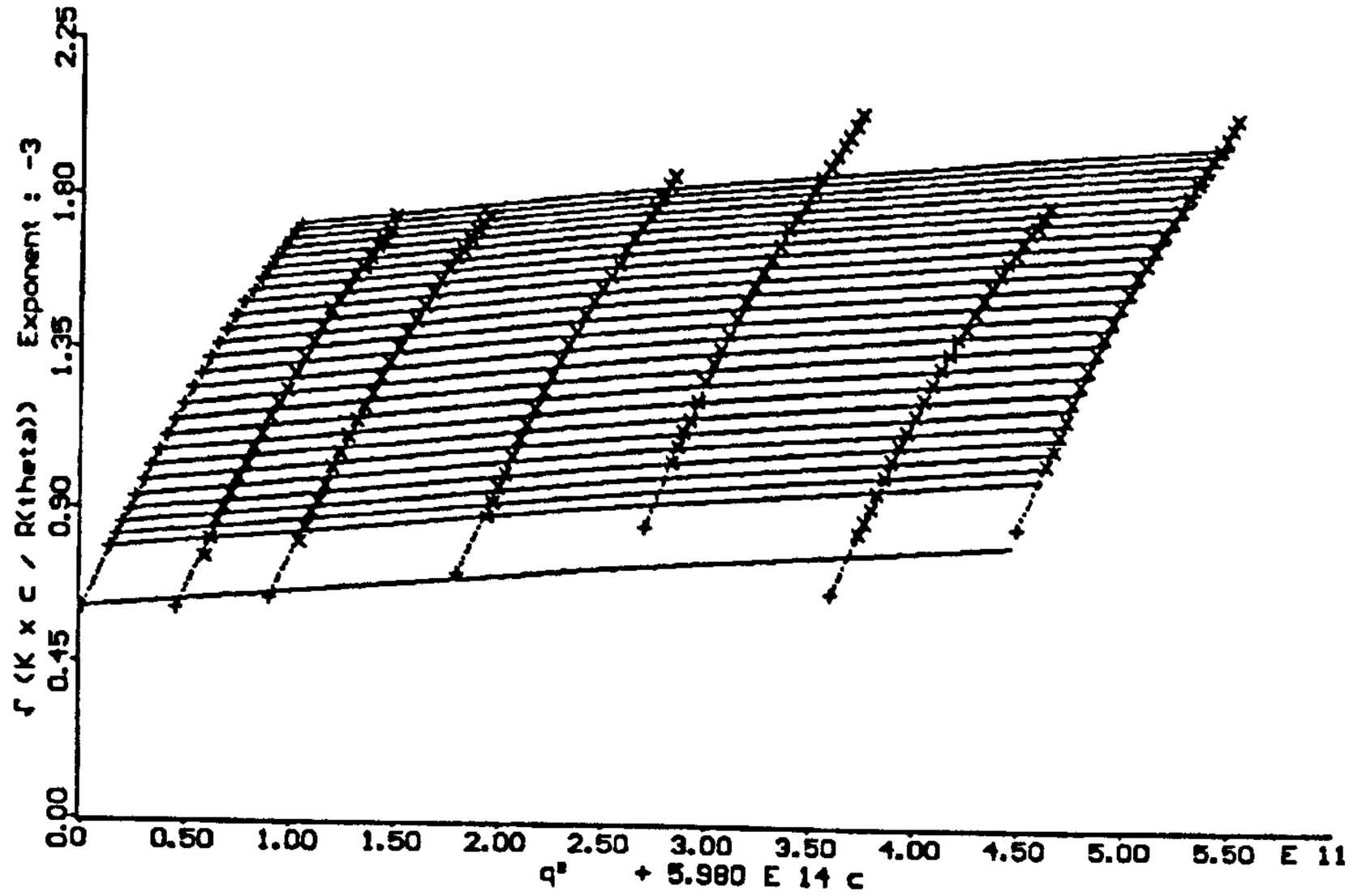

Fig. 5.7 Berry plot for sample XG5. The vertical shifts of some of the experimental data reflect slight concentration errors.

Most importantly, the M_w and R_gs showed no significant change either with length or maximum temperature of heating, or even when remeasured after 24 hours (Table 5.1). The latter, in particular, is a clear sign that the very pronounced time-dependent supramolecular aggregation, almost always seen in light scattering of polysaccharides, and most other water-soluble polymers (Huglin, 1972), appears to have been eliminated by the high temperature and pressure treatment. The former effect severely reduces the reliability of much of the literature data on polysaccharide molecular weights by light scattering.

Furthermore, the observation that M_ws obtained are effectively independent of heating temperature and time strongly suggests that we are measuring a true molecular property, rather than a time- and temperature-dependent molecular weight-degradation effect. This justifies *a posteriori* our strategy of treating the data for different treatments statistically as if they were strict replicates.

5.3.5 Intrinsic viscosity of heated samples

In order to confirm our supposition that no macromolecular changes had been induced by the pressure heating process two subsequent experiments were carried out. Firstly, one of the freeze dried samples after pressure heating from Freiburg was remeasured in London. It was noticeable how readily this sample dissolved compared to the untreated polymer. A further heat and pressure experiment was also carried out in London, although this had to be carried out using a laboratory autoclave (121°C, 15 bar total pressure) rather than the specialist pressure cell. The [η] values obtained for the sample after 20 min heating under 121°C autoclave; and for the rehydrated sample originally heated to 130°C in the pressure cell were 9.3 dl/g and 8.4 dl/g, respectively (Fig. 5.8). Although the latter value was a little lower than that seen for the original untreated sample 8.9 dl/g, this in no way suggested a significant decrease due to depolymerisation. Instead, the data are very consistent with the influence and removal of a small number fraction (but large weight, and z-average fraction) of supramolecular aggregates on the [η] of the non-heat treated samples.

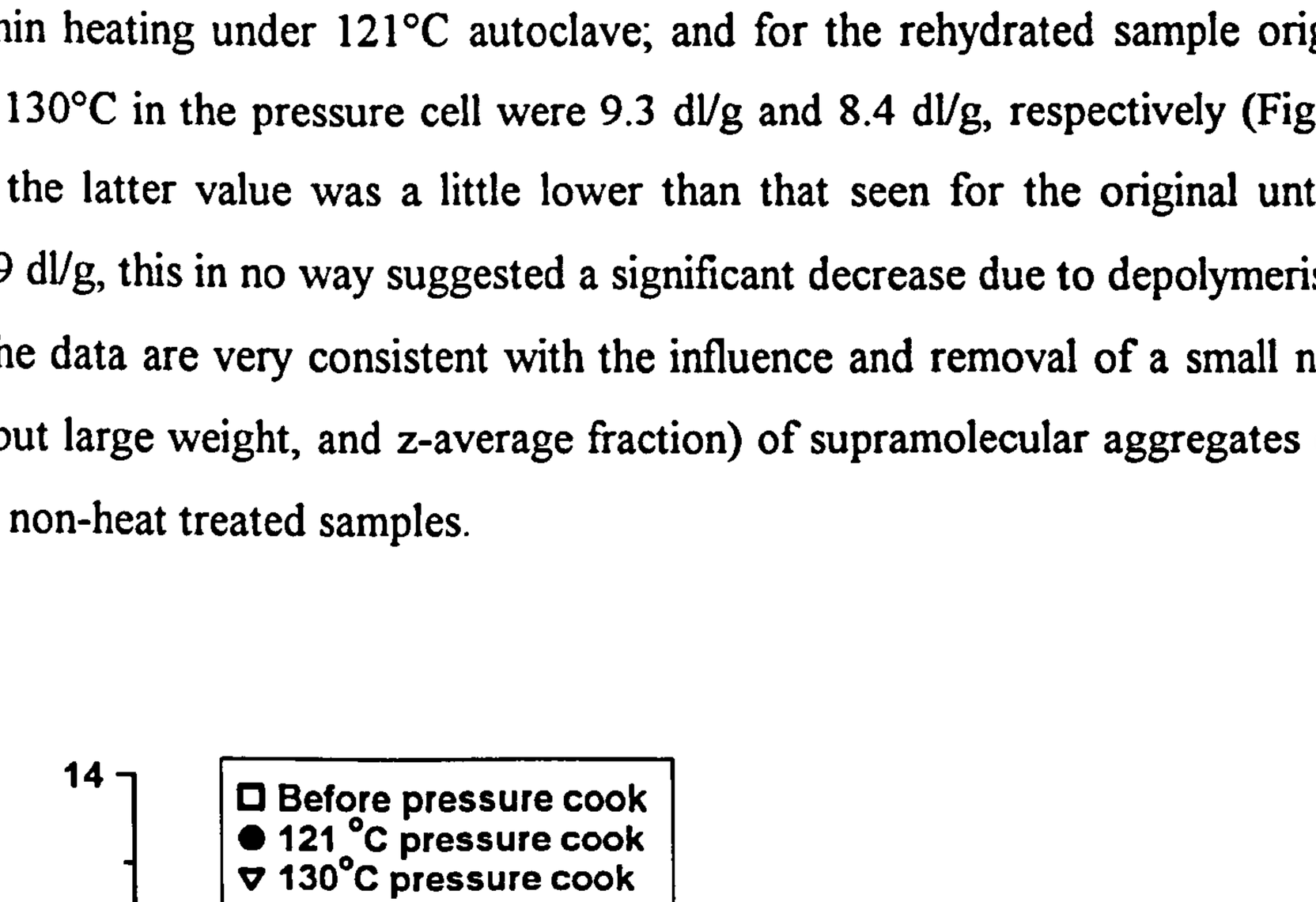

Fig. 5.8 Intrinsic viscosity of detarium measured when the sample solutions were treated in different ways.

5.4 Discussion

All the semi-dilute solution characterization work (Fig. 5.2) seems to be very largely consistent with much of the other data in the literature for the rheology of polysaccharide solutions. Nevertheless, the quality of the data are, in our view, very impressive. Fig. 5.3 illustrates the expected variation of viscosity with dimensionless overlap, with values of the two slopes quite consistent with most other published data. The shear rate dependence of viscosity at different concentrations (Fig. 5.2), and the dynamic mechanical data are all completely normal (Fig. 5.5), the linear viscoelastic strain region is quite pronounced (Fig. 5.4), and there is very strong evidence for Cox-Merz superposition of η and η^* at corresponding shear rates and oscillatory frequencies, even at relatively high concentrations (Fig. 5.6). All of this suggests that detarium gum is a well behaved linear polymer entanglement network system (Morris, *et al.*, 1981; Robinson, *et al.*, 1982; Richardson and Ross-Murphy, 1987a; 1987b; Ross-Murphy, 1984; 1994; Lapasin, *et al.*, 1995). However, the molecular weight, and angular dependence of scattering data, suggest that this conclusion is partly illusory.

As discussed earlier in this chapter, on the basis of a comparison of the intrinsic viscosity of the present sample with tamarind gum, the measured molecular weight for tamarind (Gidley, *et al.*, 1991) and the bounds of the Mark-Houwink equation for linear flexible macromolecules (0.5-0.8), the M_w for detarium gum should lie in the (albeit generously bounded) range 1.3-1.9 x 10^6. However, the measured M_w is very significantly larger than this (about 2 times greater). There are several potential explanations for this discrepancy, of which one at least is the questionable reliability of the tamarind gum results. These data (Lang and Burchard, 1993) were themselves subject to significant sample-to-sample and day-to-day fluctuations (W. Burchard, personal communication), due mainly to very pronounced time-dependent aggregation effects. Another explanation is that the detarium gum is not an essentially linear macromolecule, but is instead slightly branched. This would lower the Mark-Houwink exponent and so increase the estimated value of M_w.

Because of the high quality of the zero concentration light scattering data it should be

possible to analyse this and examine the "shape" of the macromolecule. This approach, although widely employed for synthetic macromolecules using small angle X-ray scattering or, for very high molecular weight samples, light scattering, can be applied very rarely for light scattering of polysaccharides, because the overall data are not generally reliable, nor are the molecular weights high enough. Indeed, successful application of this approach (Burchard, 1994) is limited, for example, to amylopectin and glycogen, which are both of extremely high M_w (>$2x10^7$), or to very stiff macromolecules such as xanthan. As far as we are aware, this procedure has never previously been applied successfully to any of the galactomannan, glucomannan or xyloglucan series of polysaccharides.

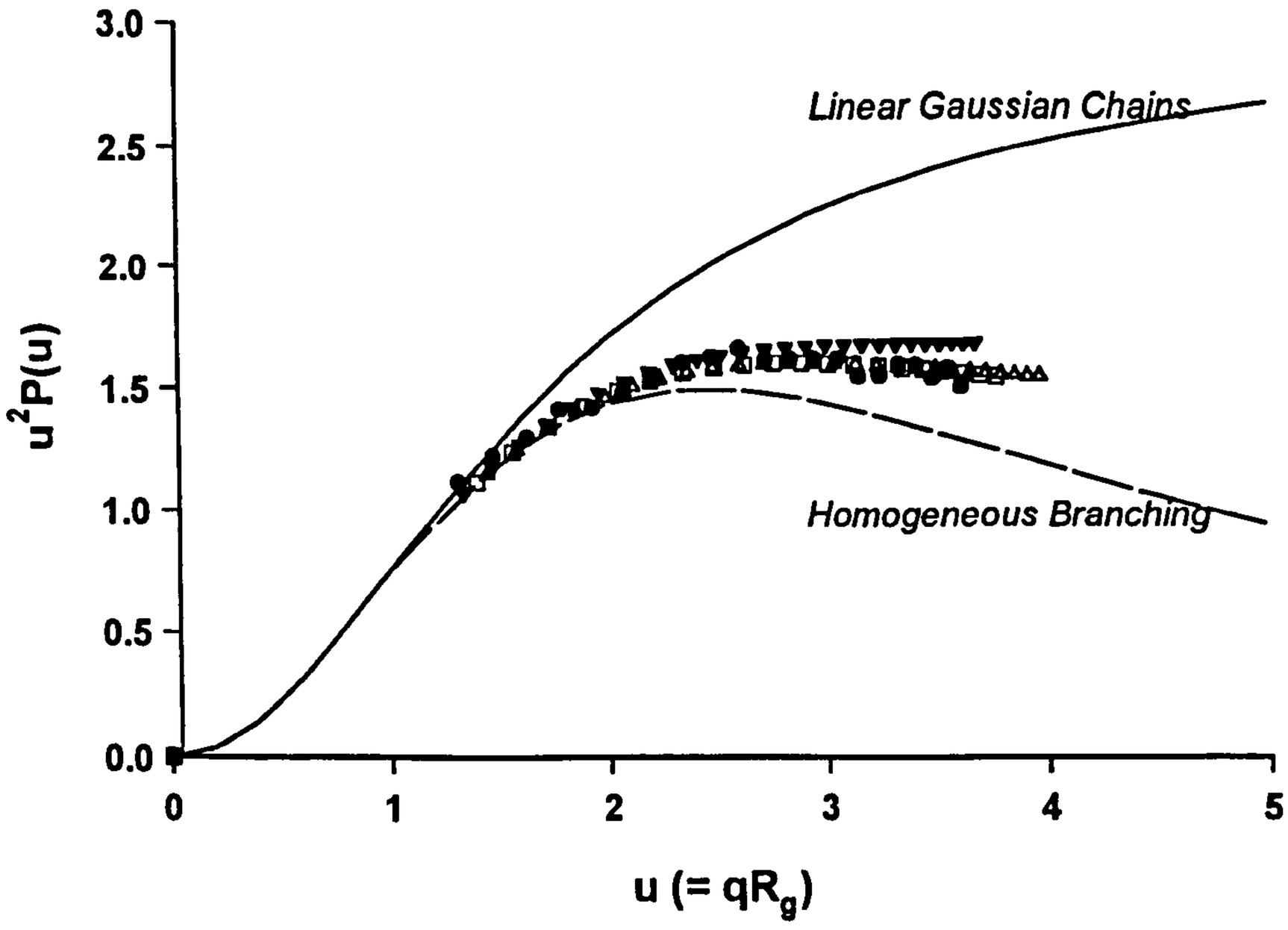

Fig. 5.9 Kratky plot for detarium gum samples. Theoretical curves calculated for models as in Burchard (1994). The upper line is for homodisperse linear chains, since both polydispersity and chain stiffness tend to increase the slope of this curve. Experimental points for samples XG1 (□), XG3 (●), XG4 (Δ), XG5 (▲).

Fig. 5.9 shows just such a procedure, using a Kratky plot of $u^2P(u)$ vs. u. Here, $u = qR_g$, $P(u) \equiv R_\theta/R_{\theta=0}$ is the so-called particle scattering factor, which reflects the angular dependence of the scattered light, and q is the scattering vector ($= 4\pi\sin(\theta/2)/\lambda$). The parameter u, which is dimensionless, measures the intramolecular probe distance relative to the incident light wavelength, and P(u) can be calculated for different chain architectures. The data from different experiments are in very good agreement (this is a particularly testing strategy) and show that at wide angles (high u) they reach an apparent plateau, where $u^2P(u)$ is ca. 1.5.

The overall grouping of data lies much below the expected profile for a Gaussian (flexible) chain, which itself lies below that for semi-flexible chains or rods (not illustrated in Fig. 5.9). The data lie above the curve for a very high degree of random homogeneous branching, and qualitatively, at least, resemble the traces calculated for low degree (three or four arm) star-branched macromolecules (also not shown in Fig. 5.9). Such a model cannot be taken too literally without including the effects of polydispersity, but what can be stated unequivocally is that the scattering profile for detarium gum is not consistent with that of a linear macromolecule, but instead strongly suggests a small element of long chain branching. The level of such branching need not be very great, say perhaps 2-10 branch points per chain. This is much below the level detectable biochemically (J.S.G. Reid, personal communication), but is quite sufficient to affect the overall chain profile. For example, at the same molecular weight, a single tetrafunctional branch point could halve the radius of gyration (Zimm and Stockmayer, 1949).

By analogy with the entanglement behaviour of branched polymer melts (Evans and Edwards, 1981), the implications of this conclusion for the rheological data are that we might expect to see, at very high concentrations, a more pronounced slope in the η_{sp} vs. $c[\eta]$ trace. Examination of Fig. 5.3 does not reveal this however, although the "breakpoint" value of $c[\eta]$ is rather low at ~2 (the corresponding value for most other polysaccharides is ~ 4; Morris, *et al.*, 1981). Such a high slope value has been observed in an apparently very highly branched polysaccharide from bacterial levan (Kasapis, *et al.*, 1994). However, the exponential increase in η_0 suggested from theory, and

sometimes observed (Ball and McLeish, 1989) for star branched polymer melts does not seem to be as obvious when considering solution behaviour.

One additional remark needs to be made. How can we be sure that the branching observed is not a consequence of either entanglements or some non-covalent interactions? For example, recent work by Goycoolea *et al.* (1995) has examined the effect of alkali treatment of polysaccharides, with a consequent reduction in [η]. Although alkali was used, in other respects the temperature regime was far less rigorous than employed in the present work. We feel that almost all non-covalent interactions would have been disrupted by the process used in the present work. Moreover, the time and heat treatment independence also argues against the presence of non-covalent bonds.

Finally, it needs to consider the longer term implications for the branched chain model. The assumption is made for a number of polysaccharides that these are linear macromolecules, although the positive evidence for this is nearly always absent. Biochemically it may even be simpler for plants to synthesise slightly branched macromolecules rather than linear chains, and the scattering part of this work, at least, suggests that there is a considerable future in re-examining the solution behaviour of a wide range of polysaccharides employing the pressure-temperature method to create time stable, molecular solutions. The use of the method to produce more readily re-hydratable materials is also worth examining.

5.5 Conclusions

In this chapter, macromolecular solution properties of detarium xyloglucan were investigated by steady and dynamic shear rheometry, and static light scattering. The intrinsic viscosity of detarium xyloglucan was found to be 8.9 dl/g. All the semi-dilute solution characterization work seems to be very largely consistent with much of the published data for the rheology of other polysaccharide solutions and suggests that detarium gum is a well behaved linear polymer entanglement network system. It has

been established that when $C < \sim C^*$, $\eta_{sp} \propto C^{1.3}$, while at $C > \sim 2C^*$, $\eta_{sp} \propto C^{4.0}$. The static light scattering technique was successfully applied to examine the molecular weight and architecture of the detarium xyloglucan macromolecule by employing pressure heating treatment of the samples. The scattering profile for detarium xyloglucan is however not consistent with that of a linear macromolecule, but instead strongly suggests a small degree of long chain branching. This slightly surprising finding may have significant implications for the future work.

Chapter 6

Development of a rheological method for the study of hydration kinetics of s-NSP powders

6.1 Introduction

The first mathematical model describing the dissolution of low molecular weight compounds appeared at the end of nineteenth century (Noyes and Whitney, 1897). Since then, the dissolution kinetics of such materials has been investigated in great detail as reviewed in Chapter 2. However, knowledge about this process in the field of macromolecules is still limited. Although numerous theories and mathematical models have been developed, most of them still have various limitations for practical use. Several attempts have been made to model particulate materials of spherical shaped and/or monodisperse in particles size only (Langenbucher, 1974; Abdou, 1989). The polydispersity in particle size and molecular weight of multi-particulate systems such as polysaccharide powders make it extremely complex to establish a theoretical model. However, the development of empirical models to describe the dissolution process of polydisperse system is still very useful for practical purposes.

In the dissolution models discussed in Chapter 2, the effect of viscosity was either ignored or was assumed to be constant during the dissolution process. This may be true under sink conditions (i.e. the dissolved molecules were removed from the dissolution surface immediately) or where the viscosity does not change significantly during the dissolution process. In the case of most high-molecular-weight polysaccharides, such as guar gum, which form highly viscous solutions above a certain concentration, the viscosity will increase by a non-linear function of concentration during the dissolution process. It is not appropriate to exclude the viscosity effects from the hydration models. Furthermore, the high-molecular-weight nature of guar galactomannan may have a

major effect on the dissolution mechanism compared to other solutes with much lower molecular weight.

Having considered the complexities of the hydration of guar gum flours, the aim of this chapter was to seek appropriate empirical models for the study of hydration kinetics of these materials. Thus, attempts were made to develop a simple empirical model by mathematical curve fitting approaches. The current hydration data of guar gum flours were also fitted to several selected models described in Chapter 2 and the comparisons were made between the results obtained from these models.

6.2 Experimental

6.2.1 Materials

Three commercial guar gum flours of different molecular weight and particle size were used in this study. These are standard food grades M150 and M90 (Meyprogat range, Meyhall Chemical Company Ltd, Switzerland), RG30 (Hercules, London, UK). A sample of guar gum granules (Master g) with medium particle size milled directly from guar seed endosperm (details for this sample is in Chapter 8) was also included in this experiment. The guar gum samples used in this chapter were from different batches of commercial products. Some physico-chemical properties, such as average molecular weight, are slightly different from other samples of the same grades. The average molecular weights of guar gum samples were estimated from measurement of intrinsic viscosity as described in Chapter 3. Particle sizes of the samples were measured by the Malvern instrument as described in Chapter 3.

6.2.2 Methods

The hydration method used in this chapter was described in Chapter 3. The mixing box rotated at a speed of 6 r.p.m. (the estimated minimum speed needed to prevent aggregation of the samples). Viscosity measurements were performed on either a

Brookfield RVT viscometer, using spindle 4 at 20 r.p.m or a RFSII (see Chapter 3), using plate-plate configurations (50 mm in diameter and 1 mm gap). In the latter case zero-shear viscosity was estimated from the mean value of the first four experimental points at the lowest shear rate, corresponding to the Newtonian plateau. The ultimate viscosity of samples of Master G was determined in a different way as described in Section 7.2.1.

In the present study, 1% (w/v) solutions were prepared on the basis of dry matter content of the materials (not on the amount of galactomannan). Thus, there would be small differences in galactomannan concentrations between the different grades of guar gum samples. Each experiment was carried out for four replicates and the mean was used in subsequent data analysis.

6.3 Results

6.3.1 Development of empirical hydration model

First order kinetics has been the most popular model for describing chemical reactions and physical process, including the hydration process. According to the first order kinetic model described in Chapter 2 the dissolution process can be expressed as:

$$\ln (1-\eta_t/\eta_\infty) = -kt \qquad (6.1)$$

or,
$$\ln (1-\eta_t^{1/3.5}/\eta_\infty^{1/3.5}) = -kt \qquad (6.2)$$

where η_t, is the viscosity of the dispersion at time t, η_∞ is the "ultimate" viscosity and k is the time constant related to the rate of viscosity development. This implies that the plots $\ln (1- \eta_t/\eta_\infty)$ or $\ln (1-\eta_t^{1/3.5}/\eta_\infty^{1/3.5})$ *vs.* time t are straight lines.

One set of the hydration data was used to test the first order kinetic model according to equations 6.1 and 6.2. As shown in Fig. 6.1, neither of these two expressions fitted the

experimental data closely. In both cases the experimental data points deviated from the initial slope according to equations 6.1 and 6.2 at about 120 minutes and 60 minutes, respectively. At these stage the viscosity of the dispersion only developed about 40% and 25% of their ultimate viscosity, respectively.

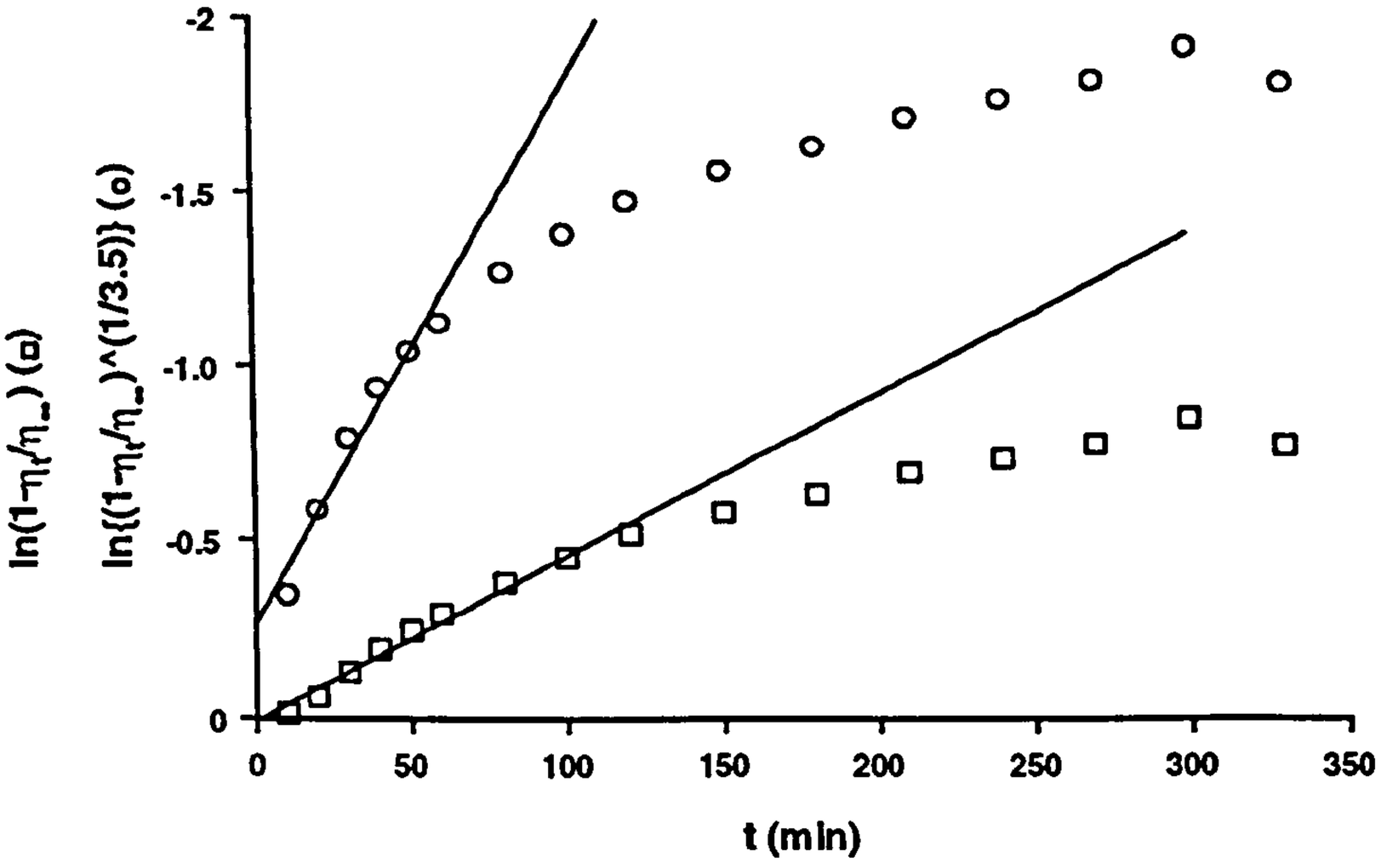

Fig. 6.1 Examples of hydration data (Master g) fitted to first order kinetic model (equations 6.1 and 6.2).

If the hydration curves in Fig. 6.1 are examined, it can be seen that the plot of ln $(1- \eta_t/\eta_\infty)$ *vs.* time t was similar in shape to the logarithmic function $y = -\log_a t$, when $0< a < 1$, $y = \ln (1-\eta_t/\eta_\infty)$. The curve of $y = -\log_a t$ passes through the point (1, 0). If we make the transformation $t' = t+1$, then the curve of $y = -\log_a (t+1)$ will pass through the origin (0, 0), which is similar in shape of our hydration curves. Since $\log_a t = \ln t/\ln a$, and to be consistent with the form of $\ln (1-\eta_t/\eta_\infty)$, the following natural logarithm function was selected initially to fit the hydration experimental data:

$$\ln (1 - \eta_t/\eta_\infty) = k \ln [a (t + t_0)] \qquad (6.3)$$

Curve fitting was performed by using the software called Fig. P for Windows. The results of the data fitting for samples of M150, M90, RG30 and Master G using equation 6.3 are summarised in Table 6.1, and illustrated in Fig. 6.2. The statistics of

the fit results in Table 6.1 showed that the present model fitted with experimental data reasonably well, as indicated by the high correlation coefficients (r^2 >0.95) and small s^2, which is the estimation of variance (s^2 = sum of squares/degrees of freedom).

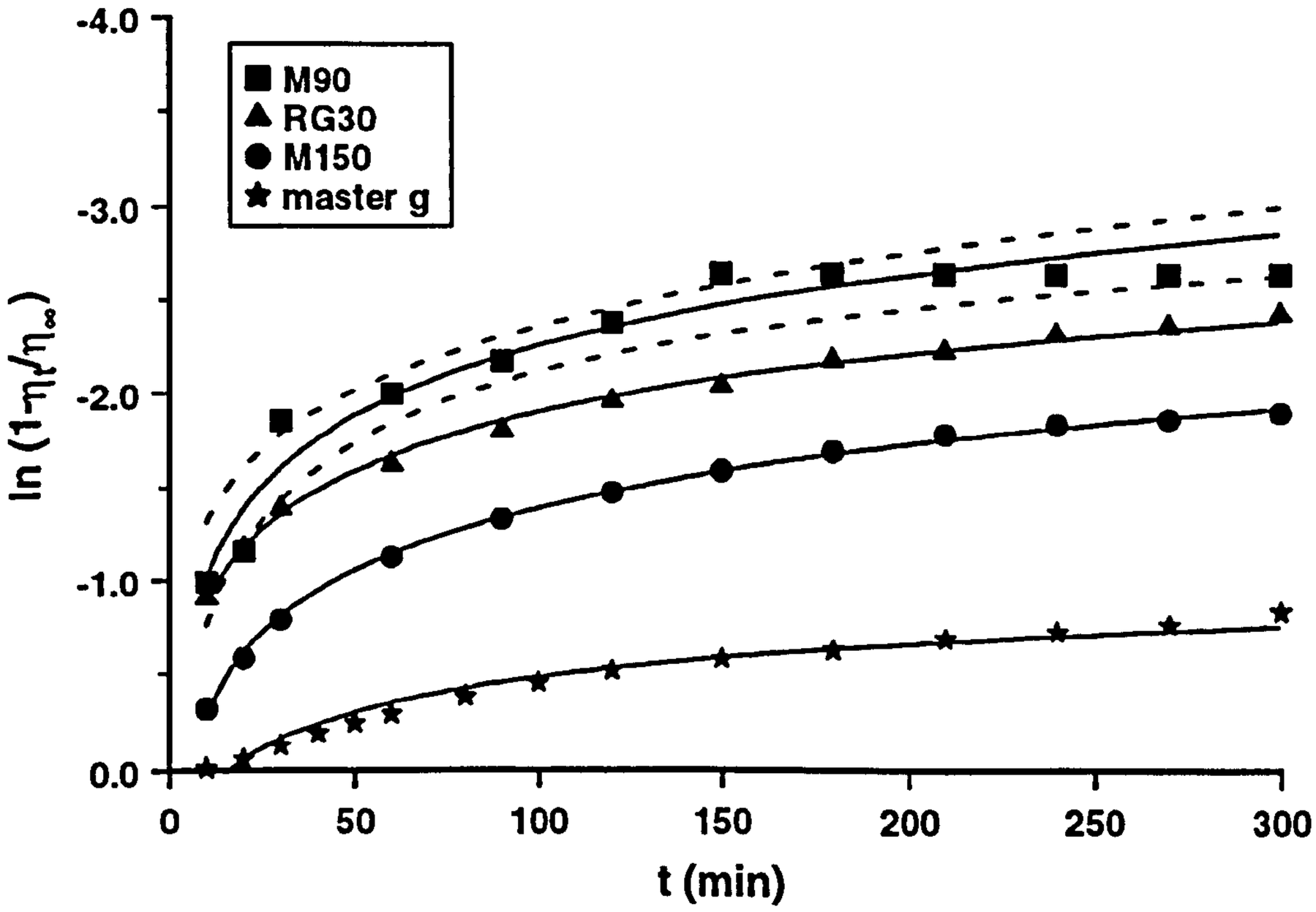

Fig. 6.2 Hydration data of different guar gum flours fitted by equation 6.3. Dotted lines indicate 95% confidence intervals.

Table 6.1 Summaries of curve fitting results of different guar gum samples according to equation 6.3.

Samples	Parameters					
	a	k	r^2	s^2	M_w x 10^{-6}	$d_{v,.0.5}$ µm
Master g	0.0629	-0.2606	0.962	0.003	2.60	75
M150	0.1764	-0.4846	0.998	0.0006	2.11	53
RG30	0.7042	-0.4461	0.996	0.001	1.85	*
M90	0.6569	-0.5384	0.952	0.02	1.39	63

* not determined.

During the above curve fitting process, t_0 was found not to be significant for any of the four samples used. This was in accordance with the initial assumption $t_0 = 1$, since $t >> 1$ immediately after the hydration starts. It is reasonable to suppose that $t_0 = 0$, thus, the initial model could be simplified as:

$$\ln (1-\eta_t/\eta_\infty) = k \ln (a\, t) \qquad (6.4)$$

which expands to: $$\ln (1-\eta_t/\eta_\infty) = b + k \ln t \qquad (6.5)$$

where $b = k \ln a$. Equation 6.5 implies that the plots of $\ln (1- \eta_t/\eta_\infty)$ *vs.* $\ln t$ should all be a group of straight lines with a slope k and an intercept b.

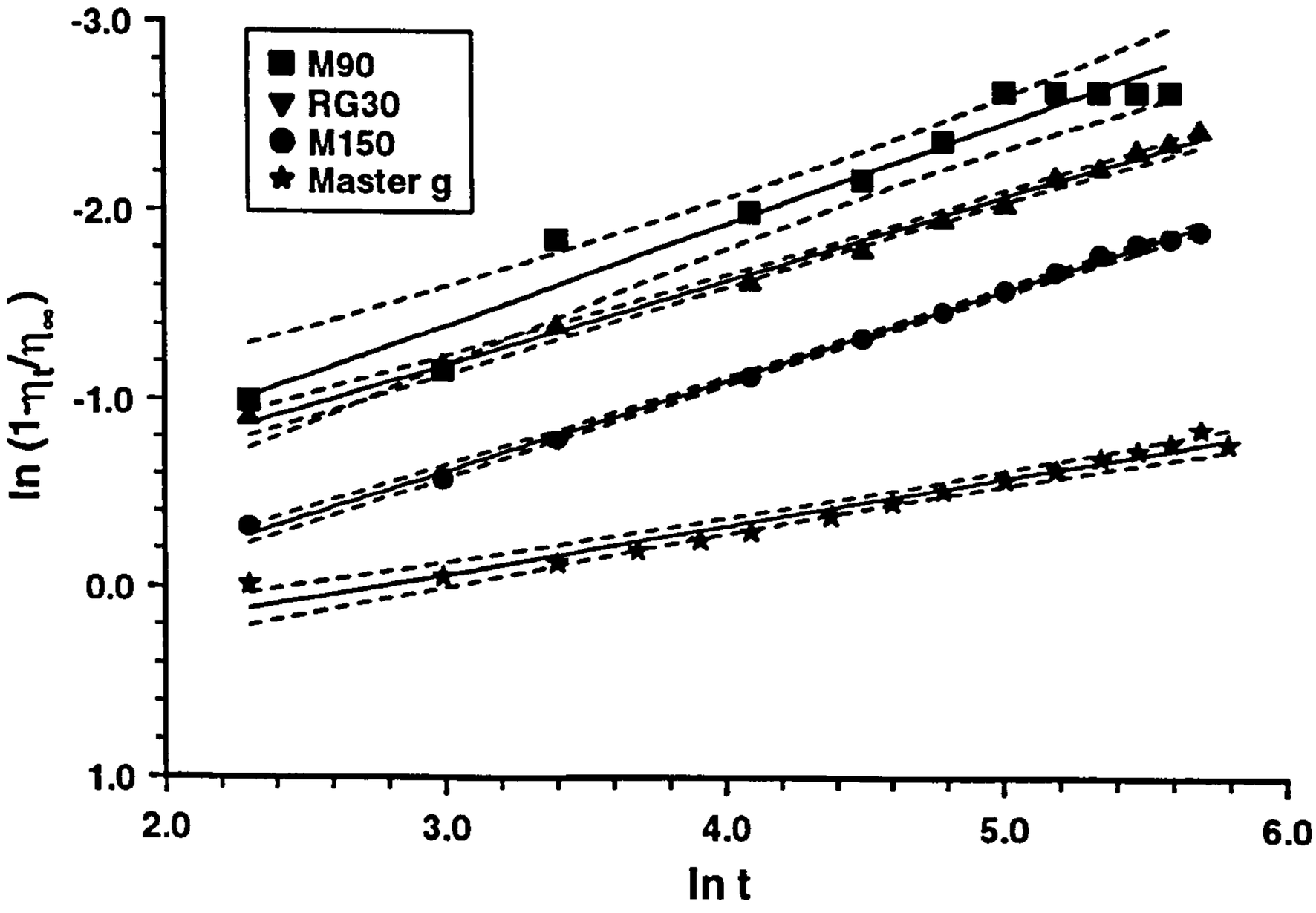

Fig. 6.3 Hydration data of different guar gum flours fitted by equation 6.5. Dotted lines indicate 95% confidence intervals.

Fig. 6.3 is the linear plots corresponding to the data in Fig. 6.2. Obviously, three of the four samples presented straight lines with excellent linearity. The curve fitting results

were tabulated in Table 6.2. For M90, a slightly poorer correlation between the present model and experimental data was obtained ($r^2 = 0.95$). Nevertheless, with all the degrees of freedom (f = 10) the fitness of this model with the data was still significant. This deviation is attributed to the quality of experimental data itself rather than the suitability of the present model. The relative lower viscosity of 1% (w/v) M90 solution made it difficult to detect the smaller changes at each time point. However, this can be improved by using a more sensitive geometry, such as couette system on the RFS II.

Because the slope (k) and the intercept (b) in the present model are not independent of each other, the hydration rate cannot be compared by comparing the hydration constants directly. Nevertheless, because this model can regenerate the hydration curves with reasonable accuracy the rate of hydration could then be defined in terms of a hydration index.

Conventionally, $t_{0.5}$, the half-life of a reaction, has been used to describe the duration of a reaction. Similarly, we can define a hydration index in terms of the time at which specified fractions of the material are found to be dissolved. In this case, it is the time at which the viscosity of the solution attains a certain fraction of the ultimate viscosity (η_∞). In the current study, $t_{0.8}$, the time needed for viscosity of the dispersion to reach eighty percent of ultimate viscosity, was selected as the index of hydration rate. The reason for choosing this time period was that it covered the main period of hydration process during which most of the viscosity had developed and also that the viscosity was approaching the plateau value (ultimate viscosity). However, when other time periods were selected, for example, $t_{0.5}$ or $t_{0.9}$, a similar profile was obtained. Thus, equation 6.5 can be re-written as:

$$\ln\left(\frac{1-\eta_t/\eta_\infty}{t^k}\right) = b \qquad (6.6)$$

thus,
$$t = \left(\frac{1-\eta_t/\eta_\infty}{e^b}\right)^{1/k} \qquad (6.7)$$

substitute $\eta_{0.8} = 0.8\eta_\infty$ in the above equation gives:

$$t_{0.8} = (\frac{0.2}{e^b})^{1/k} \quad (6.8)$$

The hydration rate of different samples, therefore, may be compared by comparing the magnitude of the hydration indices ($t_{0.8}$) predicted by the above equation. The smaller the $t_{0.8}$ value, the higher the hydration rate is. For example, the hydration indices $t_{0.8}$ calculated for guar gum samples in Fig. 6.3 are listed in Table 6.2.

Table 6.2 Curve fitting results according to equation 6.5 and hydration indices ($t_{0.8}$) of different guar gum samples.

Samples	Parameters				
	b	k	$t_{0.8}$	r^2	s^2
Master g	0.7207	-0.2606	7647	0.962	0.003
M150	0.8409	-0.4846	156	0.998	0.0006
RG30	0.1565	-0.4461	52	0.996	0.001
M90	0.2892	-0.5564	30	0.952	0.02

6.3.2 Application of the Weibull function to hydration process

This function was originally proposed by Weibull for describing the effect of the weakest link in a chain (Weibull, 1951). The chain could be anything from an electric light bulb filament to the life of a human. This equation can be written as:

$$f(t) = 1 - \exp(-(t-\Omega)/\alpha)^{\beta} \quad (6.9)$$

where t denotes time; f(t), in our experiment can be conventionally considered as the fraction remaining undissolved at time t, which is expressed as $(\eta_\infty - \eta_t)/\eta_\infty = 1-\eta_t/\eta_\infty$. Ω, α and β are the parameters in relation to viscosity development during the hydration process.

The hydration data of the different samples of guar gum was found to fit the Weibull function very well. As can be seen from Fig. 6.4, there is a reasonably good fit of the data using this model, regardless of the difference in molecular weight, particle size and types of the guar gum samples used. The fitted parameters were tabulated in Table 6.3. From Fig. 6.2 and Table 6.3 it can be seen that parameter β was a shape factor for the hydration curve. The hydration curves of sample M150, M90 and RG30 were similar in shape and their β values were approximately the same (-0.6). A relatively small absolute value of β was obtained (0.47) for the sample with the largest particle size and significant slower hydration rate (Master g). Parameter α defines a time scale of dissolution process since the larger the α value the slower the hydration process. Therefore parameter α can be used to compare the hydration rate with samples that have similar β values. For example, for samples of M150, RG30 and M90 which have similar β values, it is clearly that the hydration rate increased while α decreased. The third parameter Ω, was a measure of the apparent induction time, since dissolution started only when $(t-\Omega) > 0$. As it will be discussed in Section 6.4.2, Ω was determined by the swelling time of the polymers.

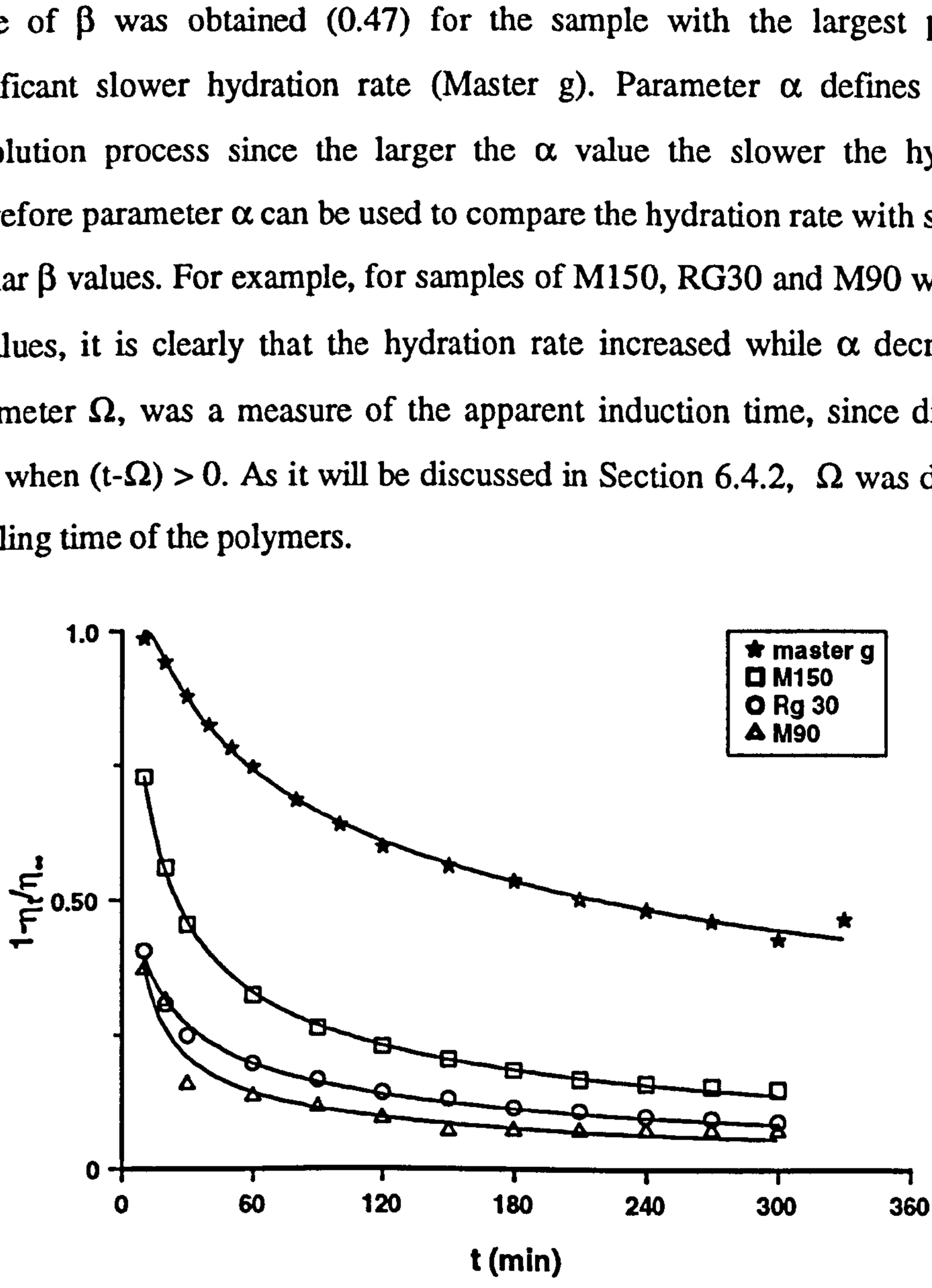

Fig. 6.4 Examples of the Weibull function fitted with hydration data of guar gum flours. Data of Master g were obtained by using RFS II, the other data by the Brookfield Rheometer.

Table 6.3 Summaries of curve fitting results for hydration data of guar gum samples by the Weibull function.

Samples	parameters				
	Ω	α	β	r^2	$s^2 \times 10^4$
Master g	10	95	-0.47	0.996	1
M150	1.9	12.6	-0.60	0.998	3
RG30	-6.6	5.3	-0.63	0.994	0.7
M90	1	2.6	-0.61	0.946	6

6.4 Discussion

6.4.1 Comparison of the Weibull function with the logarithmic model

When $\eta_{0.8} = 0.8\eta_\infty$ and $f(t) = 1-\eta_t/\eta_\infty$ are substituted into the Weibull function (equation 6.9), the hydration index, $t_{0.8}$, is given as:

$$t_{0.8} = \alpha (\ln 0.8)^{1/\beta} + \Omega \qquad (6.10)$$

The use of the hydration index $t_{0.8}$ enables us to compare the curve fitting results obtained from the logarithmic model and the Weibull function. Table 6.3 lists the hydration index $t_{0.8}$ for each guar gum sample calculated from the Weibull function (model 1) and our logarithmic model (model 2). The results obtained from these two models agree very well for the three commercial guar gum flours. However, in contrast, the $t_{0.8}$ value for Master g using model 2 was significantly higher than that obtained from model 1. This deviation may result from either the over estimation of hydration rate of model 1 or the under estimation of model 2 beyond the current experimental time (here 5 hours). It is probably more likely explained by the latter reason. This is because that model 2 only represents the hydration curves with the exponential growth in viscosity. Further experiments (in Chapter 8) showed that for some guar gum samples with larger

average particle size (and therefore slower hydration rate) the hydration curve was actually an exponential sigmoid curve. Indeed, from Fig. 6.5 it is clear that the hydration curve of Master g did exhibit a slight lag phase in the first 15 minutes and a tendency to upturn curvature after about 200 minutes. This might explain the deviations of model 2 from the experimental data after 5 hours. Nevertheless, in view of postprandial physiological effects of s-NSP, the first 5 hours is probably the most important period during which both these two models gave rise to a satisfactory prediction of the hydration behaviour of guar gum powders.

Table 6.4 Hydration index $t_{0.8}$ calculated from Weibull function (model 1) and the logarithmic model (model 2).

	Model 1	Model 2
Samples	$t_{0.8}$ (min)	$t_{0.8}$ (min)
Master g	2320	7647
M150	155	156
RG30	50	52
M90	31	30

Although both models can be used to simulate the hydration process of guar gum flours satisfactorily, the logarithmic model has the advantage that it is much easier to extract the hydration parameters from the linear transform of the model (i.e. equation 6.5). In contrast, since the Weibull function has too many arbitrary parameters, the curve fitting process was found to be very laborious. The difficulties lies in the predetermination of the parameter Ω at the beginning of the curve fitting process. The function was actually very sensitive to the pre-set Ω value. Although the Weibull function can also be transformed into a linear form, the curve fitting was not any easier to do without the correct Ω values. Furthermore, it is difficult to explain why Ω can sometimes be negative, as in the case of the RG30 sample (see Table 6.3). Langenbecher (1972) used this model for some pharmaceutical tablets with the assumption that Ω=0. However, we found this assumption was not suitable when using guar gum powders.

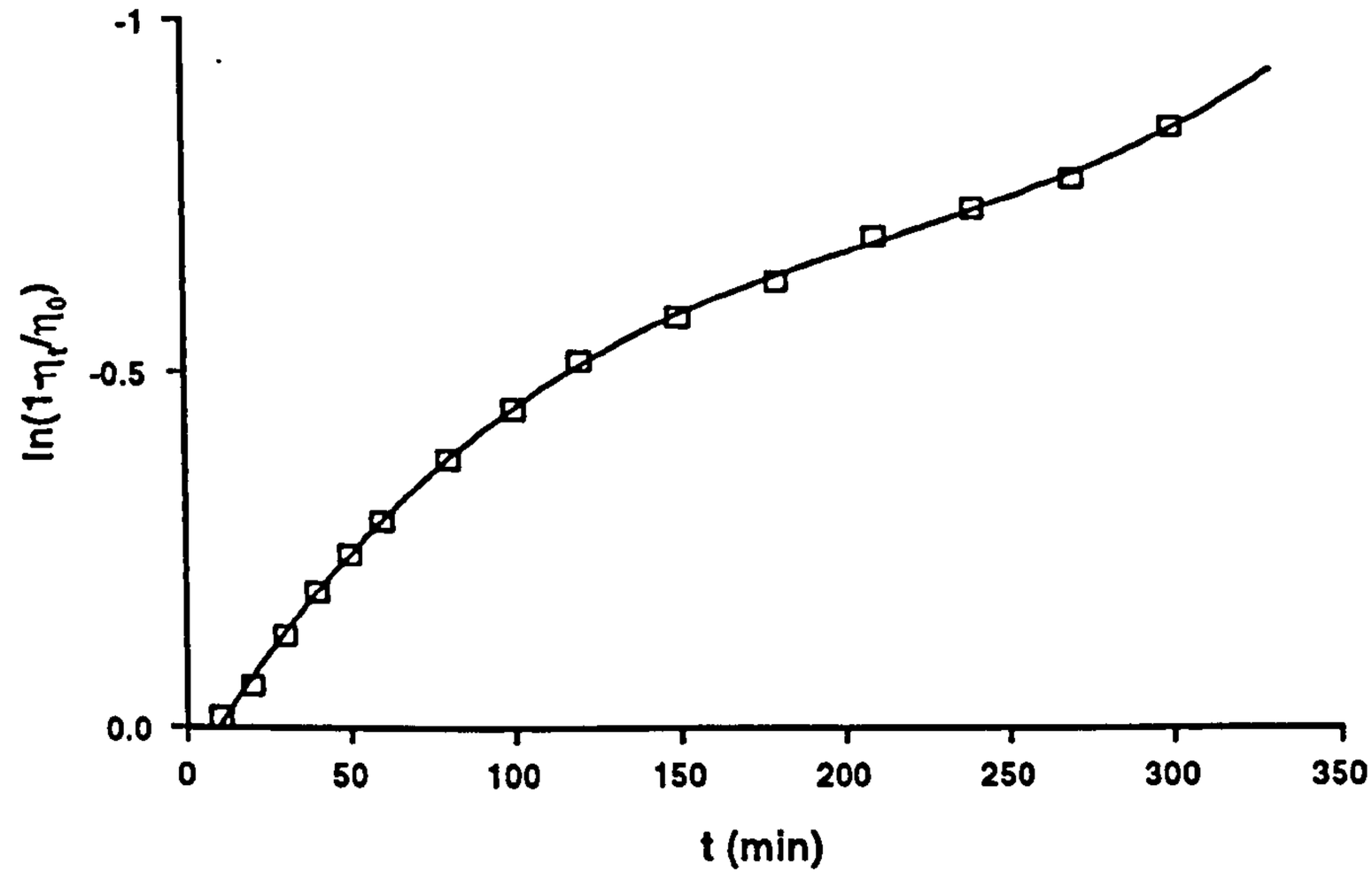

Fig. 6.5 Hydration curve of Master g showing the time lag in the first 15 minutes and the upturn after about 200 minutes. Solid line was the cubic polynomial regression of the data point (r^2=0.999).

The limitation of the logarithmic model is that it is only applicable when the hydration curves are exponential. From our experimental data this is the case for most of the commercial available guar gum samples of interest. However, for some pharmaceutical tablets and granules with extremely large particle size the hydration curve usually produces an initial lag stage (Randall, 1982). Thus, the hydration curve will actually have a sigmoid shape instead of the simple exponential shape. In this case, our model would not allow for predicting the initial time lag.

6.4.2 Mechanistic explanation of the logarithmic model

Further experiments (in Chapters 7, 8 and 9) over a wider range of sampling time, especially in the first twenty minutes, have indicated that the single linear plots for guar gum flours according to equation 6.5 can be divided into two straight lines with different slopes as shown in Fig. 6.6 as an example. The slopes of the initial stage of the hydration process were found to be always smaller than those produced for the rest of the data. This indicated that the viscosity of the solution increased with time at a lower rate in the

first stage than the second stage. Normally this first stage corresponds to the first 10 to 20 minutes after the samples were added into water and it was more pronounced for the samples with low hydration rate. Due to experimental limitations, in each experiment there were only two experiment points obtained in this time period. Although the hydration behaviour in this initial stage may need further investigation using other techniques, the finding in this experiment seems in agreement with the findings of other hydration studies and it can be explained in the following ways.

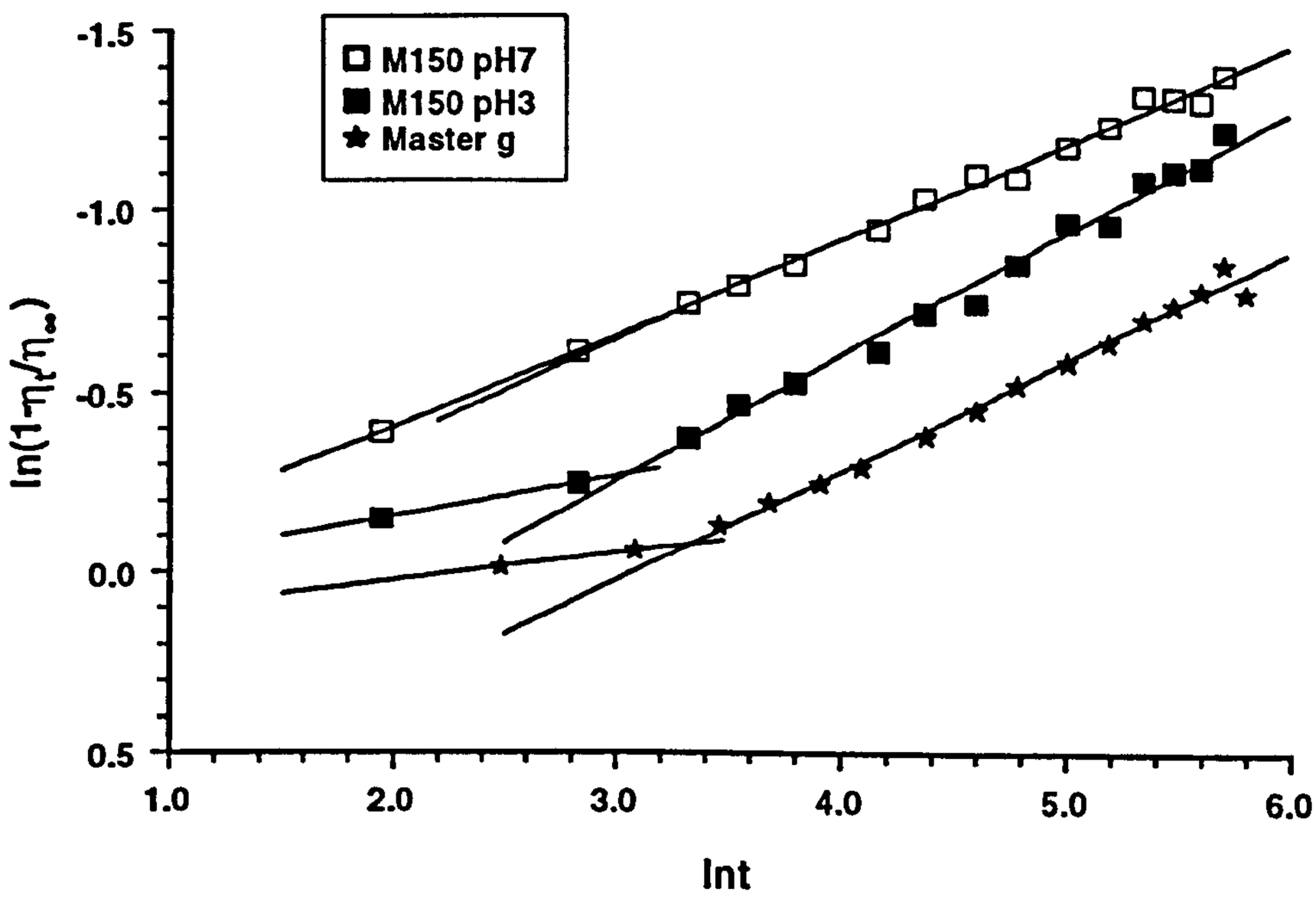

Fig. 6.6 Examples of hydration profiles of guar gum showing the two stages of hydration process.

Let us consider the hydration process of a single spherical particle as in Fig. 6.7. In the initial stage of the process the particle starts to swell as a result of the solvent (here water) diffusing into the particle and a simultaneous transition from the solid state to a gel-like state at a characteristic solvent volume fraction. Thus, two distinct fronts were observed: a solvent-polymer front (F_s), which moved outwards, and a gel-solid front (F_g), which moved inwards to the centre of particle. A gel layer phase was formed with thickness h. According to the study by Peppas *et al.* (1994; 1997), there were three distinct dissolution stages. During the early stage, the solvent diffused into polystyrene

and the sample swelled without significant dissolution (Fig. 6.7b). After the initial swelling period, dissolution was exhibited and soon reached a stationary phase. In this stage, the gel layer thickness became constant (Fig. 6.7c). At the end of the stationary stage the gel-solid F_g front reached the centre and disappeared, while at the same time, the solvent-gel interface moved rapidly towards the centre until the polymer sample was completely dissolved (Fig. 6.9d). This acceleration in the dissolution rate could be attributed to the higher solvent volume fraction at the final dissolution stage, which gave rise to a shorter disentanglement time of the polymer molecules.

It is reasonable to assume that the first stage of the hydration process of guar gum corresponds to the swelling stage. For example, the swelling time t_s has been found to be about 5 minutes for monodisperse polystyrene (M_n = 153,000) in toluene (Ueberreiter, 1968). Because of the polydispersity in molecular weight and as well as the initial particle size of the guar gum powders used in the present study, the apparent swelling stage should be relatively longer than a monodispersed sample with similar average molecular weight.

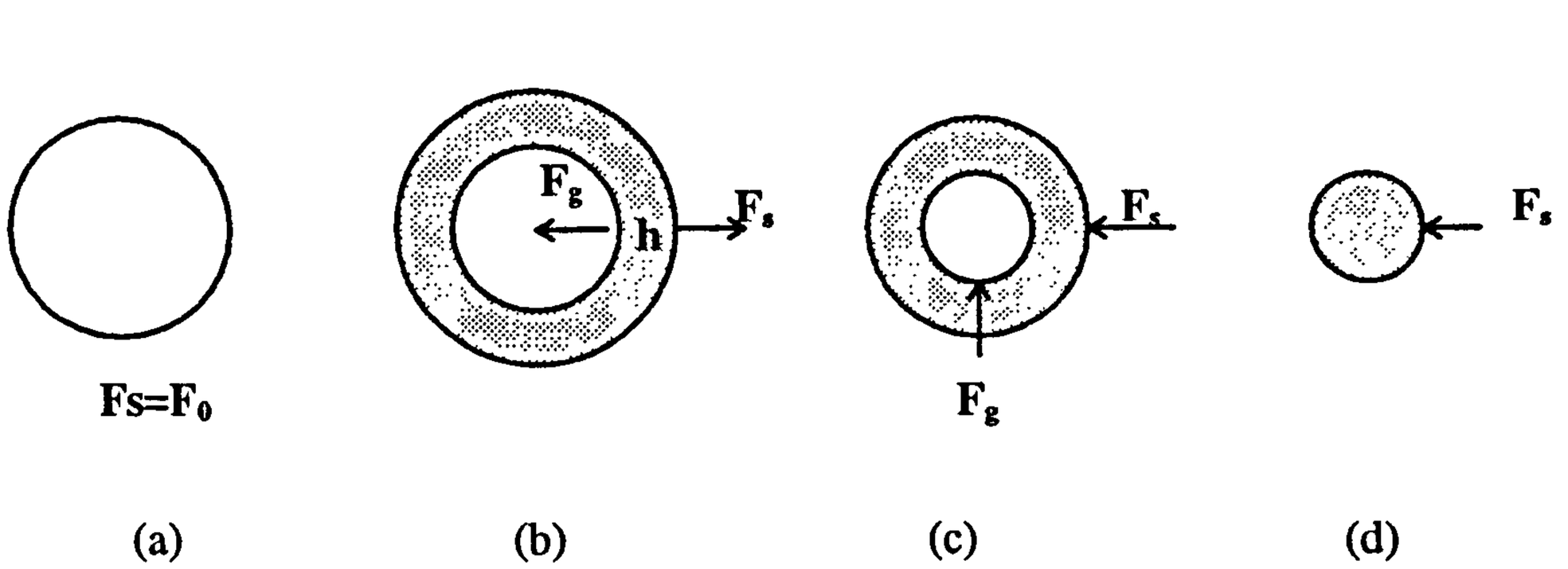

Fig. 6.7 Schematic representation of a spherical particle solvent diffusion and particle dissolution process: (a) initial particle; (b) the initial swelling stage; (c) dissolution stage and (d) end of the stationary stage. F_s = Solid-polymer front; F_g = gel-solid front; h= thickness of gel layer.

Furthermore, it is well known that relationship between viscosity and polymer concentration in solution is quite different when the concentration is below or well above the critical concentrations C*, If M90 guar flour solution is used as an example,

$\eta_0 \propto C^{1.1}$ when $C < C^*$ whereas when $C > C^*$, $\eta \propto C^{4.3}$. In other words, the viscosity increases more rapidly as the concentration increases when C is well above C*(C>C**). On the other hand, at the very initial stage of dissolution process, when concentration C < C*, the viscosity does not increase significantly as the concentration increases. This effect may also partially contribute to the small slope of the first regime of hydration lines. However, since C* of the high molecular weight guar samples is very low, it will only take a short period of time for concentration to exceed C* after dissolution starts.

The studies carried out by Peppas *et al.* (1994) were under so-called sink conditions. The dissolved polymer molecules were washed out of the sample surface by a continuous flow solvent. By contrast, in our experiments the volume of solvent was constant. The polymer concentration in aqueous phase as well as the viscosity of the dispersion increased continuously during the whole dissolution process. This increase in viscosity may reduce the mixing efficiency of the dispersion. Thus, as a consequence, the effect of transport of polymer molecules from the interaction surface to the bulk solution becomes gradually more pronounced. This can become one of the limiting steps of the dissolution process. This effect partially offsets the acceleration in the dissolution rate at the final stage observed by Peppas *et al. (1994).* This may explain why the hydration process in the present study did not show the final acceleration stage.

The first stage of the hydration process usually accounted for less than 20 minutes of the incubation time and so the viscosity level that developed at this stage was very limited. For some guar gum flours with a high hydration rate the first stage was actually not detectable under current experimental conditions. Thus, in our later studies only the second stage was considered.

6.5 Conclusions

In this chapter, several commonly used hydration models were evaluated for the hydration process of guar gum flours. The Weibull function has been found to be useful for describing the hydration kinetics of those polymer. However, the use of this model

was limited because of the complexity of the curve fitting process. A simple logarithmic model was also developed and found to be more suitable for describing the common commercial guar gum flours with satisfactory accuracy. By using this model the hydration process can simply be described by two hydration constants which may be obtained from a linear plot. This model was selected for the further study of hydration kinetics of guar gum powders. It is expected that this model would be also useful for studying other high-molecular-weight polymer powders, although further experiments would be needed for these polymers.

Chapter 7

Effects of polymer concentration and molecular weight on hydration rate of guar gum powders

7.1 Introduction

A rheological method has been designed for determining the hydration rate of guar gum flour in Chapter 6. The empirical logarithmic model for describing the hydration kinetics of guar gum powder was also established and found to be a reliable model for predictive purposes. Subsequent work using the same technique and model will involve studying a number of physico-chemical variables that are likely to influence the hydration behaviour of guar galactomannan. These include galactomannan concentration, molecular weight, particle size and pH environment. The first two are covered in the current chapter and the last two in Chapters 8 and 9, respectively.

The effects of molecular weight and polymer concentration on the rheological properties of polysaccharide systems have been well established (Launay, 1986). However as discussed in Chapters 1 and 2, when considering the physiological activity of dietary non-starch polysaccharides the hydration rate of the polymer is of critical importance. It is known that molecular weight influences the hydration rate of macromolecular materials, and, in this respect, the polystyrene-toluene system has been the most commonly used system for the studies of polymer dissolution (Ueberreiter, 1968). However, there is no study reported in detail on the hydration behaviour of guar galactomannan in relation to its molecular weight. It will be particularly useful to know to what extent the hydration rate is affected by the molecular weight of guar samples that are of practical interest in the food industry, especially those that are of use in clinical nutrition.

One of the aims of the present chapter was to investigate and compare the hydration rate of the commercial guar gum flours (Meyprogat series) of different average molecular weights. Thus, the guar gum flours were used for each experiment without any pre-treatment except for the adjustment of the moisture content. The effects of concentration on the hydration rate will also be investigated. The main objective of this study is to determine if the polymer concentration will significantly affect the hydration rate of guar gums in the concentration range normally used in clinical trials. It hoped that the results of this study could help us to understand some aspects of the physiological effects of guar gum and provide useful information about the types, doses and mode of administration of guar gum and other s-NSP that should be used to optimise their therapeutical effects.

7.2 Materials and methods

7.2.1 Study of molecular weight effects on hydration rate

Commercial guar gum flours of different average molecular weight (Meyprogat series, Meyhall Chemical AG, Switzerland) were used in this study. The moisture content of samples were adjusted to approximately the same level before hydration experiments. Each sample was placed in a container and left in a sealed incubator containing saturated sodium chloride solutions (in a beaker) for about 24 h at 27°C. Sample characterization including chemical composition, galactomannan content, average molecular weight and particle size were carried out according to the methods described in Chapter 3.

The hydration experiments were carried out according to the method described in Chapter 3 with small modifications. The mixing box rotated at a speed of 6 r.p.m. The ultimate viscosity was determined in a different ways. After the homogenising step the samples were allowed to hydrate for a further 3 h at higher tempterature (40 °C). The moisture loss during the homogenising step was compensated. 1% (w/v) solutions based on galactomannan content and 1.1% (w/v) solutions based on the dry matter weight content of different guar gum flours were used, respectively. Viscosity measurements

performed on the Rheometrics Fluids Spectrometer (RFSII). A plate-plate geometry (50 mm in diameter, 1 mm gap) was used for high-molecular-weight samples including guar gum grades M150 and M120. The couette geometry (for details see Chapter 3) was used for the rest of the samples. The zero-shear viscosity was calculated as the average value of the first four experimental points at the lowest shear rate used (five measurements were made per decades during the viscosity measurement).

7.2.2 Study of concentration effects on hydration rate

This experiment was conducted using M120 guar gum at different concentrations between 0.5% - 1.4% (w/w). The same hydration method was used as described in Chapter 3, but the rotating speed of mixing box was 15 r.p.m. in order for the experiment to cover a wider concentration range. The viscosity was measured using Brookfield rheometer with a small sample adapter and different spindles (see Chapter 3). The zero-shear viscosity was calculated as the average value of the first two points at the lowest range of shear rate used (between 0.1-1s^{-1}).

7.3 Results and discussions

7.3.1 Sample characterizations

7.3.1.1 Chemical compositions

Chemical compositions of guar flours including galactomannan content are summarised in Table 7.1. The galactomannan content of all six samples were found to be slightly different. Generally, the samples of high molecular weight contained a high concentration galactomannan. Apart from galactose and mannose, there were small amount of other monosaccharides present such as glucose and arabinose which accounted for approximately 3% - 5% of total NSP contents and varied in different samples. In contrast, samples of low molecular weight contained a larger proportion of ash than the samples of high molecular weight. This is due to the higher salt content that

is introduced as a result of the hydrolysis treatment when preparing the low molecular weight samples.

Table 7.1 Chemical compositions of guar gum flours (g/100g dry matter). Results are mean of duplicates (n=2) except for the galactomannan content which is the mean of triplicates (n=3). S.D. was the pooled standard deviation of all the samples.

Samples	Protein (Nx5.7)	Fat	Ash	Galacto-mannan	Uronic acid	Total NSP
M7	2.3	0.5	7.9	80.7	1.9	85.6
M30	3.0	0.5	4.5	83.0	1.2	87.3
M60	3.2	1.3	3.1	82.1	1.6	87.0
M90	4.0	1.2	1.7	91.3	2.6	98.0
M120	3.8	1.4	0.5	91.4	2.0	96.6
M150	3.7	1.2	0.6	87.8	1.3	92.8
± S.D.	0.5	0.1	0.1	4.6	0.4	4.9

7.3.1.2 Density

The pycnometer used measures the true volume of a powder sample (i.e. the volume bounded by the outer surface layer and excluding the open pores). From the volume data the true density is calculated. The accuracy of this method is 0.05 g/cm^3. The densities of the six guar gum flours were found to be almost identical as shown in Table 7.2. Although the density of M150 was slightly lower than the others, this may be due to its relatively higher moisture content rather than any real difference in sample density.

Table 7.2 Density of guar gum flours. Results are the mean of triplicates (n=3).

Samples	M7	M30	M60	M90	M120	M150
Moisture (%)	11.9	8.6	9.8	8.6	7.9	12.8
Density (g/cm^3)	1.54	1.58	1.56	1.54	1.51	1.50
S.D. (±)	0.01	0.01	0.005	0.004	0.002	0.001

7.3.1.3 Particle size and specific surface area

Table 7.3 and Table 7.4 tabulated the average particle size (d_m) and specific surface area (A_{sp}) measured by Fisher sub-sieve sizer and Malvern instrument, respectively. All values are the average of triplicates. From the Fisher measurements, the average particle size and specific surface area between each samples were very close to each other except for samples M90 and M60 which had slightly larger d_m and small A_{sp}. There were also small differences in particle size between these samples when measured by the Malvern instrument. The particle size of sample M90 was significantly larger than those of other samples. This is consistent with the results obtained from Fisher measurements. The distribution of particle size was also found to be different as shown in Figs. 7.1a - 7.1f. For example, compared to M150, M120 has a slightly broad range of particle size distribution. The particles with mean diameter smaller than 25μm accounted for 12% of the total particles in M120 (Fig. 7.1b), whereas there was only 6.5% of this fraction in M150 (Fig. 7.1a). This difference also can be seen in SEM images in Figs. 7.2a - 7.2f. It is clear that M120 has a greater proportion of finer particles than M150. The shapes of particles between each sample were also found not to be the same. For example, M90 appears to have more roundish shaped particles compared to M150 and M7 which were more rod shaped.

Table 7.3 Surface volume mean diameter (d_m) measured by Fisher sub-sieve sizer. The specific surface area (A_{sp}) was calculated according to equation 3.8 (see Chapter 3).

Sample	Porosity ± S.D.	d_m (μm)± S.D.	A_{sp}(m^2/g)
M7	0.543±0.003	22.1±0.6	0.176
M30	0.477±0.003	23.2±0.6	0.164
M60	0.454±0.002	24.3±0.1	0.159
M90	0.448±0.004	23.7±0.4	0.164
M120	0.458±0.003	23.1±0.1	0.172
M150	0.508±0.005	23.2±0.1	0.173

Table 7.4 Mean particle size (d_m) and specific surface area (A_{sp}) measured by Malvern instrument.

Samples	$d_m \pm$ S.D. (μm)	$A_{sp} \pm$ S.D. (m^2/g)
M7	55.5±4.3	0.130±0.03
M30	52.7±4.6	0.139±0.03
M60	54.5 ±1.6	0.167±0.04
M90	70.8±3.7	0.128±0.03
M120	50.9±6.7	0.155±0.03
M150	60.7±1.5	0.126±0.02

From the results of above particle size analysis, it is worthy of noting that although the mean particle size and the distribution of the particle size of all the guar gum flours studied here are close to each other, there are still small differences. In particular, sample M120 has a higher proportion of finer particles, and M90 has the largest mean particle size. As it will be discussed below, these differences may have effects on the hydration behaviour of these samples.

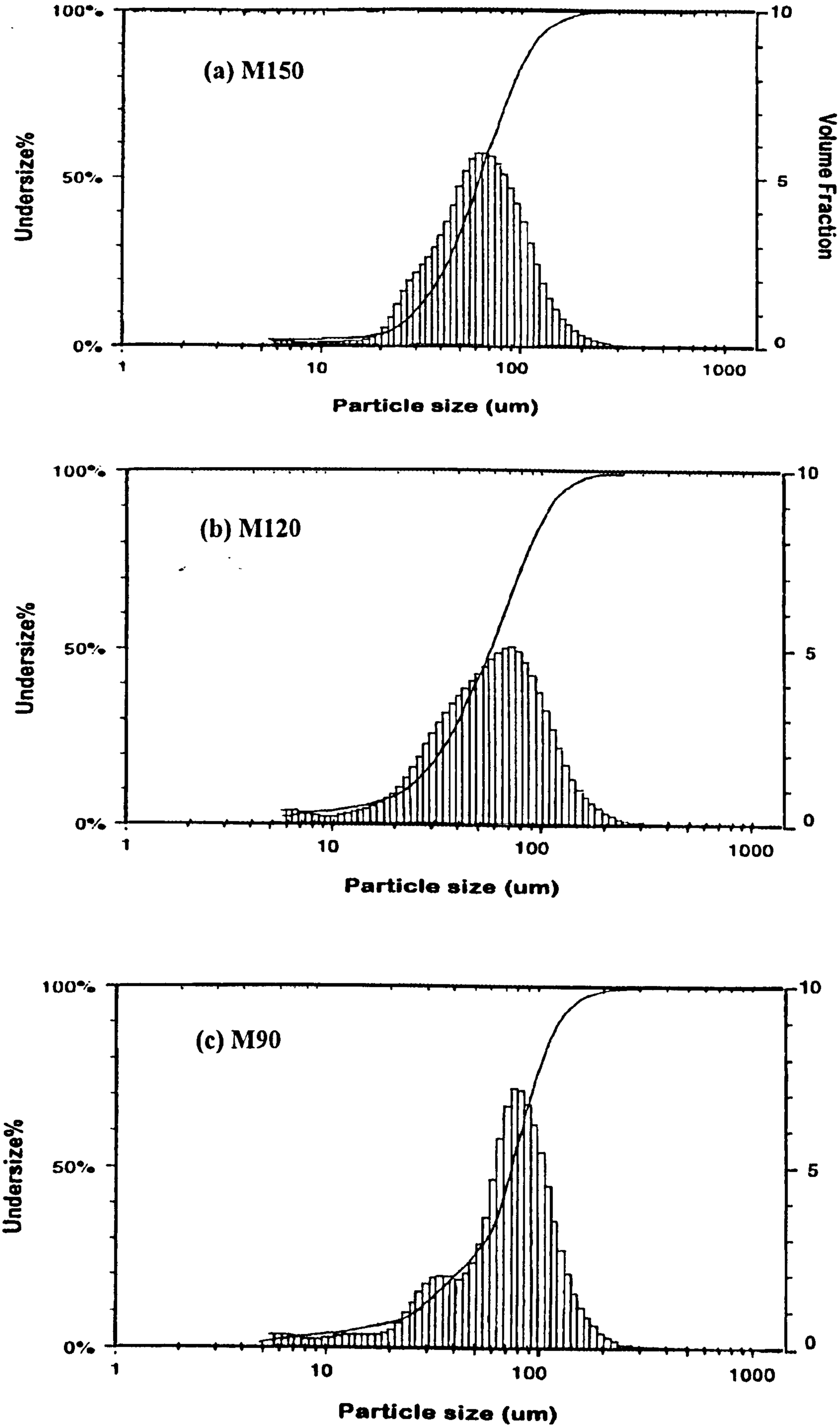

continuing to next page →

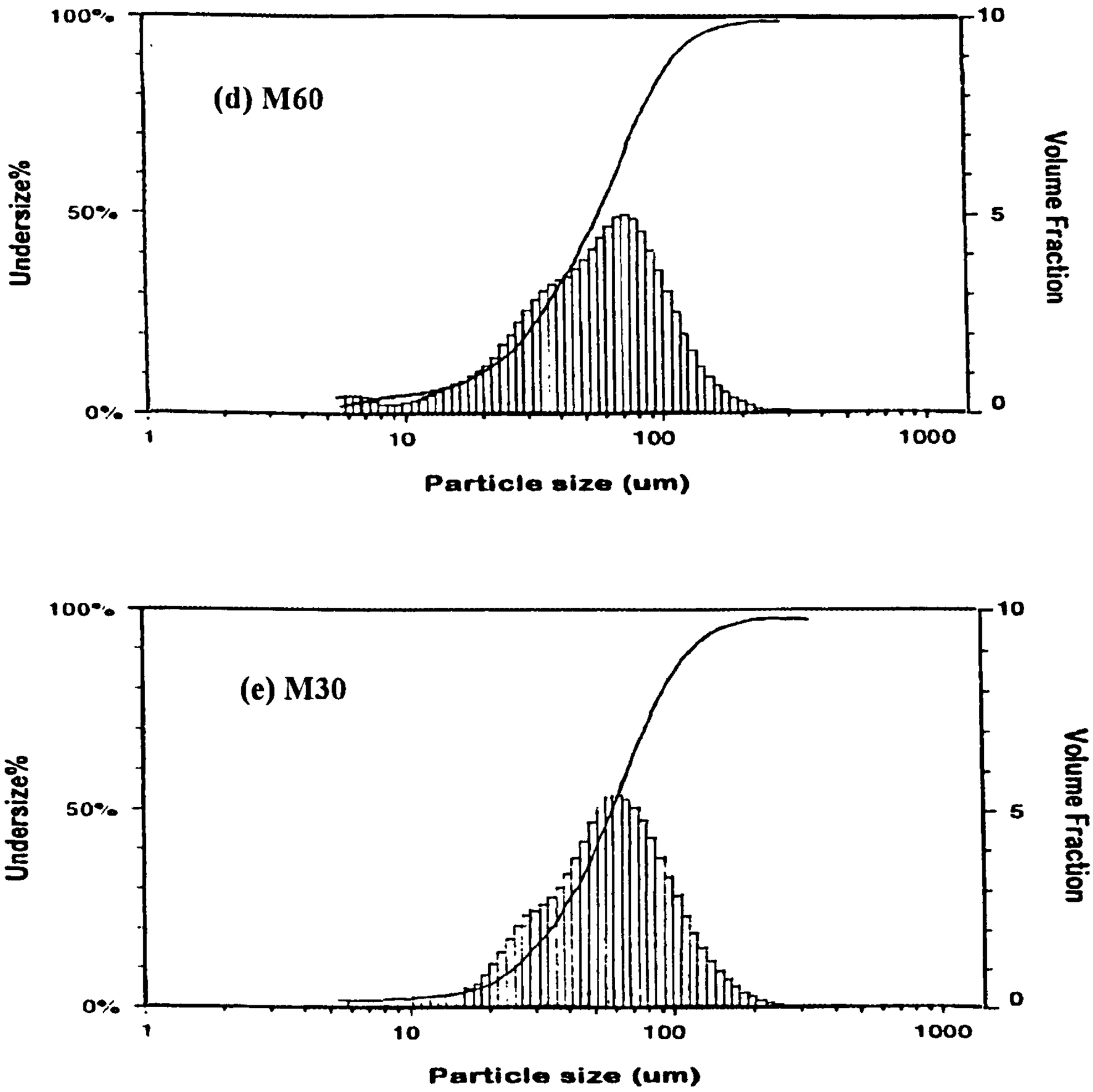

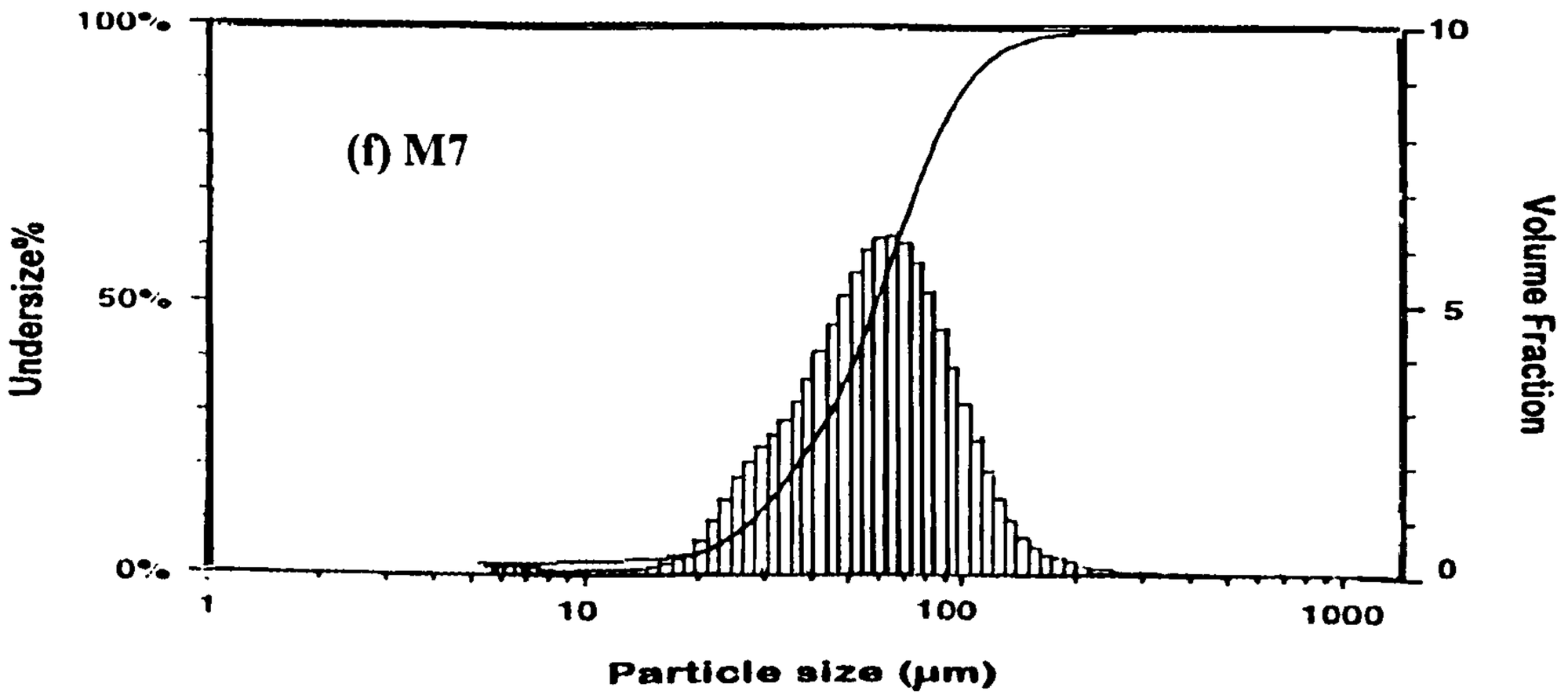

Figs. 7.1a - 7.1f Particle size distributions of guar gum samples measured by Malvern Instrument.


100UM 7.2KV SED 03/5080 M150

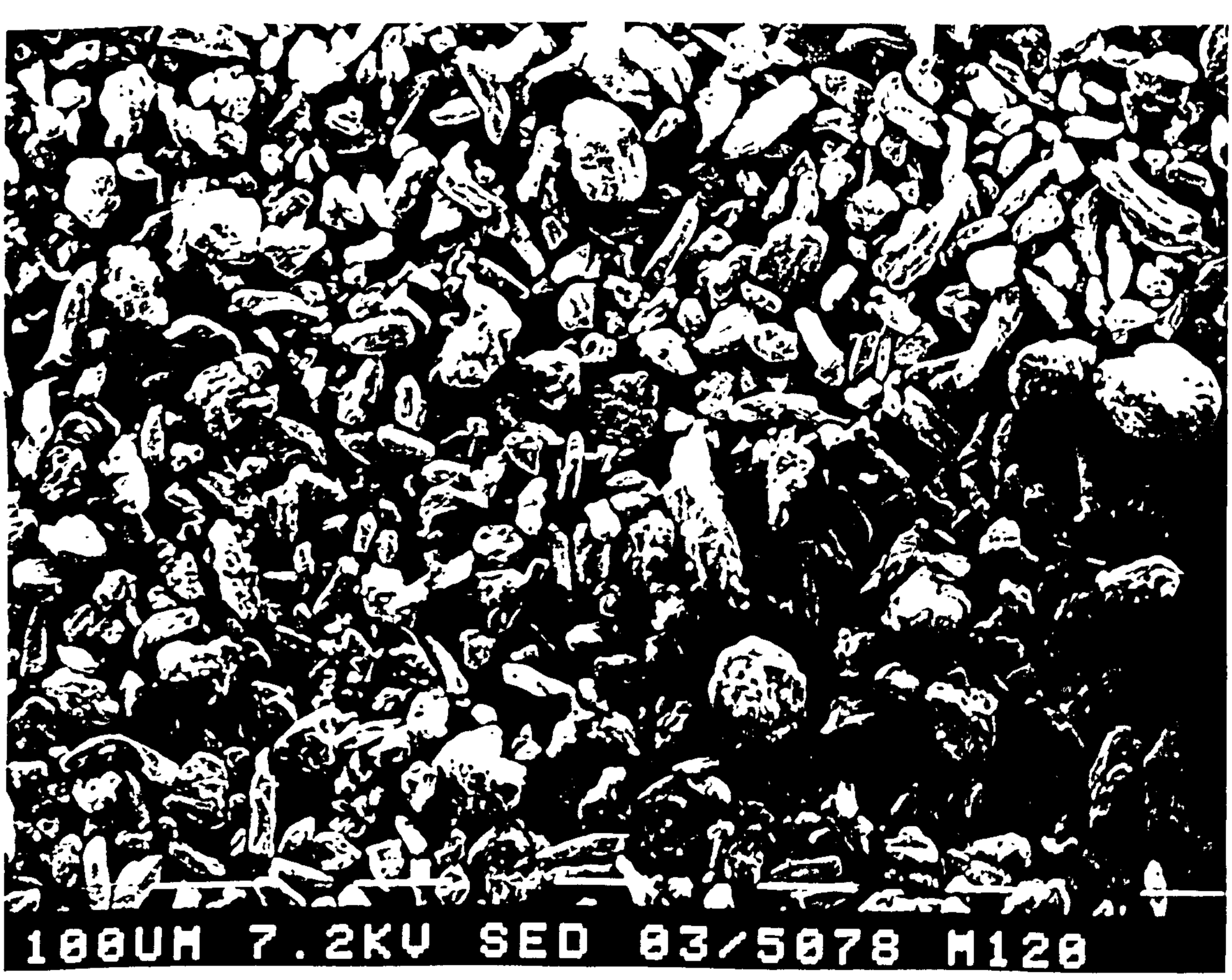
100UM 7.2KV SED 03/5078 M120

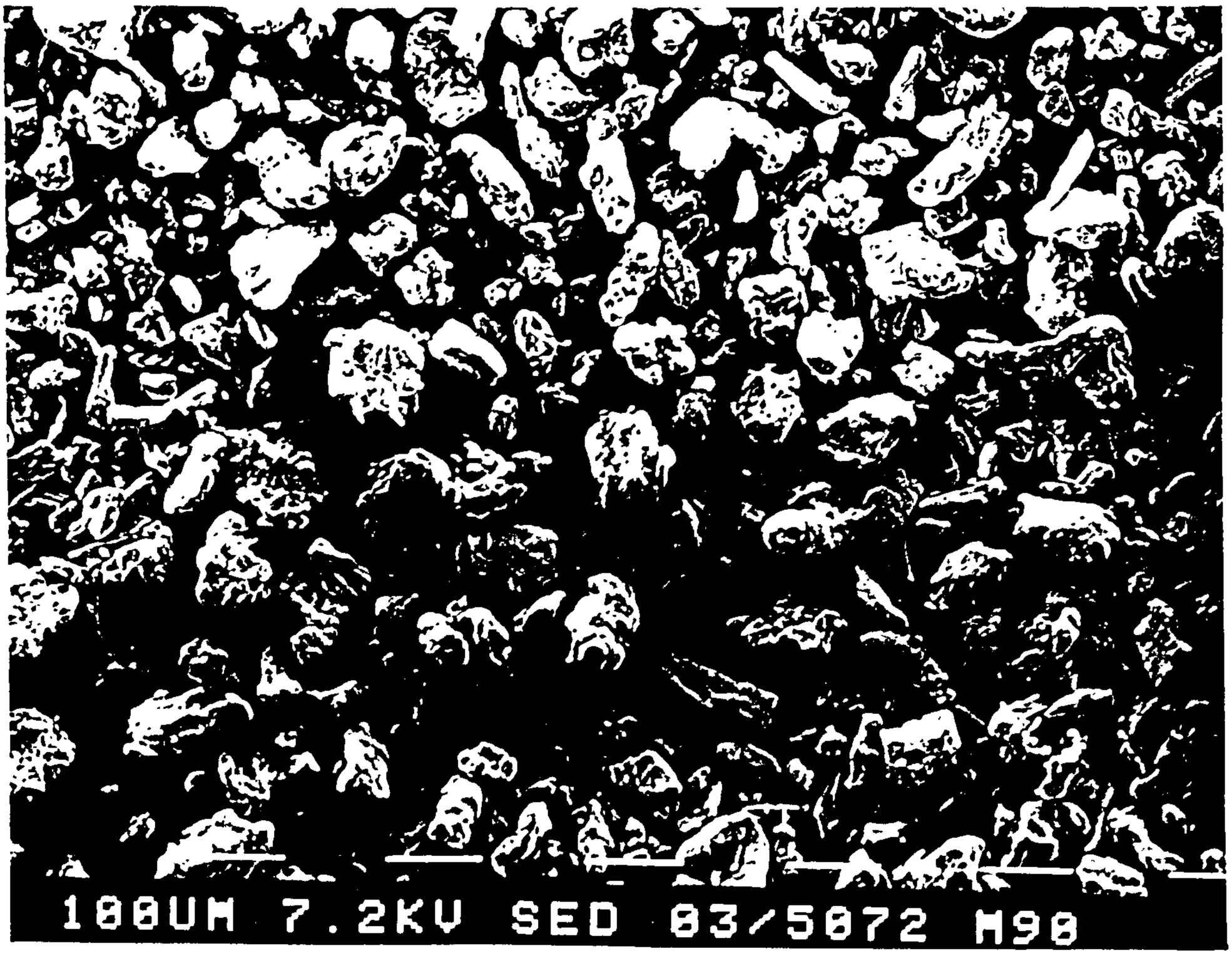
100UM 7.2KV SED 83/5872 M90


100UM 7.2KV SED 83/5869 M60

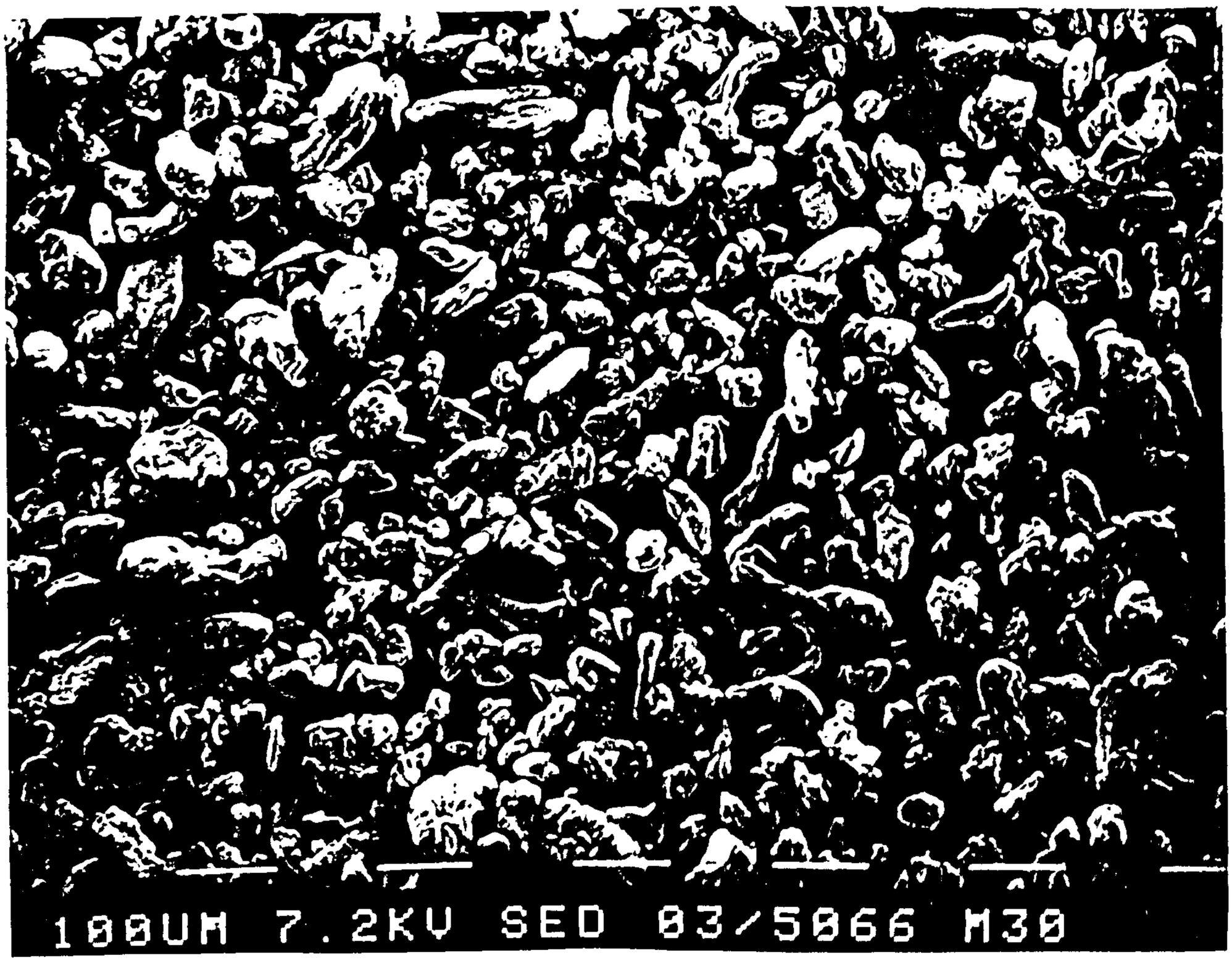

Figs. 7.2 a - 7.2 f Scanning electron microscope images of guar gum flours (Meyprogat series: M150 - M7).

7.3.1.4 Molecular weight estimation

The molecular weight of different samples was again estimated by measurement of the intrinsic viscosity. The viscosity average molecular weight (M_v) was calculated by the Mark-Houwink relationship, given as: $[\eta] = k M_v^{\alpha}$ where $k = 3.8 \times 10^{-4}$, $\alpha = 0.723$. The results are tabulated in Table 7.5.

The intrinsic viscosity values (molecular weight) estimated here were generally higher than one would have expected. This is thought due to the method adopted in this analysis. That is the guar gum samples were purified before measurements were taken. Therefore, in the calculation of the intrinsic viscosity the polymer concentration was accounted for on the basis of the galactomannan content rather than on the dry weight of flour which includes other polysaccharides and impurities as in previous studies. However, it does not exclude the possibility that some small oligosaccharides might be lost during the purification process. (see Chapter 3 for details of the method). It is known (Asp, *et al.*, 1992) that oligosaccharide (normally with less than 10 ~ 15 residues) would not be precipitated in 80% ethanol, which was the concentration used to precipitate galactomannan polysaccharides during purification. Nevertheless, the oligosaccharides will have only very limited contribution to the overall average molecular weight, particularly to the high molecular weight samples.

Table 7.5 Intrinsic viscosity, molecular weight and critical concentration C(=1/[η]) of guar gum flours. All values are means of duplicates.*

Samples	M7	M30	M60	M90	M120	M150
[η] (dl/g)	1.66	3.99	6.75	10.5	15.42	17.53
$M_v x10^{-6}$(g/mol)	0.11	0.37	0.75	1.39	2.37	2.82
C*(%)	0.60	0.25	0.14	0.10	0.07	0.06

7.3.1.5 Moisture content adjustment

Guar samples were exposed to the air with saturated NaCl solution at 27 °C for about 24 hours. It was assumed that the equilibrium moisture content (EMC) was attained after that period. The EMC of all the samples (Table 7.6) are not necessarily exactly the same if the original moisture contents are different. This is because of the so-called absorption hysteresis phenomenon. At any given water activity the water content of a material will be greater during desorption then during absorption at the same temperature. Nevertheless, it is unlikely that such small differences in EMC between the samples will affect their hydration behaviour significantly.

Table 7.6 Equilibrium moisture content (EMC) of guar gum flours under saturated NaCl solution for 24h at 27℃.

Flours	M7	M30	M60	M90	M120	M150
EMC %	12.04	10.03	10.14	10.33	10.19	11.74

7.3.2 Effects of polymer concentration on hydration rate

In Chapter 6 the following double logarithmic model was developed to describe the hydration process of guar gum flours:

$$\ln (1- \eta_t/\eta_\infty) = b + k \ln t \qquad (7.1)$$

where hydration constants k and b can be extracted from the plots of $\ln (1- \eta_t/\eta_\infty)$ *versus* $\ln t$, which is a group of straight lines with slope k and intercept b. The hydration index $t_{0.8}$ defined in Chapter 6 was also used here for comparing the hydration rate of different concentrations.

$$t_{0.8} = (\frac{0.2}{e^b})^{\frac{1}{k}} \qquad (7.2)$$

The experiments were carried out on M120 at a concentration (C) range of 0.5 - 1.4%, corresponding to a C/C* range of 8 - 22. Beyond this concentration range the viscosity was either too low or too high to measure using the Brookfield viscometer (DVII). The experimental results are summarised in Table 7.7 and Figs. 7.3-7.5.

Table 7.7 Hydration constants k, b and $t_{0.8}$ obtained from hydration experiments of different concentrations of M120 guar gum.

C(%w/w)	C/C*	k	b	$t_{0.8}$
0.5	7.7	-0.379	0.321	163
0.6	9.2	-0.399	0.455	176
0.8	12.3	-0.501	0.698	100
1.0	15.4	-0.564	0.737	65
1.2	18.5	-0.585	0.826	64
1.3	20.0	-0.436	0.35	90
1.4	21.5	-0.414	0.288	97

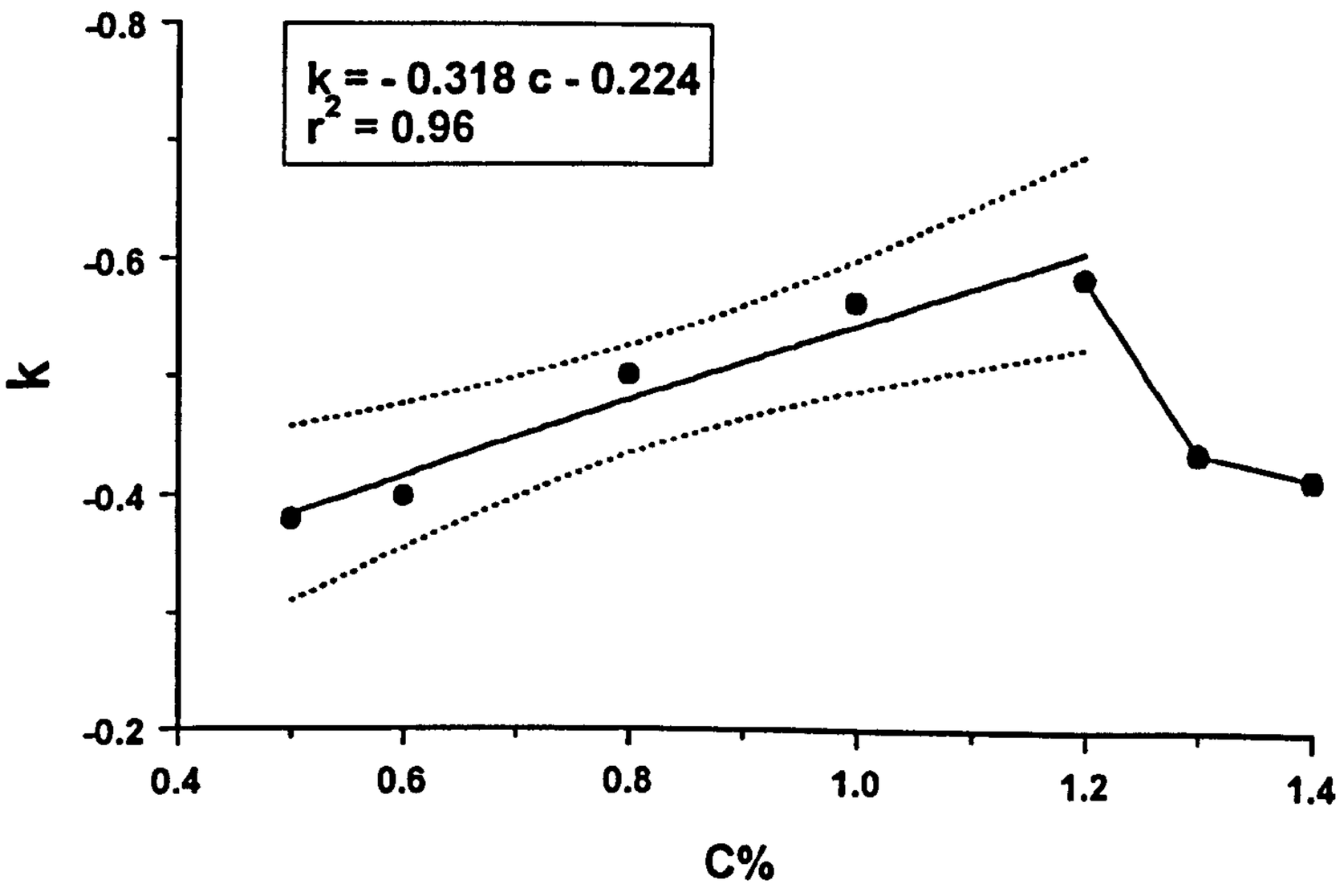

Fig. 7.3 Hydration constant k vs. concentration (C) for M120 guar gum of different concentrations.

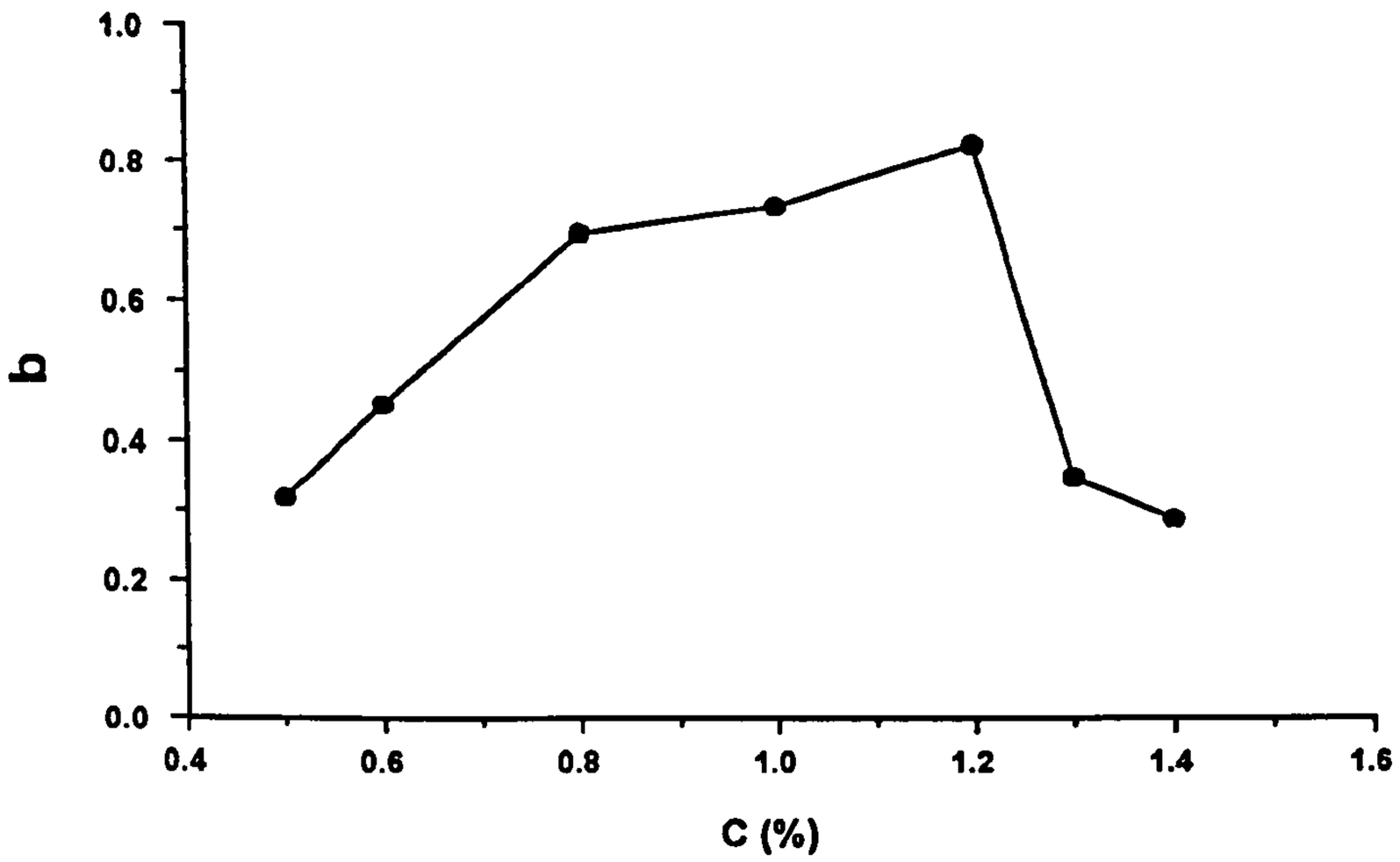

Fig. 7.4 Hydration constant b vs. concentration (C) for samples of M120 of different concentrations.

From Figs. 7.3 and 7.4, it can be seen that in the concentration range 0.6% - 1.2%, both the magnitudes of the slope k and intercept b of hydration curves increase with the increase in concentration. There is an approximately linear relationship (r^2 =0.96, df=3, $p<0.05$) between k and C. According to equation 7.2, the corresponding values of $t_{0.8}$ would decrease with increase in k, but increase with increase in b. Consequently, as shown in Fig. 7.5, $t_{0.8}$ actually decreases with increase in concentration. This indicates that the higher the polymer concentration, the faster the hydration process is within this concentration range. However, at a concentration of 1.2% there was a marked change in this tendency. When C > 1.2%, $t_{0.8}$ increased with respect to concentration increase, indicating that the hydration rate reduced at the concentration above 1.2% (see Fig. 7.5).

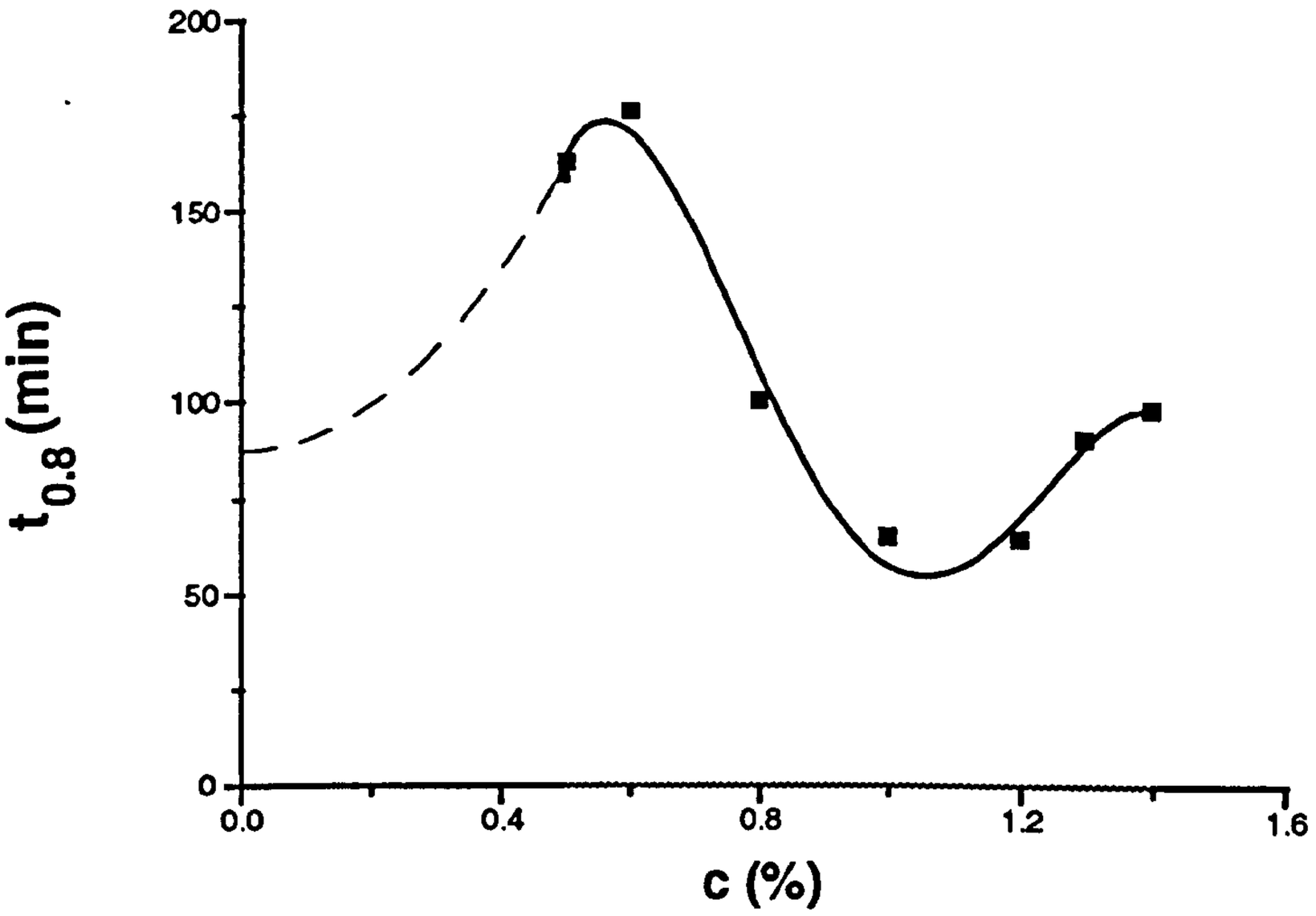

Fig. 7.5 Hydration index $t_{0.8}$ vs. concentration for M120 guar gum. Solid line was the polynomial regression (quadratic) of the experiment data (r^2 =0.960). Dotted line is a prediction of the theoretical behaviour.

From the above results and discussions the relationship between the hydration rate and concentration can be visualised as occurring in three regions, dilute solution region (C < 0.5%), intermediate region (0.6-1.2%) and concentrated region (C>1.2%). Unfortunately, the results of the present experiment did not provide sufficient evidence to illustrate the first region due to technical limitation, apart from the first two concentrations, which showed that the hydration rate of 0.6% was lower than that of 0.5%. Nevertheless, from the consideration of theory, there may be several possibilities. One of these is that the hydration rate is independent of concentration, but only determined by the hydration rate of each single particle. In this case, hydration is achieved mainly through the diffusion process of the polymer molecules since the difference of the concentration between the swollen layer of particle surface and the bulk solution was large and the deposition of the polymer molecules from the solution to the particle surface was limited. However, because the increase in concentration will stimulate the deposition process of the polymer molecules onto the surface of swollen

particles, it is likely that at some stage the hydration rate decreases with the increase in concentration.

In the medium concentration range (0.6 - 1.2%), the hydration rate increased with increasing concentration. It seems difficult to interpret these results at the first sight. Generally, the hydration rate increases with increase the 'effective' specific surface area (m^2/g) of the sample. Thus, contrary to the results of the present study, in the concentration range 0.6 - 1.2%, an increase in hydration rate with an increase in concentration would not be expected, because the initial specific surface area is not change with concentration. Although the mechanism of this process needs more careful study, one possible explanation for the increase in hydration rate in the concentration range 0.6 - 1.2% is that the shear force caused by the rotation of the mixer plays a more important role in this situation.

As has been described in the previous chapter, the powder particles form a swollen gel layer during the hydration process. The deformation of this layer would depend on the viscosity ratio η_{gel}/η_{sol}, here η_{gel} is the viscosity of the gel layer and η_{sol} is the viscosity of the continuous medium, i.e. the solution. The deformation of the gel layer would only occur when this ratio is lower than certain level under a given shear rate. For example, Tolstoguzov *et al.* (1974) have demonstrated that the deformation of a dispersed emulsion droplets in flow was only obtained when the viscosity ratio (η_{emu}/η_{sol}) < 0.7 when $0 < \eta_{emu}/\eta_{sol} \leq 1$, and the deformation increased in proportion to the decrease of this ratio in the range $\eta_{emu}/\eta_{sol} > 1$. Similarly, in the current experiment, deformation is unlikely to have occurred in dilute solutions because of the high viscosity ratio (small η_{sol}). As the concentration increases this viscosity ratio decreases because of the increase in solution viscosity (η_{sol}). The deformation would occur at some stage when this ratio is low enough under a given shear rate. Moreover, in some concentration range, this deformation would be expected to increase with the increase in concentration. The deformation of the outer gel layer facilitated the removal of the polymer molecules from the particle surface. In addition, the deformation also created a new hydration surface, which further enhanced the hydration process.

It is not difficult to explain the mechanism by which the hydration rate decreased with increasing polymer concentration when C>1.2%. It is obvious that the ratio $\eta_{gel}/\eta_{sol} \geq 1$ for the hydration system of guar gum. This implies that the deformation should reach a plateau when η_{gel}/η_{sol} is close to 1 under a given shear rate. Meanwhile, when high viscosity developed, the diffusion of the polymer molecules was highly suppressed, and on the contrary, the deposition of the polymer molecules onto the swollen surface of the particles was increased because of the small difference in concentration between the gel layer of the particles and bulk solution. Moreover, the competition for water molecules increased with the increasing concentration of guar gum; this would also limit the further hydration of guar gum at higher concentrations.

7.3.3 Effects of molecular weight on hydration rate

The initial objective of this experiment was to investigate the differences in the hydration rate of guar gum flours of different average molecular weight. One point that needs to be borne in mind is that the values for many physical factors that influence hydration, such as particle size, shape and surface properties, density etc., are not exactly the same between different guar samples. Thus, it is difficult to distinguish between the effects of M_w and all the other physical factors that are likely to influence hydration. Nevertheless, the molecular weight difference is obviously the most significant factor amongst all these factors.

Because there were difference in galactomannan contents of different grades of samples selected for study (see Table 7.1), this experiment was carried out in two groups in order to take into account of this difference. That is, the hydration rates of different samples were compared at the same concentration at 1% w/v on the basis of galactomannan content (group 1) and at 1.1% (w/v) on the basis of the dry matter content (group 2).

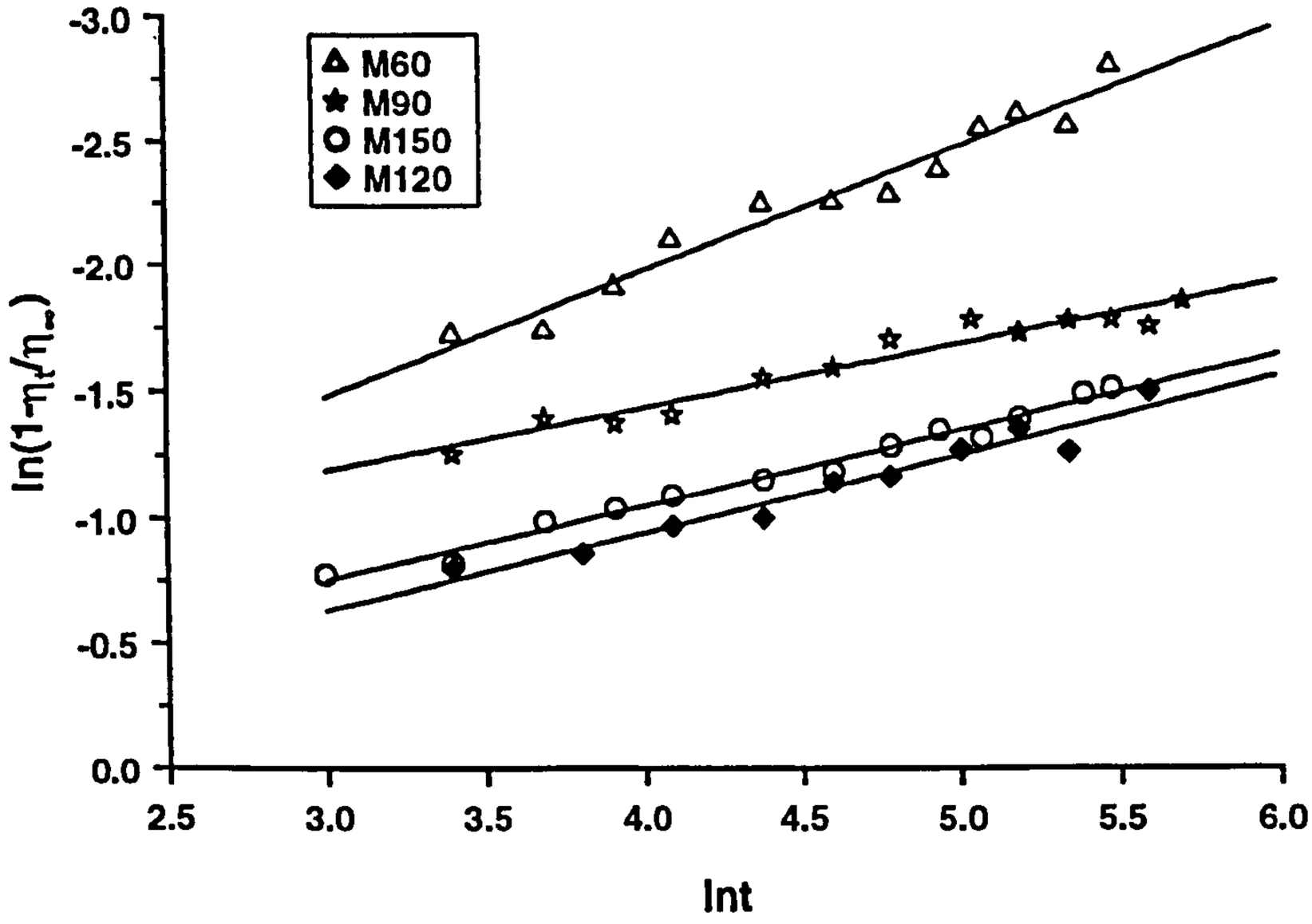

Fig. 7.6 Examples of hydration curves of different guar gum samples according to equation 7.1.

The logarithmic model for hydration was found to fit the hydration curves of all the guar gum samples studied except for the two lower molecular weight samples M30 and M7. Fig. 7.6 is an example of the hydration profiles for 1% M150, M120, M90 and M60 when plotted according to equation 7.1. Samples of M7 and M30 were found to hydrate so rapidly that no viscosity change could be easily and reliably recorded using the present method.

The hydration indices, $t_{0.8}$, calculated for the four guar gum samples were summarised in Table 7.8 and plotted in Fig. 7.7 as a function of molecular weight. The hydration rate were found indeed to be affected by the average molecular weight of the samples. The results showed that the low molecular galactomannan was more rapidly hydrated than high molecular weight polymer, using a polymer concentration (1%, w/w) based either on the same polymer weight or the same dry matter content. This was also in accordance with the hydration behaviour of samples of M30 and M7, which hydrated

extremely quickly. For example, the 1% dispersion of M150 calculated on the polymer basis required approximately 7 times longer to achieve 80% ultimate viscosity compared to M60 of the same polymer concentration. When the comparison was made on these two samples for 1.1% dispersions on the dry weight basis, the $t_{0.8}$ value of M150 was 13 times larger than that of M60.

The only exception to this general trend was sample M120, of which the hydration rate was not so different from M150, despite the fact that it has a lower molecular weight compared to the latter. Indeed, statistics showed that the difference in hydration rate between these two samples was not significant as shown by the error bars which denote 2xS.E. (i.e. 2 times standard error) ($p<0.05$). This indicates that the hydration rate of samples of M150 and M120 were not significantly different.

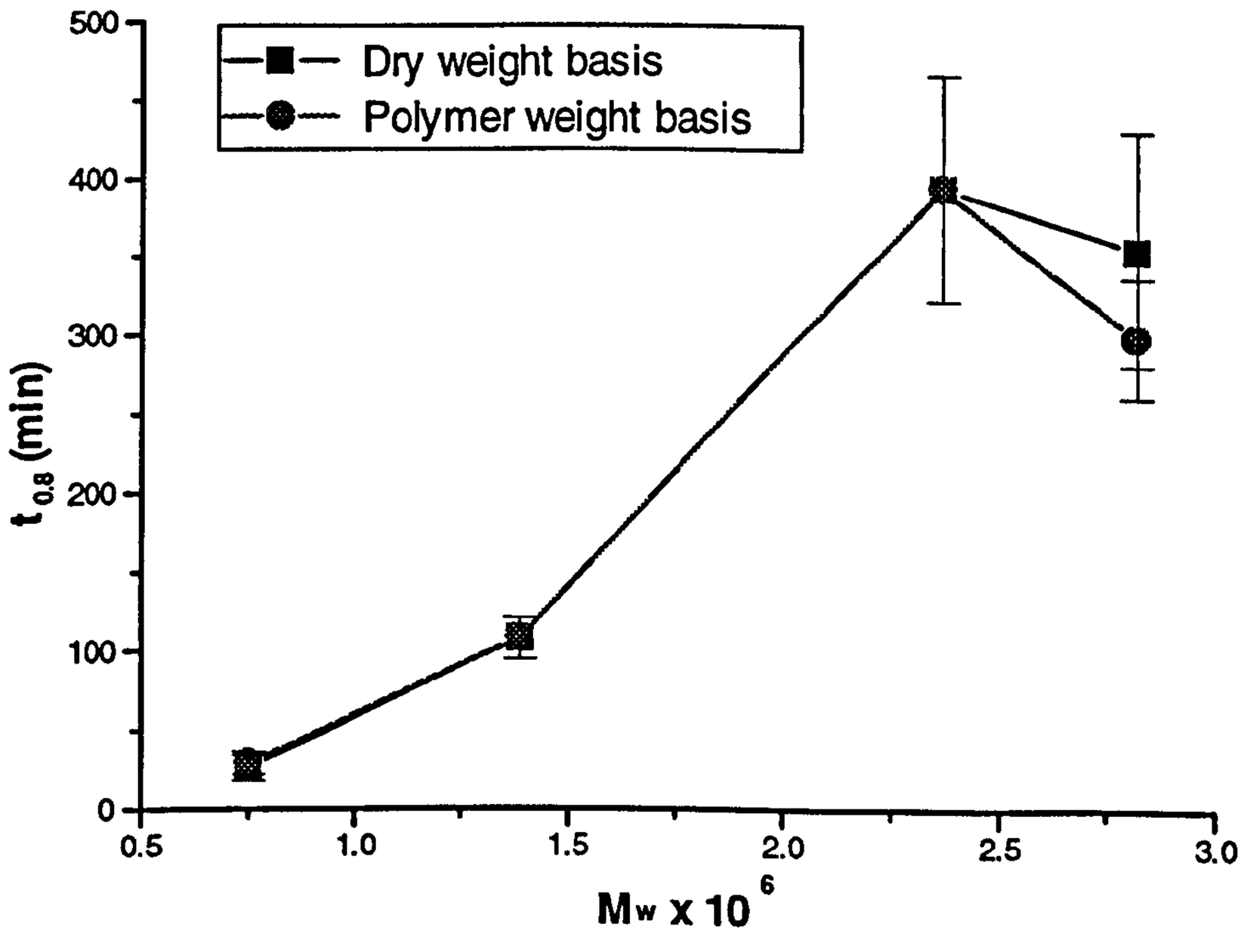

Fig. 7.7 Hydration indices ($t_{0.8}$) of samples of M150, M120, M90 and M60 in relation to average molecular weight. Error bars denote 2xS.E. (p=95%).

Table 7.8 Summaries of hydration experiments of guar gum samples with different molecular weight. GM% denotes galactomannan content. r^2 is correlation coefficient. Values are means of triplicates.

Samples	Polymer basis				Dry weight basis		
	$t_{0.8}$±S.D. (min)	2xS.E.	r^2	GM%	$t_{0.8}$±S.D. (min)	2xS.E.	r^2
M150	307±34	39	0.94	88%	359±65	75	0.93
M120	363±62	72	0.97	91%	363±62	72	0.97
M90	103±11	13	0.90	91%	103±11	13	0.90
M60	29±5	6	0.89	82%	26±6	7	0.90

It is not difficult to explain the apparent abnormal hydration behaviour of M120 when compared to M150. The difference between the average molecular weight of M120 and M150 is relatively small (less than 20%, see Table 7.5). Also, from the SEM images of the sample powders (Fig. 7.2), it is clear that some whole cellular inclusions of galactomannan were still remaining in the M120 sample as in the M150. This indicates that some of the galactomannan inclusions were not degraded at all during the industrial hydrolysis treatment of the M120. Furthermore, as mentioned previously, M120 contains a larger fraction of very fine particles (D_v<25μm) compared to M150. It is likely that most of these particles were mainly produced during the hydrolysis treatment, and therefore contained mainly low-molecular-weight galactomannan. If this was the case, then during the hydration process the molecules from this fraction would hydrate rapidly, but would contribute less to the overall viscosity of the solution because of their relatively low average molecular weight. On the other hand, the fractions with large particle size would tend to hydrate slowly, but make a larger contribution to the solution viscosity because of the relatively higher average-molecular-weight of the galactomannan. In addition to this, the actual polymer concentration of this fraction (with high molecular weight) was actually lower than the proposed concentration (i.e. 1.0%) and therefore lower than that used for M150. For instance, if the low molecular weight fraction accounts for 10% of the total weight of the sample, a 1% solution based

on total sample weight is actually a 0.9% solution based on the high M_w fraction). This concentration difference reduced the hydration rate of M120 even further as previously explained in Section 7.3.2.

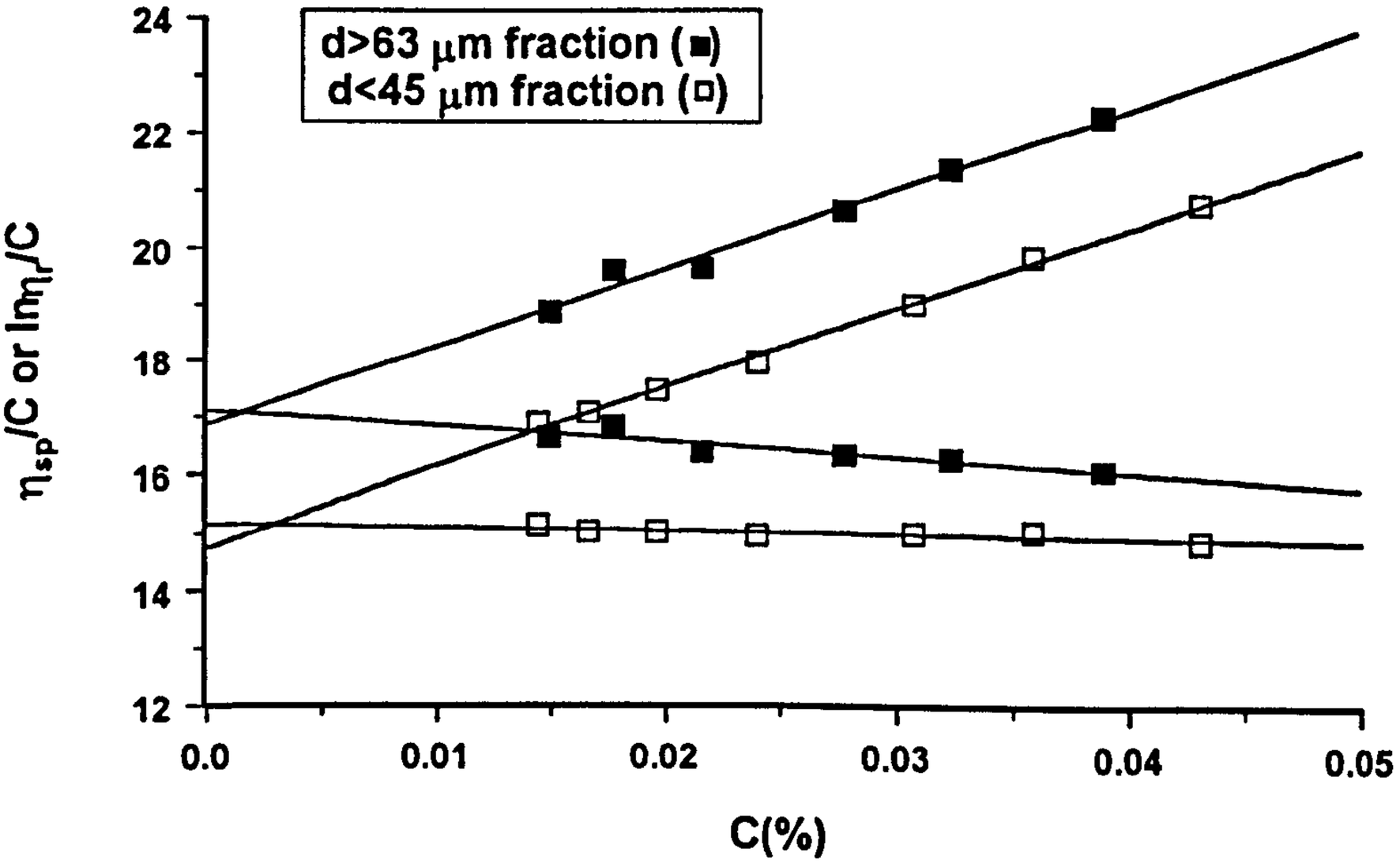

Fig. 7.8 Intrinsic viscosity of two fractions of M120 samples showing that the distribution of the molecular weight was related to particle size distribution.

In order to determine whether there is a difference in molecular weight between different particle size fractions of M120, the intrinsic viscosity of these fractions were measured. Fig. 7.8 shows the intrinsic viscosity plots of two fractions of M120 obtained by seiving method. Fraction 1 accounted for 37% of the total M120 samples (by weight) and consisted of particles < 45 μm. Fraction 2 accounted for 40% of total sample, and consisted of particles > 63 μm. The intrinsic viscosity of the fraction 2 was found to be 17.0 dl/g, which is very close to the intrinsic viscosity of M150 ([η]=17.5 dl/g, see Table 7.3), whereas, the intrinsic viscosity of fraction 1 was 14.9 dl/g. This confirms the view that the lower particle size fraction of M120 contained a larger fraction of hydrolysed and therefore low-molecular-weight galactomannan. This assumption can also be tested in the future by preparing blends of skewed molecular weight distribution.

7.4 Conclusions

In this chapter, the effects of concentration and molecular weight on the hydration rate of guar gum flours have been investigated. The hydration rate was found to be strongly dependent on the polymer concentration, but this relationship is complex. At intermediate polymer concentrations, the hydration rate increases with increase in concentration. This was thought to be caused by the swollen gel layer of guar gum particles becoming deformed by the shear force of mixing. At more concentrated systems, the increase in concentration will suppress the hydration, thus hydration rate is reduced. Although this mechanism is based on the results obtained from M120 guar sample, this explanation can probably be applied to other grades of guar gum and other similar polymers.

It was also concluded that molecular weight had a significant effect on the hydration rate of the guar gum samples studied. The results clearly show that there is an inverse relationship between molecular weight and hydration rate. Although the hydration rates of M120 and M150 were found not to be significantly different, this was thought to be due to the irregularities of the distribution of the molecular weight of M120 with respect to the particle size.

Chapter 8

Effects of particle size on hydration rate of guar gum powders

8.1 Introduction

8.1.1 Background

The particle size of polysaccharide gums greatly influences their physico-chemical properties, including their rate and degree of hydration. Usually, the rate of hydration of small particles is greater than that of large ones, because the rate of hydration of particulate materials is dependent on the specific surface area in contact with the liquid medium (O'Connor and Greenberg, 1959). However, in the case of some neutral polysaccharides such as guar and tamarind gums, the uncharged molecules have a strong tendency to form large aggregates. Therefore, the effect of particle size on hydration behaviour is somewhat more complex. Coarse material with small specific surface area will hydrate slowly and sink rapidly when added to water without enough mechanical agitation. On the other hand, extremely fine particles often hydrates so rapidly that any material caught in the wet surface film will immediately agglomerate. This will delay further hydration because of the reduced "effective" surface area. Devotta *et al.* (1994) demonstrated experimentally that there is a critical particle size of the polymer particles below which the dissolution time was independent of particle size. However, this experiment was carried out using a single particle and did not take into account the possibility of aggregation of the fine particles.

In industrial applications, various methods have been developed to yield uniform dispersions of such polysaccharides. For example, the use of an inert solid material, such

as sucrose powder, or, the use of an inert water-miscible liquid, such as methanol and glycerol, may bring about a physical separation of the polysaccharides particles, thereby enabling them to hydrate independently without "lumping". The added materials may be removed by dialysis, or, in the case of the more volatile alcohol, by evaporation. However, when polysaccharides are used as food supplements for certain therapeutical purposes and consumed in solid form, selecting the appropriate particle size for obtaining the desired hydration rate becomes extremely important.

The aim of this chapter is to investigate the hydration behaviour of guar gum with respect to different particle size using the hydration method described in Chapter 6. The particle size selected here covers a broad range of size including the usual size range of commercial guar gum flours (Meyprogat M150 to M7).

8.1.2 Previous studies

There have not been many systematic studies reported in the area of hydration of polysaccharides, especially regarding the effects of particle size on hydration rate. Pittet (1965) cited that coarse particles of Guaran (a commercial granulate guar sample) may be dispersed into water by hand-stirring, whereas a finely powdered guar gum sample required vigorous mechanical agitation to obtain a smooth 1% w/w dispersion. Ellis *et al.* (1991) studied the physiological properties of wheat breads containing guar gum samples with respect to molecular weight and particle size. They reported marked difference in the development of viscosity for samples of different particle size *in vitro.* To *et al.* (1994) also investigated the hydration rate of three guar gum flours of size range between 50μm-150μm. They observed that the hydration rate increases with reduction in particle size. These studies further stressed the importance of investigating the effect of particle size on the hydration properties of polysaccharides with regards to their biological function.

Kroger (1993) reported that the thermal stability of guar gum was improved with increasing particle size. Although the author did not mention this, a higher proportion of undissolved polysaccharides in coarse samples may be partially responsible for the

improved thermal stability. This is because for most plant cell wall polysaccharides, a proportion of water-soluble polysaccharide is likely to be trapped in the cell wall, thus remaining undissolved. The proportion of material remaining undissolved may be greater in coarse materials than in fine particles. Thus, although on the one hand, excessive heating may cause polysaccharide degradation, on the other hand, it can also increase the proportion of the dissolved polysaccharide. As a consequence, the reduction in viscosity caused by polymer degradation was partially compensated by an increase in concentration of the hydrated polysaccharide. The solubility of polymer materials has been observed to depend on particle size previously (Irani and Callis, 1963).

8.2 Experimental

8.2.1 Materials

Samples used in this experiment were kindly provided by Dr. W. C. Wielinga *et al.* (Meyhall Chemical AG, Kreuzlingen, Switzerland). All the six guar gum powders were ground directly from the same batch of guar endosperm in order to minimise differences in physical and chemical properties such as molecular weight, polymer content etc. Special care was taken to minimise the possibility of molecular degradation. The control of particle size was achieved by the control of milling time and passage times. The molecular weight was examined by the measurement of intrinsic viscosity as described in Chapter 3. The galactomannan content was analysed according to the Englyst method (see Chapter 3).

8.2.2 Particle sizing

The choice of methods of particle size analysis is limited by the particle size range and also the available experimental conditions. The particle size of the samples used in this experiment covers a wide range of size. Nowadays, there are many modern techniques to analyse the particle size. However, the sieving method is still one of the easiest and most widely used methods. In this experiment the samples of large particle size (Master

C, D, E, G) were analysed by the sieving method and those of small particle size were analysed with a Malvern laser diffraction particle sizer at the Department of Pharmacy, King's College London. Both methods and their principles have been described in detail in Chapter 3.

8.2.3 Modified hydration method

The hydration method described in Chapter 3 was modified slightly in this experiment. For samples of large particles the measurement of viscosity was affected by the inclusion of the undissolved particles. At present it is difficult to evaluate the contribution of these particles to the viscosity of the dispersion. The difficult lies in the lack of information of factors such as the fractional volume of the particles and the size and shape of the particles, which are continuously changing during the hydration process. Thus, before viscosity measurements were made aliquots of the guar solution were centrifuged on a microcentrifuge (Eppendorf 5414S, 15000 r.p.m.) for about 60-90 seconds. The supernatants were used for the measurements of the viscosity development during hydration process. Therefore, the viscosity measurements for each time point was delayed by about 3 min. The rotating speed of mixing box was 10 r.p.m. in this experiment. The ultimate viscosity was measured as described in Section 7.2.1.

8.3 Results

8.3.1 Particle size analysis

Surface area and volume are two important parameters of particles and they are proportional to the square and cube, respectively, of some characteristic dimension. The constants of proportionality depend upon the dimension chosen to characterise the particle. The surface area per unit volume is called volume-specific surface (S_v). In sieve analysis, S_v can be obtained by:

$$S_v = \alpha_{sv} \Sigma \frac{w_r}{d_{a,r}} \qquad (8.1)$$

where w_r is the fractional weight residing between two sieves of average aperture $d_{a,r}$ (Allen, 1990) and α_{sv} is surface-volume shape coefficient. $\alpha_{sv} = 6$ for spheres and increases when the particles become rod-like or flaky. The complete standards may be obtained from British Standards BS4359 (1970) Part 3. In the present study $\alpha_{sv} = 10$ was selected by examining the shapes of the powder particles through SEM images.

If a particle analysis is carried out by two different techniques, the two results can be brought into coincidence by multiplying by a shape factor provided that particle shape does not change with particle size (Allen, 1990). In the present study, one of the samples of medium size (Master G) was analysed using both sieving and laser diffraction methods. The ratio ψ_d (i.e. the shape factor) was obtained from these two measurements as follows:

$$\psi_d = \frac{d_s}{d_m} \tag{8.2}$$

where d_s and d_m are the characteristic size obtained by sieving and Malvern techniques as described in Chapter 3, respectively. This ratio was applied to convert the results obtained by Malvern to that of the standard sieving result. In other words, a diameter determined by Malvern analysis multiplied by the ratio ψ_d would yield the sieving distribution. This procedure and results are demonstrated in Fig. 8.1.

From Fig. 8.1, ψ_d was calculated as:

$$\psi_d = \frac{d_{s,0.5}}{d_{m,0.5}} = \frac{75.6}{112.5} = 0.67 \tag{8.2a}$$

where $d_{s,0.5}$ and $d_{m,0.5}$ are the median size of sample g obtained by sieving and Malvern methods, respectively (i.e. it is the 50% size on the cumulative frequency curve).

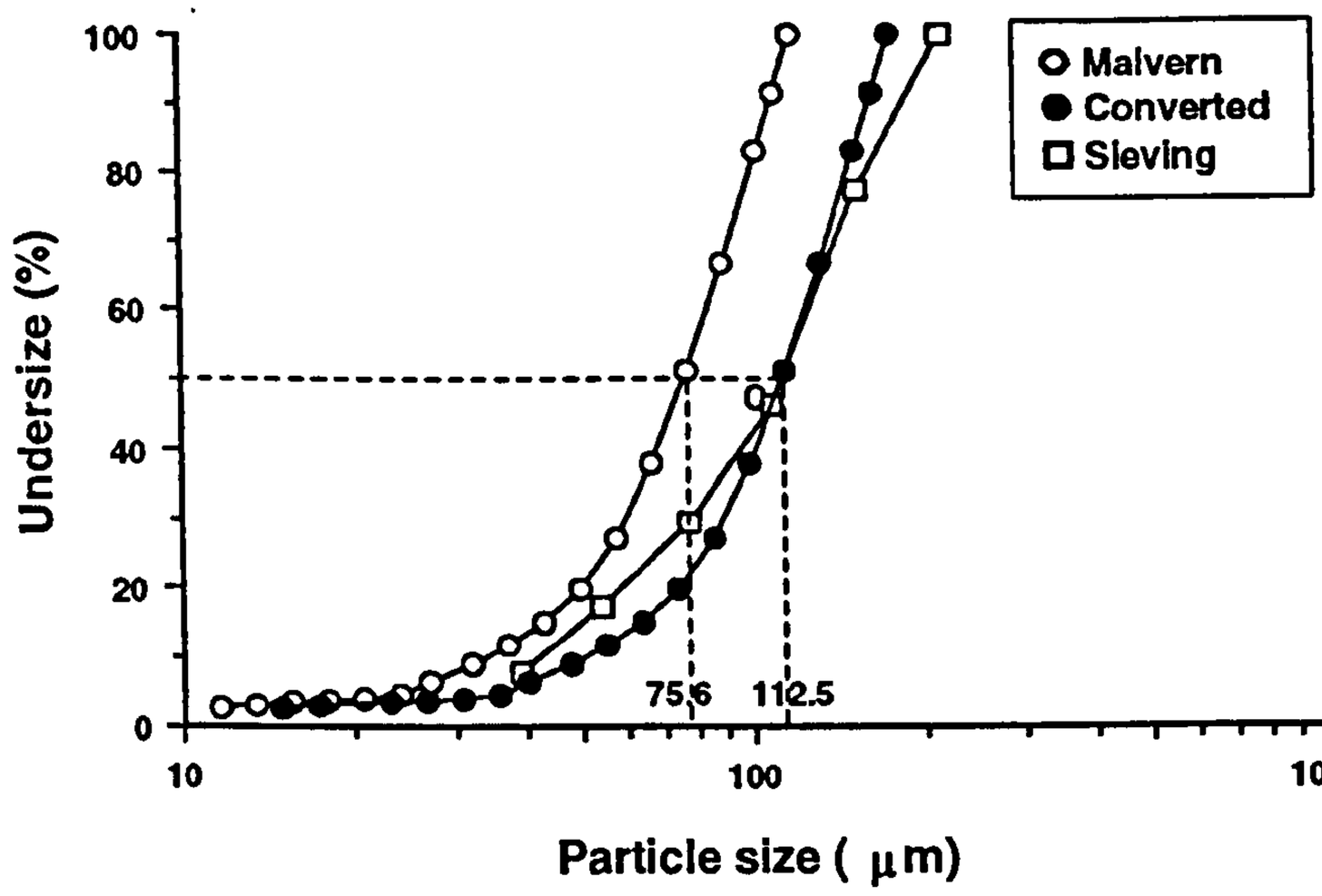

Fig. 8.1 An example (Master G) of converting particle sizing distribution of Malvern data to sieving size using ratio ψ_d (see equations 8.2, 8.2a). where $d_{s,0.5}$ =112.5 and $d_{m,0.5}$=75.6 are the median size of Master G obtained by sieving and Malvern methods, respectively.

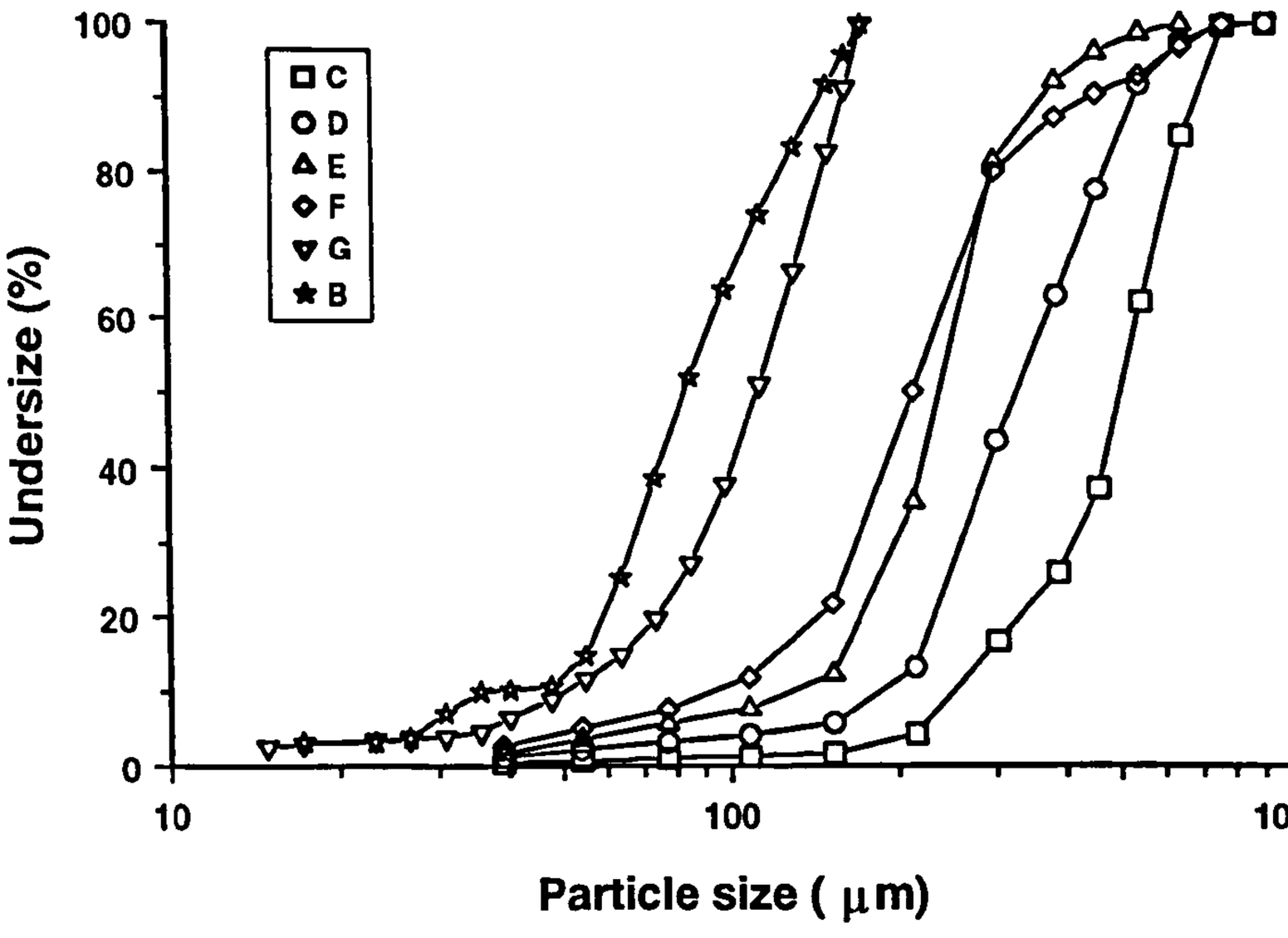

Fig. 8.2 Cumulative percentage curves for samples B to G. Data of samples B and G were produced from Malvern measurement and converted to sieving size using ratio ψ_d. The rest of the data was obtained by sieving analysis.

The results of particle size analysis are presented in the form of cumulative undersize percentage frequency curve in Fig. 8.2, in which the curves of samples B and G are converted sieving size using ratio ψ_d, and the others were obtained by sieving analysis. From equation 8.1 the volume-specific surface (S_{sv}) and mean diameter $d_{sv} = \alpha_{sv} / S_{sv}$ were calculated and tabulated in Table 8.1.

Table 8.1 Volume-specific surface area (S_{sv}) and mean diameter (d_{sv}) for guar samples of different particle size. Data of samples B and G were produced from Malvern measurement and converted to sieving size using ratio ψ_d. The rest of the data was obtained by sieving analysis.

	S_{sv} ($x10^{-4}$ m^2/m^4)			d_{sv} (μm)		
Samples	t_1	t_2	Mean	t_1	t_2	Mean
B	16.4	17.6	17.0	61	57	59
C	2.0	2.2	2.1	500	454	469
D	3.3	3.4	3.4	303	294	297
E	4.4	4.8	4.6	227	208	218
F	5.1	5.4	5.2	196	185	192
G	12.9	11.9	12.4	78	84	81

8.3.2 Galactomannan content

The galactomannan content of guar sample was analysed using the Englyst method. From the initial analysis, the total galactomannan contents of the six samples were found to be significantly different. The galactomannan contents were found to be higher in samples of small particle size compared to those of larger particle size. In order to investigate this further, the samples of larger particle size were finely ground by a laboratory hand grinder and re-analysed. From Table 8.2 it can be seen that the total galactomannan contents of all the samples (including these re-ground) are then reasonably close to each other. The (pooled) standard deviation of the mean

galactomannan content of all the samples was ±1.5%, which was well within experimental error.

*Table 8.2 Galactomannan content and intrinsic viscosity of guar gum samples of different particle size. * denotes intrinsic viscosity obtained after solutions were homogenised, or galactomannan content of re-ground samples.*

Samples	B	C	D	E	F	G	S.D. (±)
Moisture (%)	10.5	11.4	11.5	11.8	11.8	10.3	0.7
Particle size d_{sv} (μm)	59	469	297	218	192	81	
Galactomannan(%)	89.4	86.2*	87.5*	86.2	87.9	85.3	1.5
Intrinsic viscosity (dl/g)	16.0	16.1* 15.1	16.7* 15.3	16.9* 16.1	16.4	17.3	0.5

8.3.3 Molecular weight

The molecular weight of samples was estimated by intrinsic viscosity measurement. Just as in the case of the galactomannan analysis, intrinsic viscosity was also dependent on particle size. Thus, the larger the particle size samples produced smaller intrinsic viscosity. However, when the solutions of larger particle size guar gum were homogenised using a sonic mixer for about five minutes and left for further mixing for a couple of hours at room temperature, the intrinsic viscosity significantly increased compared to unhomogenised solutions (the compensation for water evaporation was always made). As shown in Fig 8.3 and Table 8.2, after this treatment the standard deviation of mean intrinsic viscosity was only ±0.5 for the mean of all the samples. This indicated that, in materials of large particle size a higher proportion of the water-soluble galactomannan is unavailable for hydration unless vigorous disruption. Thus, the initial variation in intrinsic viscosity between the guar samples was caused by differences in concentration of hydrated galactomannan rather than any real difference in molecular weight. This further confirmed that the solubility of guar gums is indeed particle size dependent.

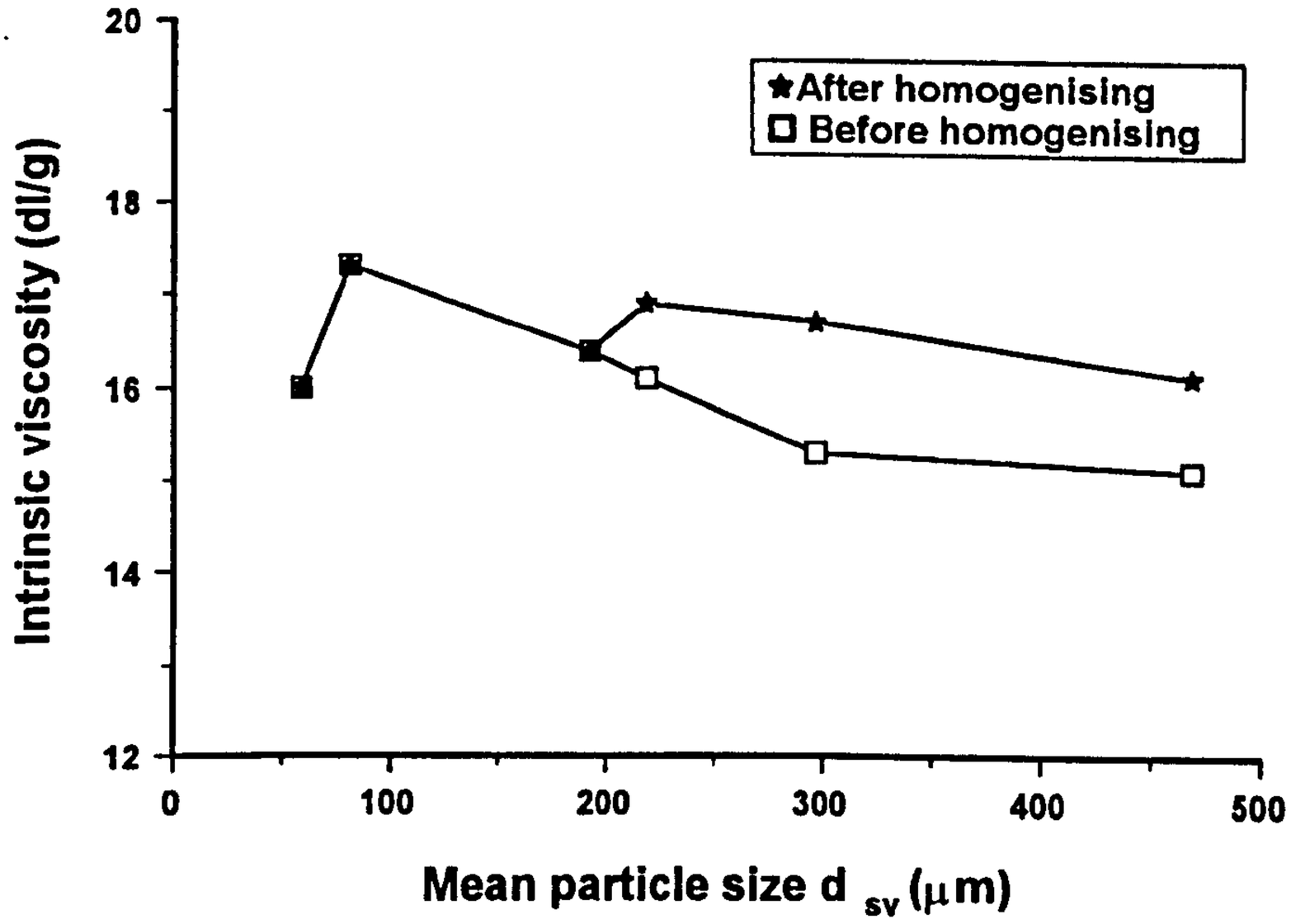

Fig. 8.3 Plots of measured intrinsic viscosity [η] vs. mean particle size d_{sv}, showing the effect of the homogenising of the sample solutions on [η].

8.3.4 Hydration properties

Fig. 8.4 describes the hydration profiles of all six samples over 6 h. Each sample was measured in duplicate or triplicate. The difference between the replicates was reasonably small as can be seen from Fig. 8.4. The ultimate viscosity was taken after the dispersion was homogenised for about 6 min (the temperature did not exceed 40°C), and then allowed to hydrate for a further 3 h at 40°C. A measurement after 24 h was also taken and compared to the previous value. In most cases, there was little difference between these two values. On a few occasions, the viscosity decreased slightly after 24 hours. Two factors which might be responsible for this decrease in viscosity are microbial degradation and/or enzymatic hydrolysis. It has been reported previously that a dispersion of guar gum gradually lost its viscosity after 24 hours at 25°C depending on the levels of bacteria in the sample (Goldstein and Alter, 1973). The ultimate viscosities of all the samples were found to be similar, which correlates with the galactomannan content. However, as discussed in the previous section this does not mean that the

proportion of water soluble fraction of all the samples is the same. Without the homogenisation step used in the current study, the hydration time needed for all the galactomannan to go into solution, may reach infinity for samples of very large particle size. For example, the dispersion viscosity of sample C had only developed about 10% of its ultimate viscosity after 6 h hydration.

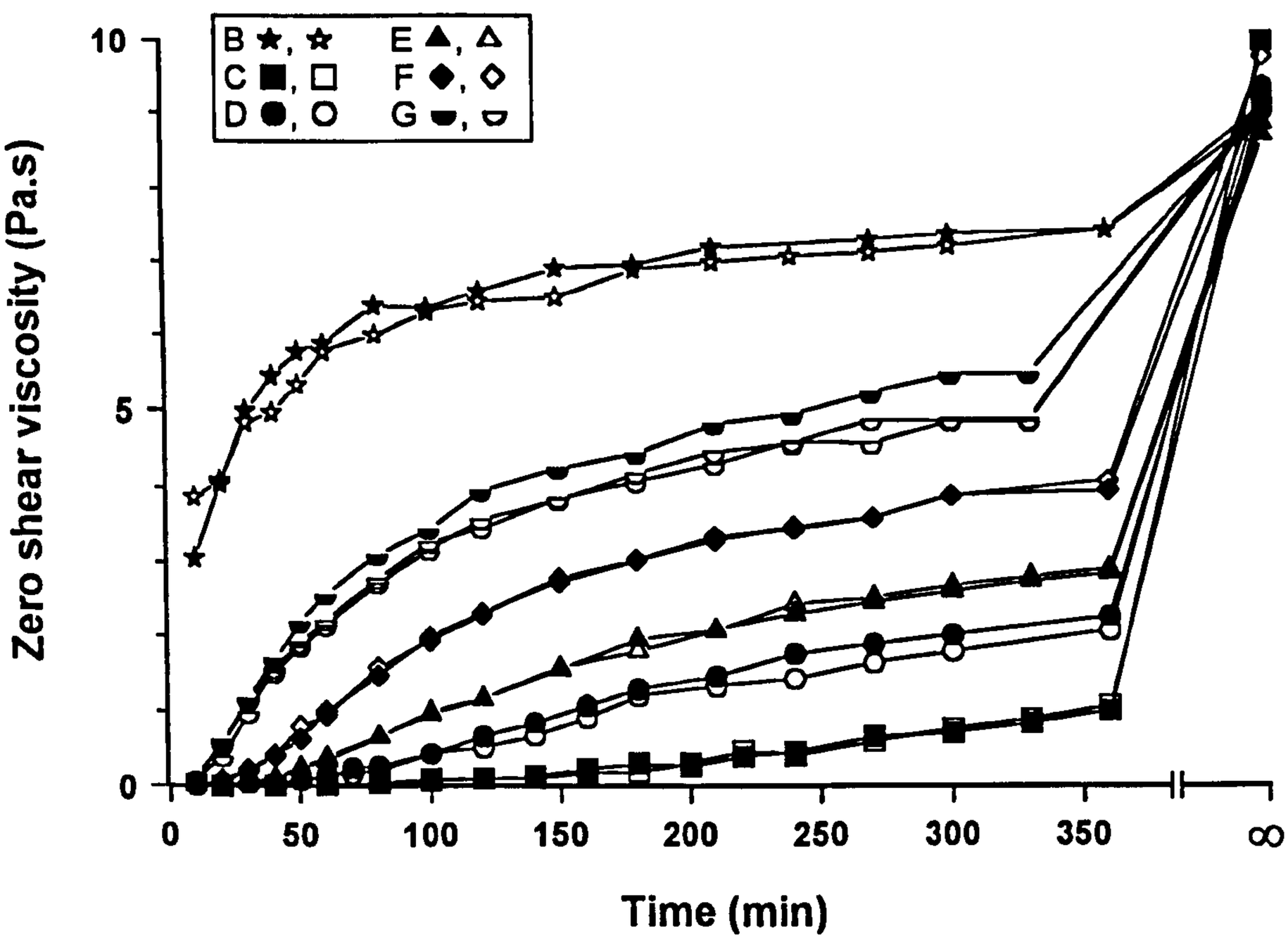

Fig. 8.4 Hydration profiles of guar gum samples of different particle size measured by zero-shear viscosity development.

The hydration model developed in Chapter 6 was found to fit very well with data of samples B, G and F. But it was not suitable for samples of big particle size (samples C, D and E). In order to compare the hydration rate of all the samples a new hydration index had to be introduced. By applying a polynomial regression, each hydration profile in Fig. 8.4 can be expressed by the following equation:

$$\eta(t) = a_0 + a_1 t + a_2 t^2 + a_3 t^3 + a_4 t^4 \ldots\ldots \qquad (8.3)$$

Thus, $d\eta/dt$ is the instantaneous hydration rate measured by viscosity development at each time point. $d\eta/dt$ may be obtained by differentiating equation 8.3:

$$\eta'(t) = d\eta/dt = a_1 + 2a_2 t + 3a_3 t^2 + \ldots\ldots + na_n t^{n-1} + \ldots\ldots\ldots \qquad (8.4)$$

Then, by applying the first-derivative test or the second-derivative test the maximum value of $\eta'(t)$ can be obtained: $m = (d\eta/dt)_{max}$. Here, m is actually the maximum hydration rate during the hydration process. There is a corresponding time point t_{max}, at which the fastest hydration rate lies. At this point we define our new hydration index as:

$$\nu = m/t_{max} \qquad (8.5)$$

The physical meaning of equation 8.5 will be discussed later in this chapter.

All data were found to be fitted well by no more than a cubic model. The regression results were tabulated in Table 8.3 and illustrated in Fig. 8.5. Fig. 8.6 represents the corresponding derivatives of data in Fig. 8.5, (i.e. the curves of instantaneous hydration rate *vs.* time). The maximum hydration rate (m) and the corresponding time (t_{max}) may also be read approximately from this figure or calculated from the regression equations. From these, the hydration index can be calculated according to equation 8.5 for each sample.

Table 8.3 Polynomial regression results (equation 8.3) for viscosity development of samples B to G during the hydration process.

	B	C	D	E	F	G
a_0	3426	27.5	-61.03	-2.48E2	-5.267E2	-3.149E2
a_1	44.0	-1.116	1.766	1.133E1	3.066E1	5.269E1
a_2	-0.1814	1.572E-2	4.23E-2	9.14E-3	-7.159E-2	-1.918E-1
a_3	2.486E-4	-1.386E-5	-8.75E-5	-4.67E-5	5.951E-5	2.474E-4
r^2	0.97	0.996	0.994	0.998	0.995	0.994

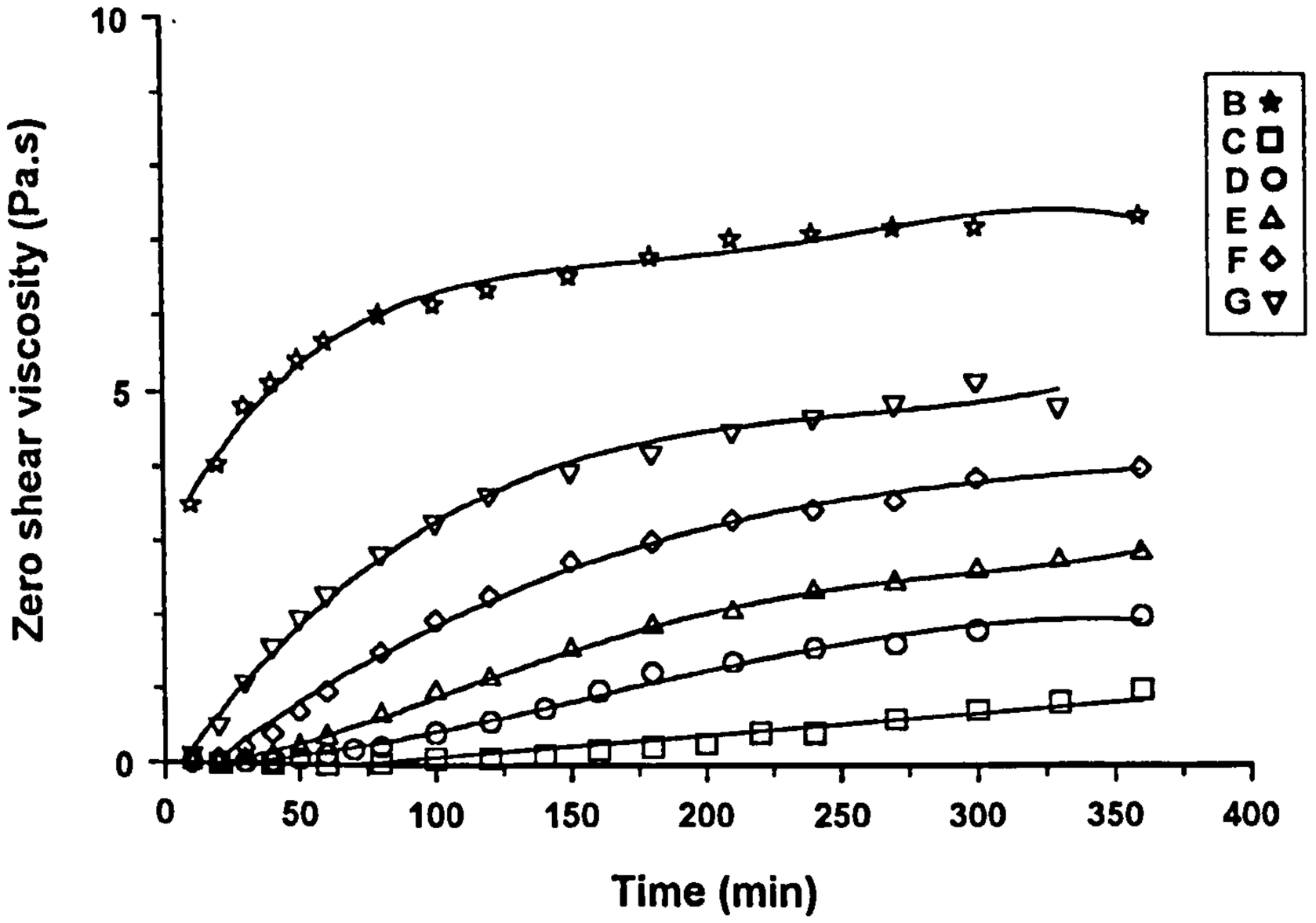

Fig. 8.5 Results of polynomial regression of hydration profiles for samples B to G. Data points are mean values of duplicates or triplicates.

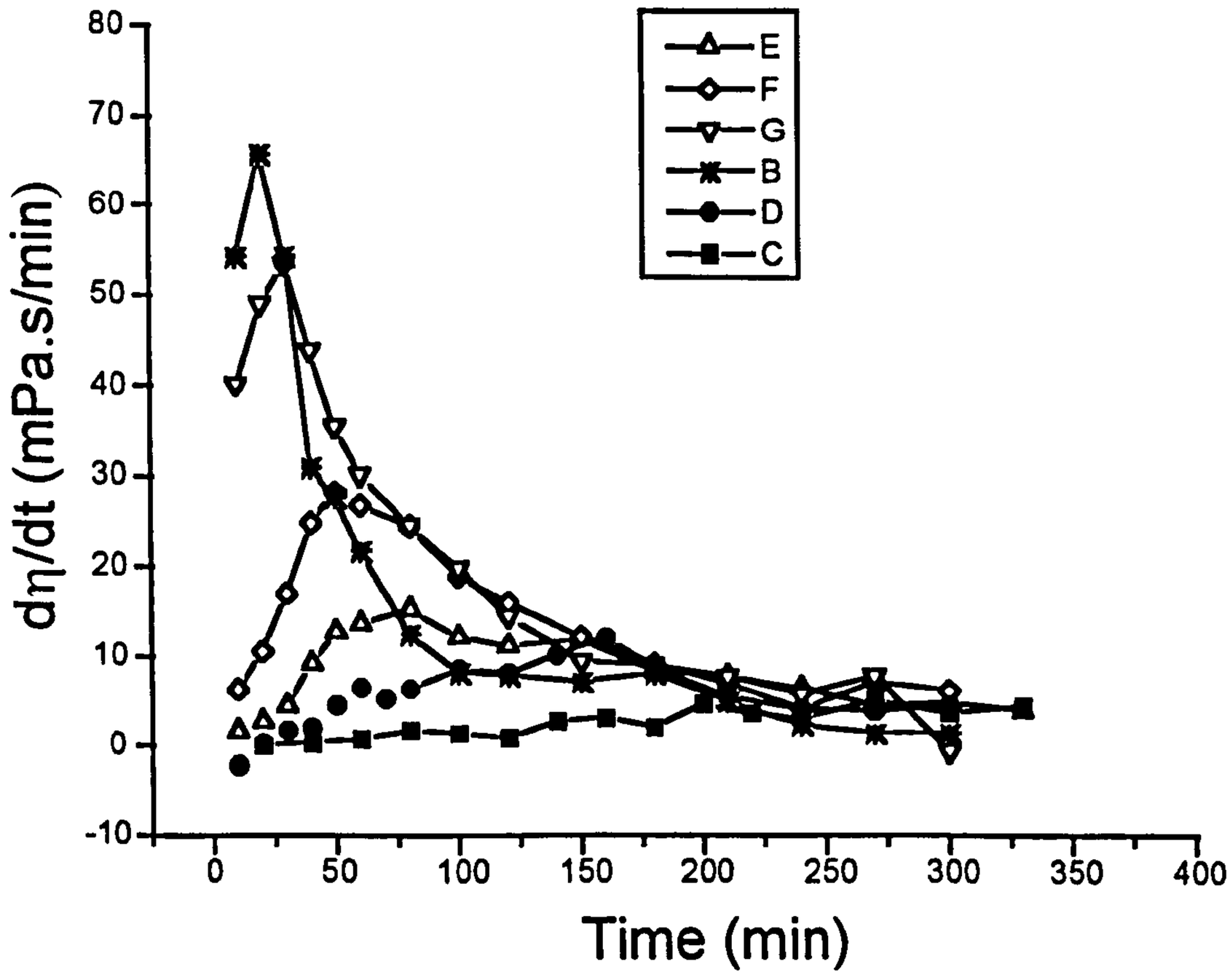

Fig. 8.6 Hydration rate (dη/dt) profiles of samples B to G obtained from the derivation of hydration profiles in Fig. 8.5.

The hydration indices and the mean particle size of the experimental samples are listed in Table 8.4 and illustrated in Fig. 8.7. From the results it can be seen, there is clearly a inverse relationship between hydration index ν and particle mean diameter (d_{sv}). A plot of log ν *vs.* d_{sv} exhibited a linear relationship in the particle size range around 60~300μm (r^2 = 0.97, df = 3). However, the hydration index dropped more rapidly when the particle size increased further. The ν value of sample C cannot be taken too literally, because the predicted t_{max} from the regression function exceeds the actual experimental time. But, what can be stated unequivocally is that the hydration rate decreases more rapidly with increasing particle size when the particle size is larger than certain level (~ 300 μm in this experiment). As expected, ν increased significantly with increasing specific surface area of the samples (Fig. 8.8). These results indicate the strong effects of particle size on the hydration rate of guar gum samples.

*Table 8.4 Maximum hydration rate (m), their corresponding time (t_{max}) and hydration indices (ν) for guar samples B to G. * calculated values from regression function (see equation 8.3 and Table8.3).*

	B	C*	D	E	F	G
d_{sv} (μm)	59	469	297	218	192	81
t_{max} (min)	20	720	159	75	50	30
m	65.9	0.017	12.3	14.9	28.4	53.9
ν	3.3	2.3E-5	0.08	0.2	0.57	1.8
logν	0.52	-4.6	-1.10	-0.7	-0.24	0.26

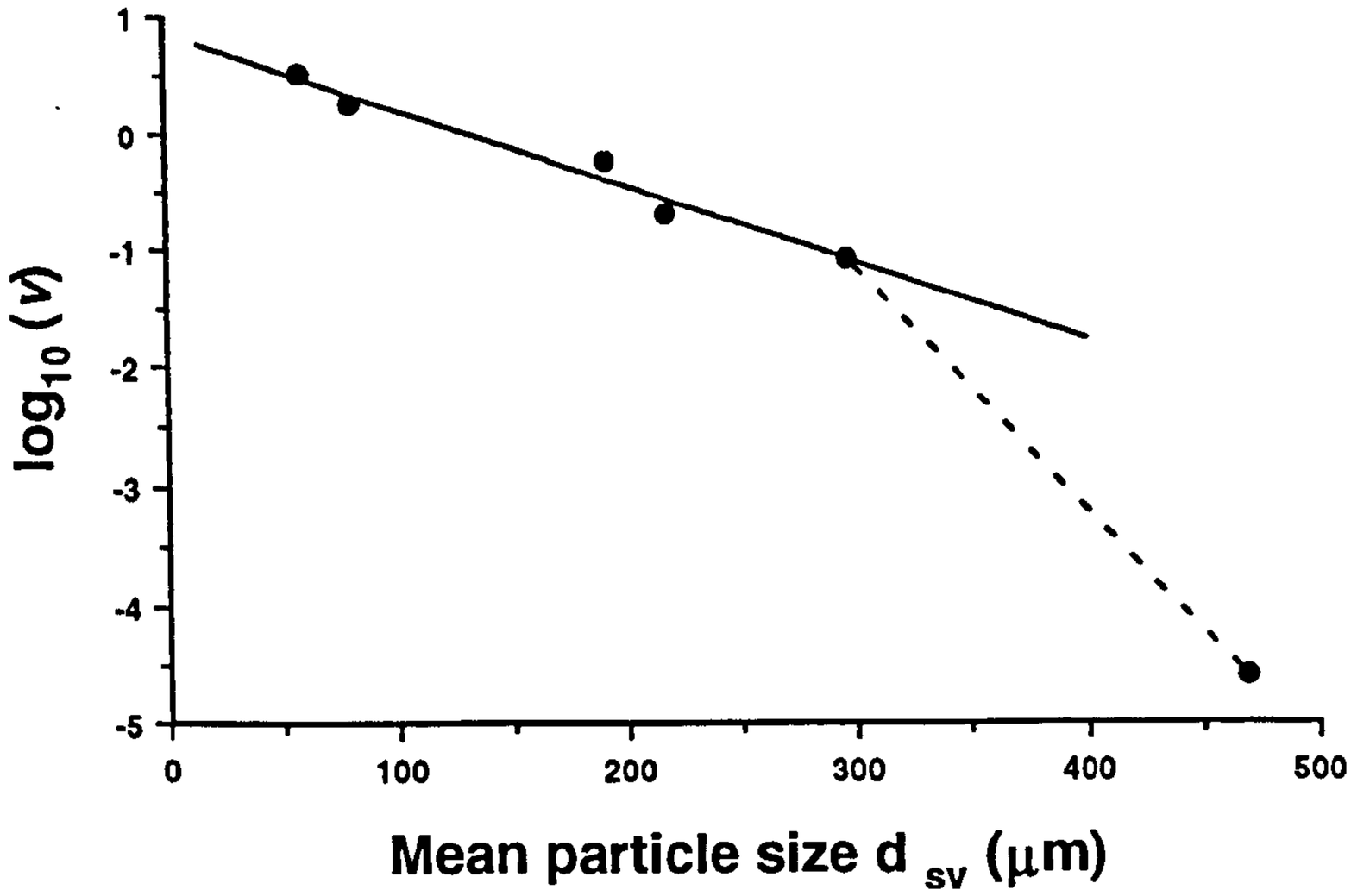

Fig. 8.7 The effect of mean particle size (d_{sv}) on the hydration index (ν) of guar gum samples showing the linear relationship of log ν vs. d_{sv} (r^2 =0.97) at small particle size and the rapid drop in log ν at large particle size .

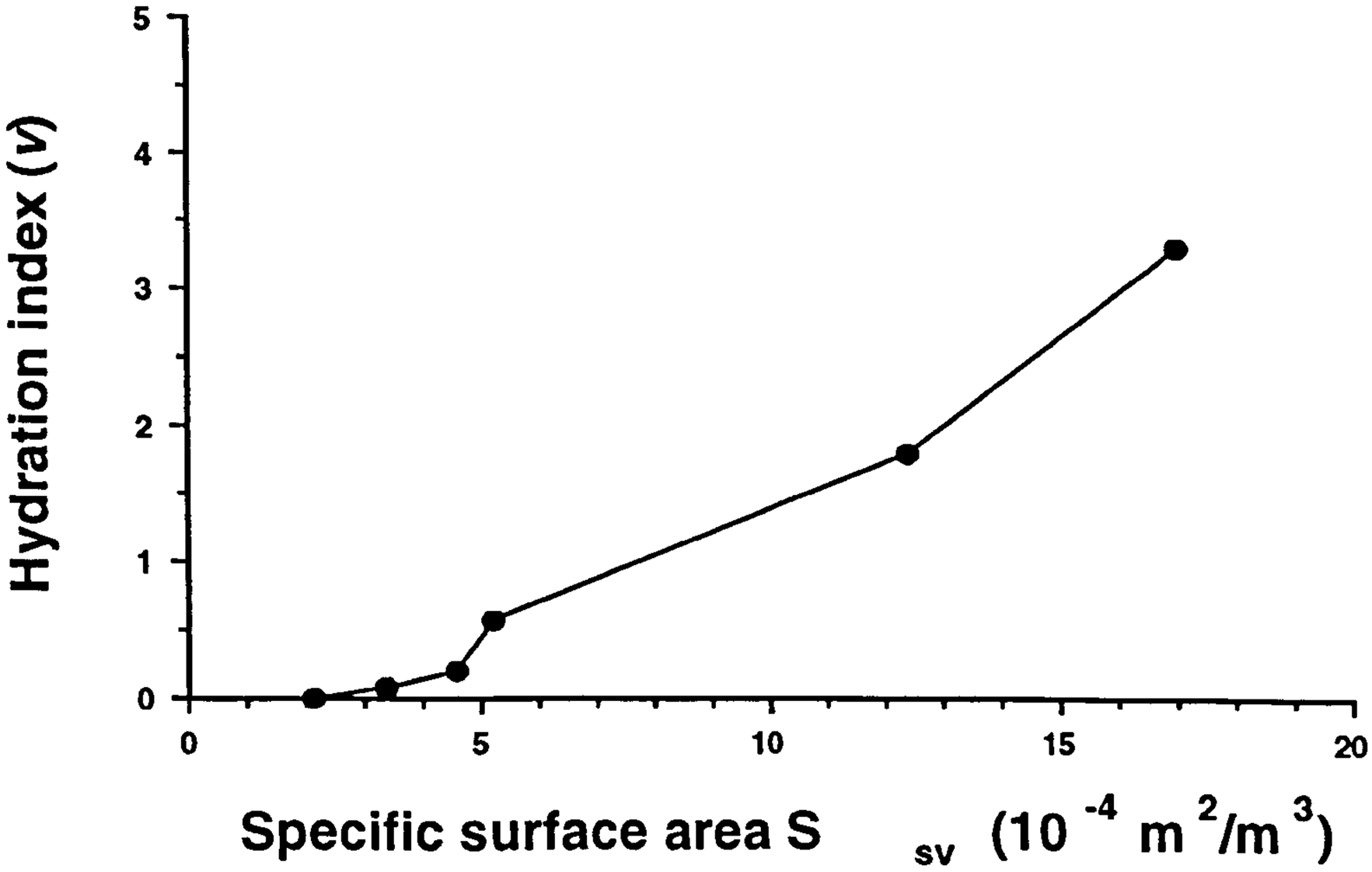

Fig. 8.8 Relationships between hydration index (ν) and specific surface area (S_{sv}) of guar gum samples.

8.4 Discussions

8.4.1 Effects of particle size

The results of this chapter clearly showed that there was an inverse relationship between hydration rate and mean particle size. This inference was based on the fact that the particle has been uniformly dispersed into the water with vigorous mixing. During the experiment we found that samples of extreme particle size are more likely to lead to clumping. A fine-mesh gum sample has a greater requirement for good dispersion when samples are added into water. On the other hand, a coarse material requires enough mixing rate during the whole hydration process. This is because the slowly developed viscosity is not able to keep the sample particles well suspended, which results in clumping of partially hydrated particles.

A specific particle size should be carefully selected to suit particular applications in order to obtain desired hydration properties. The way in which particles hydrate is the first critical factor of concerned here. This includes how the particles are exposed to water, and the mixing rate during the hydration process. For example, the actual mixing rate in the human gastrointestinal lumen could be very different from that used when preparing industrial solutions. Whether or not polysaccharide gum is premixed with other ingredients, such as when they are incorporated into foods, also cause significant difference in hydration properties (Ellis and Morris, 1991). There are many other factors that may affect the hydration properties which are beyond the scope of this chapter, and thus are omitted here.

8.4.2 Use of polynomial regression

Although the regression equation has less physical meaning in describing the kinetics of hydration process itself, it has been proved very useful in comparing the hydration rate data of several samples that could not be fitted by one single model. It is particularly convenient to use in the studies where the ultimate viscosity is different, or difficult to determine accurately.

The hydration index defined in this chapter has actual physical meaning. As illustrated in Fig. 8.9, ν actually defines a straight line with m/t_{max} as slope and zero as the intercept. This index not only takes into account the maximum hydration rate, but also the time needed to attain this maximum hydration rate. In the situation seen in Fig. 8.9, samples X and Y have the same maximum hydration rate (m), whereas samples Y and Z need the same time t_{max} to reach the maximum hydration rate. If either m or t_{max} is used we cannot distinguish the hydration rate for all three samples, since X and Y have the same m values, whereas Y and Z have the same t_{max} value. However, by comparing m/t_{max} the difference in hydration rate is obviously $X>Y>Z$ since $\nu_X > \nu_Y > \nu_Z$.

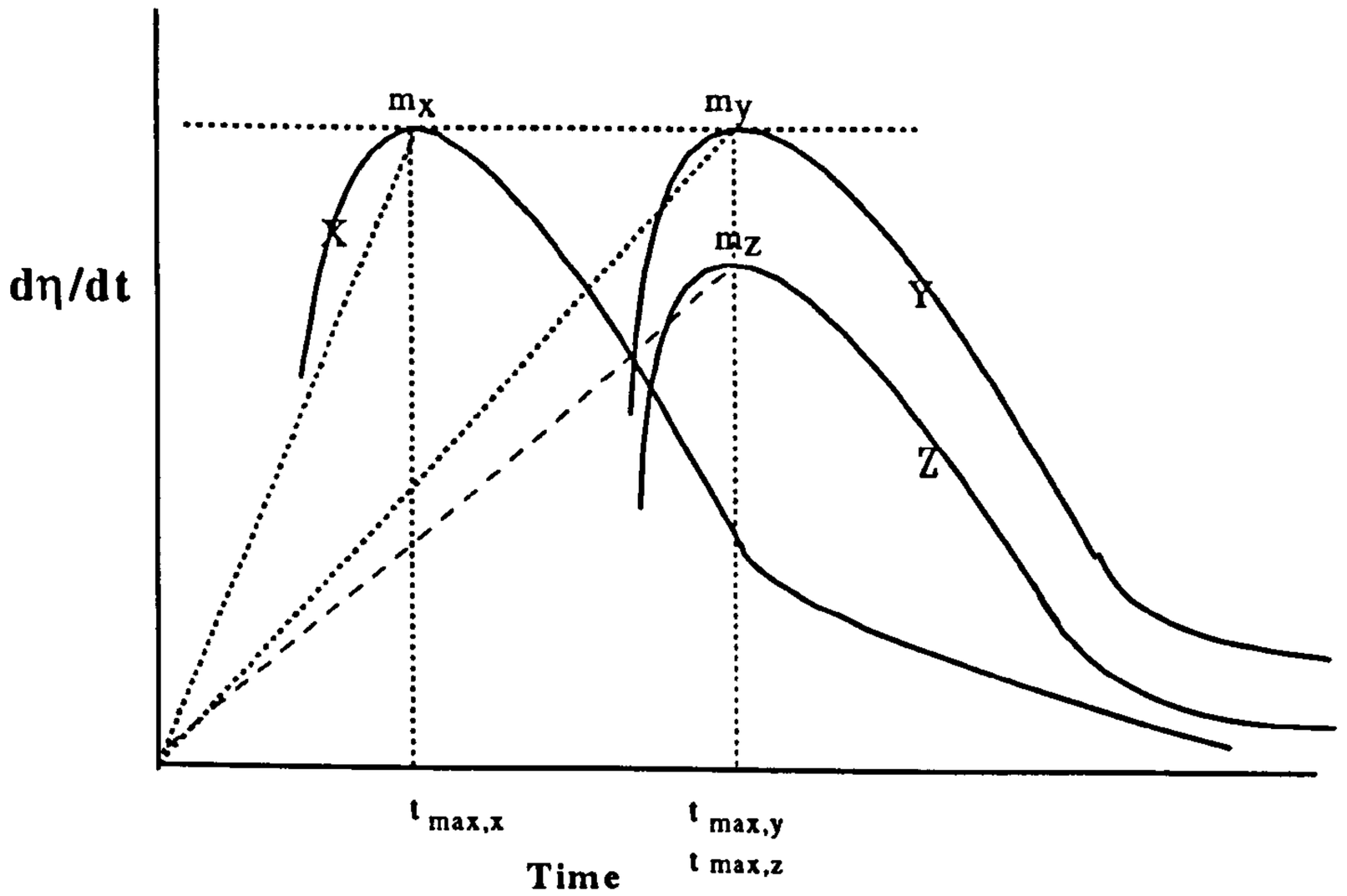

Fig. 8.9 Schematic graph to illustrate the physical meaning of the hydration indexν.

8.5 Conclusions

The effects of particle size of guar gum on the hydration properties was comprehensively studied and discussed in this chapter. A clear inverse relationship between hydration rate and mean particle size was found. The importance of selecting proper particle size to suit specific applications was further stressed. The polynomial regression method was successfully applied to describe the hydration process and a useful hydration index (ν) was defined for the comparison of hydration rate. This approach was found to be very useful to compare the hydration rate of several samples, especially when the ultimate viscosity is different or difficult to determine.

Chapter 9

The stability of guar gum in solutions and the effects of pH on hydration rate under acidic conditions

9.1 Introduction

The pH of the human stomach is normally acidic but not lower than pH 1.5 after a meal (Rayding, *et al.*, 1984; Savarino, *et al.*, 1988). Therefore, the study of hydration behaviour in acidic environments is of particular interest in the area of digestive physiology and nutrition. Many polysaccharides are readily degraded in extreme conditions, such as high temperature, acid or alkali media, or even severe mechanical disruption. The stability of guar gum under acid conditions has not yet been thoroughly investigated. It will be useful therefore to obtain information on the susceptibility of guar galactomannan to acidic depolymerisation before investigating the pH effects on the hydration behaviour under acidic conditions.

Foster (1967) reported that the viscosity of 1% guar and locust bean gums at 75°C decreased significantly after the solution was adjusted to pH 4.0 for about one hour. This decrease in viscosity was terminated after neutralisation. Bolliger (1959) studied the influence of hydrogen-ion concentration on the viscosity of guar gum slimes. The results showed that the stability of the guar solution (0.5% w/w) was optimum at pHs 6 - 7 and also a maximum in the viscosity was obtained at this pH. At pHs 5 and 8 the same solution gave a relatively high viscosity, whereas pHs 3 and 10 gave a minimum viscosity. The thermal-degradation of guar gum has been studied by several other groups (Bradley, *et al.*, 1989; Kroger, *et al.*, 1993), again using polymer concentrations > 0.5% (w/w).

Although the results of these studies reflect certain aspects of the stability of guar gum under different conditions, it is difficult to draw a whole and clear picture of it to meet our requirements in the present study. There are three reasons for this. Firstly, it would seem more appropriate to use dilute solutions (close to C*) for the study of stability of guar gum in aqueous solution. If high polymer concentrations are used the viscosity reduction detected may not necessarily be caused by polymer degradation, but merely by a reduction in the intermolecular aggregation. Secondly, the pH condition and temperature have interactive effects on the stability of guar gum solutions. For example, in Foster's study (1967) degradation occurred at 75°C and 55 °C at pH 4 and 2, respectively. However, at lower temperatures such as human body temperature (37°C), the solution may be relatively stable at these pHs. Thirdly, when using viscosity reduction as an indicator of polymer degradation it will be more useful to monitor the time course of each treatment rather than only simply measuring the ultimate viscosity as in previous studies (Bolliger, 1959; Foster, 1967).

The experiments in this chapter are divided into two stages. The first stage includes an investigation of the stability of guar gum solution at 25°C, 37°C and 50°C and at different pH levels. A special device was designed to allow the polymer degradation process to be monitored by determining changes in viscosity. The present study was not designed to investigate the kinetics of guar gum hydrolysis *per se*, but the main interest was merely to find out to what extent the viscosity of guar gum solutions will change under various conditions of pH and temperature. This approach allowed the time course of hydrolysis to be followed by measuring the changes in relative viscosity without interrupting the process and also without removing aliquots of the sample from the reaction vessel for viscosity measurements. On the basis of the information obtained from the above experiments, the hydration kinetics of guar gum solution was then studied under pH conditions where the polymer is stable or readily degraded.

9.2 Experimental

9.2.1 Preparation of sample solutions

Fully hydrated M150 guar gum solutions at a concentration of 0.07% (w/w, dry weight, corresponding to C/C* ~ 1.2) were prepared by dispersing the known weights of guar gum flour in deionised water for 0.5 h at 80 °C and then mixing overnight using a magnetic stirrer at room temperature. Solutions were filtered through a 0.2/0.8 μm syringe filter before measurements were taken. The experiment solutions were adjusted to the required pH by using different concentrations of hydrochloric acid (0.01 - 2M HCl) to ensure that the final concentration of guar gum was always the same. The amount of HCl needed to attain certain pH levels was previously determined and recorded. Therefore, the hydrolysis process could be recorded immediately after adding the required amount of acid into the sample.

9.2.2 Hydrolysis device

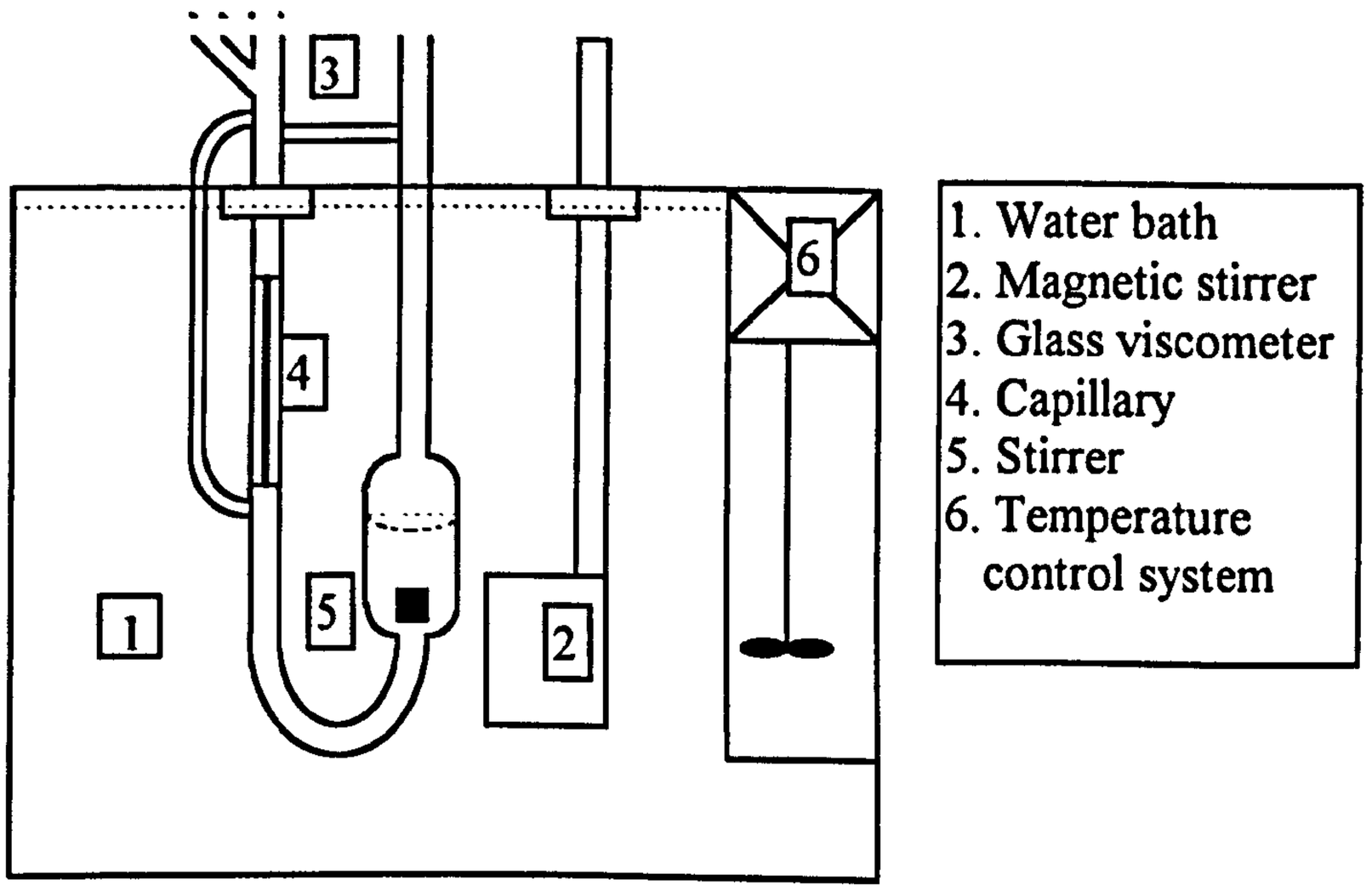

Fig. 9.1 Illustration of experimental rig for studying the degradation of guar gum in dilute solution.

The viscosity was determined by using a dilution capillary viscometer (Cannon Ubbelohde Dilution B glass viscometer. Glass Artefact Viscometers, Braintree, Essex, CM7 5JQ, UK) immersed in a water bath to maintain the temperature at 25 °C ± 0.1°C. An L-shaped magnetic stirrer with a long arm (see Fig. 9.1) was also immersed in the water bath to allow vigorous mixing of sample solutions in the viscometer during the experiments. The stirrers was chosen carefully in order to minimise the disturbance on the measurement of viscosity. During the measurements the stirrer was suspended in the solution without touching the wall of the viscometer.

9.2.3 Estimation of molecular weight during degradation process

Using a capillary viscometer (see Fig. 9.1) the relative viscosity (η_r) was measured, from which the specific viscosity was calculated ($\eta_{sp} = \eta_r - 1$). Intrinsic viscosity is normally determined by measuring reduced viscosity η_{red} ($= \eta_{sp}/C$) at various concentrations in dilute solution and extrapolating to concentration C = 0. The concentration dependence is often expressed in terms of the following relationship (Tanford, 1961):

$$\eta_{sp}/C = [\eta] + K[\eta]^2 C \qquad (9.1)$$

where K is a constant known as the Huggins constant. For flexible polymer molecules in good solvents K is often near to 0.35. Somewhat higher values occur in poor solvents. Equation 9.1 was used in the present study to calculate intrinsic viscosity by measuring specific viscosity at finite concentrations. Thus, equation 9.1 was rewritten as:

$$[\eta] = \frac{\sqrt{1 + 4K\eta_{sp}} - 1}{2KC} \qquad (9.2)$$

from the intrinsic viscosity [η], the viscosity average molecular weight (M_v) is calculated by using the Mark and Houwink equation with $\alpha = 0.732$ and $k = 3.8 \times 10^{-4}$ (Robinson, *et al.*, 1982).

9.2.4 Hydration method

The hydration experiments of guar gum under different conditions were conducted using the hydration method described in Chapter 3. The speed of mixing box was set at 6 r.p.m and the ultimate viscosity was determined as described in Section 7.2.1. All experiments were carried out using M150 guar gum at concentration 0.8% (w/w) on a dry content basis. Before the guar gum sample was hydrated, the distilled water was adjusted to the desired pH level using dilute hydrochloric acid (0.01 - 2M). During the hydration process the zero-shear viscosity was measured on the RFSII, employing a plate-plate geometry (diameter 50 mm, gap 1 mm, for details of method see Chapter 3).

9.3 Results

9.3.1 Stability study of guar gum

9.3.1.1 Kinetics of acidic degradation of guar gum in solutions

As it has been discussed in Chapter 2, assuming that the degradation reaction of guar gum under acidic conditions is a random scission process, the reciprocal of average molecular weight ($1/M_v$) should have a linear relationship with the reaction time. In other words, the reaction obeys first order kinetics.

The reciprocal of average molecular weight of guar gum was plotted against incubation time in Fig. 9.2 taking temperature at 50°C as an example. A strong linear relationship was obtained between $1/M_v$ (which is proportional to the reciprocal of degree of polymerisation) and reaction time. All the correlation coefficients (r^2) were higher than 0.98, and the estimated variances (sum of square/degrees of freedom) were small. This indicates that, as predicted, the degradation of guar gum solution under acidic condition follows first order kinetics.

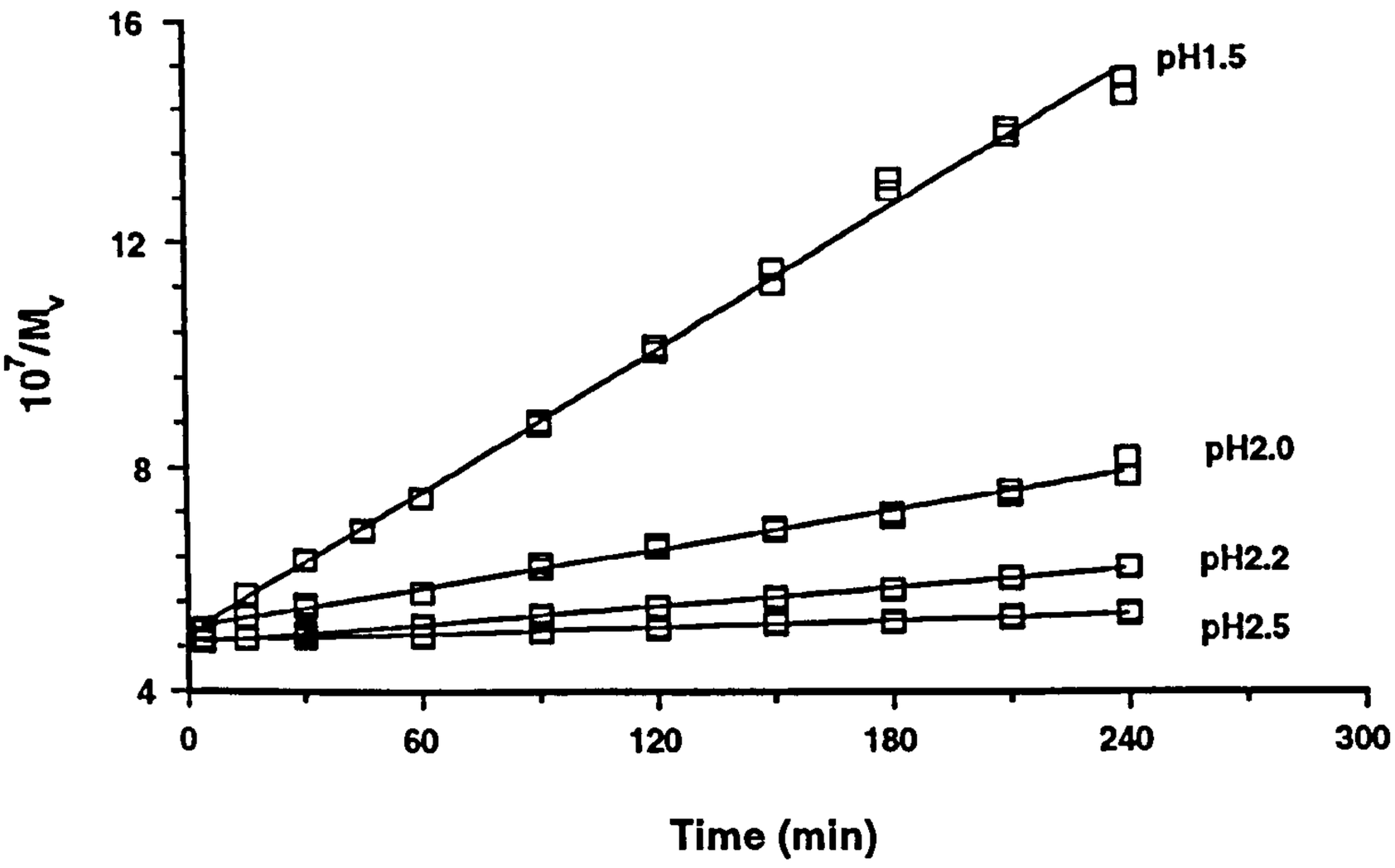

Fig. 9.2 Plots of degradation process of guar gum in solutions (0.07% w/w) showing the linear relationship between reciprocal of molecular weight ($1/M_v$) and reaction time. T = 50°C. Experiments were conducted in duplicate.

9.3.1.2 pH effects on the degradation rate of guar gum in solution

At a given temperature the rate of degradation was found to depend significantly on the pH level. The depolymerisation process was much more rapid in a higher [H^+] environment, which was indicated by the reaction lines as seen in Fig. 9.2 with steeper slopes at lower pH levels. Fig. 9.3 shows the reduction in relative viscosity during the degradation process at 50°C. At a given temperature there was a pH level above which the reduction in viscosity was negligible, as was the case at temperature of 50°C when pH>3.0.

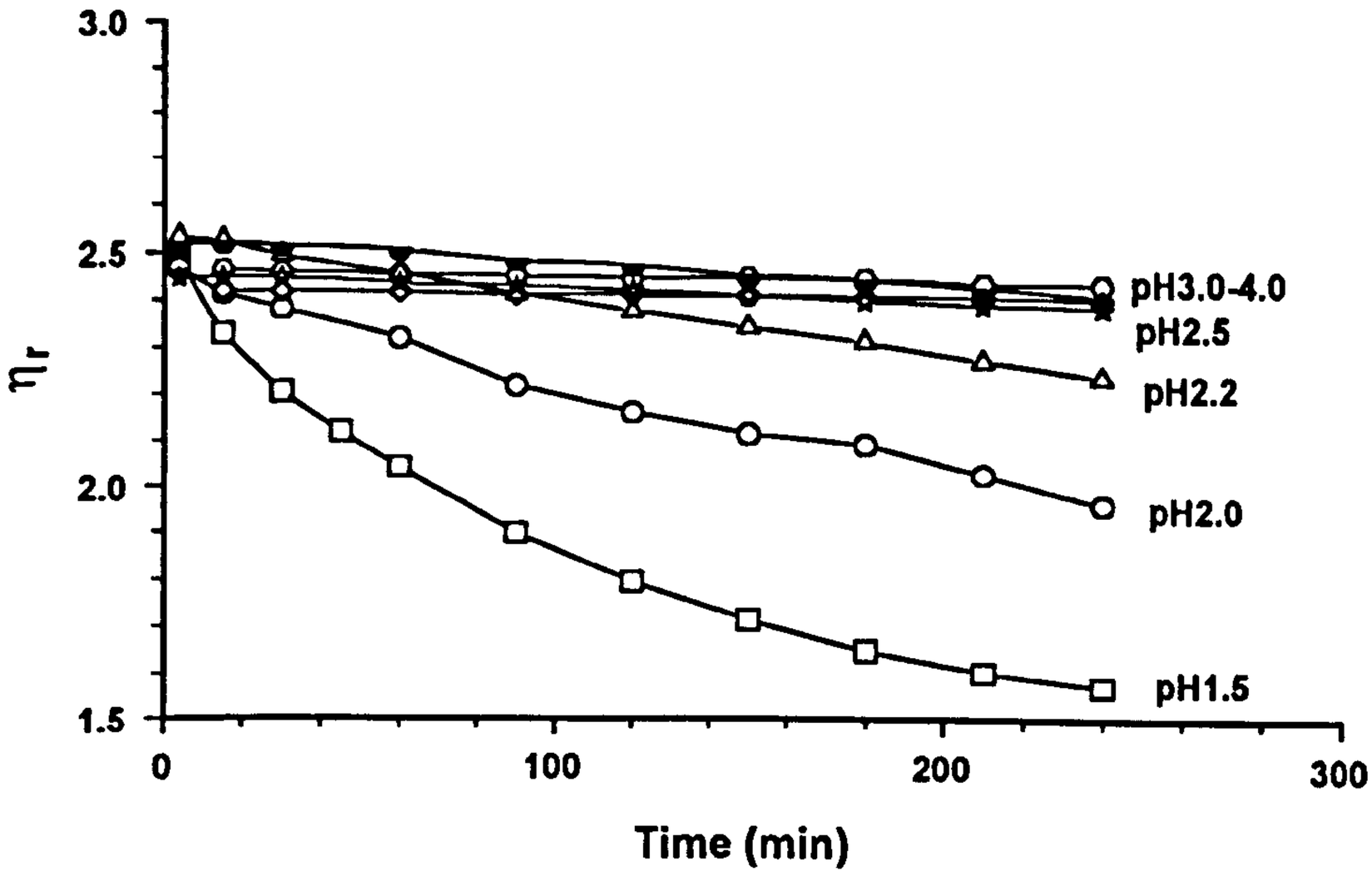

Fig. 9.3 The relative viscosity (η_r) changes of guar gum solutions (0.07% w/w) under different pH levels at 50℃. All values are means of duplicates.

9.3.1.3 Effects of temperature on the degradation of guar gum in solution

Temperature had a pronounced effect on the degradation of guar gum polysaccharides. For example, as shown in Fig. 9.4, at pH 1.5 the molecular weight decreased rapidly at 50°C, whereas at 25° it was hardly changed. High temperature would obviously accelerate the degradation process. At t = 37°C and pH 1.5, which is the most relevant pH from a biological perspective, the degradation rate was found to be very slow. After four hours incubation under these conditions the viscosity decreased by only 11%, whereas at 50°C it decreased by 37%. The viscosity reduction was calculated as the difference between the initial relative viscosity and the relative viscosity at 4 hour divided by the initial relative viscosity (it will be same in the following text). The reductions in relative viscosity under different conditions after 4 h incubation are summarised in Fig. 9.5 and Table 9.1.

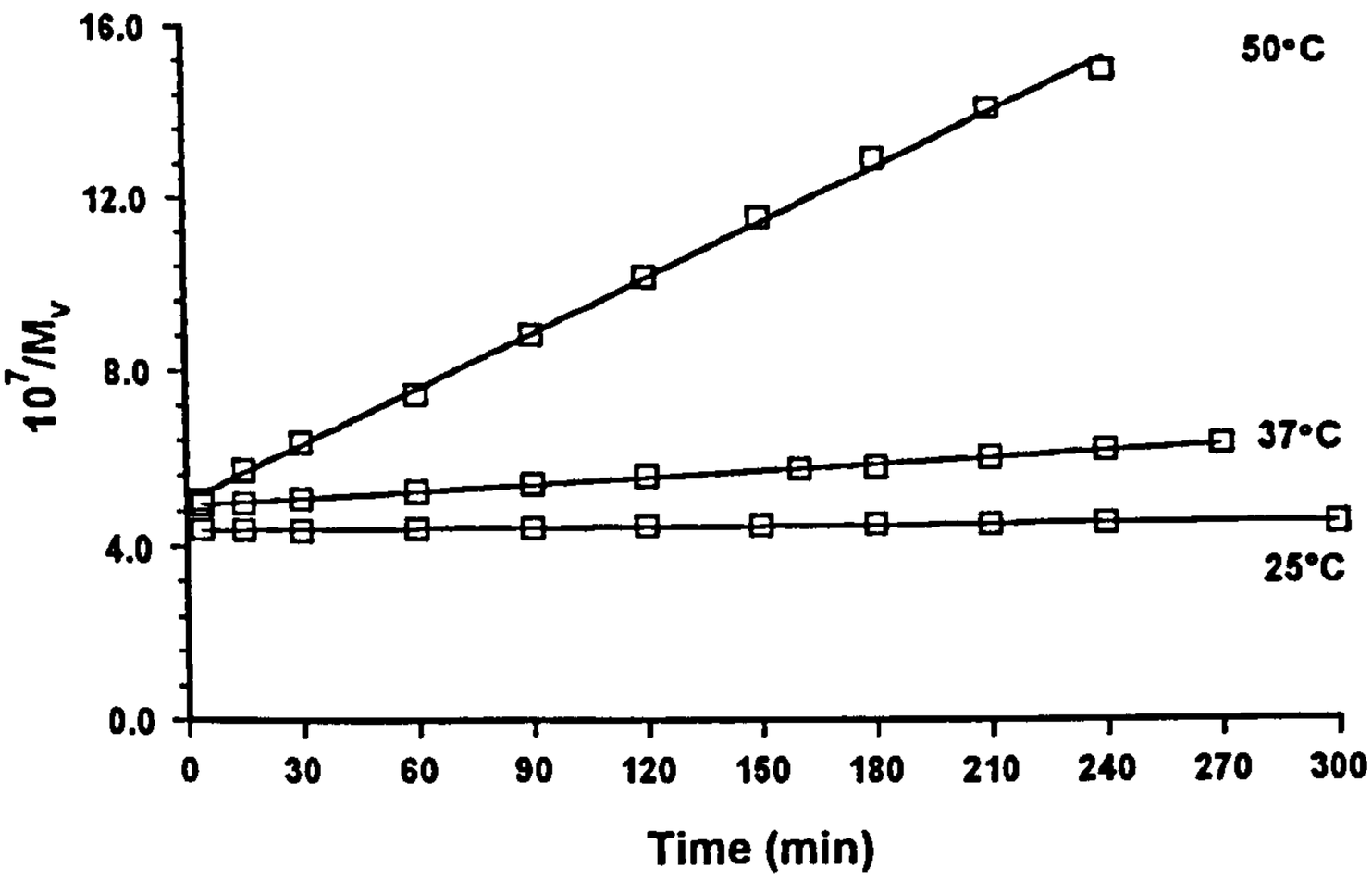

Fig. 9.4 Plot of reciprocal molecular weight against time showing the effect of temperature on degradation rate of guar gum (0.07%, w/w) at pH 1.5. All values are means of duplicates.

*Table 9.1 Summaries of viscosity reduction of guar gum solutions (0.07%, w/w) after 4 h incubation at different temperature and pH levels. * not determined.*

Temperature	25°C	37°C	50°C
pH	Viscosity reduction (%)		
1.0	*	23.8	*
1.5	2.0	11.0	36.7
2.0	0.9	4.7	20.5
2.5	*	2.1	4.4
3.0	0.4	1.2	2.7

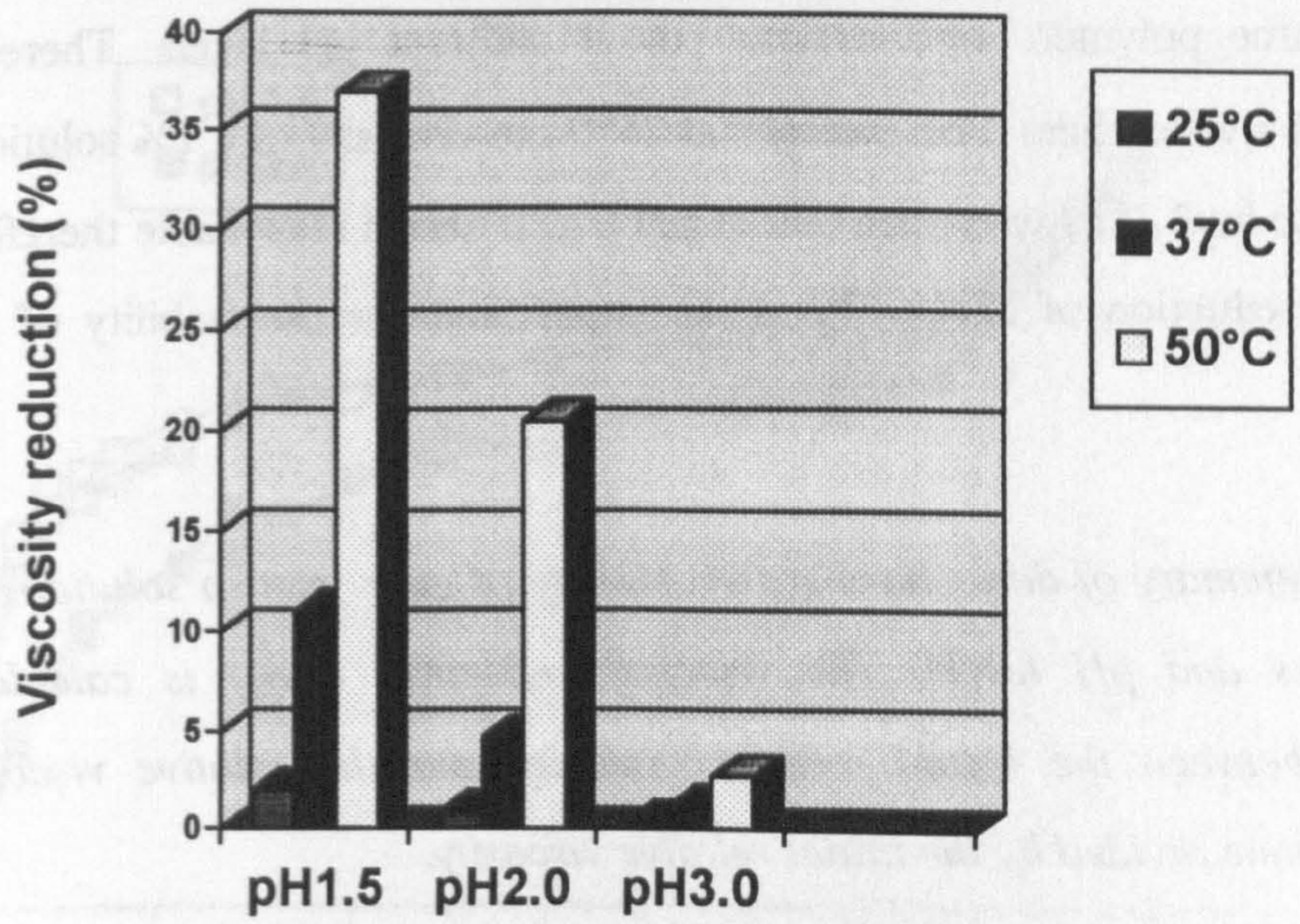

Fig. 9.5 Viscosity reductions after 4 h incubation at three pH levels showing the temperature effect on the degradation of guar gum (0.07%, w/w).

9.3.1.4 The lowest pH that guar gum remains stable in solutions

Experiments were carried out at 25°C, 37°C and 50°C and at pH levels between pH 1.0-pH 4.0. The above results have shown that, as expected, the temperature and pH had a interactive effect on the stability of guar gum solutions. Table 9.2 lists the lowest pH at which guar gum was found to be stable at temperature 25, 37 and 50°C. In this study, the guar gum was considered to be stable when the viscosity of guar gum solution was not reduced by more than 2% after 4 h incubation at a stipulated temperature. The slight decrease of solution viscosity seen at all levels of pH below neutral is probably not due to the depolymerisation of guar galactomannan, but merely because of the change in water structure affecting the interaction between the water/galactomannan and galactomannan/galactomannan molecules. The mechanism for this could be complex. One possible explanation is that this reduction in viscosity is caused by the dissociation of aggregates of galactomannan molecules. The weak protonation of the hydroxyl groups in the galactomannan chains caused by high $[H^+]$ may reduce the intermolecular hydrogen bonding, thus disrupting the aggregation of the galactomannan chains. We

have also compared the viscosity of semi-dilute solutions of fully hydrated guar gum with the same polymer concentration but at different pH levels. There are indeed differences between them. For example, at 25°C the viscosity of a 1% solution at pH 3.0 was found to be 2.3% lower than that at pH 6.5. It seems reasonable therefore to select a viscosity reduction of about 2% as the upper limit for the stability of a guar gum solution.

Table 9.2 Summary of data showing the stability of guar gum in solutions at different temperatures and pH levels. The viscosity reduction ($\Delta\eta_{rr}$) is calculated as the difference between the initial relative viscosity and the relative viscosity at 4 h incubation time divided by the initial relative viscosity.

Temp. (°C)	*25*	*37*	*50*
Stable pH	1.5	3.0	3.5
$\Delta\eta_r$ (%)	2.0	1.2	1.4

9.3.2 pH effects on hydration rate

9.3.2.1 Under conditions where polymer degradation is negligible

A comparison of the hydration rate of guar gum was made at pH 3.0 and pH 6.5 at 25°C, i.e. the conditions under which no degradation take place. There were noticeable differences between the hydration profiles of pH 3.0 and pH 6.5 as can be seen from Fig. 9.6. The initial hydration rate was slower at pH 3.0 compared to pH 6.5, which was reflected by a lower starting viscosity in solution of pH 3.0 than that of pH 6.5. For example, after 8 min incubation the relative difference in viscosity between these two dispersions was found to be 80% using the following equation:

$$\Delta\eta_0\% = \frac{100 \times (\eta_{pH\ 6.5} - \eta_{pH\ 3.0})}{(\eta_{pH\ 6.5} + \eta_{pH\ 3.0})/2} \qquad (9.3)$$

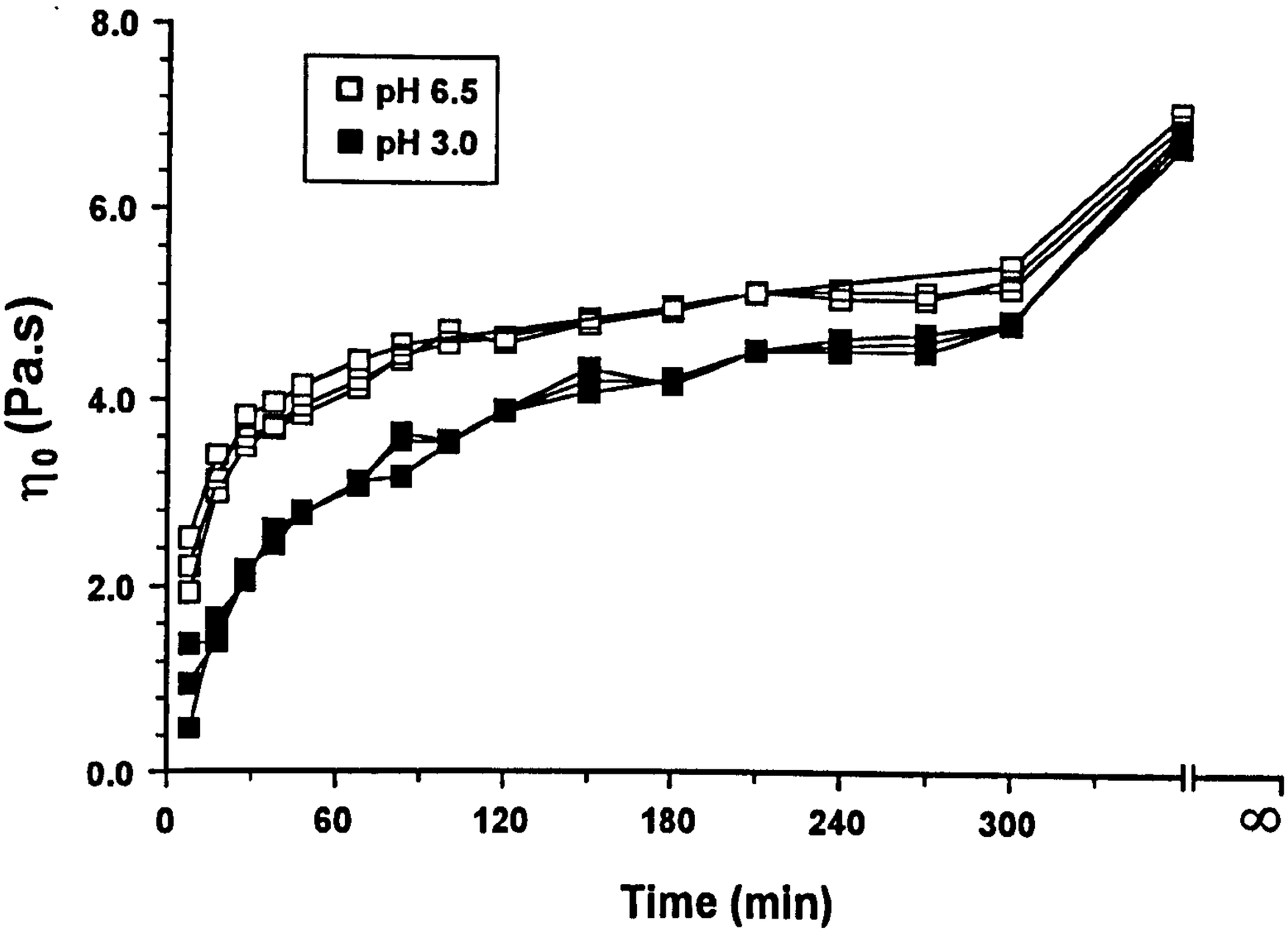

Fig. 9.6 Effects of pH on hydration behaviour of guar gum prepared as 0.8% (w/w) solutions at 25℃, when no polymer degradation took place.

However, as can be seen from Fig. 9.7, $\Delta\eta_0$ decreases gradually with hydration time, indicating that the hydration rate was higher at pH 3.0 than at neutral conditions at later times. After 4 h hydration, $\Delta\eta_0$ reduced to 8%. Fig. 9.8 shows the same hydration data in Fig. 9.6 fitted with the logarithmic model for hydration described in Chapter 6. It can been seen that the hydration curve at pH 3.0 has a steeper slope than that at pH 6.5 in the later time periods, indicating that the former hydrated faster at this later stage. The hydration index $t_{0.8}$, which was calculated according to the logarithmic model, for pHs 6.5 and 3.0. was 710 and 1050 min, respectively. Therefore, the overall hydration rate of guar gum is higher at neutral pH than in acidic conditions within the time period studied.

The ultimate viscosity levels of these two solutions are not very different, 2.3% lower in viscosity at pH 3.0 compared to pH 6.5. If we compare this result with degradation experiments (see Table 9.2), it seems to suggest that the effect of reducing pH on

viscosity loss is concentration dependent. The viscosity reduction caused by decreasing pH is more pronounced in concentrated solutions than in dilute solutions.

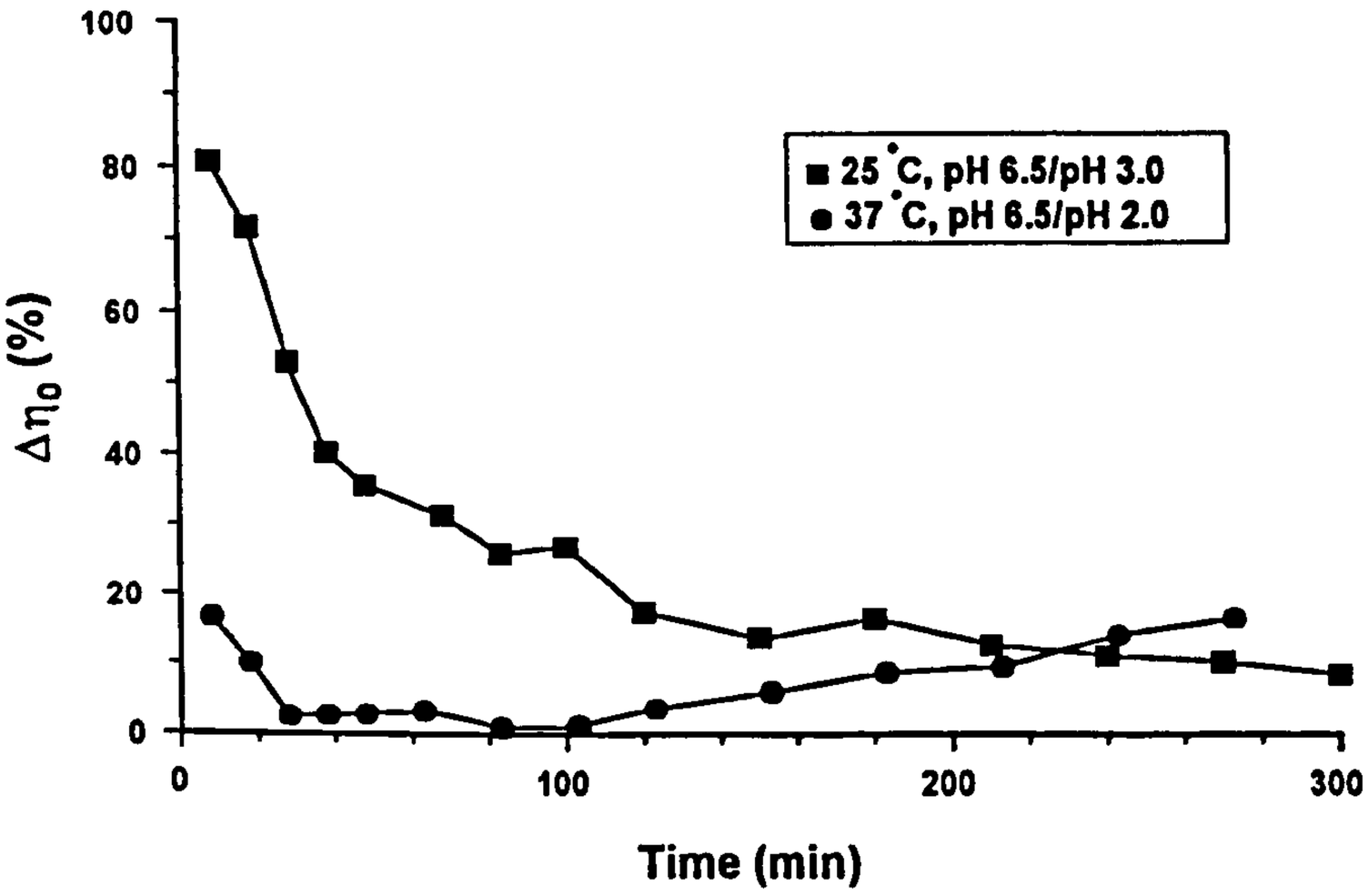

Fig. 9.7 Time courses for viscosity differences $\Delta\eta_0$ between 0.8% (w/w) guar gum solutions hydrated at two different pH levels. Values are means of triplicates.

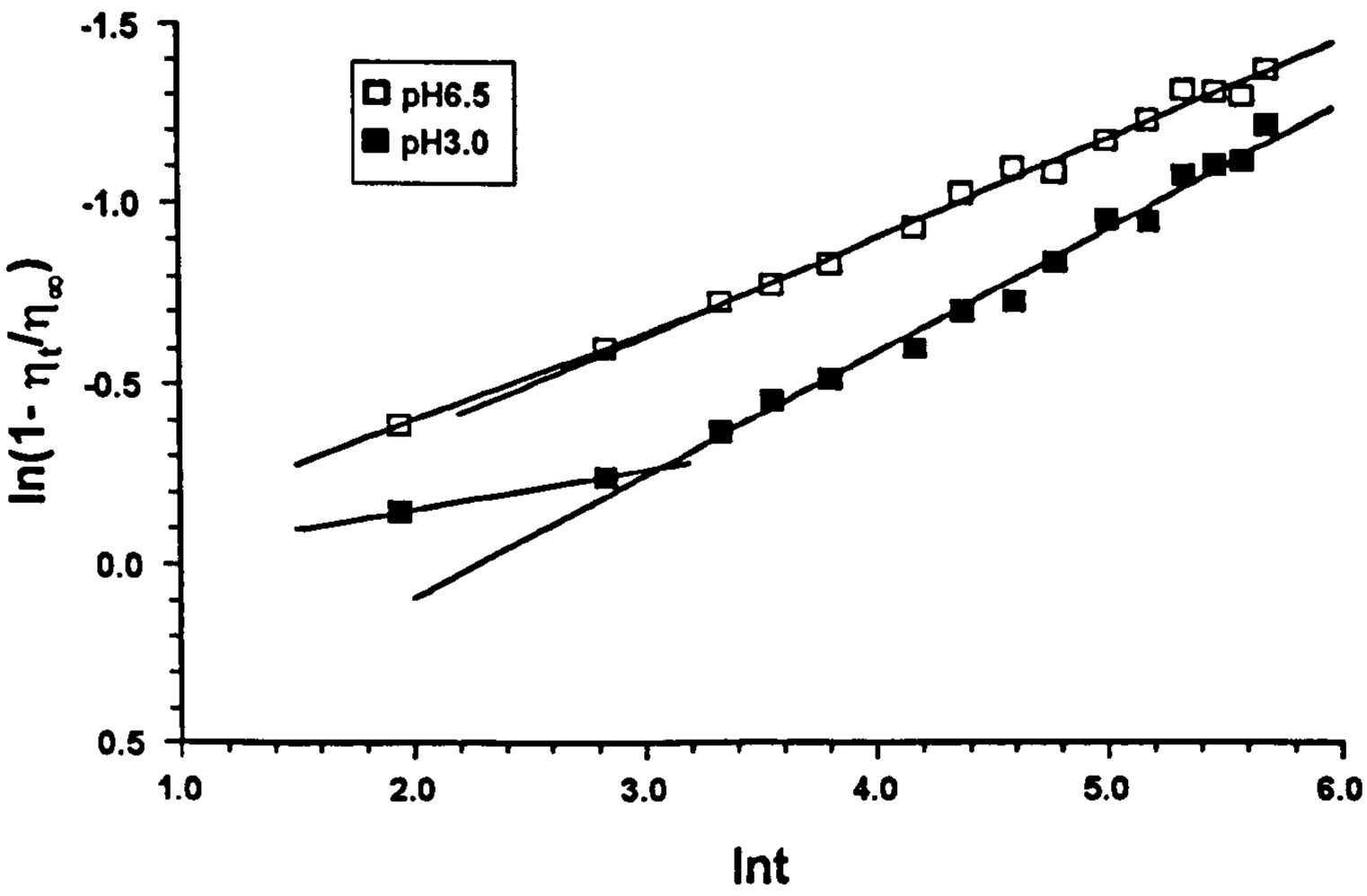

Fig. 9.8 Plots for corresponding data in Fig. 9.6 fitted by logarithmic model of hydration (see Chapter 6).

9.3.2.2. Under conditions at which polymer degradation occurs

Fig. 9.9 is the hydration profiles of 0.8% (w/v) guar gum (M150) at pH 2.0 and pH 6.5 at 37°C. The above degradation study has shown that under conditions of pH 2.0 and 37°C guar gum was readily degraded in solution. It can be seen that the viscosity is again lower in pH 2.0 dispersion than that in pH 6.5 at the initial stage. The mean difference in viscosity was also presented in Fig. 9.7. After 10 min incubation the viscosity of pH 2.0 dispersion was about 17% lower than that of pH 6.5. This difference became smaller gradually in the first 30 minutes and then remained at an approximate constant level until the first two hours. At this stage, the increase in viscosity induced by continuing hydration was partly offset by a viscosity reduction caused by polymer degradation. After two hours, the effects of degradation at pH 2.0 became more pronounced because of the reduction in hydration rate. A gradual decrease in viscosity was then observed and the viscosity difference between pH 2.0 and pH 6.5 increased significantly. After 4.5 hours incubation this difference was about 16%.

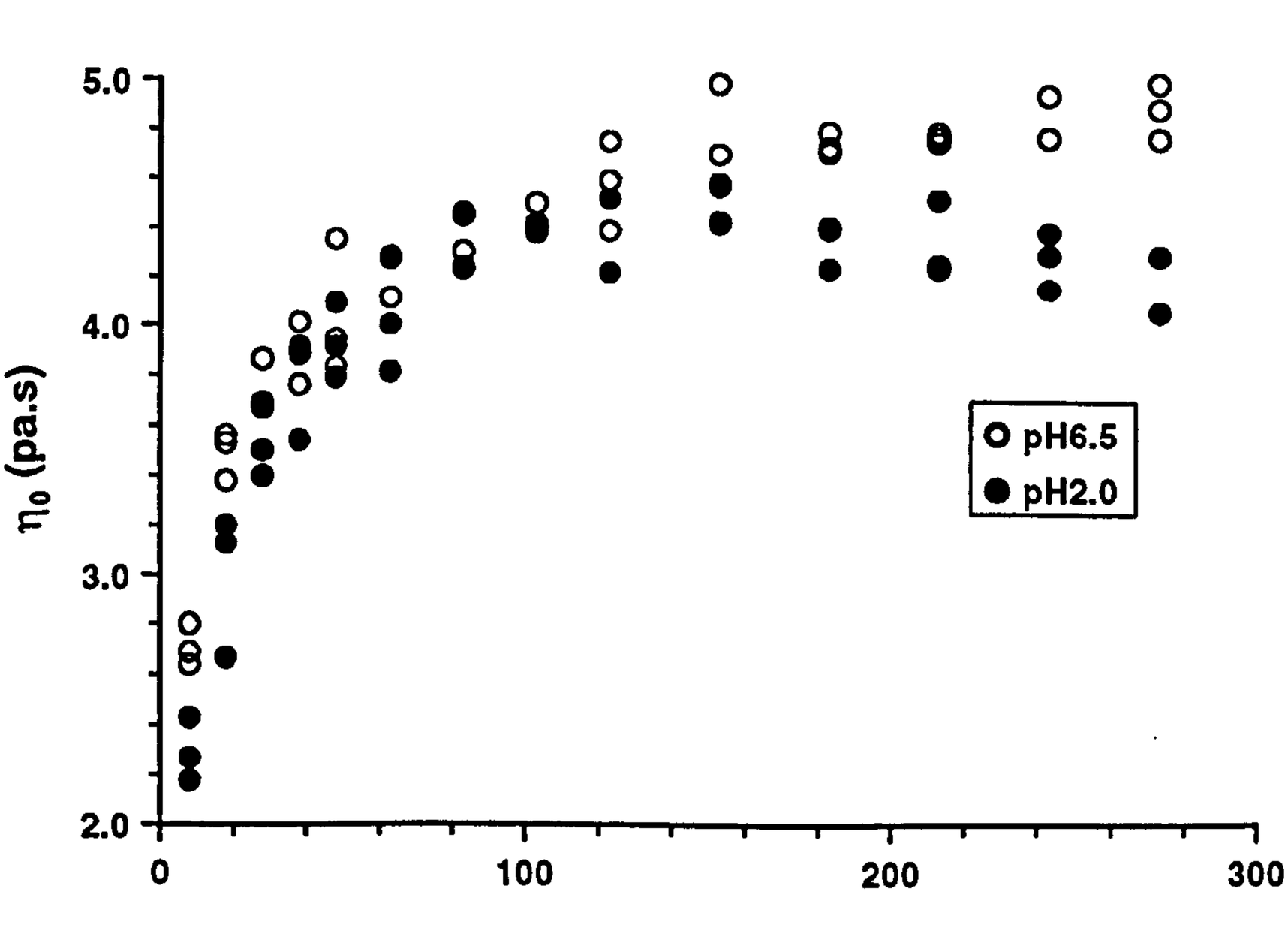

Fig. 9.9 Example of pH effects on hydration behaviour of M150 guar gum when polymer degradation occurs during the hydration process. Samples were prepared as 0.8% (w/v) solutions on the dry weight basis and hydrated at two pH levels at 37°C.

9.4 Discussions

The depolymerisation study carried out in this chapter was not intended to simulate the physiological conditions occurring *in vivo*. However, it is useful to discuss the implications of the results in terms of the likely behaviour of guar gum in the stomach and small intestine.

A number of groups have investigated postprandial gastric pH profiles (Harju, 1985; Savarino, *et al.*, 1988). Following a normal meal the pH of the gastric contents decreases from about 5 to between 2 and 1.5. For example, Rayding *et al.* (1984) measured the intragastric pH (median values) in healthy human volunteers fed meals containing guar gum. The pH of gastric contents increased from pH 1.4 immediately after ingesting the meal to a peak value about pH 4.0, and then gradually decreased to pH 1.5 after 1.5 h as shown in Fig. 9.10. It is clear that the presence of food in the stomach behaves in a manner similar to a buffer in neutralising the acidity of gastric juice. Therefore, in the first hour (pH>2.0) there is unlikely to be any significant acidic degradation of guar galactomannan contained in the food. It is possible that some polymer degradation take place after the pH returns to the baseline value of 1.5 after 2 hours, assuming that some food, as is probably the case, still remains in the stomach. However, it would be expected that any depolymerisation at this stage is likely to be limited.

The reason for this is obvious. It is easier for the polymeric molecules to be degraded in solution than it is in a more solid state such as large granules. For example, it has recently been reported that the thermal stability of guar gum in aqueous solution improves with increasing granule size (Kroger, *et al.*, 1993). However, it was reported that when guar gum was incorporated into a food matrix the hydration of the guar gum will continue in the gut post ingestion (Brennan, *et al.*, 1996). Only a variable proportion of guar gum hydrates during transit in the upper gastrointestinal tract. Our recent *in vitro* experiments (not shown in this thesis) also showed that guar gum *per se* hydrated much more slowly than on its own when it was incorporated into wheat bread. Thus, the extent of degradation of guar gum when incorporated into a food complex will

certainly be much less than that in a fully hydrated solution under the same conditions. From Table 9.2 we can see, that at T = 37°C and pH 1.5 and with thorough mixing for 4 h the viscosity reduction caused by degradation is only about 11% in a fully hydrated solution.

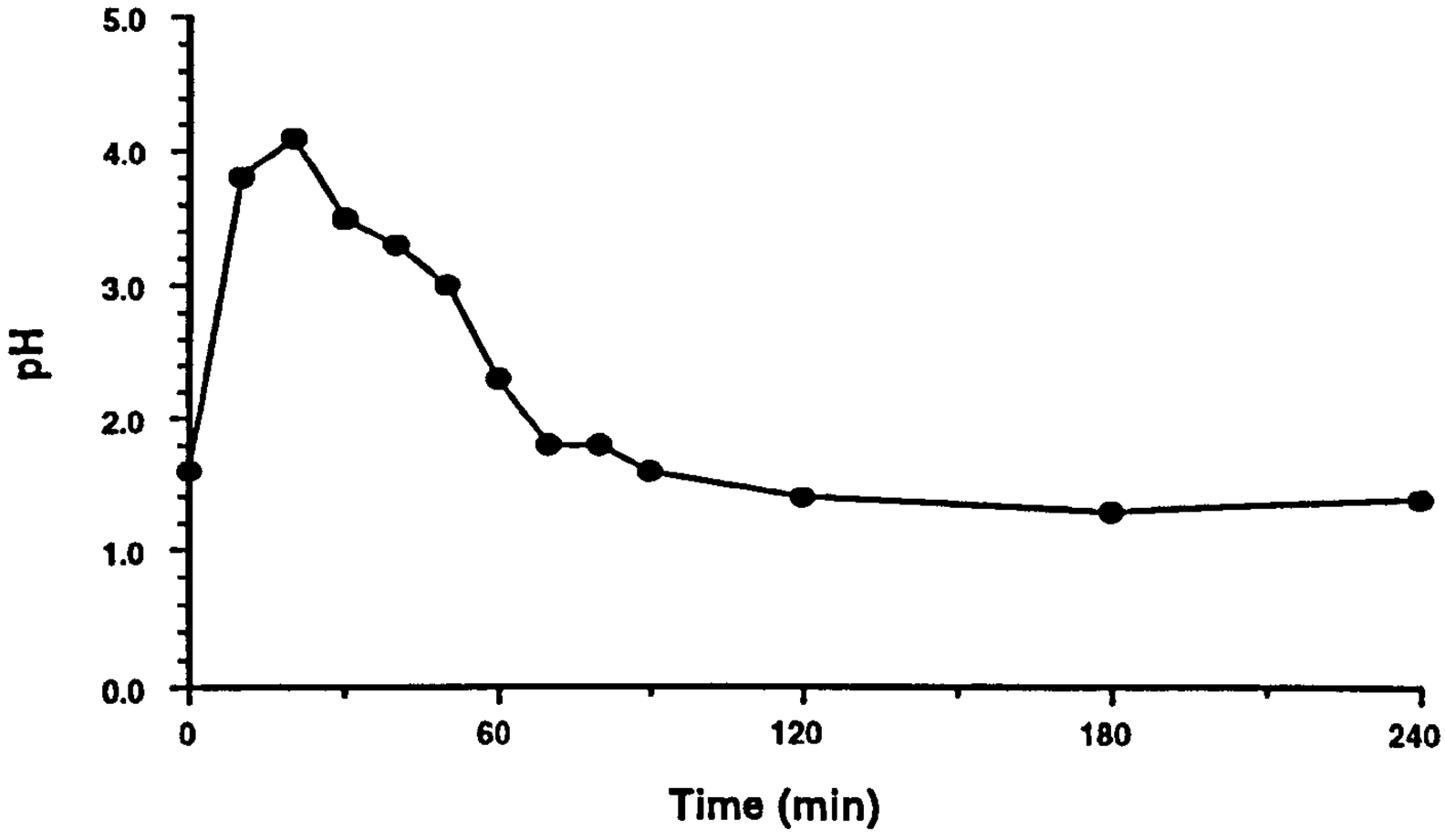

Fig. 9.10 Intragastric pH changes with time after ingesting meals containing guar gum (Rayding et al., 1984).

Although the acidic hydrolysis of guar gum may be limited *in vivo,* this does not exclude the possibility of degradation caused by bacterial enzymes in the upper gastrointestinal tract. It has been reported that the degradation of oat gum took place after passage through the stomach and the proximal small intestine of pigs (Johansen, *et al.,* 1993). This degradation was ascribed mainly due to the enzymatic digestion, originating from microbes present in the gut. However, there is no evidence that this is happening to guar gum, although bacterial degradation of guar gum in the colon is known to be extensive.

9.5 Conclusions

The stability of guar gum polysaccharides under acidic condition was investigated using dilute solutions at temperature 25, 37 and 50°C. The lowest pH that guar

galactomannan remains stable under these temperatures were found to be 1.5, 3.0 and 3.5, respectively. The degradation process under the acidic conditions is likely to be a random scission process with first order kinetics. Current experimental results suggest that severe acidic degradation of guar gum is unlikely to take place in the upper gastrointestinal tract of humans.

The hydration experiments carried out in the acidic condition indicated that the hydration rate of guar gum was influenced by pH. It was found that reducing pH would tend to decrease the hydration rate, mainly at the initial stage of hydration process. Although the hydration rate at acidic condition is slightly higher at the later time period than at neutral, the overall hydration rate was found higher at neutral than at acidic conditions.

The viscosity of a fully hydrated guar gum solutions at acidic pH was found to be lower than it was at neutral. This reduction in viscosity was affected by the concentration of the polysaccharide, *i.e.* it is more pronounced at higher polymer concentrations. This effect was thought to be due to the reduced molecular aggregation of galactomannan molecules.

Chapter 10

General conclusions and future work

10.1 General conclusions

10.1.1 Detarium gum

In this part of work, a seed polysaccharide extracted from *detarium senegalense* Gmelin was characterised by the use of a number of physico-chemical techniques. Chemical analysis indicates that the main s-NSP component of detarium gum is structurally similar to tamarind seed xyloglucan, but with slightly less galactose substitution on the detarium xyloglucan core than that found in tamarind.

Rheological and light scattering measurements have shown that the intrinsic viscosity and molecular weight of detarium xyloglucan are relatively higher than that reported for tamarind xyloglucan. This in turn implies that detarium gum is likely to have greater viscosity-enhancing capacity than tamarind gum. The macromolecular solution properties investigated by steady and dynamic shear rheometry suggest that detarium xyloglucan is a well behaved linear polymer entanglement network system. However, the result from static light scattering measurements is not consistent with that of a linear macromolecule, but instead strongly suggests a small degree of long chain branching. Thus, a long chain branching architecture is proposed for detarium polysaccharide from this finding.

In conclusion, it can be asserted that, the high molecular weight, high viscosity characteristics, together with the food origin of detarium gum strongly indicate that it is a very promising source of water-soluble dietary fibre for use as a nutritional supplement or more specifically as a therapeutical agent in the treatment of diabetes. The results of

preliminary human studies are consistent with this view (Onyechi, 1995). In common with many other polysaccharide gums extracted from plant materials, it also has other potentially important commercial applications, particularly in the food and pharmaceutical industries.

10.1.2 Hydration kinetics of guar gum powders

In this part of work, an improved method for determining the hydration rate of guar galactomannan flour was successfully developed. A logarithmic model for describing the hydration kinetics of guar gum flour was also established. In this model the hydration rate of different samples was compared using a simple hydration index. It is thought that this method could also be used to study the hydration kinetics of other polymers and other materials, such as foods supplemented with s-NSP, assuming that these materials are able to generate a certain level of viscosity during hydration.

This hydration method was subsequently used to investigate the effects of a number of important factors that influence the hydration rate of guar gum. These factors are polymer concentration, molecular weight, particle size and pH levels. Although the experiments were conducted using commercial guar gum flours, which are highly heterogeneous with regard to their physical properties, some general conclusions may be drawn from these results with carefully explanations.

From this experiments we can conclude that there is, in general, an inverse relationship between hydration rate and molecular weight. The hydration rates of different grades of guar gum flours (Meyprogat range) are significantly different, except for M120, which has similar hydration rate as M150. The hydration rate increases with increasing polymer concentration at a low polymer concentration (low viscosity) range, but at higher concentration the hydration rate decreases. Guar gum hydrates slightly slower at acidic conditions when compared to neutral conditions, particularly in the initial stage of hydration. Finally, particle size was also found to greatly affect the hydration rate of guar gum. The effects of particle size on hydration rate need to be considered in conjunction with the way by which the polysaccharide powder is to be hydrated. Under

the present experimental conditions a significant inverse relationship was found between the mean particle size and hydration rate.

The conclusions obtained from this study confirmed that the hydration rate of guar gum is greatly influenced by their physico-chemical properties and environmental conditions. It helps us to explain some of the phenomenon about the mechanisms of the actions of guar gum. It is also addressed the importance of choosing appropriate mode and grade of guar gum and other s-NSP to achieve optimum hydration properties. Moreover, many of the conclusions drawn from guar gum may also be applicable to similar polysaccharides.

10.2 Future work

10.2.1 Detarium gum

Detarium gum has been shown to be a very promising polysaccharide in various applications, particularly as a good source of water-soluble dietary fibre. Although the physico-chemical properties of detarium gum have been characterised over a fairly wide spectrum of techniques in this study, there are still much work need to be done towards the applications of this material in treatment of disease such as diabetes and hyperlipidemia. Moreover, it potential use in the food, clinical and drug industries have yet to be explored.

As far as the physiological effects of this material are concerned, one of the important topics that needs further investigation is the study of solubility and hydration properties under various conditions. This should include both purified polysaccharides and the original flour of detarium seed because the hydration property of these could be very different. The stability of this polymer under acidic conditions in vitro, or ideally in the gastrointestinal tract is also worth investigating.

Regarding the applications of detarium gum in food and pharmaceutical industries, it will be useful to look at the compatibility of this polymer with other substances presented, such as proteins, other polysaccharides and salts. Over the last 20 years or so, a considerable amount of research has been done on the study of the synergistic interactions between different polysaccharides. It will be especially interesting to look at the possible interactions between this long chain branching, non-gelling polymers and other charged or neutral polysaccharides. An initial suggestion might be to examine mixtures with xanthan, which is known to interact with galacto- and glucomannans.

The static light scattering technique was successfully applied to examine the molecular weight and architecture of polysaccharides other than starch by employing pressure heating treatment of the samples. This result suggests a considerable future in re-examining the solution behaviour of a wide range of polysaccharides, employing the pressure-temperature method to create time-stable molecular solutions. The use of this method to produce more readily rehydratable materials is also worth examining.

10.2.2 Guar gum

Work presented in this thesis has answered a number of questions concerning the mode of action of guar gum using as dietary fibre supplements. It also raises a number of interesting points that need to be explored in the future.

The result of experiments looking at pH effects indicate that severe acidic depolymerisation of guar galactomannan is unlikely to occur in the upper gastrointestinal tract of humans. However, *in vivo* studies are necessary to look at the stability of guar gum in the gut environment. Although it has been reported that the degradation of oat gum by microbial enzymes occurs when it passes through the stomach and the proximal small intestine of pigs (Johansen, *et al.*, 1993), no such study has been carried out using guar gum in either animal models or humans. However, it is well known that guar gum and similar s-NSP are fermented by bacteria in the colon as mentioned previously in Chapter 2. This work is currently in progress in our group using pigs as a model.

The hydration rate of commercial guar gums of different molecular weight has been found to be significantly different. Although samples of high molecular weight produce high viscosity after fully hydration, they tend to hydrate at a lower rate compared to lower molecular weight samples. Therefore, the effects of molecular weight on viscosity and hydration rate have to be considered at the same time when selecting appropriate samples for clinical and nutritional use. The combination of polymer samples of different molecular weight in one preparation is also worth attempting to try and create certain desirable hydration profiles.

10.2.3 Hydration kinetic study of s-NSP

During the last one or two decades, the crucial importance of the hydration property in determining the physiological effects of s-NSP has become increasingly by research workers. The hydration properties of s-NSP has been studied by a number of groups in different ways. There is a need to establish a relatively standard hydration method in order to compare the results obtained from different sources. The present work has made an good attempt on producing such a method. The hydration method developed in this study could be also applicable to a wide range of polysaccharides.

Most natural polysaccharide gums are highly heterogeneous in terms of physical properties, such as molecular weight, particle size and surface properties. Directed by the practical applications of guar gum, the present project has used the original guar gum flours as the study objects. However, for a more theoretically focused study of hydration kinetics, particular efforts should be made to prepare more homogeneous samples, although absolutely homogeneous sample never exist in practice, especially with biopolymer materials. Thus, the use of synthetic materials is a alternative way to avoid this.

10.2.4 Hydration study of food system

One serious problem encountered when administrating clinically effective types of s-NSP is their poor palatability when ingested as a viscous solution. To try and overcome this problem, pharmaceutical preparations, which hydrate slowly when mixed with water, were developed. Pharmaceutical preparations of guar gum (granules) are normally taken orally mixed with water or fruit juice immediately before a meal. In some cases however, these formulation have shown markedly diminished therapeutic properties. Recently, many s-NSP has been incorporated into a variety of food products, such as breads and breakfast cereals. Therefore, the next step of the study is to investigate the hydration behaviours of these s-NSP when they are incorporated into food systems.

Foods containing s-NSP are even more complex systems to study. Some of the conclusions drawn from guar gum flour in the present project cannot necessarily be applied to studies of guar-containing foods. A study by Brennan *et al.* (1996) has shown that guar gum is closely associated with other components (such as starch) when incorporated into a food system, such as bread. In this case, the association between guar gum and other components become an important issue for the hydration of guar gum. Our preliminary studies have shown (results not shown in this thesis) that, the hydration rate of guar gum is considerably less in a food than on its own. Thus, it is obviously very important to investigate the hydration behaviour of food systems containing s-NSP for a better understanding of the mechanisms of the physiological effects of s-SNP.

References

Abdou, H. M. (1989). Theory of dissolution. In *Dissolution, Bioavailability and Bioequivalence.* Mack Publishing Company, Easton, Pennsylvania.

Aberle, T., Burchard, W., Vorwerg, W. and Radosta, S. (1994). Conformational contributions of amylose and amylopectin to the structural-properties of starches from various sources. *Starch* **46** (9), 329-335.

Allen, T. (1990). Particle size, shape and distribution. In *Particle Size Measurement.* 4th edition. Chapman and Hall, London.

American Association of Cereal Chemists (1983). *Approved Methods of the AACC*, 8th Edition, The Association, St Paul, **1** (2).

Anderson, J.W. and Tietyen-Clark, J. (1986). Dietary fiber: Hyperlipidemia, hypertension, and coronary heart disease, *Am. J. Gastroenterol.* **81**, 907-919.

Aro, A, Uusitupa, M. Voutilainen, E., Hersio, K., Korhonen, T and Siitonen, O. (1981). Improved diabetic control and hypocholesterolemic effect induced by long-term dietary supplementation with guar gum in type-2 (insulin-independent) diabetes. *Diabetologia* **21** (1), 29-33.

Asp, N.-G., Schweizer, T.F., Southgate, D.A.T. and Theander, O. (1992). Dietary fibre analysis. In *Dietary Fibre - A Component of Food, Nutritional Function in Health and Disease,* eds. T.F. Schweizer and C.A. Edwards. Springer-Verlag, London.

Asplund, J.M., Orskov, E.R., Hovell, F.D. and Macleod, N.A. (1985). The effect of intragastric infusion of glucose, lipids or acetate on fasting nitrogen excretion and blood metabolites in sheep. *Br. J. Nutr.* **54**, 189-195.

Baker, P. (1988). Placebo-controlled trial of guar in poorly controlled type 2 diabetes. *Practi. Diabetes* **5**, 36-38.

Ball, R.C. and McLeish, T.C.B. (1989). Dynamic dilution and the viscosity of star polymer melts. *Macromol.* **22** (4), 1911-1913.

Balogun, A.M. and Fetuga, B.L. (1986). Chemical-composition of some underexploited leguminous crop seeds in Nigeria. *J. Agric. Food Chem.* **34**(2), 189-192.

Bathgate, G.N., Palmer, G.H. and Wilson, G. (1974). Action of endo-β-1,3-glucanases on barley and malt β-glucans. *J. Inst. Brew. (London)* **80**, 278-285.

Bell, S., Onyechi, U.A., Judd, P.A., Ellis, P.R. and Ross-Murphy S.B. (1993). An investigation of the effects of two indigenous African foods, Detarium microcarpum and Cissus rotundifolia on rat plasma cholesterol levels. *Proc. Nutr. Soc.* **52**, 372A.

Blackburn, N.A., Redfern, J.S., Jarjis, H., Holgate, A.M., Hanning, I., Scarpello, J.H.B., Johnson, I.T. and Read, N.W. (1984). The mechanism of action of guar gum in improving glucose tolerance in man. *Clin. Sci.* **66**, 329-336.

Bolliger, R. (1959). The influence of the methods of preparation and the hydrogen-ion concentration on the viscosity of guar gum slimes. *Congr. Sci. Pharm.*, 515-525.

Braaten, J.T, Wood, P.J., Scott, F.W., Braaten, M.K.L., Bradleywhite, P., Wolynetz, M.S., Railton, K. and Collins, M.W. (1993). Cholesterol lowering effect of oat gum in hypercholesterolemic subjects. *FASEB J.* **7** (4), 721.

Bradley, T.D., Ball, A., Harding, S.E., Mitchell, J. R. (1989). Thermal-degradation of guar gum. *Carbohydr. Polym.*, **10**(3), 205-214.

Brennan, C.S. Blake, D.E., Ellis, P.R. and Schofield, J.D. (1996). Effects of guar galactomannan on wheat bread microstructure and on the *In vitro* and *in vivo* digestibility of starch in bread. *J. Cereal Sci.* **24,** 151-160.

Brochard, F. and de Gennes, P.G. (1983). Dynamics of compatible polymer mixtures. *Physica. A.* **118A,** 289-299.

Brockman, P.R. (1982). Insulin and glucagon responses in plasma to intraportal infusions of propionate and butyratein sheep *Comp. Biochem. Physiol.* **73A,** 237-238.

Buckeridge, M.S., Rocha, D.C., Reid, J.S.G. and Dietrich S.M.C.(1992). Xyloglucan structure and post-germinative metabolism in seeds of *Copaifera langsdorfii* from savanna and forest populations. *Physiol. Plant.* **86,** 145-151.

Burchard, W. (1983). Static and dynamic light scattering from branched polymers and biopolymers. *Adv. Polym. Sci.* **48**, 1-120.

Burchard, W. (1994). Light scattering. In *Physical Techniques for the Study of Food Biopolymers,* ed. S.B. Ross-Murphy. Blackie Academic and Professional, Glasgow, UK.

Burchard, W. (1994). Light scattering. In *Physical Techniques for the Study of Food Biopolymers,* ed. S.B. Ross-Murphy. Blackie Academic and Professional, Glasgow, UK.

Carpron, I., Yvon, M. and Muller, G. (1996). *In vitro* gastric stability of carrageenan. *Food Hydrocoll.* **10**(2), 239-244.

Cassidy, M. and Calvert, R.J. (1993). Effects of dietary fibre on intestinal absorption on lipids. In *Handbook of Dietary Fiber in Human Nutration, 2nd Edition*, ed. G.A. Spiller. CRC Press, London.

Clark, A.H. and Ross-Murphy, S.B. (1987). Structural and mechanical properties of biopolymer gels. *Adv. Polym. Sci.* **83,** 57-192.

Goycoolea, F.M., Morris, E.R. and Gidley, M.J. (1995). Viscosity of galactomannans at alkaline and neutral pH: evidence of 'hyperentanglement' in solution. *Carbohydr. Polym.,* **27,** 69-71.

Cross, M.M. (1965). Rheology of non-Newtonian fluids: a new flow equation for pseudoplastic systems. *J. Colloid. Sci.* **20,** 417-437.

Cummings, J. H. (1993). The effect of dietary fiber on fecal weight and composition. In *Handbook of Dietary Fiber in Human Nutration, 2nd Edition*, ed. G.A. Spiller. CRC Press, London.

Dalbe, B. (1991). Interactions between xanthan gum and konjac mannan. *Gums and Stabilisers for the Food Industry 6*, eds. G.O. Phillips, P.A. Williams, and D.J. Wedlock. IRL Press at Oxford University Press, Oxford. 201-208.

de Gennes, P.G. (1971). Reptation of a polymer chain in the presence of fixed obstacles. *J. Chem. Phys.* **55,** 572-579.

Dea, I.C.M. and Morris, E.R. (1977). Synergistic xanthan gels. In *Extracellular Microbial Polysaccharides, eds.* P.A. Sandford and A. Laskin. ACS, Washington DC.

Dea, I.C.M. and Morrison, A. (1975). Chemistry and interactions of seed galactomannans. *Adv. Carbohydr. Chem. Biochem.* **31,** 241-312.

Devotta, I., Ambeskar, V.D., Mandhare, A. B. and Mashelkar, R. A. (1994a). Life time of a dissolving polymer particle. *Chem. Engng. Sci.* **49,** 645-654.

Doi, M., and Edwards, S.F. (1978). Dynamics of concentrated polymer systems. *J. Chem. Soc. Faraday Trans. II* **74,** 1789-1817.

Edwards, C.A., Johnson, I.T. and Read, N.W. (1988). Do viscous polysaccharides reduce absorption by inhibiting diffusion or convection? *Eur. J. Clin. Nutr.* **42,** 307-312.

Edwards, C.A., Blackburn, N.A., Craigen, L., Davison, P., Tomlin, J., Sugden, K., Johnson, I.T. and Read, N.W. (1987). Viscosity of food gums determined *in vitro* related to their hypoglycaemic actions. *Am. J. Clin. Nutr.* **46,** 72-77.

Egan, H., Kirk, R.S. and Sawyer, R. (1981). *Pearson's Chemical Analysis of Foods,* Churchill Livingstone, Edinburgh. pp.7-34.

Eliasson, A.C. and Gudmundsson, M. (1996). Starch: Physicochemical and functional aspects. In *Carbohydrates in Food.* Marcel Dekker. New York.

Ellis, P. R., Apling, E.C., Leeds, A.R. and Bolster, N.R. (1981). Guar bread: acceptability and efficacy combined. Studies on blood glucose, serum insulin and satiety in normal subjects. *Br. J. Nutr.* **46,** 267-276.

Ellis, P.R., Dawoud, F.M. and Morris, E.R. (1991). Blood glucose, plasma insulin and sensory responses to guar-containing wheat breads: effects of molecular weight and particle size of guar gum. *Br. J. Nutr.* **66,** 363-379.

Ellis, P.R. and Morris, E.R. (1991). Importance of the rate of hydration of pharmaceutical preparations of guar gum; a new *in vitro* monitoring method. *Diabetic Medicine* **8,** 378-381.

Ellis, P.R. (1994). Polysaccharide gums: their modulation of carbohydrate and lipid metabolism and role in the treatment of diabetes mellitus. In *Gums and Stabilisers for the Food Industry 7,* eds. G.O. Phillips, P.A. Williams and D.J. Wedlock. Oxford University Press, Oxford. pp.207-216.

Ellis, P.R. Roberts, F.G., Low, A.G. and Morgan, L.M. (1995). The effect of high-molecular-weight guar gum on net apparent glucose absorption and net apparent insulin and gastric inhibitory polypeptide production in the growing pig - relationship to rheological changes in jejunal digesta. *Br. J. Nutr.* **74** (4), 539-556.

Englyst, H., Quigley, M.E., Hudson, G.J. and Cummings, J.H. (1992). Determination of dietary fibre as non-starch polysaccharides by gas-liquid chromatography. *Analyst* **117**, 1707-1714.

Englyst, H., Quigley, M.E., Hudson, G.J. and Cummings, J.H. (1992). Determination of dietary fibre as non-starch polysaccharides by gas-liquid chromatography. *Analyst* **117**, 1707-1714.

Ekström, L.G, Kuivinen, J. and Johansson, G. (1983). Molecular-weight distribution and hydrolysis behavior of carrageenans. *Carbohydr. Res.* **116** (1), 89-94.

Ekström, L.G. (1985). Molecular-weight-distribution and the behavior of k-carrageenan on hydrolysis. *Carbohydr. Res.* **135**(2), 283-289.

Evans, K.E. and Edwards, S.F. (1981). Computer simulation of the dynamics of highly entangled chains, I. Equilibrium dynamics; II. Static properties of the primitive chain; III. Dynamics of the primitive chain. *J. Chem. Soc. Faraday Trans. II* **77**, 1891-1912, 1913-1927, 1929-1938.

Fanutti, C., Gidley, M.J. and Reid, J.S.G. (1991). A xyloglucan-oligosaccharide-specific α-D-xylosidase or exo-oligoxyloglucan-α-xylohydrolase from germinated nasturtium (*Tropaeolum majus* L.) seeds. *Planta.* **184**, 137-147.

Ferry, J.D. (1980). *Viscoelastic properties of polymers,* 3rd edition, Wiley, New York.

Flory, P.J. (1936). Molecular-size distribution in linear condensation polymers. *J. Am. Chem. Soc.* **58**, 1877-1885.

Food and Agriculture Organization (1988). *Traditional Food Plants: A source Book for Promoting the Exploitation and Consumption of Food Plants in Arid, Semi-arid and Sub-humid Lands of Eastern Africa,* Food and Agriculture Organization XI, Rome, p.593.

Foster, S.E. (1967). *Treatment of manno galactan gums.* U.S. Patent 3346556 (Cl. 260-209).

Fry, S.C., York, W.S., Albersheim, P., Darvill, A., Hayashi, T., Joseleau, J.-P., Kato, Y., Lorences, E.P., Maclachlan, G.A., McNeil, M., Mort, A.J., Reid, J.S.G., Seitz, H.U., Selvendran, R.R., Voragen, A.G.J. and White, A.R. (1993). An unambiguous nomenclature for xyloglucan-derived oligosaccharides. *Physiol. Plant.* **89**, 1-3.

Gaisford, S.E., Harding, S.E., Mitchell, J.R. and Bradley, T.D.(1986). A comparison between the hot and cold water-soluble fractions of 2 locust bean gum samples. *Carbohydr. Polym.* **6** (6), 423-442.

Gatenby, S.J. (1990). Guar gum and hyperlipidaemia - a review of the literature. In *Dietary Fibre Perspectives: Reviews and Bibliography 2* ed. A.R. Leeds. John Libbey, London. 100-115.

Gee, J.M., Blackburn, N.A. and Johnson, I.T. (1983). The influence of guar gum on intestinal cholesterol transport in the rat. *Br. J. Nutr.* **50**(2), 215-224.

Gerard, T. (1980). Tamarind gum. In *Handbook of water-soluble gums and resins,* ed. R.L. Davidson , McGraw Hill, New York.

Gidley, M.J., Lillford, P.J., Rowlands, D.W., Lang, P., Dentini, M., Crescenzi, V., Edwards, M., Fanutti, C. and Reid, J.S.G. (1991). Structure and solution properties of tamarind-seed polysaccharide. *Carbohydr. Res.* **214** (2), 299-314.

Girhammar, U. and Nair, B.M. (1992). Isolation, seperation and characterization of water soluble non-starch polysaccharides from wheat and rye. *Food Hydrocoll.* **6,** 285-299.

Glicksman, M. (1986). Tamarind seed gum. In *Food hydrocolloids Vol. 3*, ed. M. Glicksman, CRC Press, Florida. 191-202.

Goldstein, A.M. and Alter, E.N. (1973). Guar gum. In *Industrial Gums,* eds. R.L. Whistler and J.N. BeMiller. Academic Press, London.

Goyan, J.E. (1985). Dissolution rate studies, III. Penetration model for describing dissolution of a multiparticulate system. *J. Pharm. Sci.* **54**(4), 645-647.

Goycoolea, F.M., Morris, E.R. and Gidley, M.J. (1995). Viscosity of galactomannans at alkaline and neutral pH: evidence of 'hyperentanglement' in solution. *Carbohydr. Polym.* **27**, 69-71.

Graessley, W.W. (1967). Viscosity of entangling polydisperse polymers. *J. Chem. Phys.* **47**(6), 1942-1953.

Hansen, I. (1990). Dietary fiber products, their characteristics. In *Dietary Fiber: Chemical and Biological Aspects, eds.* D.A.T. Southgate, K. Waldron, I.T. Johnson and G.R. Fenwick. Royal Society of Chemistry, Cambridge.

Harju, E. (1985). Increases in meal viscosity caused by addition of guar gum decrease postprandial acidity and rate of emptying of gastric contents in healthy-subjects. *Panminerva Medica* **27**(3), 125-128.

Harju, E. (1985). Increases in meal viscosity caused by addition of guar gum decrease postprandial acidity and rate of emptying of gastric contents in healthy-subjects. *Panminerva Medica* **27**(3), 125-128.

Hayes, C.E. and Goldstein, I.J. (1974). α-D-galactosyl-binding lectin from *Bandeiraea simplicifolia* seeds- Isolation by affinity chromatography and characterization. *J. Biol. Chem.* **249**(6), 1904-1914.

Heppell, L.M.J. and Rainbird, A.L. (1985). Effect of the physical form of dietary guar gum on nutrient absorption in the pig. In *Proceeding of the Third International Seminar on Digestive Physiology and Nutrient Absorption in the Pig*. 58-60, eds. H.J. Just and J.A. Fernandez. National Institute of Animal Sciences, Copenhagen.

Herald, C.T. (1986). Guar gum. In *Food Hydrocolloids Vol 3* ed. M. Glicksman. CRS Press, Boca Raton.

Herman, M.F. and Edwards, S.F. (1990). Reptation model for polymer dissolution. *Macromol.* **23**, 3662-3670.

Hermansson, A.-M., Eriksson, E. and Jordansson, E. (1991). Effects of potassium, sodium and calcium on the microstructure and rheological behaviour of kappa-carrageenan gels. *Carbohydr. Polym.* **16**, 297-320.

Hiemenz, P.C. (1984). Polymer Chemistry- The Basic Concepts. Marcel Dekker, Inc. New York.

Hixson, A. and Crowell, J.H. (1931). Dependence of reaction velocity upon surface and agitation. I. Theoretical considerations. *Ind. Eng. Chem.* **23**, 923-931.

Higuchi, W. I. (1967). Diffusional models useful in biopharmaceutics drug release rate processes. *J. pharm. Sci.* **56**(3), 315-324.

Hipsley, E.H. (1953). Dietary fiber and pregnancy toxaemia, *Br. Med. J.* **2**, 420-422.

Holman, R.R., Steemson, J., Darling, P.and Turner, R.C. (1987). No glycaemic benefit from guar administration in NIDDM. *Diabetes Care* **10**, 68-71.

Holt, S., Heading, R.C., Carter, D.C. and Prescott, L.F. (1979). Effect of gel fibre on gastric emptying and absorption of glucose and paracetamol. *Lancet.* **1**, 636-639.

Huglin, M.B. (1972). *Light Scattering from Polymer Solutions*. Academic Press, New York.

Jelinek, Z.K. (1970). Mechanical methods. In *Particle Size Analysis.* Ellis Horwood Ltd., Coll House, Westergate Chichester, U.K.

Jenkins, D.J.A., Goff, D.V., Leeds, A.R., Alberti, K.G.M.M., Wolever, T.M.S., Gassull, M.A. and Hockaday, T.D.R. (1976). Unabsorbable carbohydrates and diabetes: decreased post-prandial hyperglycaemia. *Lancet* **2**, 172-174.

Jenkins, D.J.A., Wolever, T.M.S., Leeds, A.R., Gassull, M.A., Haisman, P., Dilwari, J., Goff, D.V., Metz, G.L. and Alberti, K.G.M.M. (1978). Dietary fibres, fibre analogues, and glucose tolerance: importance of viscosity. *Br. Med. J.* **1**, 1392-1394.

Johansen, H.N., Wood, P.J. and Knudsen, K.E.B. (1993). Molecular weight changes in the (1→3)(1→4)-β-D-Glucan of oats incurred by the digestive processes in the upper gastrointestinal tract of pigs. *J. Agric. Food Chem.* **41**, 2347-2352.

Johnson, I.T. and Gee, J.M. (1981). Effect of gel forming gums on the intestinal unstirred layer and sugar transport *in vitro. Gut* **22**, 398-403.

Kasapis, S, Morris, E.R., Gross, M. and Rudolph, K. (1994). Solution properties of levan polysaccharide from *Pseudomonas syringae* pv. *phaseolicola*, and its possible primary role as a blocker of recognition during pathogenesis. *Carbohydr. Polym.* **23**, 55-64.

Kato, K., Watanabe, T. and Matsuda, K. (1970). Chemical structure of konjac mannan. II. Isolation and characterization of oligosaccharides from the enzymic hydrolyzate of the mannan. *Agric. Biol. Chem.* **34**, 532-539.

Kay, R.M. and Truswell, A.S. (1980). Dietary fiber: Effects on plasma and biliary lipids in man. In *Medical Aspects of Dietary Fiber*, ed. G.A. Spillar, Plenum Press. New York. pp.153-173.

Koedritz, L.F., Harvey, A.H. and Honarpour, M. (1989). *Introduction to Petroleum Reservoir Analysis.* Gulf Publishing Company, Houston.

Kohyama, K., Iida, H. and Nishinari, K. (1993). A mixed system composed of different molecular weights konjac glucomannan and κ-carrageenan: large deformation and dynamic viscoelastic study. *Food Hydrocoll. 7* (3), 213-226.

Kooiman, P. (1960a). On the occurrence of amyloids in plant seeds. *Acta Bot. Neerl.* **9**, 208-219.

Kohyama, K., Iida, H. and Nishinari, K. (1993). A mixed system composed of different molecular weights konjac glucomannan and κ-carrageenan: large deformation and dynamic viscoelastic study. *Food Hydrocoll. 7* (3), 213-226.

Kooiman, P. (1960a). On the occurrence of amyloids in plant seeds. *Acta Bot. Neerl.* **9,** 208-219.

Kooiman, P. (1960b). A method for the determination of amyloid in plant seeds. *Rec. Trav. Chim. Pays-Bas Belg.* **79,** 675-679.

Kritchevsky, D. and Story, J.A. (1993). Influence of dietary fiber on cholesterol metabolism in experimental animals. In *Handbook of Dietary Fibre in Human Nutrition.* 2nd edtion, ed. G.A. Spiller. CRC Press, London.

Kroger, G, Buschstockfisch, M., Wilhelmi, F. (1993). The thermal-stability of guar gums in dependence of granule size. *Zeitschrift Fur Lebensmittel-Untersuchung Und-Forschung.* 540-546.

Lang, P. and Burchard, W. (1993). Structure and aggregation behaviour of tamarind seed polysaccharide in aqueous-solution. *Makromol. Chem. - Macromol. Chem. Phys.* **194** (11), 3157-3166.

Lang, P., Kajiwara, K. and Burchard, W. (1993). Investigations on the solution architecture of carboxylated tamarind seed polysaccharide by static and dynamic light scattering. *Macromol.* **26,** 3992-3998.

Langenbucher, F. (1972). Linearization of dissolution rate curves by the Weibull distribution. *J. Phar. Pharmac.* **24** (12), 979-981.

Langenbucher, F. (1974). Material and method parameters in dissolution rate studies. *Pharm. Acta Helv.* **49** (5-6), 187-192.

Lapasin, R., Delorenzi, L., Pricl, S. and Torriano, G. (1995). Flow properties of hydroxypropyl guar gum and its long-chain hydrophobic derivatives. C*arbohydr. Polym.* **28** (3), 195-202.

Lapasin, R. and Pricl, S. (1995). Industrial application of polysaccharides. In *Rheology of Industrial Polysaccharides.* Blackie Academic and Professional, London.

Lauer, O. (1966). *Grain Size Measurements on Commercial Powders.* Ausberg: Alpine AG, Ausberg.

Launay, B., Doublier, J.L, and Cuvelier, G. (1986). Flow properties of aqueous solutions and dispersions of polysaccharides. *In Functional Properties of Food*

Levy, G. and Knox, F.G. (1961). The biological activity of orally administered desiccated thyroid. *Am. J. Pharm.* **133**, 255-266.

Ling, T.F., Lee, H.K., and Shah, D.O. (1987). Surfactants in enhanced oil recovery. In *Industrial Applications of Surfactants*, ed. D.R. Karsa, The Royal Society of Chemistry, London. pp.126-178.

Maeda, M., Shimahara, H. and Sugiyama, N. (1980). Detailed examination of the branched structure of Konjac glucomannan. *Agric. Biol. Chem.* **44** (2), 245-252.

Maier, H., Anderson, M., Karl, C., Magnuson, K. and Whistler, R.L. (1993). Guar, locust bean, tara, and fenugreek gums. In *Industrial Gums: Polysaccharides and Their Derivatives. 3rd edition*, eds. R.L. Whistler and J.N. BeMiller. Academic Press, London.

Marupov, R., Shishko, A.M., Zhbankov, R.G., Ivanova, N.V., Khorevskaya, N.M., Korolik, E.V., Volkovich, S.M. (1975). Effect of temperature on the hydrolysis of cellulose I. *Izv. Akad. Nauk Tadzh. SSR, Otd. Fiz.-Mat. Geol.-Khim. Nauk.* **4**, 10-13.

Meier, H. and Reid, J.S.G.(1982). Reserve polysaccharides other than starch in higher plants. In *Encycl. Plant Physiology Vol. 13A, eds.* F.A. Loewus and W. Tanner. Springer-Verlag, Berlin. pp.418-471.

Meyer, J.H. and Doty, J.E. (1988). GI transit and absorption of solid food: multiple effects of guar. *Am. J. Clin. Nutr.* **48**, 267-269.

Morris, E.R., Rees, D.A. and Robinson, G. (1980). Cation-specific aggregation of carrageenan helixes: domain model of polymer gel structure. *J. Mol. Biol.* **138**, 349-362.

Morris, E.R., Cutler, A.N., Ross-Murphy, S.B., Rees, D.A. and Price, J. (1981). Concentration and shear rate dependence of viscosity in random coil polysaccharide solutions. *Carbohydr. Polym.* **1**, 5-21.

Morris, E.R. (1990a). Shear-thinning of 'random coil' polysaccharide: Characterisation by two parameters from a simple linear plot. *Carbohydr. Polym.* **13**, 85-96.

Morris, E.R. (1990b). Physical properties of dietary fibre in relation to biological function. In *Dietary Fibre: Chemical and Biological Aspects,* eds. D.A.T. Southgate, K. Waldron, I.T. Johnson and G.R. Fenwick. Royal Society of Chemistry, Cambridge. pp.91-102.

Morris, E.R. (1990b). Physical properties of dietary fibre in relation to biological function. In *Dietary Fibre: Chemical and Biological Aspects,* eds. D.A.T. Southgate, K. Waldron, I.T. Johnson and G.R. Fenwick. Royal Society of Chemistry, Cambridge. pp.91-102.

Munk, P. (1989). *Introduction to Macromolecular Science*. John Wiley and Sons, New York. pp.392-394.

Narasimhan, B. and Peppas, N.A. (1997). The physics of polymer dissolution. Modeling approaches and experimental behavior. *Adv. Polym. Sci.* **128,** 157-208.

Nelson, E. (1957). Solution rate of theophylline salts and effects from oral administration. *J. Am. Pharm. Assoc.* **46**, 607-614.

Nishinari, K., Williams, P.A. and Phillips, G.O. (1992). Review of the physico-chemical characteristics and properties of konjac mannan. *Food Hydrocoll.* **6**, 199-222.

Noyes, A. and Whitney, W. (1897). *J. Am. Chem. Soc.*, **19**, 930-.

O'Connor, N., Tredger, J. and Morgan, L. (1981). Viscosity differences between various guar gums. *Diabetologia* **20**, 612-615.

O'Connor, T.L. and Greenberg, S.A. (1959). Kinetics for the solution of Si_2O in aqueous solutions. *J. Phys. chem.* **62**, 1195-1198.

Onyechi, U.A., Judd, P.A. and Ellis, P.R. (1993). The effect of two Nigerian foods containing of non-starch polysaccharides on postprandial blood glucose and insulin levels in healthy subjects. *Proc. Nutr. Soc.* **52**(3), 377A.

Onyechi, U.A. (1995). PhD thesis. Potential role of indigenous Nigerian foods in the treatment of non-insulin dependent diabetes mellitus. London University, UK.

Papanu, J.S., Soane, D.S., Bell, A.T. and Hess, D.W. (1989). Transport models for swelling and dissolution of thin polymer films. *J. Appl. Polym. Sci.* **38**, 859-885.

Penner, M.H. and Liaw, E. (1990). Utilization of purified cellulose in fibre studies. *In New Developments in Dietary Fibre,* eds. I. Furda and C.J. Brine. Plenum Press, New York.

Peppas, N.A. Wu, J.C. and von Meerwall, E.D. (1994). Mathematical modelling and experimental characterisation of polymer dissolution. *Macromol.* **27**, 5626-5638.

Pittet, A.O.(1965). Dissolution of polysaccharides. In: *Methods in Carbohydrate Chemistry Vol. V, General Polysaccharides*, ed. R. L. Whistler. Academic Press, London.

Rainberd, A.L. (1986). Effect of guar gum on gastric emptying of test meals of varying energy content in growing pigs. *Br. J. Nutr.* **55**, 99-109.

Rainberd, A.L. and Low, A.G. (1986). Effect of guar gum on gastric emptying in growing pigs. *Br. J. Nutr.* **55**, 87-98.

Randall, N. (1982). PhD thesis. The kinetics of dissolution of Atensine Tablets. Chelsea College, London University.

Rayding, A., Nelson, A. and Basted, A. (1984). Influence of fibre on postprandial intragastric juice acidity, pepsin and bile acids in healthy subjects. *Scand. J. Gastroenterol.* **19**, 1039-1044.

Rees, D.A. (1977). *Polysaccharide shapes*. Chapman and Hall, London.

Reid, J.S.G. (1985). Cell wall storage carbohydrates in seeds - Biochemistry of the seed "gums" and "hemicelluloses." *Adv. Bot. Res.* **11**, 125-155.

Reid, J.S.G., Edwards, M. and Dea, I.C.M.(1987). Biosynthesis of galactomannan in the endosperms of developing fenugreek (*Trigonella foenum-graecum* L.) and guar (*Cyamopsis tetragonoloba* [L.] Taub.) seeds. *Food Hydrocoll.* **1**, 381-385.

Reiser, S. (1987). Metabolic effects of dietary pectins related to human health. *Food Tech.* **41**, 91-99.

Richardson, R.K. and Ross-Murphy, S.B. (1987a). Non-linear viscoelasticity of polysaccharide solutions. I. Guar galactomannan solutions. *Int. J. Biol. Macromol.* **9** (5), 250-256.

Richardson, R.K. and Ross-Murphy, S.B. (1987b). Non-linear viscoelasticity of polysaccharide solutions. II. Xanthan polysaccharide solutions. *Int. J. Biol. Macromol.* **9** (5), 257-264.

Robert, R.S.and Verne, A.V.F.V. (1990). The chemistry and properties of plant cell walls and dietary fiber. In *Dietary Fiber: Chemistry, Physiology, and Health Effects, eds.* D. Kritchecsky, C. Bonfield and J.W. Anderson. Plenum Press, New York.

Robinson, G., Ross-Murphy, S.B. and Morris, E.R. (1982). Viscosity-molecular weight relationships, intrinsic chain flexbility, and dynamic solution properties of guar galactomannan. *Carbohydr. Res.* **107**, 17-32.

Ross-Murphy, S.B. (1984). Rheological methods. In *Biophysical Methods In Food Research. Critical Reports on Applied Chemistry Vol. 5*, ed. H.S. Chan. Blackwell Scientific Publications. Blackwells, Oxford, UK.

Ross-Murphy, S.B. (1994). Rheological methods. In *Physical Techniques for the Study of Food Biopolymers, ed.* S.B. Ross-Murphy, Blackie Academic and Professional. Glasgow. pp. 343-392.

Sabater de Sabates, A. (1979). Contribution à l'étude des relations entre caractéristiques macromoléculaires et propriétés rhéologiques en solution aqueuse concentrée d'un épaississant alimentaire: la gomme de caroube, Doctorate Thesis, Univ. Paris XI-ENSIA.

Sandford, P.A. and Baird, J. (1983). Industrial utilization of polysaccharides. In *The Polysaccharides* vol. 2, ed. G.O. Aspinall. Academic Press. p.462.

Savarino, V., Mela, G.S., Scalabrini, P., Sumberaz, A., Fera, G. and Celle, G. (1988). 24-hour study of intragastric acidity in duodenal-ulcer patients and normal subjects using continuous intraluminal pH-metry. *Dig. Dis. Sci.*. **33**(9), 1077-1080.

Sharman, W.R., Richards, E.L. and Malcolm, G.N. (1978). Hydrodynamic properties of aqueous solutions of galactomannans. *Biopolym.* **17**(2), 2817-2833.

Schneeman, B.O. and Gallaher, D. (1986). Effects of dietary fibre on digestive enzymes. In *Handbook of Dietary Fiber*, ed. G.A. Spiller, CRC Press, Florida.

Selvendran, R.R. (1987). Chemistry of plant-cell walls and dietary fiber. *Scand. J. Gastroenterol.* **22**, (s129) 33-41.

Selvendran, R.R. and Verena, A.V.F.V. (1990). The chemistry and properties of plant walls and dietary fiber. In *Dietary Fiber, Chemistry, Physiology and Health Effects,* eds. D. Kritchevsky, C. Bonfield and J.W. Anderson. Plenum Press, New York.

Shimahara, H., Suzuki, H., Sugiyama, N. and Nisizawa, K. (1975). Isolation and characterization of oligosaccharides from an enzymic hydrolysate of konjac glucomannan. *Agric. Biol. Chem.* **39**, 293-299.

Shinoda, K. (Becher, P. translate) (1978). Surfactant solutions. In *Principles of Solution and Solubility.* Marcel Dekker, New York.

Southgate, D. A. T. (1977). The definition and analysis of dietary fiber, *Nutr. Rev.* **35**, 31-37.

Spiller, G.A. (1993). Definitions and physico-chemical properties of dietary fibre. In *Handbook of Dietary Fibre in Human Nutrition.* 2nd edtion, ed. G.A. Spiller. CRC Press, London.

Stokke, B.T., Elgsaeter, A., Bjørnestad, E.Ø. and Lund, T. (1992). Rheology of xanthan and scleroglucan in synthetic seawater. *Carbohydr. Polym.* **17**, 209-220.

Tanford, C. (1961). *Physical Chemistry of Macromolecules.* John Wiley and Sons, New York. p.12.

Tanford, C. (1961). Transport processes. In *Physical Chemistry of Macromolecules.* John Wiley and Sons, London.

To, K.-M., Mitchell, J.R., Hill, S.E., Bardon, L.A. and Matthews, P. (1994). Measurement of hydration of polysaccharides. *Food Hydrocoll.* **8**, 243-249.

Tolstoguzov, V.B., Mzhel'sky, A.I. and Gulov, V.Y. (1974). Colloid Sci/ Kolloide: Deformation of emulsion droplets in flow. *Colloid Polym. Sci.* **252**, 124-132.

Trowell, H.C. (1972). Ischaemic heart disease and dietary fibre. *Am. J. Clin. Nutr.* **25**, 926-932.

Trowell, H.C. (1974). Definition of dietary fiber. *Lancet*, 503-514.

Trowell, H.C. (1976). Definition of dietary fiber and hypotheses that it is a protective factor in certain diseases. *Am. J. Clin. Nutr.* **29**, 417-427.

Ueberreiter, K. (1968). The solution process. In *Diffusion in Polymers, eds.* J. Crank and G.S. Park. Academic Press, London.

Uragami, T. and Shinomiya, H. (1992). Concentration of aqueous dimethyl-sulfoxide solutions through a chitosan membrane by permeation with a temperature difference. *J. Membrane Sci.* **74** (1-2), 183-191.

Vorwerg, W. and Radosta, S. (1993). Molecular characterisation of starches in aqueous solution. Presented at 44th Starch Conference, Detmold, Germany.

Wang, Q., Ellis, P.R., Ross-Murphy S.B. and Reid, J.S.G. (1996). A new polysaccharide from a traditional Nigerian plant food: *Detarium senegalense* Gmelin. *Carbohydr. Res.* **284** (2), 229-239.

Weibull, W. (1951). A statistical distribution function of wide applicability. *J. Appl. Mech.* **18**, 293-297.

Whistler, R.L. and Corbett W.M. (1957). Polysaccharides. In *The Carbohydrates - Chemistry, Biochemistry, Physiology, ed.* W. Pigman. Academic Press, New York.

Williams, P.A., Clegg, S., Langdon, M.J., Nishinari, K. and Phillips, G.O. (1991). Studies on the synergistic interaction of konjac mannan and locust bean gum with kappa carrageenan. *Gums and Stabilisers for the Food Industry 6*, eds. G.O., Phillips, P.A. Williams, and D.J. Wedlock. IRL Press at Oxford University Press, Oxford. 209-216.

Wood, P.J., Siddiqui, I.R. and Paton, D. (1978). Extraction of high viscosity gums from oats. *Cereal Chem.* **55**, 1038-1049.

Wood, P.J., Braaten, J.T. and Scott, F.W. (1992). Effect of oat gum on postprandial hyperglycemia-reply. *Am. J. Clin. Nutr.* **55** (1), 143-144.

Wurster, D.E. and Taylor, P.W. (1965). Dissolution rates. *J. Pharm. Sci.* **54** (2), 169-175.

York, W.S., van Halbeek, H., Darvill, A.G. and Albersheim, P. (1990). Structural analysis of xyloglucan oligosaccharides by ^{1}H-n.m.r. spectroscopy and fast-atom-bombardment mass spectrometry. *Carbohydr. Res.* **200,** 9-31.

Zimm, B.H.(1948). The scattering of light and the radial distribution function of high polymer solutions. *J. Chem. Phys.* **16,** 1093-1099.

Zimm, B.H. and Stockmayer, W.H. (1949). The dimensions of chain molecules containing branches and rings. *J. Chem. Phys.* **17,** 1301-1304.

List of Figures

List of Tables